NUCLEIC ACID DELIVERY SYSTEMS: FROM BIOPHYSICS TO BIOLOGICAL ACTIVITY

Ana Maria Sequeira Cardoso

UNIVERSIDADE DE COIMBRA

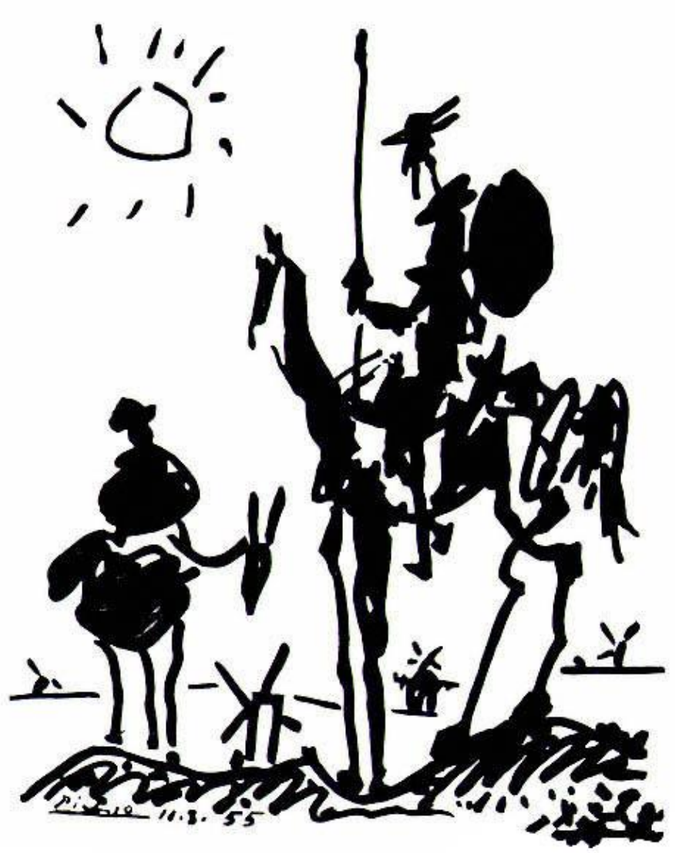

Ana Maria Sequeira Cardoso

NUCLEIC ACID DELIVERY SYSTEMS: FROM BIOPHYSICS TO BIOLOGICAL ACTIVITY

Tese de Doutoramento em Biociências na especialidade de Bioquímica, orientada por Prof. Doutora Maria Amália da Silva Jurado e por Prof. Doutora Maria da Conceição Pedroso de Lima.
Apresentada à Faculdade de Ciências e Tecnologia da Universidade de Coimbra.

setembro 2014

· U C ·

UNIVERSIDADE DE COIMBRA

Ana Maria Sequeira Cardoso

Nucleic Acid Delivery Systems: From Biophysics to Biological Activity

Sistemas de Entrega de Ácidos Nucleicos: Da Biofísica à Actividade Biológica

Tese de Doutoramento em Biociências na especialidade de Bioquímica,
apresentada ao Departamento de Ciências da Vida da Faculdade de Ciências e Tecnologia
da Universidade de Coimbra para obtenção do grau de Doutor

Coimbra
[2014]

Front cover: Dom Quixote
Pablo Picasso

Dissertação apresentada à Faculdade de Ciências e Tecnologia da Universidade de Coimbra, para prestação de provas de Doutoramento em Biociências, na especialidade de Bioquímica.

Dissertation presented to the Faculty of Sciences and Technology, University of Coimbra in partial fulfillment of the requirements for obtaining a Doctoral degree in Biosciences, specialty in Biochemistry.

Este trabalho foi realizado no Centro de Neurociências e Biologia Celular de Coimbra, Universidade de Coimbra, Coimbra, Portugal, sob supervisão da Professora Doutora Maria Amália da Silva Jurado e da Professora Doutora Maria da Conceição Pedroso de Lima. A realização deste trabalho foi apoiada pela Fundação para a Ciência e a Tecnologia (Bolsa de Doutoramento: SFRH / BD / 63288 / 2009 e Bolsa do CNC PEst-c/SAU/LA0001/2013-14).

This work was performed at the Center for Neuroscience and Cell Biology of Coimbra, Coimbra, Portugal, under the supervision of Professor Maria Amália da Silva Jurado and Professor Maria da Conceição Pedroso de Lima. The execution of this work was supported by the Portuguese Foundation for Science and Technology (Ph.D. grant SFRH / BD / 63288 / 2009 and CNC grant PEst-c/SAU/LA0001/2013-14).

Agradecimentos

Estes quatro anos foram uma espécie de aventura de cavalaria, com novos amigos, histórias, viagens, investidas, sucessos, imprevistos e até alguns gigantes, que depois se revelaram moinhos de vento. Pelo caminho fui encontrando as pessoas que contribuíram para contar esta história. Esta Tese resume o trabalho dessa excelente equipa.

Por isso, quero agradecer à Professora Doutora Maria Amália da Silva Jurado e à Professora Doutora Maria da Conceição Pedroso de Lima terem-me aceitado no grupo de investigação como aluna de doutoramento. Agradeço a ambas terem trabalhado horas a fio para consertar os rascunhos mal amanhados de projecto de doutoramento, artigos e tese, que eu lhes ia entregando, com paciência e disponibilidade inesgotáveis, e, claro, o rigor e a qualidade da orientação científica proporcionada ao longo destes anos. Mais do que orientadoras, revelaram-se boas amigas, que estimo muito.

Este trabalho não teria sido possível sem o valioso contributo das minhas colegas do Grupo de Vectores e Terapia Génica Catarina Morais, Ana Luísa Cardoso, Sara Trabulo e Rita Cruz, que desenharam e executaram experiências a par comigo.

Também as colaborações que estabelecemos com outros grupos de investigação foram indispensáveis ao sucesso desta empreitada.

À Sandra Silva, à Professora Doutora Luísa do Vale e ao Professor Doutor Eduardo Marques agradeço a colaboração na forma de síntese dos tensioactivos, assim como a disponibilidade para interessantes discussões e a amizade. À Sandra, em particular, agradeço a amizade, a disponibilidade e a forma calorosa como sempre fui recebida pelo grupo.

À Doutora Paula Gomes, agradeço a disponibilidade para a síntese dos péptidos utilizados neste trabalho.

To Professor Margus Pooga and Annely Lorentz who allowed us to benefit from their TEM expertise.

À Doutora Salette Reis, Cláudia Nunes e Marlene Lúcio agradeço a oportunidade de realizar experiências de difracção de raios-X.

To Professor Bo Nyström, who provided the polymers used in this work, resulting in a fruitful collaboration, hopefully with a bright future ahead.
À Teresa Calejo, que no pouco tempo em que esteve em Coimbra se tornou uma grande amiga.

O bom ambiente de trabalho que se vive no Grupo de Vectores e Terapia Génica do Centro de Neurociências e Biologia Celular, tanto no laboratório como no aquário e nos corredores, foi fundamental para levar a bom termo este trabalho. O companheirismo e o espírito de entreajuda presentes neste grupo são uma mais-valia para uma prolífica produção científica de qualidade.

Agradeço à Professora Doutora Catarina Resende de Oliveira, por me ter permitido realizar este trabalho no Centro de Neurociências e Biologia Celular da Universidade de Coimbra.

Aos meus amigos e família, que estiveram presentes sempre e para tudo, agradeço isso mesmo.

Contents

Abbreviations

2-AS, 2-(9-anthroyloxy) stearic acid

6-AS, 6-(9-anthroyloxy) stearic acid

12-AS, 12-(9-anthroyloxy) stearic acid

16-AP, 16-(9-anthroyloxy) palmitic acid

A

AFM, atomic force microscopy

AGO2, Argonaute 2

AMPTMA, (3-acrylamidopropyl)trimethylammonium chloride

AntpHD, *Drosophila* Antennapedia homeodomain protein

ATPR, atom transfer radical polymerization

C

cac, critical aggregation concentration

CD, circular dichroism

CM, maternally inherited cardiomyopathy

cmc, critical micellar concentration

CPEO, chronic progressive external ophthalmoplegia

CPP, cell-penetrating peptide

CTAB, cetyltrimethylammonium bromide

D

DAD, diode-array detector

DIPEA, *N*-ethyl-*N*,*N*-diisopropylamine

DLS, dynamic light scattering

DMF, *N*,*N*-dimethylformamide

DMPC, 1,2-dimyristoyl-sn-glycero-3-phosphocholine

DMPG, 1,2-dimyristoyl-sn-glycero-3-phospho-(1'-rac-glycerol)

DOPE, 1,2-dioleoyl-sn-glycero-3-phosphoethanolamine

DOPG, 1,2-dioleoyl-sn-glycero-3-phospho-(1'-rac-glycerol)

DOTAP, 1,2-dioleoyl-3-trimethylammonium-propane

DOTMA, 1,2-di-O-octadecenyl-3-trimethylammonium propane

DPH-PA, 3-(p-(6-phenyl)-1,3,5-hexatrienyl)phenylpropionic acid

DPPC, 1,2-dipalmitoyl-sn-glycero-3-phosphocholine

DPPE, 1,2-dipalmitoyl-sn-glycero-3-phosphoethanolamine

DPPG, 1,2-dipalmitoyl-sn-glycero-3-phospho-(1'-rac-glycerol)

DSC, differential scanning calorimetry

DSPC, 1,2-distearoyl-sn-glycero-3-phosphocholine

dsRNA, double-strand RNA

E

EPR, enhanced permeation and retention

ESI/IT/MS, electrospray ionization/ion trap/mass spectrometer

F

FBS, fetal bovine serum

FITC, fluorescein isothiocyanate

G

GAG, glycosaminoglycans

GFP, green fluorescent protein

H

H_I, hexagonal phase

H_{II}, inverted hexagonal phase

HA, hexylacrylate

HBTU, *O*-(benzotriazol-1-yl)-*N,N,N',N'*-tetramethyluronium-hexaflurophosphate

HOBt , 1-hydroxybenzotriazole

HPLC, high-performance liquid chromatography

I

IAP, inhibitor of apoptosis

K

KSS, Kearns-Sayre syndrome

L

LC-ESI/IT/MS, liquid chromatrography-electrospray ionization/ion trap/mass spectrometer

LCST, lower critical solution temperature

LHON, Leber's hereditary optic neuropathy

LUV, large unilamellar vesicles

M

MELAS, mitochondrial encephalopathy with lactic acidosis and stroke-like episodes

MERRF, myoclonic epilepsy with ragged red fibers

miRNA, micro RNA

MLP, mitochondrial leading peptide

MLV, multilamellar vesicles

MW, microwave

N

NARP/MILS, neuropathy, ataxia, and retinitis pigmentosum/maternally inherited Leigh syndrome

NIPAAM, *N*-isopropylacrylamide

NLS, nuclear localization signal

NMP, *N*-methylpyrrolidone

NMR, nuclear magnetic resonance

O

ODN, oligodeoxynucleotides

ONs, oligonucleotides

OTC, ornitine transcarbamylase

P

PAMPTMA, poly(3-acrylamidopropyl)trimethylammonium chloride

PCS, photon correlation spectroscopy

PDMAEMA, poly(2-(dimethylamino)ethyl methacrylate)

PEI, polyethyleneimine

PG, proteoglycans

PLGA, Poly(D,L-lactic-co-glycolic acid)

PMO, phosphorodiamidatedmorpholino-oligomer

PNA, peptide nucleic acids

PNIPAAM, poly-*N*-isopropylacrylamide

POPC, 1-palmitoyl-2-oleoyl-sn-glycero-3-phosphocholine

POPG, 1-palmitoyl-2-oleoyl-sn-glycero-3-phospho-(1'-rac-glycerol)

PS, phosphatidylserine

Q

QRT-PCR, quantitative real time-polymerase chain reaction

R

R9, nonarginine

RISC, RNA-induced silencing complex

RNAi, RNA interference

ROS, reactive oxygen species

S

SAXS, small angle X-ray scattering

SCID, severe combined immunodeficiency

siRNA, small interfering RNA

SCID, severe combined immunodeficiency

SPPS, solid-phase peptide synthesis

SUV, small unilamellar vesicles

T

TEM, transmission electron microscopy

TFA, trifluoroacetic acid

U

UTRs, untranslated regions

V

VDAC, voltage-dependent anion channels

W

WAXS, wide angle X-ray scattering

Resumo

Um número crescente de formulações, contendo moléculas conhecidas ou sintetizadas de novo, tem vindo a ser utilizado na terapia génica. A eficiência dos sistemas não-virais na entrega de ácidos nucleicos tem mostrado elevada dependência das suas características estruturais intrínsecas, que, por sua vez, condicionam as interações que estabelecem com as membranas celulares e as alterações conformacionais que sofrem no ambiente intracelular. Essas características têm, por isso, sido modeladas empiricamente com vista a aumentar a capacidade dos vetores para protegerem os ácidos nucleicos, ultrapassarem as barreiras biológicas e garantirem a libertação das moléculas transportadas nos devidos compartimentos intracelulares (citoplasma, núcleo ou mitocôndrias). É neste contexto que se insere o presente trabalho, tendo como objetivo estabelecer critérios e diretrizes que possam contribuir para uma preparação racional de novos vetores ou reformulação dos já existentes, poupando tempo, custos e recursos humanos. Com este propósito, compostos convencionais e sintetizados de novo, pertencentes a diferentes famílias químicas (tensioativos gemini, péptidos permeantes e polímeros termossensíveis) foram testados, em combinação ou não com lípidos auxiliares, como sistemas não-virais para a entrega de ácidos nucleicos, procurando, em paralelo, identificar as características estruturais de cada formulação responsáveis pelo sucesso ou insucesso da mesma na transfeção.

Pequenas variações na estrutura de tensioativos gemini, tais como um aumento do comprimento das cadeias hidrocarbonadas e do espaçador, mostraram ter impacto direto na formação de arranjos supramoleculares, *per se* ou após complexação com DNA, com consequente repercussão na eficiência de transfeção e na citotoxicidade dos complexos. Por outro lado, o tipo de ligação (amina, amida ou éster) estabelecido entre os grupos polares e o espaçador de tensioativos gemini derivados de serina, condicionando a sua biodegradabilidade e as suas características estruturais, com impacto na complexação e proteção do DNA, bem como na extensão da sua libertação intracelular, revelou-se determinante para a eficácia de transfeção. Interações fracas entre os complexos e a membrana celular, resultando numa expectável desestabilização tardia dos complexos, com libertação do DNA na proximidade do seu alvo intracelular, revelaram contribuir igualmente para elevados níveis de transfeção.

No entanto, a eficiência da entrega de DNA na mitocôndria mostrou uma boa correlação com a capacidade dos complexos com tensioativos gemini para uma extensa interação com modelos membranares de composição semelhante à das membranas mitocondriais.

Por outro lado, a interação de sistemas de entrega de material genético com membranas, levando à segregação de domínios lipídicos e à formação de fases não-lamelares em membranas modelo e celulares, mostrou ser responsável pela aptidão do péptido permeante e cariofílico S4(13)-PV para transpor a membrana celular e entregar eficientemente ácidos nucleicos à célula. Além disso, a modificação estrutural deste péptido, por adição de uma cadeia de histidinas, originou complexos com eficiente capacidade endossomolítica, melhorando a entrega de DNA plasmídico e de siRNA.

Finalmente, a habilidade de co-polímeros para mediarem eficientemente o silenciamento de genes mostrou beneficiar com um ajuste das proporções relativas dos respetivos blocos termossensíveis e catiónicos, repercutindo-se no equilíbrio entre interações eletrostáticas repulsivas e interações hidrofóbicas. A ocorrência de uma transição de fase dependente da temperatura revelou-se importante para que os polímeros condensassem os ácidos nucleicos em solução à temperatura ambiente e, após contacto com as células a 37 °C, os expelissem por dissociação dos complexos.

Em suma, utilizando diferentes tipos de vetores, foi possível demonstrar a relevância da sua estrutura em cada etapa do processo de transfeção, desde a complexação dos ácidos nucleicos à sua libertação intracelular, evidenciando como uma modelação minuciosa das suas características estruturais os pode tornar capazes de vencer as diversas barreiras celulares. Este trabalho presta, assim, um contributo para uma melhor compreensão dos mecanismos através dos quais a composição, as propriedades físico-químicas e a arquitetura final de uma variedade de vetores não-virais influenciam a sua eficiência de transfeção, o que representa um avanço para o desenho racional de novos sistemas de entrega de ácidos nucleicos.

Abstract

Increasing efforts have been made to synthesize new molecules and to prepare new formulations with pre-existing molecules aiming at their application in gene delivery. Growing evidence shows that efficient nonviral nucleic acid delivery depends on intrinsic structural characteristics of the delivery systems, as well as on their ability to interact with cellular membranes and undergo conformational changes in the intracellular environment. These properties are interdependent and have been modulated by a "trial and error" approach towards the establishment of an optimized set of architectural characteristics that provide nanocarriers with the capacity to complex and protect nucleic acids, to overcome the biological barriers imposed to nucleic acid delivery and to ensure cargo release at or close the adequate intracellular target (cytoplasm, nucleus or mitochondria). It is in this context that the present work was developed with the ultimate goal of contributing for establishing criteria and guidelines for the preparation of new vectors or the reformulation of conventional ones, as a hypothesis driven procedure, sparing time, costs and human resources. With this purpose in mind, conventional and novel compounds from different chemical families, namely gemini surfactants, cell-penetrating peptides and thermoresponsive polymers, with or without helper lipids, were tested as nonviral nucleic acid delivery systems, in an attempt to identify the structural peculiarities of each formulation responsible for its success or failure in mediating transfection.

Small variations in the structure of gemini surfactants, such as the progressive increase of tail and spacer length, showed to be able to generate different supramolecular arrangements of gemini surfactants and their complexes with DNA, thus being important for the modulation of transfection efficiency and cytotoxicity of the complexes. Furthermore, the type of linkage (amine, amide or ester) established between the headgroups and spacer of serine-derived gemini surfactants produced surfactants varying in spacer length, flexibility, and biodegradability, which showed to be implicated in the structural arrangement of their complexes with DNA, their ability to release the cargo, and their transfection efficiency. These small structural alterations modulated the strength of surfactant-DNA interactions, with impact on the extent of DNA complexation and protection, and on the intracellular release of DNA.

High transfection efficiency was associated with low extent of complex-membrane interactions, which resulted in late destabilization of the complexes and DNA release near its intracellular target. However, the efficiency of gemini surfactant-based complexes to deliver DNA to mitochondria showed to be dependent on enhanced interactions with membranes of composition mimicking that of mitochondrial membranes.

On the other hand, nanocarrier interaction with membranes leading to lipid domain segregation and formation of nonlamellar phases in model lipid bilayers and in cell membranes showed to be responsible for the ability of the karyophilic cell-penetrating peptide S4(13)-PV to transpose the cell membrane and efficiently deliver nucleic acids into the cell. Additionally, structural modification of this peptide by the addition of a histidine tail provided the corresponding nucleic acid complexes with effective endosomolytic ability, improving plasmid DNA and siRNA delivery.

Finally, change of the relative proportions of thermoresponsive and cationic blocks constituting co-polymers, which resulted in the modification of the delicate interplay between repulsive electrostatic forces and hydrophobic interactions, guided their ability to efficiently mediate gene silencing. The occurrence of a temperature-dependent phase transition allowed for the polymers to condense the nucleic acids in solution and, upon heating, the collapse of the polymer structure expelled them from the aggregates, the complexes being thus dissociated.

This work provides deep insights into the mechanisms through which the composition, the physicochemical properties, and the final architecture of a variety of nonviral delivery systems, whose structure is susceptible of systematic modulation, influence their efficiency in mediating transfection. Using different types of nucleic acid delivery systems, we were able to show the relevance of their structure to each step of transfection, from complexation of nucleic acids to their intracellular release. This work shows that the modulation of structural features of the molecules used for nucleic acid delivery allows a fine tuning of the overall ability of the vectors to overcome the barriers imposed by the cells, thus representing a step forward towards the rational design of new nucleic acid delivery systems.

Synopsis

This work was motivated by the growing interest in unraveling the structural properties that endow a compound with the capacity to complex nucleic acids, to mediate their delivery into the cell and promote their activity. The ultimate goal of this research is to contribute to the rational design of new and efficient gene delivery systems obviating extensive *in vitro* and *in vivo* screening of new molecules, almost exclusively conducted by trial and error.

The work developed in the present Thesis aims at contributing to consolidate knowledge in this field, evaluating three types of nucleic acid delivery systems – based on gemini surfactants, cell-penetrating peptides (CPPs) and thermoresponsive polymers –, in terms of their physico-chemical properties, interactions with membranes and ability to mediate intracellular gene delivery. In this regard, Chapter 1 (Introduction) consists of a comprehensive approach of the gene therapy goals, strategies, and types of the most currently used nucleic acid delivery systems. From the variety of compounds with potential for application in nucleic acid delivery, special attention will be paid to gemini surfactants, cell-penetrating peptides and stimulus-responsive polymers. The reason for the selection of these categories of gene carriers stems from the fact that they are amenable to structural manipulation, thus having been used to develop the experimental work, thanks to a joint collaboration with researchers from national and foreign laboratories where the synthesis of these compounds was performed. In the Introduction chapter, emphasis will be given to the structural characteristics that, for each class of compounds, are more relevant for their ability to act as gene delivery systems, either by forming covalently linked conjugates with the nucleic acids or originating complexes through electrostatic interactions. Studies focusing on interactions of nucleic acid complexes with synthetic models or cellular membranes will also be referred to underline the importance of conformational changes of the nucleic acid delivery system and of the structural lipid rearrangements in membranes for the success of the delivery approach. From the virtually infinite number of possible structural variations in gemini surfactant, CPP and polymer molecules, those that showed to improve their

ability to mediate gene delivery, by promoting interactions with the cell surface and facilitating complex internalization or overcoming natural barriers imposed in one or more of the multiple steps involved in the intricate intracellular trafficking leading to gene expression or silencing, will be addressed.

The hypothesis that was on the basis of the present work as well as the general aims of this Thesis, including the intermediate milestones that were pursued and that contributed to reach the ultimate goals, will be presented in Chapter 2.

Chapter 3 will give an overview of the theoretical basis underlying each methodology used in the Chapters 4 to 9, which consist of the reproduction of scientific articles already published (Chapters 4, 7, 8 and 9) or under revision (Chapter 5 and 6) in peer-reviewed international scientific journals. The methodologies briefly described in the articles that originated Chapters 4 to 9 will be described in detail in Chapter 3 in order to facilitate the replication of each experiment by other researchers.

Chapters 4 to 6 approach the use of gemini surfactants as gene delivery systems targeting nuclear and mitochondrial gene expression.

Chapter 4 addresses conventional *bis-quaternary* gemini surfactants from the alkanediyl-α,ω-bis(alkyldimethylammonium bromide) family, containing different spacer and hydrocarbon chain lengths, which were systematically studied regarding their ability to mediate gene delivery. The results are discussed in terms of the importance of an optimal tail and spacer length for efficient complexation and release of the cargo and of the relevance of complex-membrane interactions for their ability to enter the cells. The existence of a linker (spacer) between the two headgroups of gemini surfactants, maintaining them closer than the optimal distance defined by the entropic/enthalpic balance of surfactant molecules in solution, provides these systems with special aggregation properties, which were shown to contribute to their potential for gene delivery.

Modifications of gemini surfactants with natural structural motifs, such as sugars, lipids or aminoacids, which are recognized by organisms as blocks for their intrinsic anabolic pathways rather than unfamiliar and potentially harmful elements that should be eliminated, have the capacity to reduce the toxicity of those compounds. In

this context, the ability of members from a serine-derived gemini surfactant family to mediate transfection will be addressed in Chapter 5. Amide and ester linkages, introduced between the surfactants' headgroups and spacer, showed to produce gemini surfactants with biodegradability potential, contributing to decrease the toxicity of the delivery system, as well as to favor the release of cargo inside the cells, upon eventual digestion of the compounds by intracellular enzymes.

Alternative targets for transfection are provided by other organelles containing the machinery to produce their own proteins. In animal cells, mitochondria are the only organelles to meet this requirement. Cell energy production became the quintessential role of mitochondria. Optimization of eukaryotic cell resource, by concentration of a great part of the energy producing enzymes in mitochondria, resulted in the generation of toxic oxygen reaction species at high concentration in these organelles. Therefore, and adding to this the fact that mitochondrial DNA is not protected by histone-condensation, oxidation of mitochondrial DNA is much more likely to occur than oxidation of nuclear DNA. The identification of a large number of point mutations in mitochondrial DNA related with several diseases, mostly affecting high energy-consuming organs, has driven the interest towards the development of transfection agents able to specifically target mitochondria. The recent design of a plasmid DNA construct that codes for GFP protein, which is specifically expressed by the mitochodrial machinery, propelled the study performed in the present work regarding the potential of gemini surfactants as mitochondria-targeting gene delivery systems. In this regard, in Chapter 6, members of both families of gemini surfactants previously used to deliver DNA into the nucleus were shown to be able to deliver mtpDNA into mitochondria. The extent of gemini surfactant-DNA complex interactions with model membranes of specific lipid compositions, mimicking those of different cellular structures faced by complexes along their intracellular trafficking towards mitochondria, showed a strict correlation with their ability to mediate efficient mitochondrial gene expression.

Cell-penetrating peptides are the focus of Chapters 7 and 8. In Chapter 7, the S4(13)-PV cell-penetrating peptide and its derivative with scrambled sequence are compared in terms of their ability to interact with model and cell membranes. The

results are discussed regarding membrane lipid phase transitions induced by the presence of peptides, and their commitment in the molecular mechanisms underlying the success of peptide membrane translocation and, consequently, their capacity to be used as gene delivery systems. Chapter 8 regards the use of S4(13)-PV and its derivatives (scrambled, reverse NLS and a derivative containing an additional histidine tail) as DNA and siRNA delivery systems. The histidine tail was added to improve endosomal escape of the complexes internalized by endocytosis, taking advantage of the buffering ability provided by the imidazole groups in this aminoacid residue. Survivin, which is overexpressed in the majority of cancers and is responsible for switching off apoptosis, being hence involved in the survival and recurrence of several types of cancer, showed to be efficiently silenced by a siRNA complexed to histidine tail-containing S4(13)-PV peptide. The transfection efficiency of the different peptides is here compared and data are interpreted in terms of their structural peculiarities.

Finally, Chapter 9 explores the use of thermoresponsive co-polymers, containing different ratios of a thermoresponsive block and of a cationic block, to mediate gene silencing. The silencing efficiency of the polymers is compared and differences are interpreted in terms of their ability to complex and release DNA, the success of the latter event being driven by the phase transition temperature (cloud point) of these polymers near the physiological temperature.

General conclusions and future perspectives are presented in Chapter 10, summarizing the most important results obtained in the course of this work and providing an overview of new studies envisaged as potentially contributing to gain further insight into this interesting research field.

Chapter 1

General Introduction

General Introduction

1.1 GENE THERAPY

Gene therapy emerged as a new therapeutic modality to treat genetic diseases, both inherited and acquired. The diseases that can be targeted with this type of therapy are characterized by anomalous expression of one gene (monogenic disorders), such as severe combined immunodeficiency (SCID), cystic fibrosis and hemophilia, or several genes (polygenic disorders), which include cancer and cardiovascular diseases, (Opalinska & Gewirtz 2002; Verma & Somia 1997). The basic concept of gene therapy consists of inserting genes into target cells in order to prevent, halt or reverse a pathological process (Verma & Weitzman 2005; Somia & Verma 2000; Mountain 2000; Glover et al. 2005). The most used gene therapy strategies consist of the replacement of a nonfunctional gene with its normal version, the introduction of a gene that is dysfunctional or absent as a consequence of a disease, or the addition of a therapeutic gene. The simultaneous deletion of a damaged gene and introduction of its functional form implicate the controlled recombination of DNA fragments. To overcome this difficulty, a plasmid DNA (pDNA) containing a functional or a therapeutic gene is usually introduced into the target cells, in order to correct a genetic deficiency.

As opposed to the abovementioned approaches, gene knockdown, which takes advantage of the recently discovered RNA interference (RNAi) technology, uses RNA molecules, which can be siRNAs or miRNAs, to impair the translation of messenger RNA into proteins that are overexpressed as a consequence of a disease (Opalinska & Gewirtz 2002; Hannon 2002). These small non-coding RNA molecules exhibit regulatory functions, acting as a fine tuning of the mRNA available for protein synthesis. In this regard, siRNAs target specific mRNA sequences, to which they bind with specific complementarity, leading to their cleavage. On the other hand, miRNAs do not require perfect complementarity with their target sequence (Whitehead et al. 2009). Depending on the degree of complementarity between the miRNA and the target mRNA, translation can be blocked (imperfect complementarity) or the mRNA strand can be degraded (perfect complementarity) (Hannon 2002; de Fougerolles et al. 2007; He & Hannon 2004; Cullen 2004). The application of small non-coding RNAs in gene silencing takes advantage of the cellular machinery endogenously used for processing these molecules, namely the RNAse III enzyme Dicer and the RNA-induced silencing complex (RISC), leading to the inactivation of the target mRNA.

1.2 NUCLEIC ACID DELIVERY SYSTEMS

The major drawback of gene therapy is the inability of nucleic acids to travel in biological fluids without being degraded and to enter the cells unaided. Investigation regarding nucleic acid delivery systems has been carried out for decades, aiming at providing a vector able to protect, to carry and deliver the nucleic acids into the cells, releasing them in or close to their target organelle. Several strategies were explored along the years, with the purpose of delivering nucleic acids into cells, both efficiently and safely. These strategies include viral and nonviral delivery approaches.

Viral vectors, which are highly efficient, are based on viral particles whose gene responsible for the virulence is replaced with a therapeutic gene. The disadvantages of these systems regard safety. On the one hand, viral particles, such as adenovirus, have the ability to trigger immunological responses, which prevents repeated administration and limits the therapeutic efficacy of the treatment (Mountain 2000). In fact, adenoviruses used to treat partial ornithine transcarbamylase (OTC) deficiency patients, promoted a strong immune response, resulting in patient death (Lehrman 1999; Somia & Verma 2000). On the other hand, some types of viruses used to prepare viral delivery systems, such as retrovirus, have the ability to insert their genetic cargo on the host's genome. The use of retroviral vectors led to tragic results in clinical trials featuring the treatment of patients with X-linked SCID, who developed leukemia (Hacein-bey-abina & Schmidt 2003; Check 2005). Despite the tragic events, an important proof-of-concept of gene therapy emerged from the clinical trials addressing SCID, with the successful treatment of this disease (Fischer et al. 2002).

Nonviral delivery of nucleic acids can be accomplished by physical and chemical methods. Physical methods to introduce nucleic acids into cells include bombarding the cells with metal particles covered with nucleic acids (gene gun) or inducing cell membrane permeability through electroporation. Both these approaches damage the cells and are, hence, highly cytotoxic (Li & Huang 2000; Mellott et al. 2013). To avoid the toxic effects of viral vectors and nonviral physical methods, a need for suitable alternatives propelled the study of chemical nonviral nucleic acid delivery systems. In this regard, several types of molecules have been explored over the years in the search of safe and efficient delivery systems.

In contrast to viral vectors, chemical nucleic acid delivery systems lack the endogenous ability to "infect" the cells, a feature that viruses have developed along millions of years of co-evolution with their host cells. Several biological barriers stand in the way of

efficient gene delivery mediated by nonviral vectors. The immune system and extracellular nucleases constitute obstacles to the delivery of nucleic acids, before those reach the target cells. At cellular level, the cytoplasmic membrane, endosomal entrapment and lysosomal degradation are other barriers that must be overcome. Therefore, an efficient nucleic acid delivery system should be able to reach the target cells, preventing nucleic acid degradation by nucleases and circumventing the immune defense, to cross the plasma membrane, thereby mediating nucleic acid internalization, to escape the endolysosomal pathway, avoiding lysosomal degradation, and to allow dissociation of the nucleic acids from the carrier near the intracellular target (**Figure 1.1**). Furthermore, pDNA delivery systems should be able to facilitate nucleic acid translocation to the nucleus or to mitochondria for gene expression to occur (Simões et al. 2005; Heitz et al. 2009).

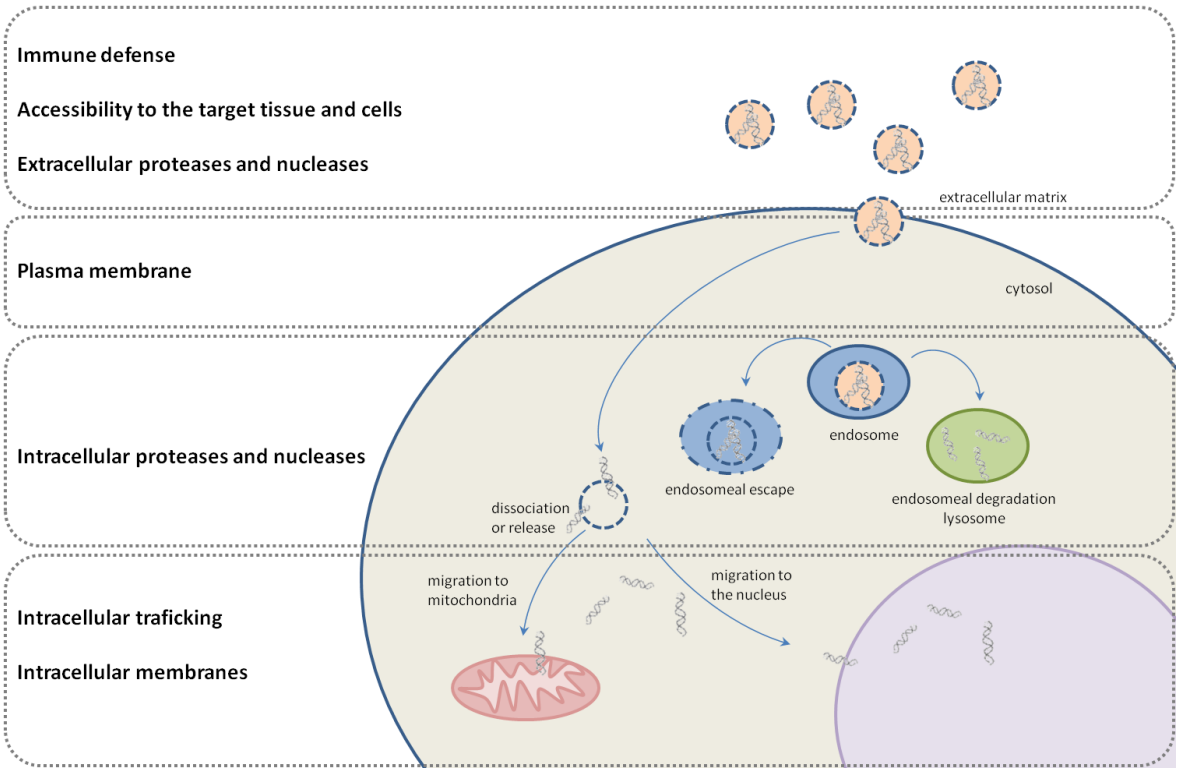

Figure 1.1 Physiological barriers to transfection. In order to efficiently accomplish its task, a successful nucleic acid delivery system should be stealthy to avoid immune reaction, reach the target tissue/organ while avoiding enzymatic degradation and diffuse through the extracellular matrix (A). Upon reaching the target cell, the delivery system should be internalized (B), either by endocytosis or through direct membrane translocation. Once inside the target cell, the delivery system should mediate endosomal escape to avoid lysosomal degradation (C). The nucleic acids should be released from the delivery system at or close to their intracellular target (D), either in the cytoplasm, in the case of siRNAs and miRNAs, or in the nucleus (E) or mitochondria (F), in the case of pDNA.

Chemical nucleic acid delivery systems should provide means to overcome the abovementioned obstacles so that nucleic acids can exhibit their therapeutic effect, either in the cytosol, in the nucleus or in mitochondria. In this regard, several classes of molecules have been studied that fulfill the requirements to efficiently carry and deliver nucleic acids into the target cells at or close to their action site. These classes of molecules include lipids, cell-penetrating peptides (CPPs), polymers and surfactants. The pioneer work of Felgner and coworkers (Felgner et al. 1987), who have synthesized a cationic lipid (DOTMA) that forms liposomes able to spontaneously interact with DNA and facilitate the delivery of functional DNA to CV-1 cells (green monkey kidney fibroblasts) and COS-7 cells (SV40-transformed CV-1 cells) in culture, paved the way to an extensive evaluation of other molecules to mediate nucleic acid delivery, such as those reported in the present work and described in detail in the next sections.

In general, efficient nucleic acid delivery systems originate from cationic molecules, able to interact electrostatically with the negative charges of the nucleic acids, leading to their complexation, and with the cell surface, which is rich in negatively charged glycosaminoglycans (GAG) and proteoglycans (PG), favoring the internalization of the delivery system. In most cases, cell uptake occurs through endocytosis rather than by direct membrane translocation, although the latter pathway has also been observed. Furthermore, the nucleic acid delivery system should have structural properties that assure conformational changes facilitating cargo release under the environmental conditions offered by the intracellular milieu (e.g. regarding temperature and pH). Cancer therapy may take advantage of such delivery system structural alterations into the tumor microenvironment, which has been described as hyperthermic and acidic.

Due to accumulated information on gene carriers resulting from biological and biophysical studies, the next sections will describe in detail the classes of nonviral gene delivery systems used in the present work, namely gemini surfactants, cell-penetrating peptides and thermoresponsive polymers.

1.2.1 GEMINI SURFACTANTS

Dicationic detergents were first synthesized in 1971 when Bunton and coworkers attempted to produce molecules able to catalyze nucleophilic substitutions of hydroxide ions with chloro- and fluoro-2,4-dinitrobenzene and hydroxide and fluoride ions with p-nitrophenyl diphenyl phosphate (Bunton et al. 1971). These new detergents were found to be more catalytically active than monomeric detergents, which was explained taking into account the critical micelle concentration (the concentration of surfactant above which micelles spontaneously form, *cmc*), dicationic detergents presenting *cmc*s two orders of magnitude lower than that of the monomeric detergent (CTAB) with the same hydrocarbon chain length. Since catalytic activity depended on the proximity of the reaction molecules, favored by their incorporation in micelles, detergents that form micelles at the lowest concentrations were the most efficient catalysts (Bunton et al. 1971). These detergents, composed of two sets of a polar headgroup and a hydrocarbon chain, linked together by a spacer at or close to the polar groups, were overlooked for some time until they were rediscovered in 1991, when the name "gemini surfactants" was coined to describe these twin molecules (Menger & Littau 1991).

The group of Menger summarized the relevant structural features that define a gemini surfactant: i) at least two hydrophobic chains (herein named tails) and two polar groups, which can be positively charged (ammonium), negatively charged (phosphate, sulphate or carboxylate) or nonionic (polyether or sugar) and ii) a spacer that can be short (2 methylene groups) or long (up to 12 methylene groups), rigid (stilbene) or flexible (aliphatic or aromatic). Later, the authors recognized that, although originally the name "gemini surfactant" described symmetrical molecules, other asymmetrical surfactants (e.g. n-s-m, instead of m-s-m, where n or m refers to the number of tails' carbon atoms and s, the number of spacer's carbon atoms) and surfactants containing three or more polar groups or tails had also been included in the "gemini" class (Menger & Keiper 2000).

1.2.1.1 Structural properties of gemini surfactants in aqueous solution

The word "surfactant" originates from the contraction of "surface-active agent", which is a molecule able to reduce the water surface tension. Gemini surfactants present surface activity three orders of magnitude higher than that of monomeric surfactants.
At an air/water interface, gemini surfactants are able to adopt a number of conformations, which are not allowed to monomeric surfactants (**Figure 1.2**). In fact, gemini surfactants could assume a linear conformation (*trans* conformation), placing one hydrophobic tail into the air and forcing the other one into the water or laying flat on the surface, or they could adopt an "horseshoe" conformation (*cis* conformation) in which both chains point to the air, while in monomeric surfactants the polar headgroup interacts with the air/water interface, and the single hydrocarbon chain points to the air (Menger & Littau 1993).

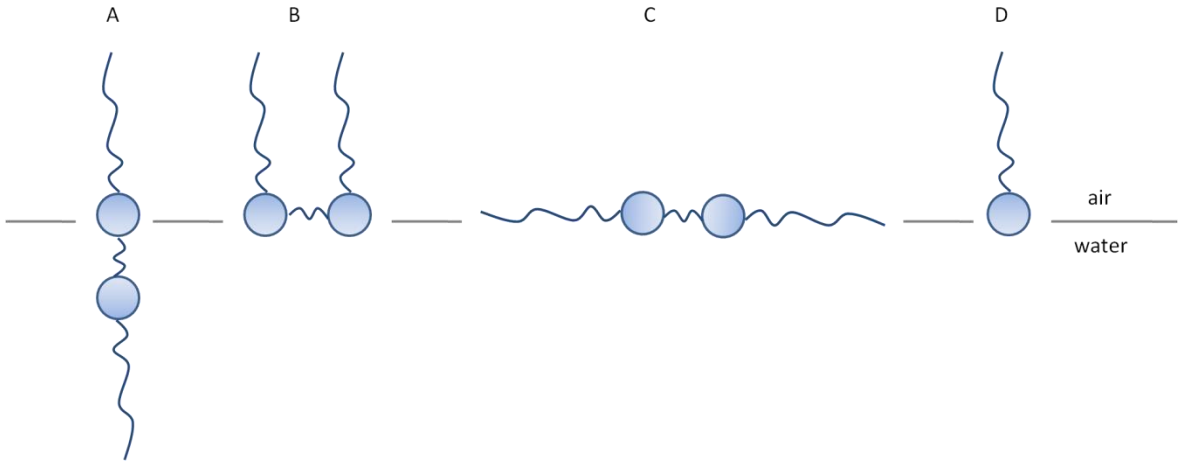

Figure 1.2 Possible orientations of gemini surfactants (A-C) and of a monomeric surfactant (D) at an air/water interface. Possible conformations adopted by gemini surfactants include: A) linear conformation perpendicular to the interface, B) "horseshoe" conformation (*cis* conformation) and C) linear conformation parallel to the interface.

The different conformations adopted by the gemini surfactants depend on the affinity of each portion of the molecule to water and on the steric hindrance between the two alkyl tails of the gemini surfactant. The spacer and tails, being hydrophobic, will avoid the water, while the headgroups will favor contact with the water. *Trans* conformation is unfavorable due to the large hydrophobic portion of surfactant in contact with water. However, for surfactants containing short spacers (s≤4), the *cis* conformation represents an overlap of the two tails. Therefore, the two alkyl tails of a dimeric

surfactant in aqueous solution are expected to adopt *trans* conformation for molecules containing short spacers and *cis* conformation as the spacer length increases (Grosmaire et al. 2002).

Gemini-induced reduction of water surface tension is more than twice that induced by single chain-surfactants and, hence, cannot be attributed solely to the presence of two sets of hydrophilic headgroup plus hydrophobic tail. This effect depends on the distance at which the headgroups are kept, due to the spacer length and rigidity. Thus, the 12–2–12 gemini surfactant was found to pack much more tightly at the air/water interface than 12–3–12 and 12–4–12 gemini surfactants due to increased chain–chain interactions, which disfavor the desorption of molecules from the surface to the bulk solution (Groth et al. 2004).

With the increase of the surfactant concentration, the air/water interface cannot accommodate all the surfactant molecules, which start to accumulate in solution. The micellization process occurs in order to minimize the free energy of a water/surfactant system and consists of the formation of supramolecular structures, which decrease the contact between the hydrophobic hydrocarbon chains of the surfactant and water molecules. In these structures, the hydrophilic headgroups are in contact with the water and are kept away from each other due to electrostatic repulsions.

The existence of a spacer with different lengths linking the two headgroups of the surfactant molecule results in an unusual behavior in aqueous solution. Thus, the *cmc* of gemini surfactants reflects a compromise regarding the conformation of the spacer, which depends both on its length and flexibility, and on the degree of repulsion between the two similarly charged headgroups. As **Table 1.1** illustrates, for 12-s-12 and 16-s-16 gemini surfactants with increasing spacer length, the *cmc* reaches a maximum for those containing a spacer of 4 and 6 carbon atoms, respectively, and decreases for those displaying longer spacers.

Table 1.1 *Cmc* of gemini surfactants of the alkanediyl-α,ω-bis(dimethylalkylammonium bromide) family measured at 25 °C (mM)*.

m-s-m	8-s-8[a]	10-s-10	12-s-12[c]	14-s-14	16-s-16[g]	18:1-s-18:1[i]
m-2-m			0.84	0.137[d]	0.021	0.0269
m-3-m	57.0	6.10[b]	0.87	0.091[e]	0.026	0.0234
m-4-m			1.17		0.027	
m-5-m			1.09	0.15[f]	0.038[j]	
m-6-m	73.0		1.03		0.043	0.018
m-8-m			0.83		0.033	
m-10-m			0.63			
m-12-m			0.37[h]			
m-16-m			0.12[h]			

* Values of *cmc* were gathered from: [a] (Frindi & Michels 1994), [b] (Wettig & Verrall 2001), [c] (Grosmaire et al. 2002), [d] (Manet et al. 2010), *cmc* was determined at 30 °C, [e] (Uhríková et al. 2005), [f] (Kabir-ud-Din et al. 2010), [g] (Zana et al. 1991), [h] (Khan et al. 2010) and [i] (Li et al. 2005).

A favorable effect of the increase of the hydrophobic spacer length on the micellization process, which is driven both by enthalpic and entropic forces, would be expected. However, similarly to the behavior at the air/water interface, spacers shorter than the equilibrium distance between the charged headgroups (s≤4-6) will force these two groups to be closer than they would be if they belonged to individual molecules. Therefore, these spacers are maintained fully extended to minimize the repulsion between the headgroups, establishing an unfavorable contact with the water. In this regard, it was proposed that the increase of the *cmc* with the increase of the spacer length up to 4-6 carbon atoms reflects a balance between the hydrophobic effect, which increases with the increase of the hydrophobic spacer length, and the repulsive electrostatic forces between the cationic headgroups, which compel the spacer to be maximally stretched up to an equilibrium distance, therefore constraining the spacer to be extensively in contact with the surrounding aqueous medium (Menger & Keiper 2000; Weihs et al. 2005; Perez et al. 2007).

On the other hand, spacers longer than the equilibrium distance will not be fully extended and will minimize their contact with the water (Karaborni et al. 1994). If the spacer is long and flexible enough, this can occur through coiling of the spacer into the hydrophobic region of the structure (Almeida et al. 2011; Zana et al. 1991). The increase of the length of the hydrocarbon spacer, above that corresponding to 4-6 methylenes, contributes to the overall hydrophobicity of the gemini surfactant,

reducing progressively the monomer solubility and, consequently, promoting self-assembly at concentrations progressively lower (Menger & Keiper 2000).

Gemini surfactants derived from aminoacids also present values of *cmc* one or two orders of magnitude lower than those of the corresponding single chain analogues, as exemplified by those based on arginine and serine (**Table 1.2**) (Weihs et al. 2005; Perez et al. 2007; Silva et al. 2012; Silva et al. 2013). Although there is no available data for these surfactants to define the spacer length that corresponds to the equilibrium distance between the headgroups, it is remarkable that the increase of the spacer from 2 to 5 methylene groups in $(12Ser)_2CONm$ gemini surfactants also promotes an unexpected increase in *cmc* values, which can be explained by the phenomenon referred above for the classical gemini surfactants.

Table 1.2 Critical aggregation concentration (*cac*)* of serine- and arginine-derived gemini surfactants measured at 25 °C (mM)*.

			m=2	**m=3**	**m=5**	**m=6**	**m=9**	**m=10**	**m=12**
Serine-based monomeric	14Ser	1.16[a]							
	12Ser	1.87[a]							
Serine-based dimeric	$(16Ser)_2N5$				0.015[c]				
	$(14Ser)_2N5$				0.042[c]				
	$(12Ser)_2Nm$				0.32[c]			0.067[c]	0.082[c]
	$(12Ser)_2CONm$		0.27[b]		0.40[b]				
	$(12Ser)_2COOm$		0.37[b]		0.26[b]				
Arginine-based monomeric	LAM[#]	6.0[d]							
	CAM[#]	16.0[d]							
Arginine-based dimeric	$C_m(LA)_2$[#]			0.56[d]		0.40[d]	0.18[d]		
	$C_m(CA)_2$[#]			2.0[d]		1.6[d]	1.1[d]		

*Critical aggregation concentration (*cac*) is used herein instead of critical micellar concentration (*cmc*) due to the broader meaning of *cac*, which includes other types of supramolecular arrangements, such as vesicles, besides micelles.

[#]nSer,*N*α-alkyl-L-serine, $(nSer)_2Nm$, Nα,Nα-bis(Nα-alkylserine)α,ω-alkylendiamines, $(12Ser)_2CONm$, Nα,Nα-bis(Nα-dodecylserine)α,ω-alkylendiamides, $(12Ser)_2COOm$ Nα,Nα-bis(Nα-dodecylserine)α,ω-alkylendiesteres,LAM, *N*α-lauroyl-L-arginine methyl ester, CAM, *N*α-caproyl-L-arginine methyl ester,$C_m(LA)_2$, Nα,Nα-bis(Nα-lauroylarginine) α,ω-alkylendiamides, $C_m(CA)_2$, Nα,Nα-bis(Nα-caproylarginine) α,ω-alkylendiamides.

[a] from (Silva et al. 2009), [b] from Silva et al. 2013, [c] from Silva et al. 2012, [d]from (Perez et al. 2002).

On the other hand, the increase in the length of the tails up to 16 carbon atoms produces an effect on *cmc* similar to that observed for monomeric surfactants, i.e. the increase of the alkyl chain length results in a decrease of the *cmc* (Zana et al. 1991; Silva et al. 2012; Perez et al. 2002)

The type of supramolecular aggregates (micelles, bilayers and inverted hexagonal phases) formed by surfactants can be inferred, similarly to those formed by other amphiphiles, from the molecular geometry of the molecules, which in the case of gemini surfactants depends on the conformation adopted and, hence, on the spacer length, as previously mentioned.

According to the most popular model to explain amphiphile mesomorphism, a critical packing parameter (P) can be defined, which depends on the shape of amphiphilic molecules and allows to predict the mesomorphic phase preferentially adopted by those molecules when dispersed in water. That parameter takes into account the volume of the hydrophobic chains (v_c), the cross sectional area of the headgroups (a) and the length of the hydrophobic chains (l_c), and is given by the equation:

$$P = \frac{v_c}{a \times l_c}$$

Thus, amphiphiles which maintain a uniform cross-sectional area along their length (cylindrical shape) tend to form planar mesomorphs, such as bilayers; molecules with larger headgroup than tail areas (conical shape) tend to form micelles or cylindrical micelles, arranged in hexagonal structures, with the hydrophilic headgroups facing the aqueous environment and the hydrophobic tails concealed inside the supramolecular structure, away from the water (H_I structures), and those which have smaller headgroup than tail areas (inverted conical shape) form inverted hexagonal structures (H_{II} phases) (**Figure 1.3**).

The approach to understanding the nonlamellar behavior of amphiphiles based on their molecular shape is simple and allows to predicting the “preferred” aggregates formed by amphiphilic molecules, when dispersed in an aqueous medium. However, this model does not adequately consider the contribution of headgroup and/or chain repulsion for the interaction free energy, nor the flexibility of the amphiphilic molecules, which can provide them with more than one molecular shape. For instance, pH changes may influence the net charge of polar groups and, consequently, the cross-sectional area per headgroup, which leads to alteration of the geometric shape of the molecules as a whole.

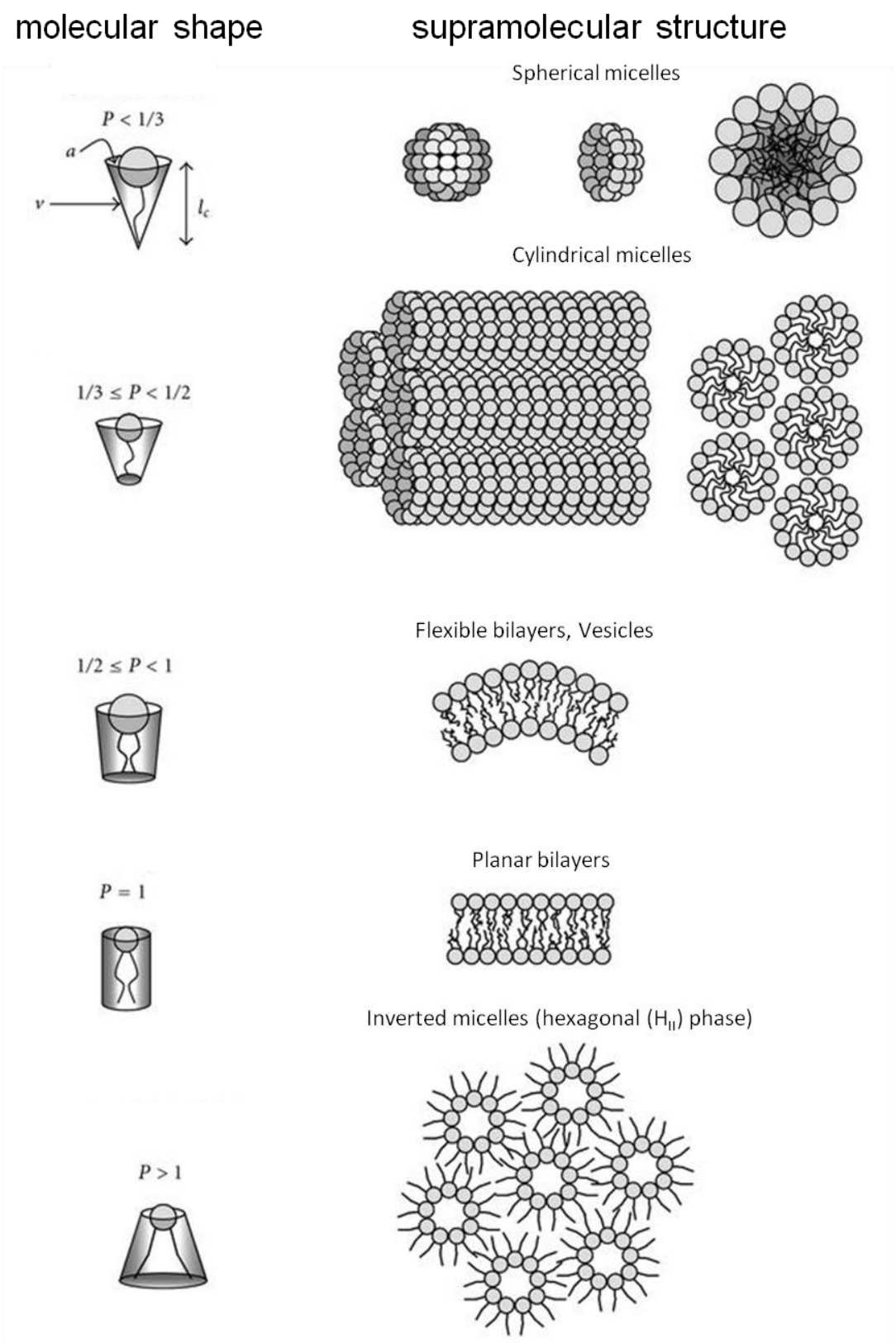

Figure 1.3 Molecular shape of amphiphiles (inverted cone, cylinder, cone) (left) and supramolecular structures adopted (right) according to the critical packing parameter (P), calculated as the ratio between the volume of the hydrophobic chains (v_c) and the product of the cross sectional area of the headgroups (a) multiplied by the length of the hydrophobic chains (l_c) (modified from Balazs & Godbey 2011).

An alternative model was proposed in which the propensity to form nonlamellar structures is evaluated in terms of a balance between opposing tendencies towards the minimization of the monolayer curvature free energy and the free energy associated with hydrocarbon chain packing. In this regard, the predisposition to form nonlamellar structures depends on the intrinsic radius of curvature, R_0, which derives from the asymmetric nature of the amphiphile molecules and endows the supramolecular structures to curl when relaxed. This curling, which is a consequence of the side-by-side packing of molecules whose cross sectional area varies systematically along the length of the molecules, defines the spontaneous curvature ($C_0=1/R_0$) of an amphiphile layer and its mesomorphic tendency. This model accommodates the essentials of the "shape" concept, since amphiphiles whose shape is defined by an uniform cross section along their length (cylindrical shape) have zero spontaneous curvature and form stable bilayers, whereas amphiphiles with inverted conic shape form layers with a positive intrinsic curvature, originating stable micelles or H_I phases, and those with conic shape generate layers with a negative intrinsic curvature, predisposing to the formation of H_{II} phases (Gunter 2004; Lewis & Mannock, David & McElhaney 1997).

As previously referred, depending on the length, the spacer of gemini surfactants imposes different conformations to molecules, which are characterized by different values of the critical packing parameter, this being reflected in the generation of micelles with different morphologies. In fact, surfactants with short spacers (s=2, 3 or 4) have been shown to originate elongated micelles, which "grow" in a single dimension with the increase of the surfactant concentration. This effect is more pronounced for surfactants with the shortest spacer, probably due to the increased geometrical constraints in the formation of aggregates (Groth et al. 2004).

In the context of the mesomorphism, gemini surfactants have been shown to present a phase behavior similar to that of their corresponding monomeric surfactants. However, the potential for gemini structure modulation is enormous and the length and chemical nature of the spacer can be modified in order to modulate their thermotropic and lyotropic behaviors (In & Zana 2007).

The study of the concentration dependence of the mesomorphic behavior (lyotropism) of gemini surfactants showed a complex sequence of phases adopted by the surfactants in solution, including spherical micelles, worm-like micelles, ribbons, multi-bilayers, multi-bilayer ribbons, lamellar and inverted hexagonal phases (Oda et al. 1999; Alami et al. 1993). This sequence may not always be followed and coexistence

of several phases is common. The average length of the "worms" is defined by two opposing forces: the electrostatic repulsions between the polar headgroups, which favors scission of the worms, and the "end-cap energy" that favors micelle growth by minimizing the number of high energy termini. Thus, it was observed that, at high concentrations of 12-2-12 gemini surfactants, the "end-cap energy" becomes dominant over the electrostatic repulsion and long worm-like micelles are formed (Menger & Keiper 2000). Micelle shape has shown to depend on the length and hydrophilicity of the spacers. Hence, short hydrophobic spacers originate nonspherical micelles ("threads") and long hydrophobic spacers lead to rod-like micelles, while hydrophilic spacers originate (more or less) spherical micelles. **Figure 1.4** illustrates the phases adopted by n-2-m surfactants in an aqueous medium and denotes the occurrence of phase transitions induced by temperature increase. For example, the symmetrical surfactants 14-2-14, 16-2-16, 18-2-18 show a temperature-induced transition from tubular lamellar phases to isotropic entangled worm-like micelles (Oda et al. 1997).

Not only the spacer length but also the type of linkage between the headgroups and the spacer contribute to the type of supramolecular aggregates formed by gemini surfactants. Serine-derived gemini surfactants containing short spacers linked to the heagroups through an amide or ester bond were shown to aggregate into micelles, whereas those containing a long spacer (12 carbon atoms-long) formed giant vesicles even at low concentration. However, the amine derivative with 12 carbon atoms-long spacer also formed micelles. This is justified by the fact that the positive charges of the headgroups of surfactants from the amide and ester series, in contrast to those of surfactants of the amine series, are actually at a distance greater than that corresponding to the spacer length (12 carbon atoms-long alkyl chain), since the chiral carbon atom and the α-carboxylate group of each headgroup also contribute to this distance. This translates into a critical packing parameter of the amide and ester derivatives close to 1, favoring the formation of bilayers, while that of the amine derivative is about 0.3-0.5, favoring micelle formation.

In contrast to gemini surfactants, monomeric surfactants present fewer types of phases with no tendency to form elongated or stacked structures (Oda et al. 1999).

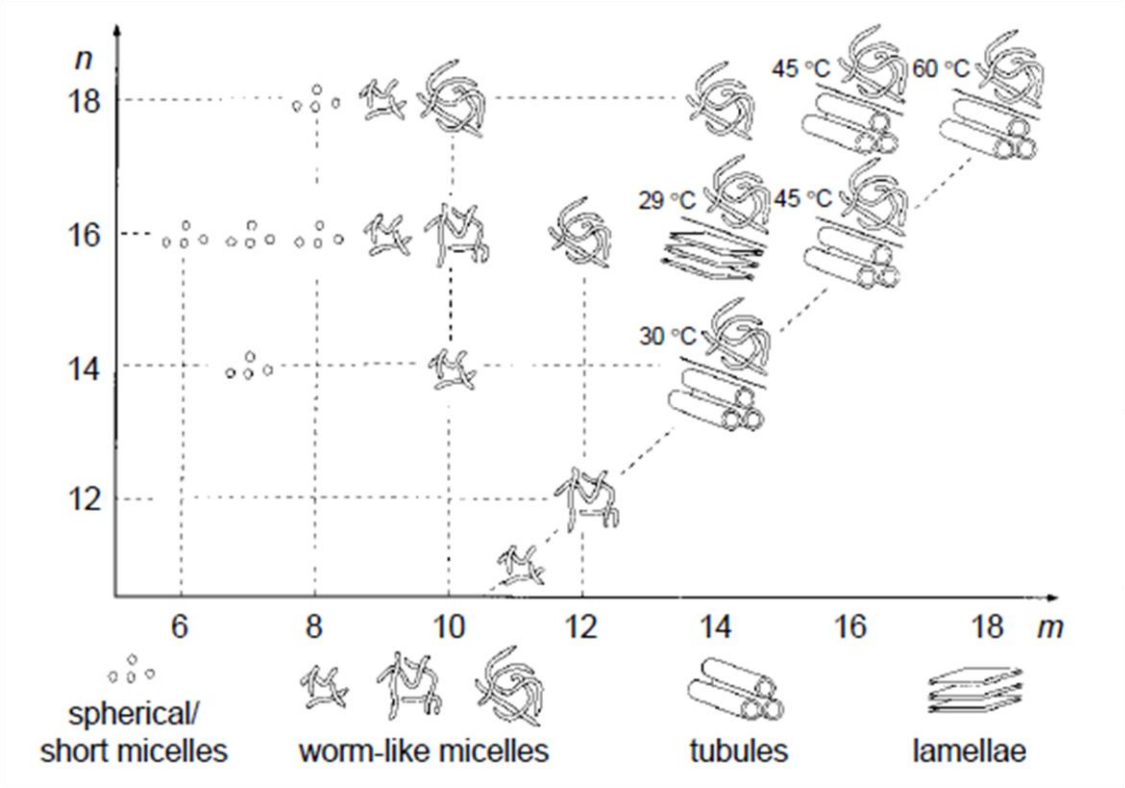

Figure 1.4 Phases observed in aqueous solutions of *n*-2-*m* surfactants as a function of *n* and *m*, at concentrations between 0.1 and 10% w/w (*ca*. 1.6–160 mM). Transition temperatures are indicated whenever a phase transition was observed upon heating (modified from Oda et al. 1997).

1.2.1.2 Structural modulation of gemini surfactants featuring their biological/ pharmacological application

In theory, any two surfactants can be linked by a spacer group. Since the early studies reporting the higher surface activity and lower *cmc* of gemini surfactants as compared to their monomeric counterparts, and their particular micelization behavior (formation of elongated, entangled micelles, rather than spherical micelles), allied to low toxicity (in general lower than that of monomeric surfactants with similar headgroups and hydrocarbon chains), several families of gemini surfactants were developed, aiming at their application in environmental, industrial and pharmacological fields. In fact, gemini surfactants revealed the capacity to act as emulsifiers, antifoaming agents, detergents, dispersants, wetting agents and thickeners (reviewed in Menger & Keiper 2000). Furthermore, some gemini surfactants, especially those containing short spacers (Hoque et al. 2012), have been shown to exhibit high antimicrobial efficiency, namely against pathogenic bacteria (Pérez et al. 1996).

The interest in gemini surfactants regarding their therapeutic use is related with the lower concentration of these surfactants that is expected to be needed to reach the *cmc* as compared to that of their monomeric counterparts. For example, in a gene delivery system, the gemini surfactant capacity to form supramolecular aggregates at low concentrations has a positive impact on cytotoxicity, the gemini surfactant-containing systems being less toxic than those containing the corresponding monomeric surfactants at higher concentrations (Karlsson et al. 2002).

Gemini surfactants were shown to be versatile vectors for nonviral gene delivery (Yang et al. 2010). This stems from the fact that there are many possibilities, through chemical modification of the alkyl tails and the spacer group of these compounds, to modulate their physicochemical behavior towards the enhancement of the efficiency of gene transfer. For example, modification of the length, degree of unsaturation and substitution of different functional groups in the spacer and alkyl chains can provide opportunities to tailor their chemical structure for specific needs (Zana et al. 1991; Zana & Lévy 1997). On the other hand, the variety of supramolecular structures adopted by gemini surfactants, depending on their concentration, which can also change upon meeting different environments in the cell (e.g. provided by membrane structures, pH and redox conditions), endows each gemini surfactant molecule with high structural versatility.

Gemini surfactants derived from sugars (van Doren et al. 2000; Menger & Mbadugha 2001; Bell et al. 2003; Johnsson et al. 2003; Wasungu et al. 2006a; Wasungu et al. 2006b; Klijn et al. 2006; Klijn et al. 2007; Liu et al. 2013), oligocations, such as ornitine and spermine (Dauty et al. 2001; Ronsin et al. 2001), lipids, such as cholesterol (Bajaj et al. 2007; Bajaj et al. 2008a; Kim et al. 2011; Misra et al. 2013) and cardiolipin (Bhattacharya & De 1999; Bajaj et al. 2008b), and aminoacids (McGregor et al. 2001; Brito et al. 2006; Fan et al. 2008; Yang et al. 2010; Luckzynski et al. 2012; Singh et al. 2012; Silva et al. 2012; Silva et al. 2013; Pérez et al. 2014) have been synthesized, characterized in terms of their mesomorphic behavior in solution and evaluated in terms of transfection efficiency. Carbohydrate- and aminoacid-based gemini surfactants represent classes of surfactants with superior properties of biocompatibility and biodegradability, due to their similarity with natural amphiphilic molecules.

The structure, synthesis, physicochemical characteristics (surface adsorption, aggregation and phase behavior) and biological properties (toxicity, antimicrobial activity and biodegradation) of aminoacid-derived gemini surfactants, as well as their potential applications, such as drug and gene delivery, have been recently reviewed by Perez 2014, and a summary of the most important properties and applications are presented in **Table 1.3**.

The structural characteristics of gemini surfactants and their supramolecular assemblies, as related to the several steps of the transfection process, will be addressed in the next sections.

Table 1.3 Physicochemical and biological properties of aminoacid-derived gemini surfactants and their potential applications.

Aminoacid	Physicochemical Properties	Biological Properties	Potential Applications	References
Alanine	The alanine residue was introduced in the alkyl chains, rather than as the headgroup.	Anti-adhesive	Antifungal agent	(Luckzynski et al. 2012)
Aginine	Thermotrpic phase transition from elongated micelles to hexagonal liquid crystal phase (surfactants containing s=3 or 6) or to lamellar phase (surfactant containing s=9)	Cytotoxic for gram negative and gram positive bacteria; hemolytic capacity increasing with the spacer and the alkyl chain lengths.	Antimicrobial agent	(Pérez et al. 1996)
Cystein (Cystine)	Tightly packed at the air/water interface and in supramolecular aggregates	-	Encapsulation and release of hydrophilic drugs	(Fan et al. 2008)
Lysine	Two units of a di- or tri-peptide, linked through their α or ε group to an alkyl chain, forming both the headgroups and the spacer.	Long (C18) alkyl chains and Lys residues linked through their ε group originate surfactants that efficiently mediate transfection in mouse muscle cells; The presence of the aminoacid residues improved DNA delivery and release	Transfection agent; scleroderma, atopic dermatitis and wound healing	(McGregor et al. 2001; Singh et al. 2012)
Serine	Formation of elongated micelles (s=2 or 5) or vesicles (s=12) in aqueous solution above their respective *cac*.	Non-toxic for eukaryotic cells (low cytotoxicity for HeLa cells)	Transfection agent*	(Silva et al. 2012 and 2013)

*This aspect is explored in the present work (Chapters 5 and 6).

Cytotoxicity

As mentioned above, the concentration of gemini surfactants needed for a given application, such as gene delivery, is significantly lower than that of their monomeric counterparts required for the same purpose. This has an obvious impact on cytotoxicity. In addition, at the same concentration, gemini surfactants have been found to be generally less cytotoxic than their monomeric counterparts. In this regard, lipid-, aminoacid- and sugar-based gemini surfactants were found to be more biocompatible and more biodegradable than monomeric surfactants or conventional gemini surfactants (Pérez et al. 2014; Wasungu et al. 2006b; Perez et al. 2002; Kim et al. 2011; Misra et al. 2013). This is mainly due to the existence of linkages in the molecules of these surfactants, which can be cleaved inside the cells, resulting in moieties (lipids, aminoacids or sugars) that are easily metabolized.

However, gemini surfactants incorporated in membranes may disturb their structure and dynamics, causing adverse effects to the cells. The reported influence of alkyl chain length of serine-derived gemini surfactants on cell viability is a clear demonstration of the impact of surfactant membrane insertion on cytotoxicity (Silva et al. 2013). Thus, the increasing hydrophobicity of surfactants containing progressively longer hydrocarbon chains (n=12, 14, and 16 carbon atoms), which should be accompanied by increasing propensity to incorporate into lipid bilayers of cell membranes, and, eventually, increasing disturbance of membrane-mediated physiological processes, should be on the basis of the resulting progressively higher toxicity. However, the surfactant with 18 carbon atoms-long chains induced less cytotoxicity than that with 16 carbon atoms-long chains, probably indicating that this chain length resembles that of the fatty acyl chains of membrane lipids, and therefore is less disturbing to the physical properties of the membrane. Serine-derived surfactants containing alkyl chains with the same length (n=12) and amine, amide or ester linkages to the spacer also showed differences in cytotoxicity, the ester and amide derivatives revealing higher cytotoxicity than the amine derivative. Furthermore, the latter presented a dose/response curve with a steep slope, indicating a potent single effect presumably involving interference with a vital metabolic function. On the contrary, the shape of the sigmoidal dose/response curves of the amide and ester derivatives was interpreted in terms of a low specificity of the toxic effects, probably involving a large spectrum of

variables. Chemical susceptibility of surfactants from the amide and ester families to pH or enzymatic degradation may explain their high cytotoxicity, since the cells would be exposed to monomeric serine-derived surfactants in a concentration twice that of the gemini surfactant (Silva et al. 2013).

DNA complexation

The interactions between cationic surfactants and polyions with opposite charges, such as DNA, leading to the formation of polymer–surfactant aggregates, have been analyzed as a basis for the design of transfection agents or gene delivery systems. The polyelectrolyte chain binds to surfactant molecules through electrostatic attractive interactions, and the hydrophobic moieties of the surfactant molecules stabilize the aggregates due to the hydrophobic effect in aqueous solution (Uhríková et al. 2005). This concept is particularly relevant to drive the search of gemini surfactant-based systems for gene delivery. In fact, the strength of the interactions established between gemini surfactants and DNA may determine the ability of the delivery system to condense and release DNA into the cell.

The structural arrangement displayed by complexes composed of gemini surfactants and DNA depends on the supramolecular aggregates gemini surfactants form on their own, when dispersed in water in the absence of DNA. Based on experiments of atomic force microscopy (AFM), Wang and coworkers (Wang et al. 2007) suggested that the addition of DNA to surfactants in the form of micelles originated compacted globular complexes, with strings of DNA connecting several globules, similarly to the "spaghetti and meatballs" model proposed for cationic liposome-DNA complexes (Sternberg et al. 1994). On the other hand, when gemini surfactants aggregated to form vesicles, DNA molecules distributed around the vesicles, which then rearranged themselves to form an inverted hexagonal lattice containing DNA. The higher transfection efficiency mediated by surfactants that form vesicles as compared to those forming micelles was assigned to the ability of the former to generate H_{II} structures upon DNA complexation (Wang et al. 2007).

The structure of the complexes also showed to depend on the cationic gemini surfactant/DNA charge ratio. In this regard, the titration of gemini surfactants with DNA showed that, at low DNA/surfactant charge ratio (0.2), the micelle-forming

18:1-6-18:1 gemini surfactant gave rise to toroidal isolated complexes, which were converted to cylindrical structures upon further addition of DNA (DNA/surfactant of 0.3-0.4), the DNA in excess acting as a bridge between the isolated complexes. In the case of a surfactant with shorter spacer, 18:1-2-18:1 surfactant, vesicles surrounded by DNA were formed at low (-/+) charge ratio (0.05), and larger "fiber-like" aggregates occurred at high (-/+) charge ratios (0.3-0.4), possibly reflecting a conversion to an inverted hexagonal phase (Wang et al. 2007).

The compaction of DNA by cationic gemini surfactants might involve an initial interaction of a small cluster of surfactant molecules with DNA and the combined effect of electrostatic and hydrophobic interactions should promote the contribution of more surfactant molecules, thus enhancing the compaction. This process results in an enthalpy gain, similarly to self-association, thus being favored by a low *cmc* (Kirby et al. 2003). The low *cmc* values presented by these surfactants was proposed to increase the stability of the surfactant/DNA complexes, due to micelle aggregation that would keep the complexes together during the delivery process, and therefore improve their transfection ability (Badea et al. 2005). The same forces driving the surfactant micellization process are also responsible for their aggregation with the negatively charged nucleic acids. Therefore, it is not surprising that a low *cmc* favors the supramolecular assemblies involving both these types of molecules.

The most efficient DNA compaction was found for gemini surfactants with short spacers (s=2, 3) (Karlsson et al. 2002). Micelles of these surfactants were shown to disassemble in the presence of DNA, which interacts with gemini surfactant monomers, creating disperse micelle-like aggregates of surfactant and DNA (Jiang et al. 2004). In this context, a molecular compaction model was suggested for DNA condensation promoted by an imidazolium-based gemini surfactant (Zhou et al. 2013). The progressive increase of the surfactant/DNA (+/-) charge ratio would result in the conversion of twisted, collapsed DNA molecules into stacked toroidal nanoparticles and, subsequently, into spherical nanoparticles with smaller sizes (**Figure 1.5**) (Zhou et al. 2013).

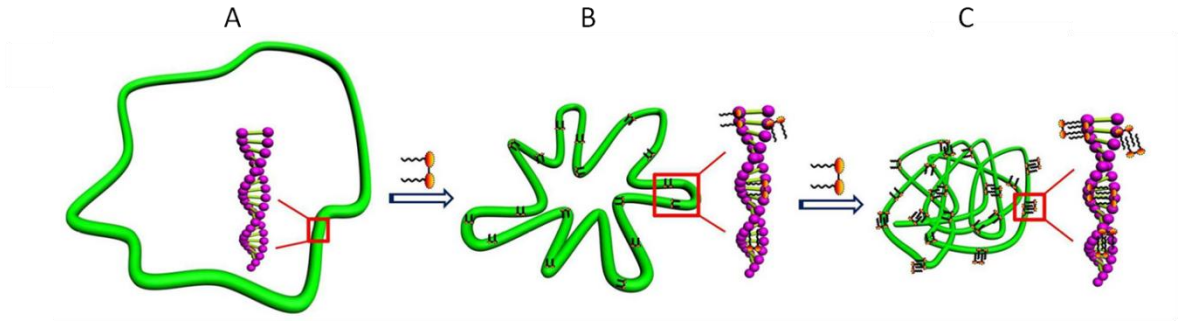

Figure 1.5 Schematic representation of the DNA condensation process with the addition of increasing amounts of imidazolium-derived gemini surfactant [12-4-12im]Br_2, from the free DNA with loose conformation (A), to condensed DNA with toroidal structure (B), and then to condensed DNA with spheroidal structure (C) (modified from Zhou et al. 2013)

Apparently, the ability to mediate gene delivery varies inversely with the spacer length, which correlates with the area occupied by the surfactant headgroup. A short spacer maintains the cationic headgroups at a distance closer to that corresponding to the distance between the phosphate groups of DNA, therefore enhancing the complexation. A distance of 4.9 Å, corresponding to three methylene groups, between gemini surfactant ammonium headgroups showed to be optimal for the interaction with the DNA phosphate groups (Wettig et al. 2007).

Additionally, the length of the alkyl chains and the type of connection between the elements of the gemini surfactants have been shown to influence their ability to complex DNA and, consequently, their transfection efficiency. In this regard, studies performed with gemini surfactants containing two lysines as headgroups, linked together through a disulfide bond, and connected, either through the α-amine group or through the ε-side chain, to alkyl chains of different length, showed that transfection efficiency improved with the increase in length of the surfactant hydrocarbon chains (the maximum complexation and transfection efficiency being achieved with the gemini surfactants containing oleoyl chains), and depended on lysine residue connection. Thus, gemini surfactants in which the lysine residues were linked through their ε-side chains promote higher transfection efficiency than those in which lysine residues were linked through their α-amine group (McGregor et al. 2001).

Cellular internalization

Cells internalize DNA complexes from their surroundings using a variety of mechanisms, including direct membrane translocation, which, while being independent of energy and of the presence of specific proteins, depends on the ability of the components of the delivery system to interact and destabilize membranes with specific composition.

In this regard, DSC and fluorescence polarization studies showed that surfactants with short alkyl chains induce a decrease of the overall order of a DPPC lipid bilayer, whereas surfactants with long alkyl chains (C16 and C18) promote an increase of lipid packing and induce the formation of new and more ordered structures, as assessed by the appearance of a new endothermic peak at temperatures above that corresponding to the gel to fluid phase transition of DPPC (Almeida et al. 2010). An increase in the spacer length was found to decrease the membrane lipid packing, especially in the region closer to the hydrophobic/hydrophilic interface, as assessed by the fluorescence probes 2-AS, 6-AS, 12-As and 16-AP, which report the gradient of lipid order across the bilayer. The presence of a long hydrophobic spacer is expected to interact and disturb the arrangement of a large number of DPPC molecules per surfactant molecule, therefore contributing to a disordering effect of the membrane at the interfacial region. The insertion of surfactant molecules with very long spacers (C10) in the lipid bilayer minimizes this effect since the two tails of this surfactant are likely to be inserted away from each other, thus allowing lipid positioning between the tails of the surfactant molecule, which helps to conceal the long hydrophobic spacer from the water, representing a stable arrangement of the surfactant molecules (Almeida et al. 2010; Almeida et al. 2011).

As an alternative to direct membrane translocation, there is a variety of energy- and protein-dependent endocytic pathways (schematized in **Figure 1.6**) that may ensure the internalization of gene delivery systems. These pathways lead to different intracellular trafficking routes, which include the endolysosomal route in the case of clathrin-mediated endocytosis, and, in some circumstances, may avoid this degradative pathway, such as in the case of caveolae- or raft-mediated endocytosis. In order to achieve efficient gene delivery, complexes internalized by endocytosis have to mediate DNA escape from the endolysosomal pathway and release their cargo in the proximities of their intracellular target to avoid nuclease degradation.

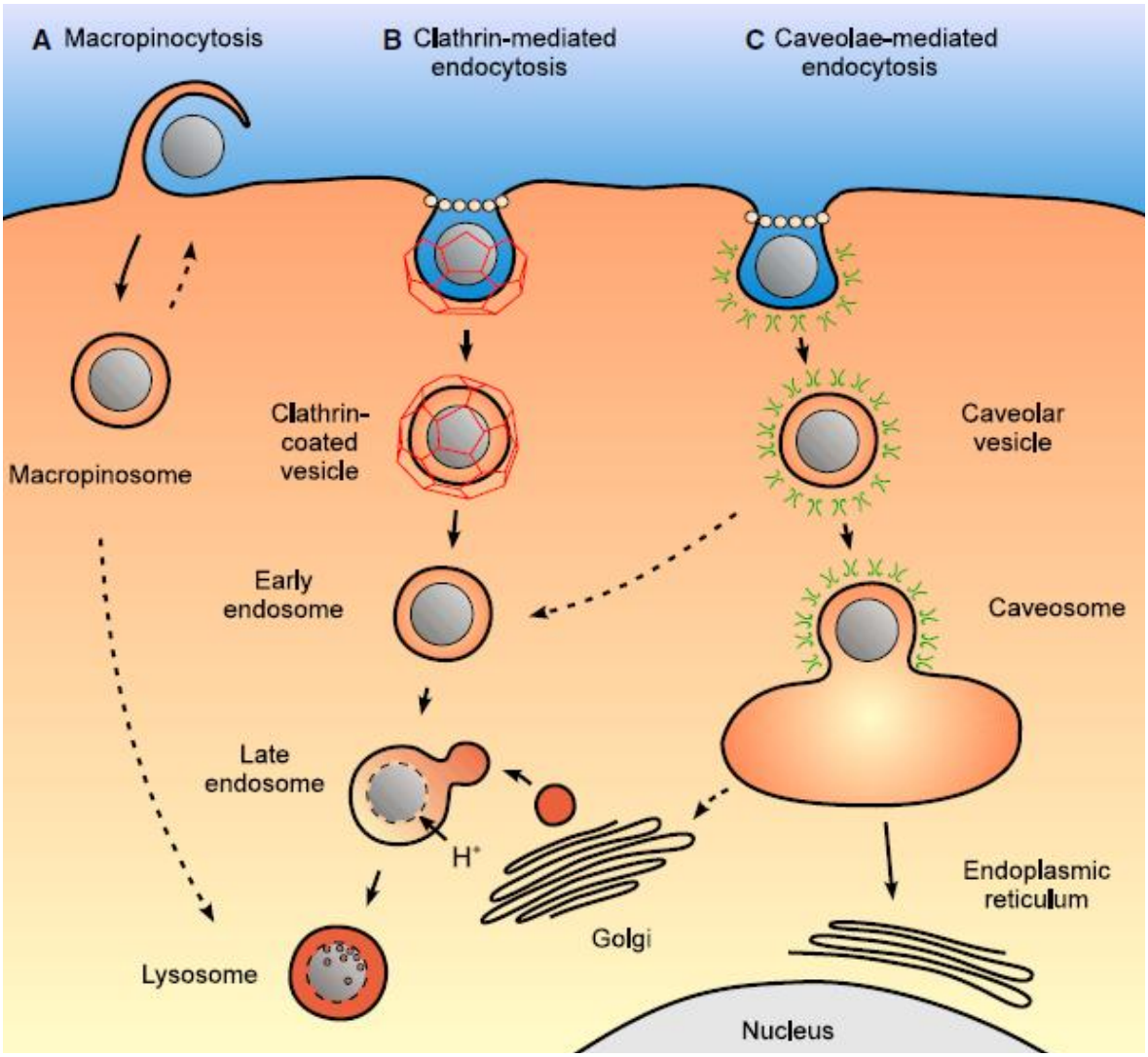

Figure 1.6 Intracellular trafficking following macropinocytosis, clathrin-mediated endocytosis and caveolae-mediated endocytosis. A) Macropinocytosis leads to the formation of a macropinosome, which is thought to eventually fuse with lysosomes or recycle its content to the cell surface. B) Clathrin-mediated endocytosis leads to the formation of an early endosome, which is acidified and fuses with pre-lysosomal vesicles containing enzymes (in red) to give rise to a late endosome and finally a lysosome, where the acidic and hydrolytic enzyme-rich environment leads to nanocarrier and drug degradation. C) Caveolae-mediated endocytosis of a nanocarrier gives rise to a caveolar vesicle, being delivered to caveosomes, which offer a neutral environment, devoid of the acid hydrolases existing in lysosomes, to the endocytosed material (reproduced with permission from Hillaireau & Couvreur, 2009).

Endosomal escape

An important feature that has been explored in several types of molecules used in gene delivery is their ability to undergo conformational changes upon interaction with the endosomal membrane, in order to promote cytoplasmic release of the carried nucleic acids. In this regard, lipids, surfactants, peptides and polymers with sensitivity to temperature, pH or redox environment have been employed in formulations of gene delivery systems.

DNA complexes of the gemini surfactant 1,9-bis(dodecyl)-1,1,9,9-tetramethyl-5-imino-1,9-nonanediammonium dibromide (12-7NH-12) and of its derivative with a glycyl-lysine dipeptide substituted spacer, both prepared with DOPE, constitute a good example to underline the relevance of endosomal escape aiming at efficient transfection. These complexes were shown to be internalized by clathrin-mediated endocytosis. However, the complexes containing the unsubstituted surfactant underwent lysosomal degradation, whereas those containing the aminoacid substitution were able to escape from the endolysosomal route due to their high buffering capacity, inducing an ATPase-driven proton accumulation in endosomes to retain their acidic pH, followed by passive chloride ion influx. The consequent high ionic concentration caused inflow of fluid and, thus, osmotic stress ("proton sponge" effect). On the other hand, the complexes increased in size in response to medium acidification, due to unfolding (relaxation) of the surfactant. These two factors contributed to disrupt the endosome and to loosen the interaction between the DNA and the surfactant, promoting DNA release to the cytosol (Singh et al. 2012).

The dependence of DNA complex supramolecular arrangements on pH has been studied with a formulation based on a sugar-containing gemini surfactant, in which the headgroups consist of pentoses. *In vitro* assays showed that a gradual acidification of the medium to simulate the endosomal lumen led to the appearance of different mesomorphic phases adopted by the complexes, namely lamellar phase, condensed lamellar phase and inverted hexagonal phase (H_{II}), as assessed by SAXS and cryo-TEM. As a result of this morphological change, it was proposed that the complexes would be able to fuse with the endosomal membrane, causing destabilization of this intracellular structure and favoring the release of DNA into the cytoplasm (Bell et al. 2003).

DNA complex sensitivity to the redox environment was assayed in gemini surfactants with decamino and lauramino chains, which exhibited disulfide bonds to bridge two monomeric subunits derived from cysteine, forming cystine-derived gemini surfactants (Fan et al. 2008). Studies of dynamic light scattering and TEM showed that these surfactants aggregated into small vesicles and micelles. However, upon reduction of the disulfide bonds, no supramolecular structures were detected, due to the higher *cmc* of the monomeric components as compared to the gemini surfactants. The supramolecular aggregates reappeared after the oxidation of thiol groups have restored the disulfide bond, indicating a reversible disassembly and rebuilding of aggregates. This behavior suggested the possibility of using these surfactants to encapsulate biologically active molecules. The water soluble dye riboflavin showed to be encapsulated only in oxidative conditions, that is, when a disulfide bond connected the monomeric subunits of the surfactants, allowing the formation of supramolecular aggregates (Fan et al. 2008).

Similarly to transfection mediated by cationic lipids, that mediated by cationic gemini surfactants also showed to be favored by the addition of DOPE, as a helper lipid, to the delivery system (Camilleri et al. 2000). Helper lipids or co-lipids are uncharged lipids that have been used to enhance transfection mediated by cationic vectors, cholesterol and DOPE being the most widely employed. Cholesterol has been used as a helper lipid due to its ability to modify hydrocarbon chain packing, resulting in more stable complexes and, therefore, with potential for large traveling periods in blood circulation (Koynova & Tchenkov 2010). DOPE, characterized by a high propensity to form inverted hexagonal phases, has been suggested to play a role in facilitating the disassembling of lipid-based DNA formulations and DNA escape from the endosmes (Hoekstra et al. 2007 Duzgunes et al. 2007).

As expected, DOPE is not a “universal enhancer” of transfection efficiency, since its action takes place at the endosomal membrane level and, on the one hand, not all complexes are internalized through the endolysosomal route, and, on the other hand, DOPE-induced destabilization of the endosomal membrane depends on the presence of other components in the complex. In fact, the addition of DOPE to DNA complexes containing *bis-quaternary* ammonium surfactants with short (C2 and C3) and intermediate (C6) spacers and long tails (C18:0 and C18:1) did not enhance their

ability to mediate transfection, probably because these complexes were not internalized by endocytic mechanisms (Rosenzweig et al. 2001).
On the other hand, phase transitions from lamellar to normal hexagonal structures (H_I) have also been found to occur in complexes able to efficiently mediate transfection, such as those containing pH-sensitive sugar-based gemini surfactants (Wasungu et al. 2006b), which underwent a bilayer-to-H_I phase transition at mildly acidic pH (Wasungu et al. 2006a).

Nucleic acid release
Nucleic acid release depends on the lability of the interaction between the carrier molecules and the polynucleotide chains. Only an efficient nucleic acid release in an appropriate intracellular location will originate high levels of transfection. Complexes containing gemini surfactants modified from the 12-7H-12 parent molecule, by introducing an aminoacid (glycine or lysine) or a dipeptide (glycyl-lysine or lysine-lysine) in the spacer, presented increased flexibility and lability, conferred by van der Waals and hydrogen bonding interactions (Yang et al. 2010). These complexes were shown to be endocytosed without significant destabilization upon interaction with the plasma membrane. Furthermore, the substituted gemini surfactants protected DNA from degradation inside the endosomes during the time necessary to occur endosomal membrane destabilization. In contrast, complexes containing the unsubstituted gemini surfactant were promptly destabilized upon interaction with the cytoplasmic membrane, leading to a premature release of the DNA into the cytoplasm or inside the caveosome, and consequent degradation (Singh et al. 2012).

1.2.1.3 Summary
Gemini surfactants emerged as new molecules presenting characteristics that allow to obtaining supramolecular assemblies and DNA compaction at very low concentration. In a toxicological context, this has a great impact on pharmacological applications, due to the possibility of minimizing cell, organism and environmental toxicity. On the other hand, gemini surfactants offer the possibility for structure modulation, allowing the introduction of biocompatible and biodegradable elements that would further decrease the toxicity, or improve the clearance rate from the organism.

In the perspective of gene delivery, gemini surfactant structure modulation may regulate surfactant affinity towards DNA, reflected in complexation efficiency and DNA protection, thus allowing a fine tuning of the nucleic acid release. The intracellular release of the cargo may be tuned, among other ways, by the introduction of labile linkages between specific groups of the gemini surfactant molecules. The mechanisms by which gemini surfactant-based complexes are taken up by cells, and, consequently, their intracellular traffic and fate, can also be modulated by the use of surfactants with different structural features. Surfactant ability to interact selectively with certain membrane regions (e.g. raft and non-raft regions), due to structural peculiarities of their own molecules or of the aggregates they form, may determine the mechanisms by which surfactant-based complexes transpose the plasma membrane, and hence the pathway of their cellular internalization. In summary, a gene therapy-addressed manipulation of gemini surfactant structure is now taking the first steps towards the development of new, more efficient and less toxic systems for gene delivery.

1.2.2 CELL-PENETRATING PEPTIDES

Cell-penetrating peptides (CPPs) present a variety of amino acid sequences, usually enriched in basic residues and with the ability to be arranged in amphipathic secondary structures, such as α-helixes and β-sheets, which contribute to their cell-penetrating properties. The ability to enter into the cells and to carry molecules across the cytoplasmic membrane makes CPPs interesting vehicles for drug delivery. In this context, considerable effort has been expended in developing new and more efficient CPPs to deliver bioactive molecules with low capacity to permeate membranes, such as nucleic acids.

Two strategies have been used in CPP-mediated nucleic acid delivery. CPPs were covalently conjugated with their cargo, mostly consisting of DNA mimic molecules or steric block oligonucleotides, such as peptide nucleic acids (PNA) (Koppelhus et al. 2002) and phosphorodiamidated morpholino-oligomer (PMO) (Abes et al. 2006a). Although the covalent approach is advantageous for delivering uncharged molecules, such as nucleic acid analogs, its use for the delivery of plasmid DNA or oligonucleotides (ONs) has proved to be more challenging, involving high costs and technical difficulties. Furthermore, although the size and stoichiometry of the CPP conjugates are relatively constant and predictable, their efficiency in releasing the cargo and the activity of carried molecules are sometimes hardly anticipated (Meade & Dowdy 2008). In contrast, the non-covalent approach is simpler and has been shown to originate complexes with net positive charge that provide nucleic acids with protection against nuclease-mediated degradation, favoring the release of the nucleic acids once inside the cell (Heitz et al. 2009; Morris et al. 1997). Thus, most studies regarding CPP use as nucleic acid delivery systems report the formation of non-covalent complexes based on electrostatic interactions between the cationic CPPs and the negatively charged nucleic acids. Peptides that can form non-convalent complexes are usually short amphipathic peptides consisting of two domains, one hydrophilic (polar) and the other hydrophobic (non-polar).

1.2.2.1 Structure versatility of CPPs

The high structural versatility of CPPs is an attractive property of this kind of vectors. The diversity of amino acid side chains, which includes charged and non-charged, polar and hydrophobic groups, allows the design of a variety of peptide sequences resulting in different secondary structures, thus influencing the final molecule conformation and the mode by which it interacts with other biomolecules and with supramolecular structures, such as biological membranes. Furthermore, the conjugation of CPPs with other small molecules, namely fatty acids, nucleic acid derivatives, and phosphoryl groups, confers different biological properties to the original peptide. Modifications have been introduced in the first generation CPPs in order to favor their complexation with nucleic acids and improve their biological activity, by promoting their interaction with the cell membrane, their internalization and their targeting to specific cell organelles. On the other hand, since most CPPs, particularly when associated with a cargo, are internalized through endocytosis, and this pathway has the potential of entrapping CPP complexes in endosomes, leading to lysosomal degradation of the cargo, chemical and structural modifications of classical CPPs have also been performed in order to provide CPPs with endosomolytic properties, favoring nucleic acid endosomal escape. With this purpose, several strategies have been developed, such as the addition of histidine residues. A typical example of the contribution of this modification to increase transfection efficiency is given by Tat peptide. The covalent fusion of histidine residues to Tat peptide, either at the N- or the C-terminal, originated CPPs with different transfection efficiencies, the most promising being that with 10 histidine residues attached to Tat peptide (Tat-10His), which mediated gene delivery 7,000-fold more efficiently than the original Tat peptide. The increase in transfection efficiency was explained as being a consequence of the "proton sponge" effect, which would be promoted by the imidazole groups of histidine residues, leading to enhanced endosomal release of nucleic acids. On the other hand, it was observed that the incorporation of 2 cystein residues into the Tat – derived peptide 5His-Tat-5His, producing Cys-5His-Tat-5His-Cys, resulted in an even higher efficacy in transfection, which was attributed to the increased stabilization of the peptide/DNA complexes, possibly due to the formation of disulfide bonds between cystein residues (Lo & Wang 2008).

Penetratin, used as a carrier for siRNA, resulting in efficient cellular uptake and knockdown, both *in vitro* and *in vivo* (Cheng et al. 2011), has been also modified, giving rise to a new peptide designated EB1, by replacing two basic amino acids with histidines and adding 6 amino acids (LIRLWS) to its N-terminal. The improved gene silencing ability of this peptide with respect to penetratin was attributed to the endosomolytic properties, provided by the histidine residues (Lundberg et al. 2007). This new peptide was further modified, by addition of a single C-terminal cysteine (Cys) to improve the ability of EB-1 to deliver plasmid DNA. Consequently, a peptide dimmer was formed, through a disulfide bond, its affinity to DNA being enhanced as compared to that of the monomers. Furthermore, when the covalent bond was reduced in the cytoplasm of the cell, the cargo was efficiently released and reached its target, resulting in pDNA expression in 50% of the cells (Åmand et al. 2012).

CPPs derived from the dermaseptin peptide are also an example of peptides whose structure has been modulated through the introduction of different modifications in the original peptide, and whose biophysical properties and biological activity as gene carriers have been extensively studied in order to establish structure-activity relationships. In this regard, the CPP S4(13), constituted by the first 13 aminoacids of the dermaseptin S4 peptide, was modified by the covalent attachment of the nuclear localization sequence (NLS) of the SV40 large T-antigen (PV) to its N-terminal, which enhanced the ability of this peptide (PV-S4(13)) to accumulate in the nucleus in an ATP-dependent manner. In contrast, the PV-S4(13) analogue containing the NLS in a reverse order (rPV-S4(13)), although presenting the same cell permeating ability as PV-S4(13) and S4(13), did not show karyophilic character. These findings propelled the study of S4(13) and its derivatives as carriers of nucleic acids to different intracellular compartments of cultured cells.

Another variation of S4(13) peptide was produced by introducing the NLS of the SV40 large T-antigen to its C-terminal (S4(13)-PV). S4(13)-PV peptide electrostatically associated to plasmid DNA showed to efficiently mediate transfection, particularly at high peptide/DNA charge ratios (5/1 and higher) (Trabulo et al. 2008). Importantly, complexes prepared with a scrambled analogue, obtained by randomization of the original sequence of amino acids, mediated transfection with significantly lower efficiency than those prepared with S4(13)-PV or S4(13)-PVr peptides, which

demonstrates the importance of the amino acid sequence of CPPs derived from the dermaseptin S4 peptide (amino acids 1–13) to the transfection process.

In comparison with other well-known CPPs, such as Tat, dermaseptin-derived peptides have the advantage of lacking intracellular functions, being hence less prone to interfere with normal metabolic pathways (Hariton-Gazal et al. 2002). **Table 1.4** presents the sequences of S4(13) and its derived synthetic peptides, as well as the corresponding modifications introduced in order to potentiate their performance.

Table 1.4 S4(13) and related peptides, amino acid sequence and type of modification introduced.

Peptide	Amino acid Sequence	Type of modification	References
S4(13)	^{1}ALWKTLLKKVLKA^{13}	Peptide fragment with residues 1-13 of Dermaseptin S4	(Hariton-Gazal et al. 2002)
PV-S4(13)	PKKKRKV^{1}ALWKTLLKKVLKA^{13}	N-terminal addition of NLS derived from SV40 large T-antigen (PV) to enhance nuclear import of the peptide	(Hariton-Gazal et al. 2002)
rPV-S4(13)	VKRKKKP^{1}ALWKTLLKKVLKA^{13}	N-terminal addition of PV in reverse order to study the role of the PV amino acid sequence in the nuclear import of the peptide	(Hariton-Gazal et al. 2002)
S4(13)-PV	^{1}ALWKTLLKKVLKA^{13}PKKKRKVC	C-terminal addition of PV to enhance nuclear import of the peptide	(Mano et al. 2006)
S4(13)-PVr	^{1}ALWKTLLKKVLKA^{13}VKRKKKPC	C-terminal addition of PV in reverse order to elucidate how NLS sequence influences the cellular uptake of S4(13)-PV peptide.	(Mano et al. 2006)
scrambled	^{1}KTLKVAKWLKKAKPLRKLVKC^{21}	Random amino acid sequence derived from S4(13)-PV peptide to elucidate how peptide primary structure influences the cellular uptake of S4(13)-PV peptide.	(Mano et al. 2006)
H_5-S4(13)-PV	HHHHH^{1}ALWKTLLKKVLKA^{13}PKKKRKVC	Addition of a five histidine tail to the N-terminal of the S4(13)-PV to facilitate endosomal release*	(Cardoso et al. 2013)

* This aspect is explored in the present work (Chapter 8).

1.2.2.2 Structural properties of CPPs and their impact on CPP-cell interactions and cellular uptake

Interaction of CPPs with the cell surface constitutes a key step for their internalization and, consequently, for their success in nucleic acid delivery. Electrostatic interactions with the extracellular matrix revealed to be a prerequisite for the uptake of the majority of cationic peptides, including Tat and Tat fusion proteins and polyarginines

(Tyagi et al. 2001). The involvement of proteoglycans (PG) and glycosaminoglycans (GAG) in S4(13)-PV cell internalization was also demonstrated (Mano et al. 2005). In this case, a strong inhibition of peptide internalization was observed in the presence of low heparin concentrations and, in genetically modified cells deficient in PG, it was observed that these membrane components potentiated peptide internalization, although their presence at the cell surface was not absolutely required. In addition, at high peptide concentrations (1 μM), dynamin, which is involved in clathrin- and caveolae-mediated endocytosis and phagocytosis, showed not to be essential for peptide uptake, whereas at low peptide concentrations (0.2 and 0.4 μM) chlorpromazine, a specific inhibitor of clathrin-mediated endocytosis, reduced peptide uptake. Therefore, two distinct mechanisms were proposed for the cellular uptake of S4(13)-PV peptide, whose dominance depended on peptide concentration, namely a GAG- and endocytosis-dependent mechanism at low peptide concentration, and a GAG- and endocytosis-independent mechanism at high peptide concentration (Mano et al. 2005).

Similarly to S4(13)-PV, MPG was shown to enter cells even in the absence of GAG, although at a lower rate than in their presence. Electrostatic interactions between MPG and GAG showed to induce significant GAG clustering. The similar propensity of MPG, which exhibits a β-sheet structure, and MPGα, a MPG derivative that forms an α-helix, to interact with GAG and induce GAG clustering suggested that the type of secondary structure is not relevant for the initial interactions between the peptide and the extracellular matrix (Gerbal-Chaloin et al. 2007).

An ultrastructural approach to peptide-membrane interactions and cellular uptake was performed with the S4(13)-PV peptide and its derivatives with a reverse NLS and a scrambled sequence, using transmission electron microscopy (TEM). The S4(13)-PV and S4(13)-PVr peptides showed to form nanoparticle-like regular spherical structures (sizes ranging 80 to 100 nm for S4(13)-PV and 140 nm for the reverse NLS peptide) at the surface of the cells, before transposing the cell membrane. On the other hand, the scrambled peptide formed larger irregular aggregates and permeated the cells less efficiently than the other two peptides, suggesting that the peptide primary structure impacts on CPP-cell surface interactions, with repercussion on their internalization. The generation of nanometer-sized particles has also been shown with other peptides, such as Pep-1 (Muñoz-Morris et al. 2007), MPG and CADY (Crombez et al. 2008). Nanoparticles of S4(13)-PV peptide generated upon interaction with cell

membranes were not found in the absence of cells, that is S4(13)-PV did not form nanoparticles when added to a culture medium containing or not serum, or in the presence of anionic GAGs, like heparin, chondroitin sulfate and hyaluronan. Therefore, the clustering of S4(13)-PV peptides seems to depend on a specific environment or on the direct interaction of the peptide with the cell surface (Padari et al. 2010).

Moreover, electron microscopy studies showed that the association of S4(13)-PV and S4(13)-PVr particles to the plasma membrane of HeLa cells promoted membrane fading, denoting an interference with the packing of bilayer lipids, which is consistent with results demonstrating that S4(13)-PV becomes buried in the lipid bilayer upon interaction with negatively charged vesicles. In contrast, scrambled peptide cellular association did not perturb plasma membrane integrity, even at high concentrations. It was proposed that both the modulation of the plasma membrane properties and the different particle assemblies might be responsible for the differences observed in the efficiency of uptake of the S4(13)-PV, reverse NLS and scrambled peptides (Padari et al. 2010).

Nanocarrier interactions with membrane lipids have shown to constitute a key element for the success of nucleic acid delivery. In this context, the study of CPP–lipid interactions using membrane models has revealed to be of crucial importance for unraveling how CPPs affect the physical properties of the lipid bilayer, and how membrane physical alterations determine the competence of CPPs to translocate the cell membrane and to deliver its cargo into the cell.

It was shown that penetratin affected the temperature, enthalpy and cooperativity of the main phase transition of the anionic lipid DMPG, while RL16 produced a strong perturbation in the lipid chain packing of bilayers composed of the zwitterionic lipid DMPC. Penetratin is unstructured in solution and also in the presence of zwitterionic lipid membranes and adopts an α-helix secondary structure upon interaction with anionic membranes. The electrostatic interactions between the cationic residues of penetratin and the negatively charged headgroups of the lipids trigger peptide structural changes, which create hydrophobic patches in the peptide allowing its partial insertion into the lipid acyl chain region. Translocation of penetratin appears to involve the formation of nonlamellar lipid structures, such as inverted micelles. On the other hand, RL16 presents an α-helix secondary structure both in solution and in the presence of lipid membranes. Upon interaction with zwitterionic membranes, RL16 inserts deeply in the lipid fatty acyl chain region, decreasing lipid order. However, in

DMPG bilayers, RL16 does not insert into the acyl chain region but rather remains anchored at the headgroup region where it establishes electrostatic interactions. In these membranes, RL16 molecules seem to act according to a detergent-like carpet mechanism, assembling at the bilayer surface and disintegrating the membrane in a detergent-like manner above a threshold peptide concentration. Although being both highly cationic, penetratin and RL16 differ in their amphipaticity. The interactions of these CPPs with anionic membranes are guided by the spatial charge distribution in the peptide sequence, involving hydrophobic interactions between the peptide sequence and the lipid bilayer core, and electrostatic interactions between the peptide charged residues and the lipid headgroups. The balance between those types of interactions determines whether CPP inserts into the lipid bilayer or lays on the membrane surface, hence influencing the internalization process (Alves et al. 2008). **Figure 1.7** schematizes the models of peptide-membrane interactions proposed for cationic peptides which adopt α-helix secondary structure, either amphipatic or non-amphipatic.

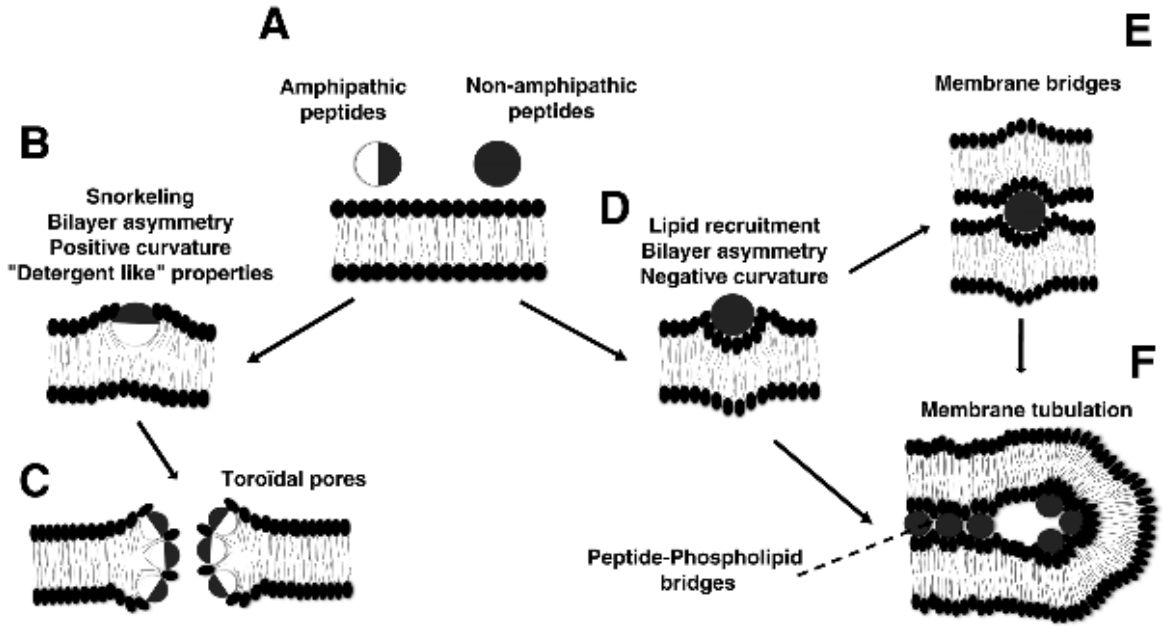

Figure 1.7 Model for peptide-membrane interactions. A) Peptide amphipathicity and net positive charge guide the perturbations induced by the peptides on membrane physical properties. Peptide surface regions are represented in dark when enriched in charged residues, and in white when hydrophobic residues predominate. B) Amphipathic peptide-membrane interaction results in positive membrane curvature; C) Detergent-like activity induces the formation of toroidal pores; D) Positively charged peptide-membrane interaction induces a negative curvature in the membrane outer monolayer. E) Membrane bridging and vesicle aggregation; F) Membrane tubulation results from curvature-induced invaginations (from Lamazière et al. 2007, no permission required).

Although a negative surface charge is common for most eukaryotic cells, due to the presence of proteoglycans, the membrane lipid composition varies with the type of cell, its differentiation and health or disease conditions. Therefore, the interactions of cell-penetrating peptides with lipids containing acyl chains with different length or different degree of unsaturation should also be taken into consideration. In fact, RL16 showed to interact preferentially with lipids containing short (DMPC) rather than long (DSPC) alkyl chains, and with saturated (DMPC) rather than unsaturated (POPC) lipids. Thus, the thickness and packing of the lipid bilayer can influence the specific membrane domains with which the peptide interacts and the extent of this interaction (Joanne et al. 2009).

In an attempt to better understand the molecular mechanism responsible for the translocation of the S4(13)-PV peptide across biological membranes, a detailed characterization of the interaction of this peptide with model membranes was performed using a biophysical approach (Mano et al. 2006). Thus, fluorescence studies based on the intrinsic fluorescence of S4(13)-PV (resulting from a single Try residue located at the N-terminus) showed the occurrence of a shift of the maximum emission wavelength to shorter wavelength values (blue-shift), in the presence of anionic membranes, suggesting a deep insertion of the peptide into those membranes. Interestingly, the magnitude of the blue shift, reflecting the incorporation of S4(13)-PV into the hydrophobic core of the membrane, was significantly higher than that reported for penetratin, transportan and Pep-1. Furthermore, circular dichroism studies showed that the helical content of S4(13)-PV increased with the negative charge density of the lipid bilayers and with the lipid/peptide ratio, a behavior that was also observed with penetratin and RL16 (Mano et al. 2006). On the other hand, the ability of S4(13)-PV and S4(13)-PVr peptides to be partially arranged in an amphipathic α-helix upon peptide-membrane interaction was not shared by the scrambled peptide. The formation of this secondary structure might be related with the capacity of S4(13)-PV and S4(13)-PVr peptides to insert into the lipid bilayer and translocate across biological membranes, which was not exhibited by the scrambled peptide. Furthermore, scrambled peptide cellular internalization through endocytosis was evidenced by the punctuated cytoplasmic pattern observed by confocal microscopy. On the contrary, the S4(13)-PV and S4(13)-PVr peptides exhibited mainly

a diffuse subcellular localization, suggesting an endocytosis-independent translocation process, also observed for penetratin and nonarginine (R9) (Lamazière et al. 2007), which might be initiated by the binding of the peptide to the membrane as a consequence of the electrostatic interactions established between the peptide and the charged cell surface PG (Mano et al. 2006; Mano et al. 2007). These data suggest that membrane-induced conformational changes strongly influence the mechanism by which the cellular uptake of the peptides occurs. The transient membrane destabilization induced by the amphipathic α-helix formed by S4(13)-PV peptide upon interaction with the membrane would result in its translocation to the intracellular milieu. In this regard, the sequence, length and conformation of the CPP were reported to play a more important role in peptide membrane penetration than the accumulation of positive charges (Mueller et al. 2008).

Table 1.5 summarizes the peptides used for cargo delivery reported in this section and their sequences, with emphasis on the structural modifications introduced to second generation peptides.

Table 1.5 Cell-penetrating peptides commonly used for cargo delivery.

Peptide	Sequence	Modification	Reference
Tat(49-57)	^{49}RKKRRQRRR^{57}	Peptide with residues 49-57 of HIV-1 TAT	(Wender et al. 2000)
R9	^{1}RRRRRRRRR^{9}	-	(Mitchell et al. 2000; Wender et al. 2000)
MPG	^{1}GALFLGFLGAAGSTMGAWSQPKKKRKV^{27}-cysteamide	Peptide containing NLS of SV40 large T-antigen	(Deshayes et al. 2004)
MPGα	^{1}GALFL**A**FL**A**AA**L**S**L**MG**L**WSQPKKKRKV^{27}-cysteamide	Substitution of Gly^{6}and Gly^{9} by alanines and Gly^{12}, Thr^{14} and Ala^{17} by leucines to increase peptide helical content	(Deshayes et al. 2004)
Penetratin (Pen)	^{43}RQIKIWFQNRRMKWKK^{58}	Peptide fragment with residues 43-58 of AntpHD	(Derossi et al. 1994)
Transportan (TP)	^{1}GWTLNSAGYLLG**K**INLKALAALAKKIL^{27}	Substitution of Pro^{13}→ Lys in Galparan to allow the attachment of cargo molecules to the Lys residue	(Pooga et al. 1998)
Pep-1	^{1}KETWWETWWTEWSQPKKKRKV^{21}-cysteamide	Substitution of the HIV-1 gp41-derived hydrophobic domain by a hydrophobic tryptophan-rich motif to improve the delivery of peptides and proteins	(Morris et al. 2001)
EB1	LIRLWS^{43}**HL**I**H**IWFQNRR**L**KWKK^{58}K	Substitution of Arg^{43}→ His; Gln^{44}→Leu; Lys^{46}→ His; Met^{54}→Leu and addition of 6 amino acids to the N-terminal and a Lys residue to the C-terminal of penetratin to enable peptide penetration into the endosomal membrane	(Lundberg et al. 2007)

Table 1.5 (cont.) Cell-penetrating peptides commonly used for cargo delivery.

EB1-Cys	LIRLWS^{43}HLIHIWFQNRRLKWKKK^{58}C	Addition of C-terminal cysteine to EB1to allow peptide dimerization by disulfide bond formation in order to enhance peptide/nucleic acid complex stability and intracellular cargo release	(Åmand et al. 2012)
RL16	^{1}RRLRRLLRRLLRRLRR^{16}	-	(Alves et al. 2008)
S4(13)	^{1}ALWKTLLKKVLKA^{13}	Peptide fragment with residues 1-13 of Dermaseptin S4	(Hariton-Gazal et al. 2002)

1.2.2.3 Summary

The interest in using CPPs to improve non-invasive cellular delivery of therapeutic macromolecules, including nucleic acids, resulted from the recognition of their remarkable ability to transpose cell membranes. Multiple factors may affect the efficiency of CPP internalization, including structural features of the CPP and its associated cargo, the target cell type and specificities of CPP-membrane lipid interactions. However, other obstacles besides transposition of cellular membranes hamper to a successful cargo delivery. Changes in the peptide amino acid sequence, fusion of additional sequences with different properties and/or association with lipophilic moieties have been performed to optimize CPP ability to deliver biologically active molecules. Most commonly, such modifications are intended to contribute to the stabilization of CPP/nucleic acid complex, the improvement of CPP cellular association and/or uptake, and the release of cargo entrapped in endosomes, ultimately to favor cargo accumulation in the target cellular compartment (nucleus, mitochondria or cytoplasm).

1.2.3 POLYMERS

Polymers are large molecules consisting of small chemical repeating units (monomers) covalently linked together. The capacity of synthetic cationic polymers to interact with nucleic acids through electrostatic interactions, forming complexes (polyplexes) that exhibit enhanced bonding to the cell surface and efficient internalization into endosomal vesicles has been explored for gene delivery applications. Several strategies have been used to improve the various steps of transfection mediated by polyplexes, from cellular internalization to the nuclear import. Cell internalization of polymer-based gene delivery systems was enhanced through the use of ligands that promote the cellular uptake, such as endogenous ligands (e.g. transferrin, folate), carbohydrates, antibodies and cell-penetrating peptides (e.g. Tat, penetratin). In order to favor nucleic acid escape from endosomes, several strategies were adopted to reinforce the "proton sponge" effect, characteristic of polymers containing a large number of protonable amine groups, such as polyethylenimine (PEI) (Won et al. 2009). These include the addition of a pH-sensitive peptide (which undergoes a conformational change from a random coil to α-helix at low pH) to the polymer formulation, and the use of pH-sensitive polymers, designed to have the same functional groups that are presumably responsible for the membrane-disrupting properties of pH-sensitive peptides (carboxyl groups which are protonated at acidic pH and alkyl groups that interact with the endosomal membrane to collectively enhance cargo escape from endosomes) (Wong et al. 2007). Another aspect that must be taken into consideration is the internal cell structure provided by the cytoskeleton, which gives rise to a viscous environment that counteracts the diffusion of large molecules such as naked DNA and large polyplexes. In order to obviate this obstacle to polymer-mediated transport of nucleic acid towards the nucleus, natural endogenous cytosolic factors, such as NLS and carbohydrates to bind to intracellular carbohydrate-binding receptors that mediate intracellular trafficking, have been used (Wong et al. 2007). To favor nucleic acid dissociation from the delivery system, disulfide bonds, which can be reduced by glutathione in the intracellular medium, and hydrolytically-sensitive ester bonds, which can act as labile crosslinkers for highly branched structures, have been incorporated into the polymers. In addition, thermoresponsive polymers, able to undergo temperature-dependent structural rearrangements with

repercussion on polyplex behavior in terms of nucleic acid condensation and release, have also been extensively explored for gene delivery (Wong et al. 2007). In the next section special attention will be drawn to this type of polymers since they were object of our studies in Chapter 9.

1.2.3.1 Temperature-responsive polymers

Some polymers have been designed to respond to exterior stimuli, such as temperature, pH, redox potential, light, ionic strength, electric and magnetic fields or the presence of enzymes or specific ligands (Alexander 2006). Thermoresponsive polymers, which undergo conformational changes as a response to small temperature variations, have been used in gene delivery, due to the possibility they offer to regulate the degree of DNA condensation in response to small temperature variations and, thus, to modulate the rate and site of cargo release (Alexander 2006). Thermoresponsive polymers also constitute a selective means of drug transport to tumor tissues, where the release can occur spontaneously due to tumor hyperthermic environment or be forced through the application of localized heating. This class of polymers undergoes a reversible coil-to-globule phase transition in response to temperature (**Figure 1.8A**). The transition temperature, above which the globule phase exists, is designated "lower critical solution temperature (LCST)" or "cloud point". This transition, which is accompanied by a sharp change in the polymer hydration state, is entropically driven. When a polymer is placed in water, the enthalpy favors dissolution/solvation due to the formation of a large number of hydrogen bonds between the solvent and the solute. However, the resulting organization of water molecules around the solute results in a loss of entropy. At low temperatures, the enthalpic contribution dominates resulting in dissolution. As the temperature increases, the hydrogen bonds weaken, resulting in a reduced enthalpic contribution and an increasing unfavorable entropic contribution. Once the temperature is raised above the LCST, the entropic contribution dominates and phase separation is favored over dissolution. Since the thermoresponsive behavior depends on the solvent interaction with the polymer and the hydrophilic/hydrophobic balance within the polymer molecule, it is not surprising that additives to the polymer/solvent system, besides polymer concentration and molecular weight, can influence the temperature at which the phase transition occurs. Such additives include salts, surfactants and co-solvents (Schmaljohann 2006).

The polymer poly(N-isopropylacrilamide), known as PNIPAAM, is one of the most widely studied thermoresponsive polymers, which exhibits a phase transition in water at 32 °C (LCST). However, this critical temperature can be increased or decreased by copolymerization with hydrophilic or hydrophobic monomers, respectively (Schild 1992; Talelli & Hennink 2011). Polymers of PNIPAAM are able to carry different molecules, such as drugs or nucleic acids.

Copolymerization of PNIPAAM with hydrophobic or hydrophilic blocks can originate micelles, with PNIPAAM located in the micellar shell or core, respectively (**Figure 1.8B** and **C**). At temperatures below the LCST, copolymers of PNIPAAM with hydrophobic blocks form micelles with a hydrated PNIPAAM shell. When heated above the LCST, micelles destabilize and aggregate due to the collapse of the micellar shell. These micelles when loaded with a drug should release it as a consequence of the phase transition. Since this phase transition occurs at a temperature below the body temperature (LCST<37 °C), PNIPAAM is not useful for *in vivo* applications, the micelles with a PNIPAAM shell being expected to aggregate upon injection. However, PNIPAAM copolymerized with hydrophilic monomers originated polymers with an LCST above 37 °C (Talelli & Hennink 2011).

Three PEI-PNIPAAM grafted co-polymers, varying in the PNIPAAM molecular weight and grafting density, were compared in terms of their thermoresponsive behavior. A temperature increase resulted in the collapse of the copolymers containing the highest PEI/PNIPAAM molar ratio, regardless of the length of the PNIPAAM grafts. The hydrophobicity of PNIPAAM grafts, resulting either from long chains or from large number of grafts, contributes to this phenomenon. PNIPAAM grafts can be envisaged as being oriented around the PEI domains below the LCST and collapsing upon heating to temperatures above the LCST. This model predicts larger hydrophobic domains above LCST and stronger association forces for the polymer with the highest grafting density. Alternatively, the copolymers in solution can be arranged with the PNIPAAM domains residing inside the structure, even below LCST, since their chains are more hydrophobic than PEI. In this case, the collapse of PNIPAAM domains above LCST would lead to large changes in apparent volume, especially for copolymers containing more PNIPAAM grafts. Most likely, large hydrophobic surface regions lead to a reduced colloidal stability (Griffiths et al. 2008).

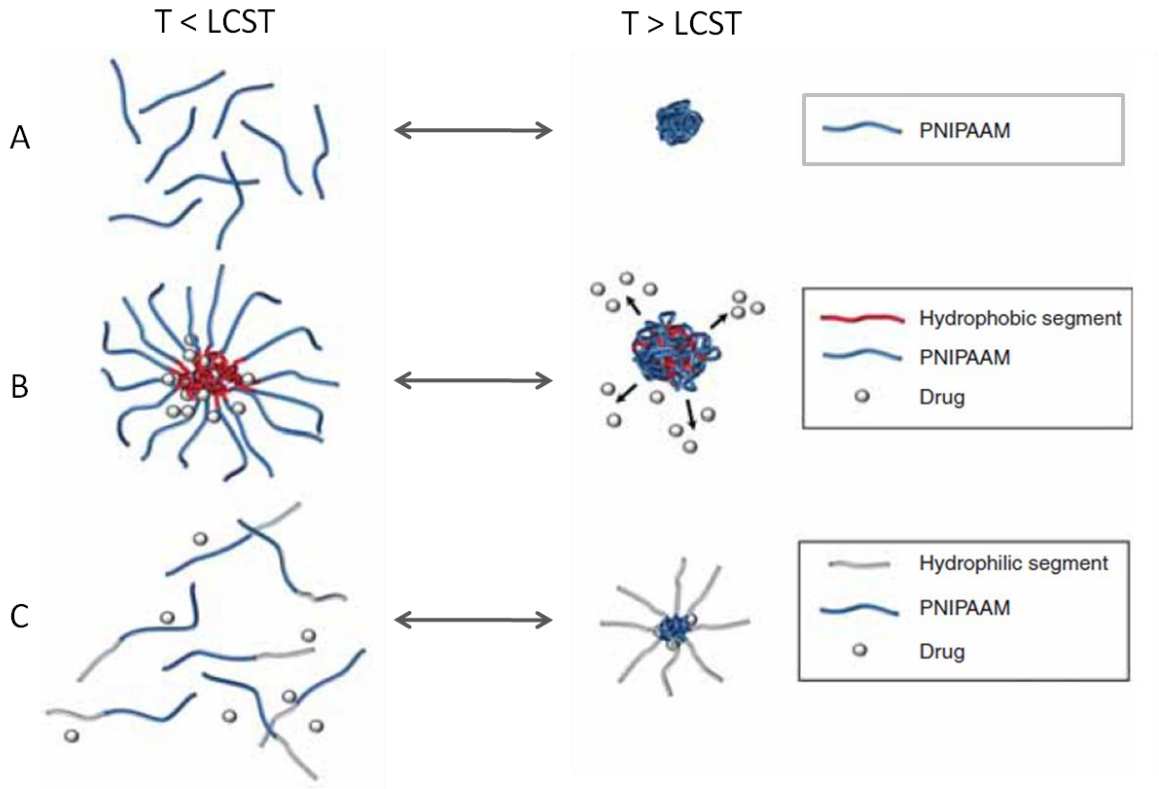

Figure 1.8 Effect of temperature (below and above LCST) on the phase behavior of PNIPAAM and on the micellization of PNIPAAM copolymers. A) PNIPAAM undergoes a 'coil-to-globule' transition above the LCST, as a result of hydrophobic associations. B) PNIPAAM copolymers containing a permanently hydrophobic segment form core-shell micelles in aqueous solution at low temperatures, where the core is hydrophobic and the hydrated PNIPAAM constitutes the shell. As the temperature increases above the LCST, the PNIPAAM shell collapses, causing the destabilization of the micelles and triggering drug release. C) PNIPAAM copolymers containing hydrophilic segments are water soluble at temperatures below LCST. At higher temperatures, the segments self-assemble into micelles, as a result of the self-association of the thermoresponsive moieties. Core-shell micelles, based on a PNIPAAM core and on a hydrophilic shell are thereby formed. In this case, drugs can be loaded (or released) in hyperthermic (or hypothermic) conditions (modified from Calejo et al. 2013a).

Another charged block, (3-acrylamidopropyl)-trimethylammonium chloride (AMPTMA), which is a quaternized acrylamide-based monomer, was copolymerized with PNIPAAM and the resulting copolymers of different lengths were characterized in terms of their thermoresponsiveness (**Figure 1.9**) (Patrizi et al. 2009). Both the LCST and the *cmc* of the copolymers were found to increase with the increase in length of the cationic block AMPTMA, for the same NIPAAM length. The increase of AMPTMA length corresponds to a decrease in hydrophobicity of copolymer molecules, which stabilizes copolymer monomers in solution, by shielding the hydrophobic NIPAAM blocks. An opposite effect is observed with variation of the NIPAAM block length for the same AMPTMA length (Patrizi et al. 2009). More recently, PNIPAAM-*b*-PAMPTMA

block copolymers were shown to interact electrostatically with oppositely charged poly-electrolytes, namely DNA, forming polymer-DNA complexes, designated mixed micelles. In this regard, the extent of polymer-DNA interaction was found to depend not only on the temperature (high temperature promotes complexation), but also on the ionic strength of the medium (high salt reduces electrostatic interactions between the polymers and DNA), providing an additional mean of controlling DNA complexation (Tardani et al. 2011).

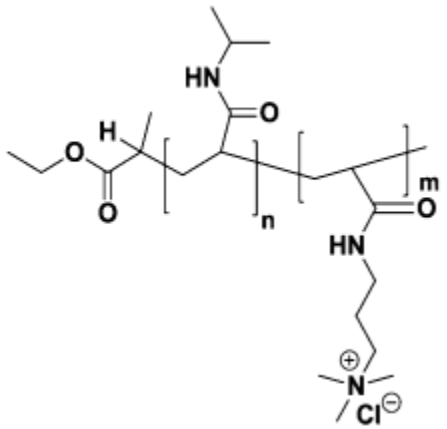

Figure 1.9 Schematic representation of the copolymer $PNIPAAM_n$-*b*-$PAMPTMA_m$ (reproduced with permission from Calejo et al. 2013b).

1.2.3.2 Transfection mediated by thermoresponsive polymers

The thermoresponsive homopolymer PNIPAAM has been used to carry and deliver oligodeoxynucleotides (ODN) into cells. The nucleic acid delivery systems were produced either by co-polymerization of the ODN with PNIPAAM (ODN-PNIPAAM) or by electrostatic association between the ODN and PNIPAAM (ODN + PNIPAAM). The ODN-PNIPAAM conjugate, but not the ODN + PNIPAAM complex, was able to protect ODN from nuclease degradation with high efficiency and to mediate successful transfection (Murata et al. 2003). However, covalent linkage between the nucleic acids and their carrier can be disadvantageous, namely if the release of the nucleic acids becomes compromised.

Copolimerization of PNIPAAM with cationic monomers was used in order to obtain thermoresponsive polymers able to interact with nucleic acids electrostatically, protecting them from degradation and facilitating their intracellular release. PNIPAAM

copolymerized with protonated poly-2-(dimethylamino)ethyl methacrylate (PDMAEMA) groups was shown to form complexes with DNA with high stability at 37 °C (those with low PNIPAAM content) or which precipitated at 37 °C (those rich in PNIPAAM). The most stable complexes proved to be the most effective in transfection, probably because they are able to delay the release of their cargo. Furthermore, maximum transfection was shown to depend on the co-polymer/DNA ratio, polyplexes prepared at 1/2 to 4/1 co-polymer/DNA ratios, which corresponded to polyplex Zeta potentials close to neutrality, being those showing the highest transfection efficiency (Hinrichs et al. 1999).

Twaites and coworkers designed PEI-PNIPAAM and PNIPAAM-PDMAEMA-hexylacrylate (HA) conjugates. The latter polymer joins together the thermoresponsive polymer PNIPAAM with the strongly hydrophilic DMAEMA and the hydrophobic HA. Each of the temperature-responsive polymers formed complexes with DNA under physiologically relevant conditions (Twaites et al. 2005). Moreover, these polymers were shown to transport DNA into mouse myoblasts and PEI-PNIPAAM was able to mediate DNA translocation to the cell nucleus. However, linear-PEI-PNIPAAM copolymer was unable to mediate gene expression, while the branched-PEI-PNIPAAM analogue efficiently transfected cells. Thermoresponsive polymer-DNA complexes were found to induce lower cytotoxicity than PEI homopolymer (Twaites et al. 2005).

Lavigne and colleagues studied two PEI-PNIPAAM conjugate polymers with different LCSTs and presenting coil-to-globule transitions when complexed with plasmid DNA. This transition was shown to lead to conformational changes of the polyplexes, reflected in differences in electrophoretic mobility of polyplexes at temperatures below and above polymer LCST. More interestingly, complexes prepared above the LCST were shown to improve their transfection efficiency in an experimental design, which included a “cold-shock” below the LCST of the polymer during transfection to initiate a change in the polymer conformation. The authors suggested that the microstructural changes in the polymer-DNA complexes, induced upon the abrupt decrease of temperature, when these were inside the endosome, facilitated DNA release thus leading to a better transfection yield. Maximal transfection efficiency corresponded to twice that of the commercially available reagent JetPEI™, and the polyplexes showed to be less toxic than this reagent (Lavigne et al. 2007).

Cationic block copolymers based on PNIPAAM-*b*-PAMPTMA were also studied regarding their transfection efficiency. Copolymers with short charged blocks showed high potential for association with DNA at 37 °C, forming compact core-shell structures that were able to protect DNA from the external environment and led to expressive transfection efficiencies. However, the increase in the length of the charged PAMPTMA, for a constant length of PNIPAAM, led to an increased degree of charge repulsion between the polymer molecules, inhibiting to some extent the thermoresponsive association of PNIPAAM with DNA, with the resulting formation of polyplexes with an 'open' structure (**Figure 1.10**). The low compactness of these polyplexes associated with their low capacity to destabilize lipid bilayers was considered to be the key factor for their low transfection efficiency. For long charged blocks, a very long PNIPAAM block was therefore found essential to ensure the formation of compact nanoparticles (**Figure 1.10**) that led to a successful gene delivery (Calejo et al. 2013b).

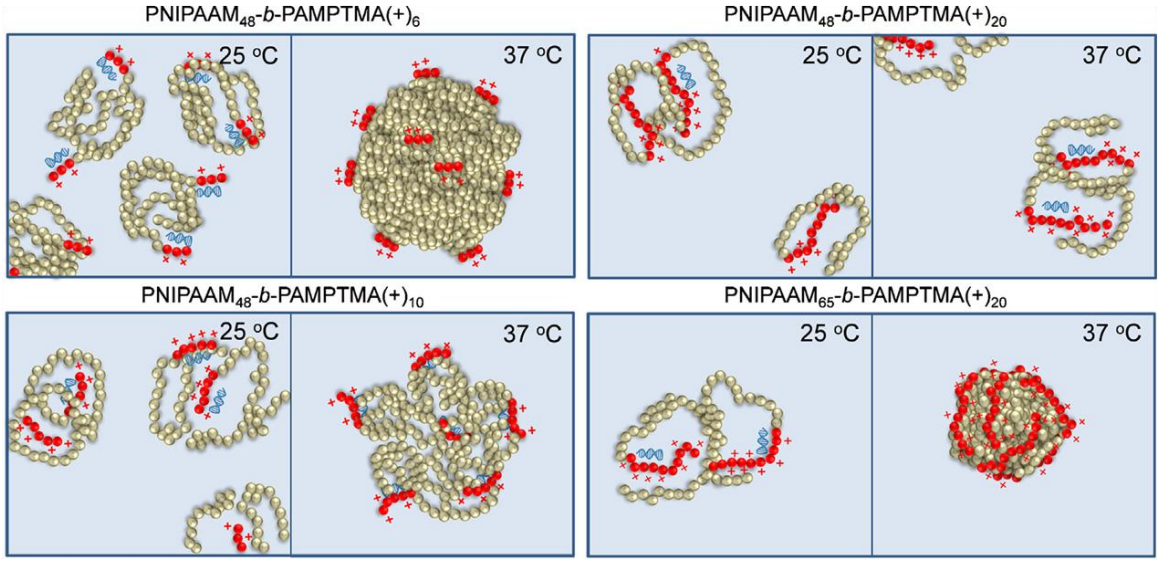

Figure 1.10 Schematic illustration showing the temperature effect on the formation of PNIPAAM-*b*-PAMPTMA/DNA polyplexes. The double-stranded molecule represents the nucleic acid payload, in this case the plasmid DNA in its supercoiled, condensed structure. At 25 °C, the polymer is in its extended, soluble form, allowing the establishment of electrostatic interactions between the positively charged PAMPTMA block and the negatively charged DNA. At 37 °C, the highest degree of aggregation takes place in the presence of the polymer with the shortest PAMPTMA(+) block (PNIPAAM$_{48}$-*b*-PAMPTMA(+)$_6$) and with the longest PNIPAAM block (PNIPAAM$_{65}$-*b*-PAMPTMA(+)$_{20}$) (reproduced with permission from Calejo et al. 2013b).

1.2.3.3 Summary

Polymeric vectors constitute promising tools for *in vivo* delivery of genes and RNAi mediators, due to their controllable structures, safety, transfection efficacy and possibility of large-scale production. Transfection efficiency of thermoresponsive co-polymers was comparable or higher than that of PEI homopolymer, which has been widely regarded as the most effective polymeric vector for *in vitro* gene delivery, although revealing high cytotoxicity. The design of block copolymers showing thermal transitions close to physiological temperature and the possibility for fine modulation of their ability to dissociate and release their cargo can revolutionize therapeutical technologies based on thermoresponsive polymers. In this regard, the synthesis and investigation of copolymers composed of PNIPAAM and biocompatible molecules open the window for the treatment of inflammatory reactions, which promote hyperthermia and are associated to a variety of diseases.

1.3 NUCLEIC ACID DELIVERY SYSTEMS TARGETING MITOCHONDRIA

Being organelles that contain their own DNA, mitochondria have been regarded as potential targets for gene delivery. Following mitochondrial genome decoding in 1981, it became apparent that these organelles did not use the "universal genetic code", which implied that mitochondrial transfer-RNAs (tRNA) recognized some codons as corresponding to certain aminoacids, different from those identified by cytosolic tRNAs (Anderson et al. 1981). In fact, four codons are different in mammalian nuclear and mitochondrial translational systems (**Table 1.6**) (Wallace 1999; Yoon et al. 2010).

Table 1.6 Differential codon usage in the mammalian nuclear and mitochondrial translation systems.

codon	Mitochondria	Nucleus
AUA	Met	Ile
AGA	Stop	Arg
AGG	Stop	Arg
UGA	Trp	Stop

Although mitochondrial genome is very small and encodes only 13 protein subunits of the mitochondrial respiratory chain (Howell 1999), a number of mitochondrial diseases have been related with point mutations in the mitochondrial genome (DiMauro & Schon 2001; Yoon et al. 2010; Wallace 1999). These disorders include encephalomyopaties, such as mitochondrial encephalopathy with lactic acidosis and stroke-like episodes (MELAS), myoclonic epilepsy with ragged red fibers (MERRF), Kearns-Sayre syndrome (KSS), chronic progressive external ophthalmoplegia (CPEO) and neuropathy, ataxia, and retinitis pigmentosum/maternally inherited Leigh syndrome (NARP/MILS), maternally inherited cardiomyopathy (CM), and Leber's hereditary optic neuropathy (LHON), which typically present highly variable multisystem defects that involve abnormalities of skeletal muscle and/or central nervous system (**Figure 1.11**) (Howell 1999).

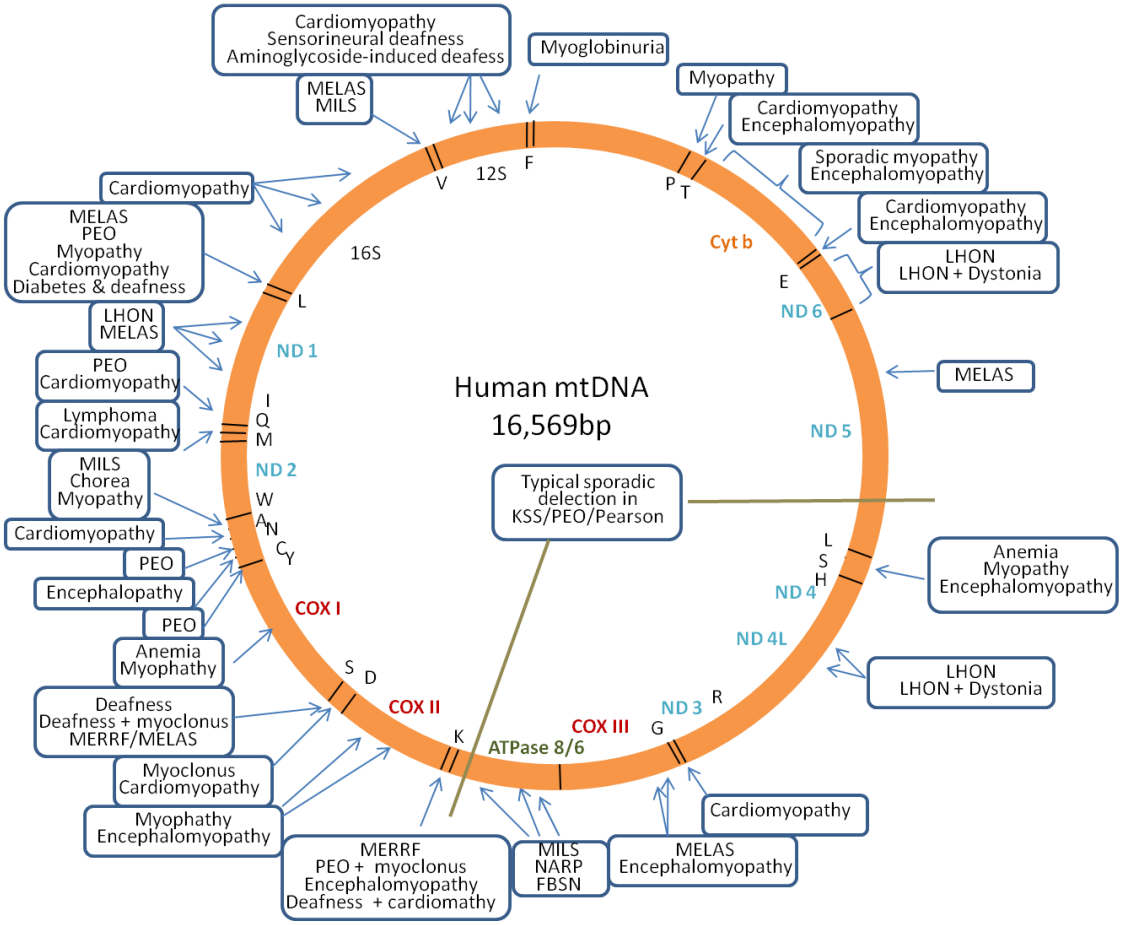

Figure 1.11 Morbidity map of the human mitochondrial genome. The map of the 16.6-kb mtDNA shows the location of the protein-coding genes for the seven subunits of complex I (ND), the three subunits of cytochrome c oxidase (COX), cytochrome b (Cyt b), and the two subunits of ATP synthase (ATPase 6 and 8); the 12S and 16S ribosomal RNAs (rRNA); and the 22 transfer RNAs (tRNA), identified by one-letter codes for the corresponding amino acids. Diseases linked to mtDNA point mutations are indicated in balloons pointing to the DNA region where the mutations occur; FBSN, familial bilateral striatal necrosis; KSS, Kearns-Sayre syndrome; LHON, Leber hereditary optic neuropathy; MELAS, mitochondrial encephalomyopathy, lactic acidosis, and strokelike episodes; MERRF, myoclonic epilepsy with ragged-red fibers; MILS, maternally inherited Leigh syndrome; NARP, neuropathy, ataxia, retinitis pigmentosa; PEO, progressive external ophthalmoplegia.

The number and variety of diseases associated with mitochondrial DNA mutations have been related to the low level of repair potential of mitochondrial DNA (Mason 2003) and to the high mutation rate promoted by the large scale production of reactive oxygen species (ROS) in mitochondria. However, the mitochondrial genome is different from the nuclear DNA so that the severity of mitochondrial gene mutations can be strongly attenuated. In fact, the circular mitochondrial DNA exists in hundreds or thousands of copies in each mammalian cell and deleterious mutations of mtDNA often affect only a few copies, thus originating mitochondria harboring both normal

(wild-type) and mutant populations of mtDNA (heteroplasmy). In addition, for a disease phenotype to appear, a minimum critical number of mutant mtDNA molecules should be present (threshold effect) (DiMauro & Schon 2001).

Mitochondria play well known and extensively studied roles in energy supply, ROS production and apoptosis, and appear as suitable targets for gene therapy of the abovementioned life limiting diseases. As with gene delivery targeting the cell nucleus, mitochondrial targeting is also limited by the inability of the nucleic acids to cross membrane barriers, including the double mitochondrial membrane. One advantage of mitochondrial targeting over nuclear targeting regards the uptake of DNA by that organelle, which is facilitated by the "natural competence" of mitochondria for DNA import (Koulintchenko et al. 2006), a process later identified as being mediated by voltage-dependent anion channels (VDAC) present in the inner mitochondrial membrane (Weber-Lotfi et al. 2009). In fact, ATP has been shown to enhance exogenous DNA uptake and to promote its integration in mitochondrial nucleoids. Large molecules of imported DNA with a proper sequence content might promote recombination with the resident mtDNA, but for small DNA molecules (smaller than 4 kb), the sequence requirements disappear (Ibrahim et al. 2011).

Lipophilic cations with delocalized charges have traditionally been identified as mitochondriotropic molecules, that is, with ability to reach mitochondria and accumulate in their matrix. However, lipophilic cations correspond only to one third of the molecular species whose mitochondrial tropism has been reported. In this regard, Horobin and coworkers performed a remarkable work in systematizing the properties presented by 100 molecules that have shown mitochondriotropism. In this study, four groups of molecules, which accumulated in or close to mitochondria, were defined: i) lipophilic cations (36%), ii) acids (potentially or actual anions), most of which were weak acids whose free acid species were lipophilic (39%), iii) hydrophilic cations (14%), and iv) electrically neutral compounds (10%). Thus, amphiphilicity was found not to be a required property of mitochondriotropic molecules (Horobin et al. 2007).

Nucleic acids were shown to be efficiently delivered to isolated mitochondria in several conditions (Seibel et al. 1995; Weissig et al. 2001a). The colocalization of nucleic acids delivered by different carriers, such as dequalinium, lipids and polymers, with mitochondria, in their natural environment, i.e. in live cells, has been also

demonstrated (Yasuzaki et al. 2010; Lee et al. 2007; Lee et al. 2013; Weissig et al. 2005) (**Figure 1.12**). DQAsomes, liposome-like aggregates formed by dequalinium, which is a dicationic amphiphile traditionally regarded as mitochondriotropic, were used to mediate gene delivery to mitochondria in live cells. This vector showed to be able to promote DNA uptake by the cells, to favor its escape from the endolysosomal route and to deliver it to the vicinity of mitochondria (D'Souza et al. 2003). Another line of work used MITO-Porter, a lipid-based system that enters the cells by promoting fusion with the cytoplasmic membrane. Colocalization of the MITO-Porter carrying DNA (labeled with a fluorescent probe) with mitochondria was observed, although a small amount of the vector also colocalized with the nucleus (Yasuzaki et al. 2010). PEI conjugated with the mitochondrial leading peptide (MLP) was also used to deliver DNA to mitochondria. Importantly, it was shown that these MLP-PEI/DNA complexes colocalized with mitochondria in living cells without promoting cytotoxicity (Lee et al. 2007). In a subsequent study, PEI was copolymerized with Poly(D,L-lactic-co-glycolic acid) (PLGA) and used in the micelle form to carry both DNA and the antioxidant α-tocopherol. The production of ROS promoted by the transfection event was shown to decrease in the experimental conditions under which the antioxidant was used. This antioxidative transfection system yielded a significant reduction in intracellular oxidative stress and mitochondrial membrane potential perturbation, leading to remarkably enhanced transfection in human cancer cell lines. However, since the authors used unmodified luciferase-coding plasmid in their transfection experiments, there is no guarantee that the produced protein has resulted from mitochondrial gene expression (Lee et al. 2013).

In this regard, three protein-encoding plasmid DNA sequences were synthesized in order to be expressed in mitochondria. In 1996, Wheeler and coworkers designed an ornithine transcarbamylase (OTC) gene flanked by mitochondrial sequences in order to be cloned and transcribed in mitochondria. These authors avoided the codons which differ from the universal code, in order to further promote translation, allowing both the mitochondrial and the cytosolic (nucleus-associated) machinery to synthesize the protein (Wheeler et al. 1996). In a subsequent work, Chrzanowska-Lightowlers and collaborators modified the firefly luciferase gene, so that it could be expressed in mitochondria. In this work, advantage was taken of the non-universal mitochondrial

genetic code, in order to produce a reporter gene which would result in intramitochondrial protein synthesis (Chrzanowska-Lightowlers et al. 1999). More recently, Lyrawati and colleagues produced an "artificial mini-mitochondrial genome", i.e. a plasmid DNA molecule, coding for a reporter green fluorescent protein (GFP) designed to be expressed exclusively in mitochondria. For this purpose, besides the use of a specific codon from the non-universal mitochondrial genetic code, the favored mitochondrial codons that are highly expressed in mitochondrial-encoded proteins were used to replace the corresponding codons used by the cytosolic machinery. The produced mitochondrial DNA was designated pmtGFP (Lyrawati et al. 2011).

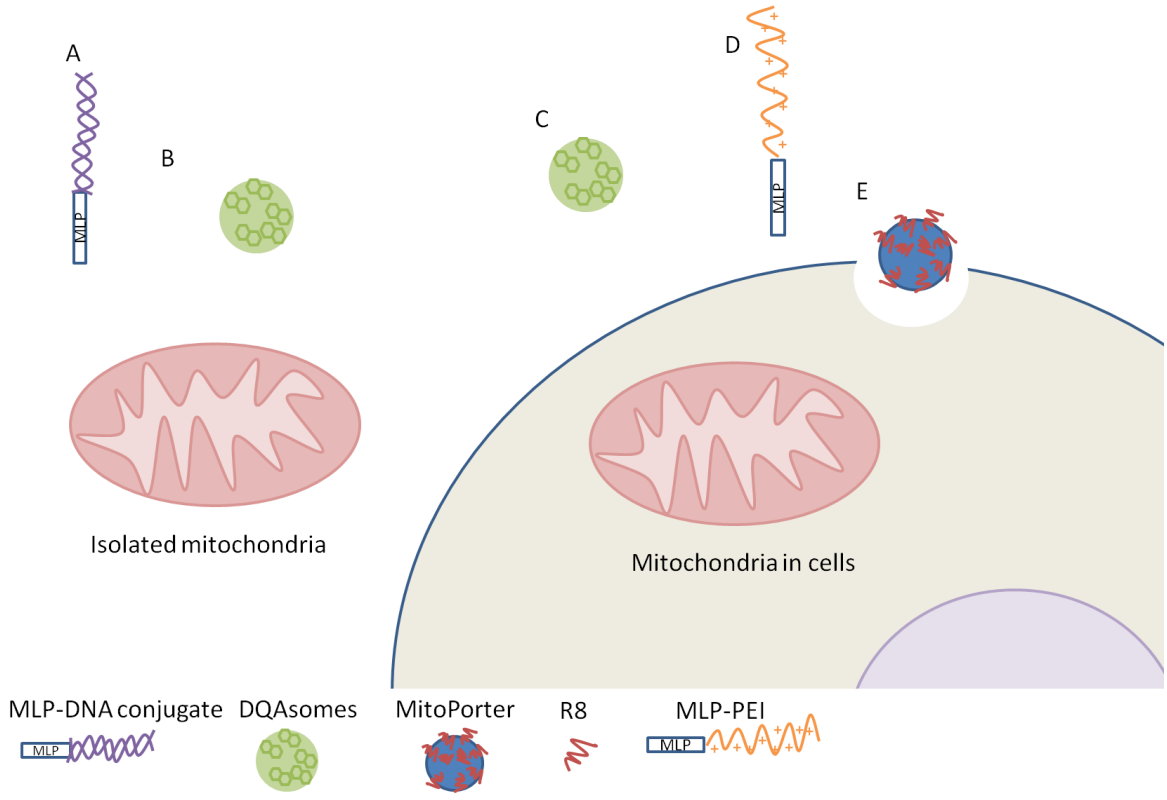

Figure 1.12 Strategies used for mitochondrial targeting. Isolated mitochondria were targeted using mitochondria leading peptide (MLP)-DNA conjugates (A) and DQasomes electrostatically associated with DNA (B). In both situations, the delivery systems were internalized by mitochondria. Mitochondria in live cells were targeted using DQasomes (C), MLP-PEI conjugates (D) and MitoPorter (E). In these three cases the DNA was electrostatically associated with the carriers and colocalization of DNA and mitochondria was observed in live cells (see text for details).

1.3.1 SUMMARY

In summary, gene delivery targeting mitochondria has emerged as a promising approach to address life-limiting diseases with origin in mtDNA mutations. Several studies described successful attempts to deliver molecules to mitochondria in living cells. On the other hand, DNA has been shown to enter isolated mitochondria and to be transcribed and translated by these organelles, originating functional proteins. The next step of this process involves the conjugation of these two abilities, i.e., to find a delivery system able to mediate both efficient cellular internalization and mitochondrial uptake of the carried nucleic acids leading to enhanced gene expression.

1.4 CONCLUDING REMARKS

The field of nonviral technology for drug delivery has benefited from the joint cooperation of chemists, biophysicists and cell biologists aiming at discovering novel molecules with ability to transfect cells and improving those already existing, by structural remodeling. The development of delivery systems has aimed at achieving high cargo transfer efficiency and avoiding cytotoxicity at the concentrations needed for a successful biological activity. Therefore, cell biological studies have been focused on selecting non-toxic molecules with high ability to transpose cellular membranes and promote intracellular cargo delivery.

On the other hand, biophysical analysis has the purpose of establishing structure-activity relationships, considering four different steps in the delivery process, namely the interaction and binding of the delivery molecules to the cell surface, eventually evoking conformational alterations, their translocation across cell membrane, their escape from endosomes, when the endocytic pathway is used for the cellular internalization of the delivery system, and their ability to release their cargo into the intracellular milieu.

Although currently there is no recipe to create the ideal delivery system, a major concern regards the chemical and structural characteristics of the carrier molecules along with the nature of their interaction with the cargo and the cell membranes. Thus, research in the field of nonviral gene delivery benefits from an integrative protocol using biological and biophysical analysis.

Electrostatic interactions between opposed charges (from cationic components of the delivery systems and the negatively charged cloud at the cell surface, conferred by glycosaminoglycans, GAGs), and hydrophobic interactions (established between amphipathic molecules composing the carrier and the lipid bilayer) guide the interactions between the delivery systems and cell membranes, and perturbation of the physical properties of the membrane lipid bilayer can also contribute to an additional gain in free energy for the translocation process.

The heterogeneous and the highly dynamic nature of cell membranes make the assessment of delivery system-cell membrane interactions a complex process, with several factors involved, which increase the difficulty of studying it in detail at a molecular level. Therefore, membrane-mimicking lipid systems, which contain neither

proteins nor sugars, have been used to evaluate the influence of membrane structure and composition on carriers' cellular uptake.

A full characterization of the nucleic acid delivery systems originated from gemini surfactants, CPPs and stimuli-responsive polymers can contribute positively to the rational remodeling of those types of molecules. This approach can be fostered by the conjugation of biological and biophysical techniques, jointly contributing to the establishment of the principles able to warrant the design of increasingly competent nucleic acid delivery systems applicable to different therapeutic purposes.

Chapter 2

Objectives

Objectives

The hypothesis that originated the work presented in this Thesis is that the chemical structure of nucleic acid delivery systems, the interactions they establish with membranes and the conformational alterations they undergo under different biological conditions are intrinsically related to their performance. Therefore, a deep understanding at a molecular-level of this relationship will provide a fundamental basis for developing new materials and strategies, in order to vastly improve the efficiency of non-viral gene delivery systems.

In order to test our hypothesis, we proposed to carry out several tasks with the following aims:

1. Development/improvement of non-toxic gene delivery systems based on cationic gemini surfactants from two families, conventional and serine-derived *bis-quaternary*.

2. Physical characterization of the gemini surfactant-based gene delivery systems developed and comparison of the properties presented by those able to efficiently mediate gene delivery with those lacking this ability.

3. Evaluation of the ability of gemini surfactant-based gene delivery systems to promote mitochondrial gene expression.

4. Assessment of the extent of the interactions between the gemini surfactant-based complexes able to efficiently mediate mitochondrial gene expression and membrane models mimicking the lipid composition of different cell membranes.

5. Characterization of the biophysical changes induced by the cell-penetrating peptide S4(13)-PV and its scrambled derivative in lipid membrane models and ultrastructural analysis of the arrangements adopted by the cell-penetrating peptides upon interaction with cellular membranes.

6. Development of new formulations for plasmid DNA and siRNA delivery based on a cell-penetrating peptide derived from S4(13)-PV by addition of a histidine sequence, in order to improve its endosomolytic capacity.

7. Evaluation of the silencing ability of PNIPAAM-*b*-PAMPTMA(+) block copolymers with different thermoresponsive and cationic block lengths, and, consequently, different charge densities and cloud points.

These objectives were defined as milestones to be achieved along the experimental plan envisaging to reach two challenging goals: *i*. to prepare innovative formulations based on cationic gemini surfactants, cell-penetrating peptides and thermoresponsive polymers, combining high performance in delivering nucleic acids into cells and mediating gene expression and silencing, without causing cytotoxicity, and *ii*. to unravel the structural characteristics of the generated nucleic acid delivery systems that, on the one hand, modulate their interaction with cellular membranes, cell uptake and intracellular trafficking, and, on the other hand, ensure their high transfection efficiency, with minimal adverse effects to cells.

Chapter 3

Materials and Methods

3.1 MATERIALS

3.1.1 GEMINI SURFACTANTS

Conventional and serine-derived *bis-quaternary* gemini surfactants were synthesized, purified and physically characterized in Centro de Investigação em Química, Department of Chemistry and Biochemistry, University of Porto (Porto, Portugal) and kindly provided to us thanks to a collaboration with Prof. Eduardo Marques and Prof. Luísa do Vale from that Institution.

3.1.2 CELL-PENETRATING PEPTIDES

Peptides of the S4(13)-PV family, namely S4(13)-PV (wild type), S4(13)-PVscr (scrambled derivative of S4(13)-PV, with the same aminoacid composition and overall charge of the wild type peptide, but a distinct primary sequence), S4(13)-PVrev (reverse NLS derivative, whose aminoacid sequence only differs from that of the wild type peptide in the sequence of three aminoacids in the NLS) and H5-S4(13)-PV (histidine derivative, resulting from the addition of a 5-histidine tail to the amine terminus of the wild type peptide), were synthesized, purified and physically characterized in Centro de Investigação em Química, Department of Chemistry and Biochemistry, University of Porto (Porto, Portugal) and kindly provided to us thanks to a collaboration with Prof. Paula Gomes from that Institution.

3.1.3 THERMORESPONSIVE POLYMERS

PNIPAAM-*b*-PAMPTMA diblock copolymers were synthesized, purified and physically characterized in Department of Chemistry, University of Oslo (Oslo, Norway) and kindly provided to us thanks to a collaboration with Prof. Bo Nyström from that Institution.

3.1.4 LIPIDS

The lipids bis(monooleoylglycero)phosphate (18:1 BMP), cholesterol (chol), 1,2-dimyristoyl-*sn*-glycero-3-phosphocholine (DMPC), 1,2-dioleoyl-*sn*-glycero-3-phosphocholine (DOPC), 1,2-dioleoyl-*sn*-glycero-3-phosphoethanolamine (DOPE), 1,2-dioleoyl-*sn*-glycero-3-phospho-(1′-rac-glycerol) (DOPG), 1,2-dioleoyl-3-trimethylammonium-propane (DOTAP), 1,2-dipalmitoyl-*sn*-glycero-3-phosphocholine (DPPC), 1,2-dipalmitoyl-*sn*-glycero-3-phosphoethanolamine (DPPE), 1,2-dipalmitoyl-*sn*-glycero-3-phospho-(1′-rac-glycerol) (DPPG), 1-palmitoyl-2-oleoyl-*sn*-glycero-3-phosphocholine (POPC), 1-palmitoyl-2-oleoyl-*sn*-glycero-3-phospho-(1′-

rac-glycerol) (POPG), 1-palmitoyl-2-oleoyl-*sn*-glycero-3-phospho-L-serine (POPS), bovine brain sphingomieline (SM) and 1',1',2',2'-tetraoleoyl cardiolipin (TOCL) were purchased from Avanti Polar Lipids (Alabaster, AL).

3.1.5 Fluorescent probes

The fluorescent probes 1,6-diphenyl-1,3,5-hexatriene (DPH), 3-(p-(6-phenyl)-1,3,5-hexatrienyl)phenylpropionic acid (DPH-PA), 2-(9-anthroyloxy) stearic acid (2-AS), 6-(9-anthroyloxy) stearic acid (6-AS), 12-(9-anthroyloxy) stearic acid (12-AS), 16-(9-anthroyloxy) palmitic acid (16-AP), N-(7-nitrobenz-2-oxa-1, 3-diazol-4-yl)-phosphatidylethanolamine (NBD-PE) and rhodamine-phosphatidylethanolamine (Rho-PE) were obtained from Molecular Probes Inc. (Eugene, OR).

3.1.6 Primers

The primers for survivin and HPRT-1 genes were pre-designed by Qiagen (QuantiTect Primer, Qiagen).

3.1.7 Antibodies

The antibody anti-survivin (goat) was purchased from Santa Cruz (Santa Cruz Biotechnology, Inc., Heidelberg, Germany), the antibody anti-α-tubulin (mouse) and the secondary antibodies were obtained from Sigma (St. Louis, MO, USA).

3.1.8 Plasmid DNA

Plasmid DNA encoding GFP (pEGFP-C1 plasmid DNA, here simply denominated pDNA) was obtained from Clontech, CA, USA, and plasmid DNA encoding mitochondrial GFP (mtpDNA) was synthesized and kindly provided by Prof. Diana Lyrawati, Brawijaya University (East Java, Indonesia).

3.1.9 siRNAs

The anti-GFP siRNA (5′-GCAAGCUGACCCUGAAGUUCAU-3′) and Cy3-labeled nonspecific siRNA sequence were purchased from Ambion (Austin, TX, USA). The anti-survivin siRNA (5′-GGACCACCGCAUCUCUACAdTdT-3′) and the non-silencing siRNA used as control were obtained from Dharmacon (Lafayette, CO, USA).

3.2 METHODS

3.2.1 PREPARATION OF NUCLEIC ACID DELIVERY SYSTEMS

Nucleic acid delivery systems were prepared through non-covalent association of nucleic acids with several carrier molecules. This process is an easy method to generate complexes from negatively charged nucleic acids and cationic carriers, and has the advantage of neither compromising the biological activity of the carried nucleic acid nor requiring the generation and testing of new constructs for any given nucleic acid cargo. However, the reproducibility of the procedure and the control of the stoichiometry are not as rigorous as those obtained with covalently linked systems (Heitz et al., 2009). The procedure that originates the most efficient complexes depends on a variety of factors, including the nature of the carrier molecules, and, for ternary complexes, i.e., those containing helper lipids besides the cationic carrier molecule and nucleic acids, the order of component addition is equally relevant.

3.2.1.1 Gemini surfactant-based complexes

The influence of the method for preparation of nucleic acid complexes based on conventional *bis-quaternary* gemini surfactants on their transfection ability was evaluated. Plain complexes of surfactant/DNA or ternary complexes of surfactant/helper lipid/DNA were prepared using two different methods (A and B). Method A, reported in Cardoso et al., 2011, consisted of dissolving gemini surfactants or their mixture with DOPE and cholesterol in chloroform, at the desired molar ratios (3:2:1 and 3:4:2). Solutions were then dried under vacuum in a rotatory evaporator and the resulting lipid films were hydrated with deionised water to a final lipid concentration of 2 mM. Surfactant or surfactant plus lipid dispersions were then sonicated for 3 min, extruded 21 times through two stacked polycarbonate filters of 50 nm pore diameter, using a Liposofast device (Avestin, Toronto, Canada), to produce small unilamellar vesicles (SUV) and, after a three-fold dilution with deionised water, they were filter-sterilized utilizing 0.22 μm pore-diameter filters (Schleicher & Schuell, BioScience, Germany). Plain complexes (surfactant/DNA) and ternary complexes (surfactant/DNA/lipid) were prepared by mixing 100 μL of a

HEPES-buffered saline solution (HBS; 100 mM NaCl, 20 mM HEPES, pH 7.4) containing 0.5 μg of pEGFP-C1 plasmid DNA encoding GFP (Clontech, CA, USA) with a volume of the previously prepared surfactant suspensions (without or with helper lipids), to obtain surfactant/DNA (+/-) charge ratios in the range of 2/1 to 8/1. The resulting mixtures were then incubated for 15 min at room temperature.

Method B consisted of an adaptation of the method described by Badea and coworkers (Badea et al., 2005). Briefly, aqueous solutions (0.5 mM) of gemini surfactants were filtered through 0.22 μm pore-diameter filters (Schleicher & Schuell, BioScience, Germany) and a solution of DOPE and cholesterol (2:1 molar ratio) in chloroform was dried under vacuum in a rotatory evaporator, the resulting lipid film being hydrated with HBS (pH 9.0) to a final lipid concentration of 0.5 mM. The resulting multilamellar vesicles (MLV) of DOPE plus cholesterol were then sonicated for 3 min and filtered through 0.22 μm pore-diameter filters (Schleicher & Schuell, BioScience, Germany). Complexes were prepared by mixing 100 μL of HBS containing 0.5 μg of pEGFP-C1 plasmid DNA encoding GFP with aliquots of the aqueous gemini surfactant solution, to obtain surfactant/DNA (+/-) charge ratios in the range of 2/1 to 8/1. These preparations were incubated 15 min at room temperature. To produce the ternary complexes, a volume of DOPE:Chol liposomes was added to surfactant/DNA complexes to obtain surfactant/lipid molar ratios in the range of 1/1 to 1/2, followed by 30 min incubation at room temperature.

The two methods are depicted in **Figure 3.1**. Since method B was less time consuming and revealed to produce the most efficient complexes with the conventional gemini surfactants as compared to method A, the former was selected to be employed in the preparation of complexes based on conventional as well as serine-derived gemini surfactants, containing either pDNA or mtpDNA.

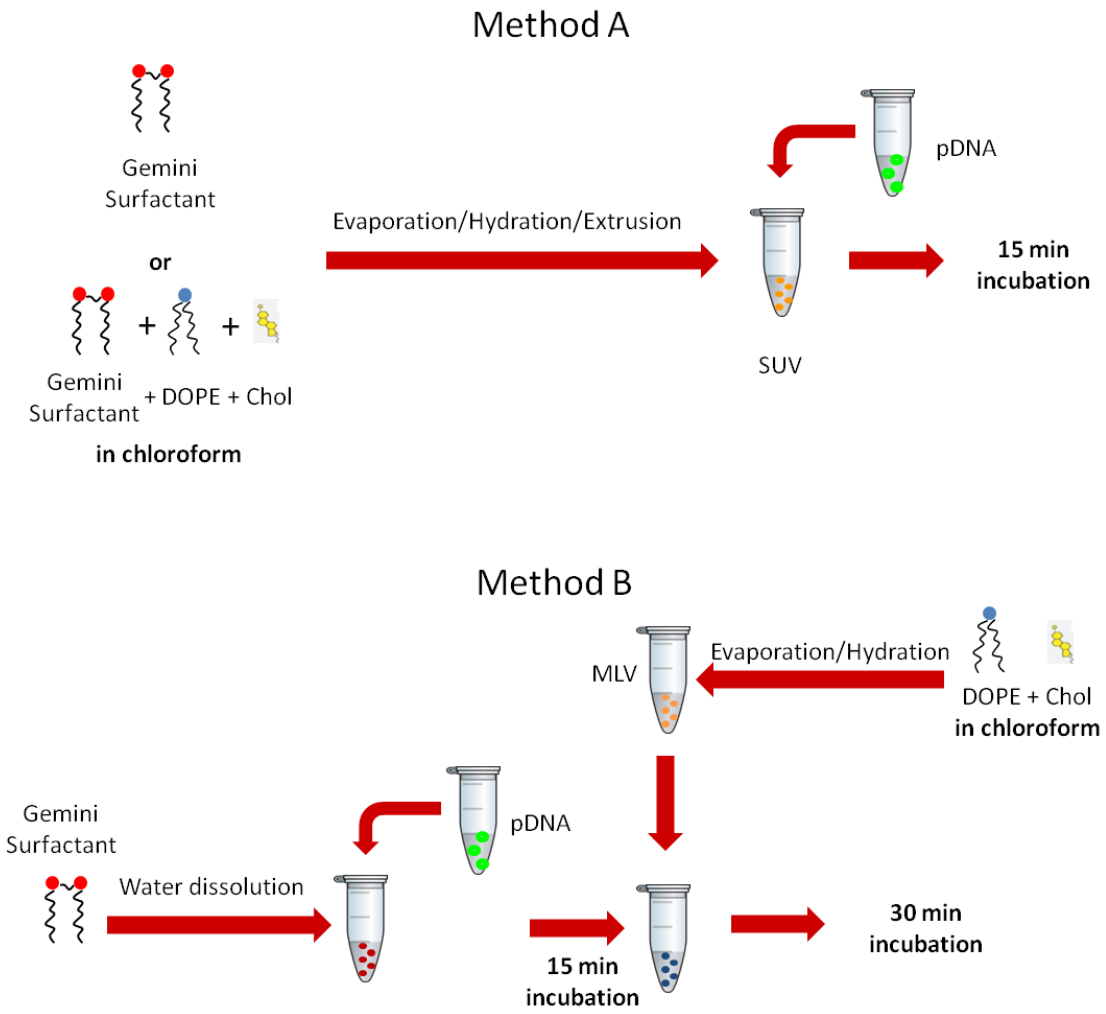

Figure 3.1 Schematic representation of the two methods used for complex preparation. Method A: gemini surfactant or gemini surfactant plus DOPE and cholesterol were dissolved in chloroform and then mixed at the desired molar ratio and dried under vacuum in a rotatory evaporator. The dried lipid films were hydrated with deionised water and the resulting MLV were sonicated and extruded. Complexes were prepared by mixing 0.5 μg of pEGFP-C1 plasmid DNA encoding GFP with an aliquot of the previously prepared SUV dispersion, to obtain the desired surfactant/DNA (+/-) charge ratio. The mixture was further incubated for 15 min at room temperature. Method B: DOPE and cholesterol were dissolved in $CHCl_3$ and then mixed at the desired molar ratio (2:1) and dried under vacuum in a rotatory evaporator. The dried lipid film was hydrated with HBS (pH 9.0) and the resulting MLV were then mildly sonicated in a sonication bath. Complexes were prepared by mixing 0.5 μg of pEGFP-C1 plasmid DNA encoding GFP with aliquots of a gemini surfactant aqueous solution prepared at 0.5 mM, to obtain the desired surfactant/DNA (+/-) charge ratios, followed by incubation at room temperature for 15 min. To obtain the ternary complexes (surfactant/DNA/lipid), a volume of DOPE:Chol liposomes was added to this mixture at the desired surfactant/lipid molar ratio, followed by an incubation for 30 min at room temperature.

3.2.1.2 Cell-penetrating peptide-based complexes

Plain complexes of CPP/DNA or ternary complexes of CPP/DNA/DOTAP:DOPE were prepared in HBS. Plain complexes were produced by gently mixing pDNA (0.5 μg) or siRNA (25 pmol) with each of the CPPs, at the desired charge ratio, followed by 15 min (pDNA complexes) or 30 min (siRNA complexes) of incubation at room temperature. Ternary pDNA complexes were obtained by gently mixing peptide/pDNA complexes, prepared at the desired charge ratio, with DOTAP:DOPE large unilamellar vesicles (LUV), prepared from MLVs (generated as previously referred). Mixtures were then incubated for 15 min, at room temperature.

Complexes of siRNA containing both CPP and LUVs composed of DOTAP:DOPE were prepared following two different methodologies. One method involved the addition of CPP to the siRNAs (50 nM), in order to obtain the desired CPP/siRNA (+/-) charge ratios, followed by the addition of the cationic LUV (CPP/siRNA/DOTAP:DOPE complexes). In the other method, CPPs were mixed with the cationic LUV, before the addition of the siRNAs (CPP/DOTAP:DOPE/siRNA complexes). After the addition of each component, the mixtures were gently mixed and incubated for 30 min at room temperature to allow the formation of the complexes exhibiting the desired (+/-) charge ratios.

3.2.1.3 Thermoresponsive polymer-based complexes

Polymers were dissolved in cell culture medium without serum (OptiMEM) or containing 10% fetal bovine serum (FBS) (DMEM-LG) and gently mixed with siRNA targeting GFP (50 nM), at the desired polymer/siRNA (+/−) charge ratios, at room temperature. The mixtures were further incubated for 20 min at room temperature.

3.2.2 Evaluation of the physico-chemical properties of nucleic acid complexes

Physico-chemical properties of the complexes, such as hydrodynamic diameter, surface charge density and colloidal stability were evaluated because of their importance in determining the success in nucleic acid delivery.

3.2.2.1 Mean diameter

Evaluation of the hydrodynamic size distribution of surfactant-, peptide- and polymer-containing particles complexed with nucleic acids (DNA or siRNA) were performed by measuring the dynamic light scattering (DLS), through photon correlation spectroscopy (PCS). In PCS, the time-dependent fluctuations resulting from the Brownian motion of particles in suspension are determined by autocorrelation spectroscopy of scattered laser light. A photomultiplier detects the light intensity scattered at a given angle, which then passes to an autocorrelator, which determines the rate of diffusion or Brownian motion of the particles, and hence their size, through a time-dependent analysis (**Figure 3.2**). The relationship between the size of a particle and its speed due to Brownian motion is defined in the Stokes-Einstein equation:

$$D = \frac{RT}{N_A} \frac{1}{6\pi\eta a}$$

where D is the diffusion coefficient of a spherical particle of radius a, R is the gas constant, N_A is the Avogadro number, T is the absolute temperature and η is the viscosity of the medium. Particle size is determined as the diameter of a sphere that would diffuse at the same speed as the particle being measured. In the present work, the detection angle was fixed at 90° and the assay was performed using a Coulter N4 Plus Instrument (Coulter Electronics, Miami, FL). The analysis was performed at room temperature, in HBS, and complexes were prepared, as recommended, immediately before analysis.

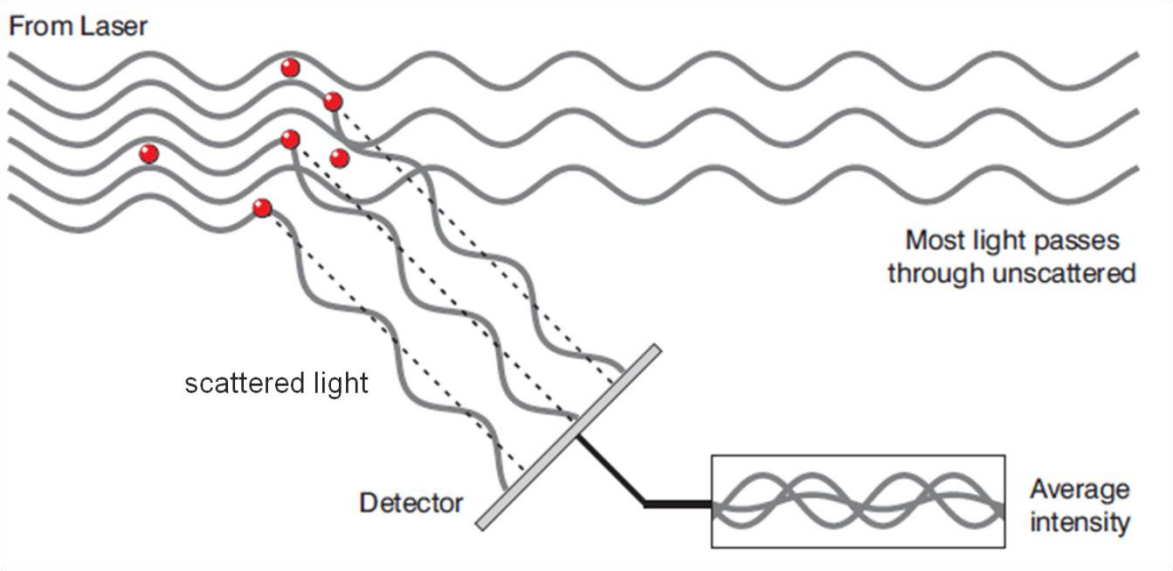

Figure 3.2 Schematic representation of the propagated waves from the light scattered by the particles dispersed in an aqueous medium (modified from Zeta Sizer Nano Series, User Manual, Ch. 13).

3.2.2.2 Zeta potential

The Zeta potential or electrokinetic potential of surfactant-, peptide- and polymer-containing particles was measured using a Zetasizer Nano ZS, ZN 3500, with a 532 nm laser (Malvern Instruments, UK). Charged particles modify the distribution of ions in the surrounding medium, resulting in an increased concentration of counter-ions close to the surface. Therefore, an electrical double layer is formed around each particle, consisting of an inner region (Stern layer), where ions are strongly bound to the particle, and an outer, diffuse region where ions are more loosely attached. Counter-ions within this double layer form a stable entity with the particle they surround, creating a boundary (slipping plane). The difference of potential between this boundary and the bulk is known as the Zeta potential (**Figure 3.3**).

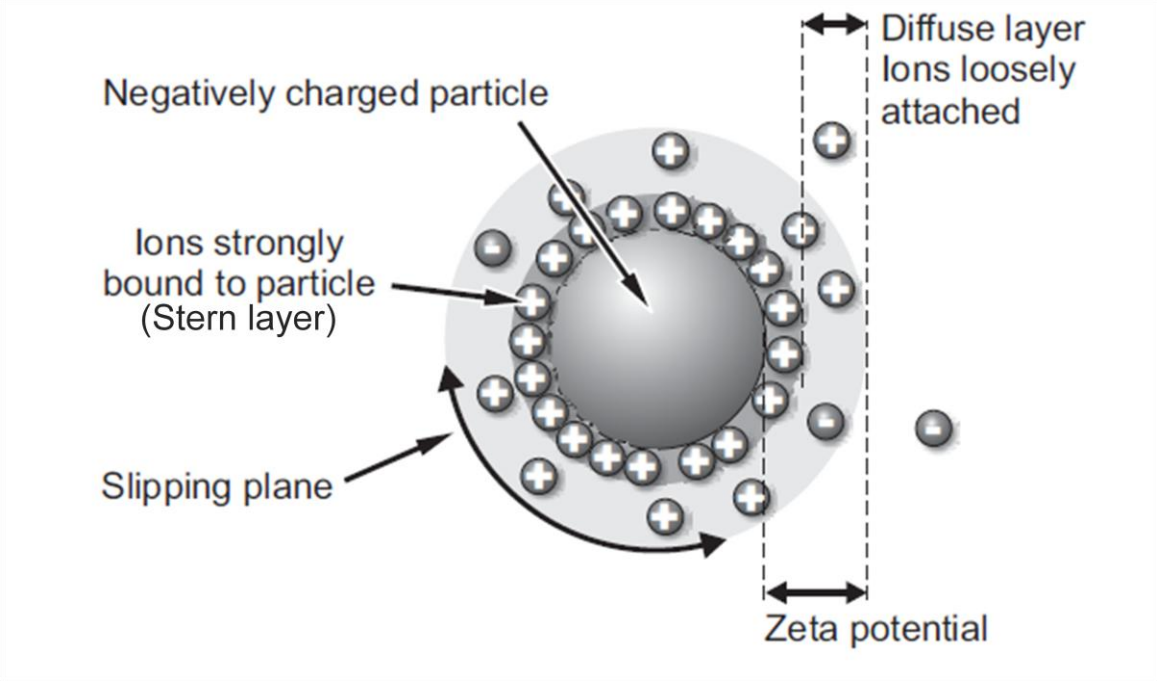

Figure 3.3 Schematic representation of the ion organization around the particle of interest (modified from Zeta Sizer Nano Series, User Manual, Ch. 1).

Zeta potential is measured using a combination of electrophoresis and Laser Doppler Velocimetry. This method measures the velocity of a particle in a liquid when an electrical field is applied. Zeta potential can be determined from the velocity of the particle and the electrical field applied, taking into consideration the viscosity and the dielectric constant of the medium.

Electrophoretic mobility is detected by the Doppler shift in frequency, Δυ, using a heterodyne method, and calculated using the equation:

$$\Delta\upsilon = U(Ek)$$

where U is the electrophoretic mobility, E is the applied electric field, and k is the scattering angle determined by the equation:

$$k = \frac{4\pi n}{\lambda} sin\frac{\theta}{2}$$

where λ is the wavelength of the helium–neon laser light in vacuum, n is the refractive index of the medium, and θ is the angle between the incident laser beam and the detector. From both equations, electrophoretic mobility can be calculated using the equation:

$$U = \frac{\Delta \upsilon \lambda}{2nEsin\frac{\theta}{2}}$$

The Smoluchowski approximation assumes that the double-layer thickness is small compared to the colloidal particle diameter, thus correlating electrophoretic mobility and Zeta potential:

$$U = \frac{\varepsilon_r \varepsilon_0 \zeta}{\eta}$$

where ζ is the Zeta potential, ε_r is the dielectric constant of water, ε_0 is the permittivity of the free space and η is the viscosity, this being a valid assumption for aqueous systems of defined electrical conductivity (Cardoso et al., 2009).

The measurements were performed in the aqueous buffer HBS, at 25 °C (for surfactants, CPPs, polymers and respective DNA complexes) or 37 °C (for polymers and respective DNA complexes), using DTS 1060C folded capillary cells and the protocol for general purposes (electric current 3.0 mA, medium viscosity 0.89 cP, medium refractive index 1.33, sample viscosity 0.89 cP, particle refractive index 1.45 and equilibration time 3 min). Values of dielectric constant of 78.5 and beam mode F(Ka) of 1.5 (Smoluchowsky) were used and Zeta potential was calculated for each scattering angle (8.6°, 17.1°, 25.6° and 34.2°).

3.2.2.3 Colloidal stability

Turbidity fluctuations of complex dispersions in HBS buffer (pH 7.4) were monitored as a function of time in a SPECTRAmax PLUS 384 spectrophotometer (Molecular Devices, Union City, CA) at a wavelength of 550 nm, in HBS buffer, pH 7.4 over a period of 48 h, in order to evaluate complex colloidal stability.

3.2.3 Structural properties of complexes and their interactions with membranes

The interactions between nanocarriers and membrane lipids may play a key role in the success of nucleic acid delivery. In this context, the use of lipid models has been revealed very helpful to address the effects of nanocarriers or corresponding nucleic acid complexes on the physical properties of cell membrane lipids, with repercussion on the transfection process. A biophysical approach is also useful to evaluate the

compactness of lipid-based complexes, which can be determinant for the protection and dissociation of carried molecules.

3.2.3.1 Fluorescence polarization analysis

Membrane fluidity can be determined from the spectroscopic parameter provided by fluorescence polarization or fluorescence anisotropy. Several fluorescent probes can be used to detect alterations in membrane physical properties at different depths of the lipid bilayer, such as 1,6-diphenyl-1,3,5-hexatriene (DPH) and its anionic and cationic analogs 3-[p-(6-phenyl)-1,3,5-hexatrienyl]phenylpropionic acid (DPH-PA) and 1-(4-trimethylaminophenyl)-6-phenyl-1,3,5-hexatriene (DPH-TMA), respectively. The high molar absorption coefficient of DPH ($\varepsilon_{350nm} \approx 80{,}000\ M^{-1}\ cm^{-1}$), as well as its high quantum yield in hydrophobic environments (0.8 in hexane, at 25 °C), negligible emission in aqueous media, and absorption and emission spectra at distinct wavelength ranges, are advantageous spectroscopic properties that invite the use of this probe in membrane studies (Shinitzky & Barenholz, 1974). The high hydrophobicity of DPH compel its insertion deep into the hydrocarbon core of the lipid bilayer (Andrich & Vanderkooi, 1976), whereas its charged derivatives are anchored at the lipid–water interface (Prendergast et al., 1981; Trotter & Storch, 1988). Steady-state fluorescence anisotropy measurements are based on the principle of photoselectivity (Gennis, 1989). The exposure of a liposome suspension labeled with a fluorescent probe to light of a suitable wavelength (340–360 nm), polarized along the z-axis, results in the excitation of the probe molecules whose transition dipole moments are also oriented in the vertical direction. Light emission at an adequate wavelength is monitored when the emitted light is polarized in a parallel and in a perpendicular direction to the exciting radiation, providing the $I_{\parallel}$ and $I_{\perp}$ components, respectively. The values of $I_{\parallel}$ and $I_{\perp}$ are used to obtain the anisotropy (r) or fluorescence polarization (P) according to the equations:

$$r = \frac{I_{II} - GI_{\perp}}{I_{II} + 2GI_{\perp}} \text{ and } P = \frac{I_{II} - GI_{\perp}}{I_{II} + GI_{\perp}}$$

where G is the grating correction factor for the optical system, obtained from the equation:

$$G = \frac{I_{\perp}}{I_{II}}$$

The constraints to the rotational diffusion and reorientation of probe molecules indicated by the value of r or P, reflect the free volume existent in the region where the probe resides within the membrane. Therefore, r and P describe (indirectly) the freedom degree and level of mobility (range and rate of motion) of phospholipid hydrocarbon chains (Trabulo et al. 2012).

For fluorescence polarization measurements, liposomes were prepared by mixing the lipids in chloroform at the desired molar ratio and hydrating the lipid films with Tris-maleate (50 mM), KCl (10 mM), pH 7.4 buffer in order to obtain a concentration of 200 μM in phospholipid. This preparation (MLV) was then sonicated in a low energy water sonifier for a few seconds to decrease light scattering. The probe DPH-PA, as well as the probes derived from stearic acid 2-(9-anthroyloxy) stearic acid (2-AS), 6-(9-anthroyloxy) stearic acid (6-AS), 12-(9-anthroyloxy) stearic acid (12-AS) or palmitic acid 16-(9-anthroyloxy) palmitic acid (16-AP) were then incorporated in liposomes, by injecting a few microliters (5-10 μL) of the concentrated probe solution in dimethylformamide into liposome suspensions to obtain a lipid/probe molar ratio of 200/1. Thereafter, the liposome suspensions were incubated for 30 min in a water bath set 7–10 °C above the transition temperature of the phospholipids, in order to favor probe incorporation into the lipid bilayers, and let to stabilize overnight at room temperature, in the dark. Blank samples were prepared with equivalent volumes of the probe solvent to correct fluorescence measurements for the contribution of light scattering, although these corrections were often found to be negligible (blank fluorescence intensity lower than 5% of that of the respective sample). To study the effect of CPPs on membrane fluidity, these were allowed to incubate with liposomes labeled with different probes for 30 minutes in a water bath set 7–10 °C above the transition temperature of the phospholipids and the fluorescence polarization of the probes was evaluated in an appropriate temperature range.

To evaluate hydrocarbon chain packing in gemini surfactant-based complexes, these were incubated with the fluorescent probes DPH or DPH-PA for 30 min and the fluorescence polarization of the probes was evaluated at 37 °C. The same formulations lacking DNA were used as controls.

The fluorescence polarization measurements were performed in a Perkin Elmer LS 55B fluorescence spectrophotometer (Perkin Elmer, U.S.A), equipped with polarization filters and a thermostated cell holder. The excitation and emission wavelengths were set at 336 nm and at 450 nm, respectively for DPH-PA and at 365 nm and 450 nm for the probes 2-AS, 6-AS, 12-AS and 16-AP, with 5 nm excitation and 6 nm emission band pass.

3.2.3.2 Differential scanning calorimetry (DSC)

Differential scanning calorimetry (DSC) is a sensitive technique that provides useful information about effects of lipid interactions with strange molecules from the perspective of the structure and dynamics of lipid aggregates. For this purpose, two conditions should be observed, firstly lipids or lipid mixtures should undergo a phase transition (or transitions) within an accessible temperature range and, secondly, this temperature range should be distinct from those at which phase transitions for other elements of the mixture occur. Depending on the objective, that is determination of the effect of nucleic acids on the compactness of lipid-based complexes, or simulation of the interaction of carrier molecules with membranes, the samples are prepared differently. In the first case, the method of complex preparation should be reproduced and, in the second case, the carrier molecules should be added to preformed liposomes of a specific composition with biological relevance (Trabulo et al. 2012). For this purpose, large unilamellar vesicles (LUV), which provide a more realistic model of a membrane lipid bilayer, or multilamellar vesicles (MLV), which present much more cooperative transitions, can be used (Alves et al. 2008).

The DSC profiles register the excess of heat capacity (Cp) of the system as a function of temperature. After defining the interpolated baseline (the line connecting the pre- and post-transition baselines) different characteristic temperatures can be determined (**Figure 3.4**). The temperature of the onset (T_{on}) and the temperature at the endothermic peak (T_m) are automatically defined in the thermotropic profiles. To define the range of the phase transition or lateral phase separation (T_f–T_{on}), the temperature of completion of the phase transition (T_c) can be determined by the intersection of a tangent to the descendent slope of the endothermic peak with the baseline. Additionally, the calorimetric enthalpy changes (ΔH) of the thermotropic

events are normalized to the exact phospholipid content in each pan, determined by quantification of the inorganic phosphate obtained after carefully opening the pans, dissolving their contents in chloroform/methanol (3:1) and digesting them with perchloric acid (70%) (Trabulo et al. 2012).

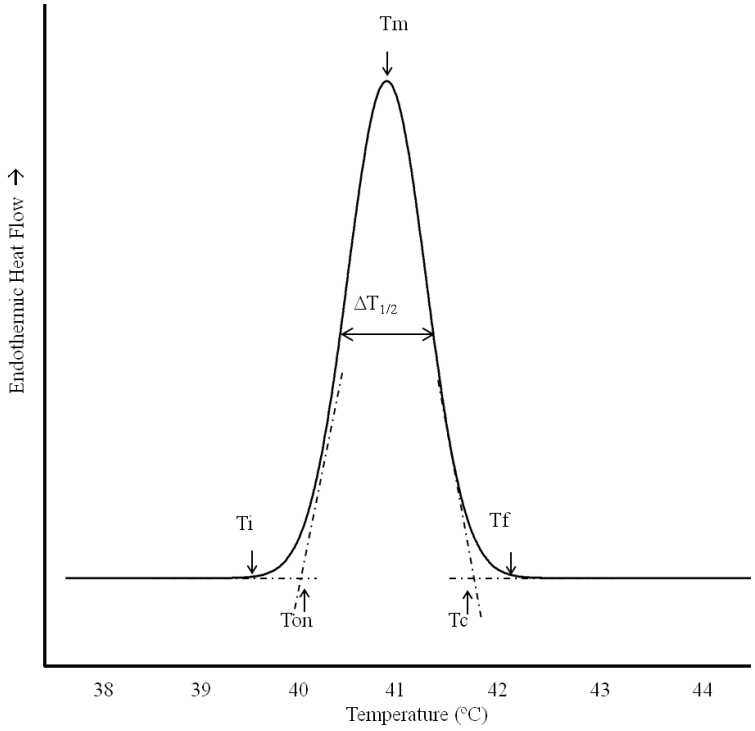

Figure 3.4 Example of a DSC profile (heating scan) of DPPG bilayers. Characteristic temperatures are indicated: T_i, when DSC record first deviates from the base line; T_{on}, determined by extrapolating to the baseline a tangent to the ascending slope of the endothermic peak; T_m, the peak maximum; T_c, determined by extrapolating to the baseline a tangent to the descendent slope of the endothermic peak; and T_f, obtained when the curve reaches again the baseline. $\Delta T_{1/2}$ (peak width at half maximum height) is also indicated (modified from Trabulo et al. 2012).

For determination of the effect of DNA molecules on the thermotropic behavior of gemini-based formulations, aqueous dispersions of gemini surfactants were incubated with plasmid DNA and, in the case of ternary complexes, a suspension of DOPE:Chol MLV was subsequently added. In parallel, equivalent formulations lacking DNA were also prepared. The preparations with gemini surfactants (2.5 to 3.0 wt%) were let to stabilize at room temperature for 15 min and for an extra period of 30 min when they also contained helper lipids.

To study the effect of CPP on the thermotropic behavior of membrane lipids, MLV suspensions (DPPC, DMPG, DPPG or a mixture of POPG/DPPE at 3/7 molar ratio, 75 mM) were incubated with peptide (lipid/peptide molar ratios in the range of 20/1 to 80/1) for 30 min in a water bath set 7-10 °C above the transition temperature of the lipids.

Gemini-based formulations or MLV suspensions containing the CPPs were centrifuged at 148,000 g for 45 min at 4 °C to obtain a pellet, which was then carefully transferred into a 50 μL capacity aluminum pan, subsequently hermetically sealed with a crimper. A void pan was used as reference.

All measurements were performed in a Perkin-Elmer Pyris 1 differential scanning calorimeter. Heating scans were performed over an appropriate temperature range, at a scan rate of 5 °C/min. To check the reproducibility of data, three heating scans were recorded for each sample. Data acquisition and analysis were performed using the software provided by Perkin Elmer.

3.2.3.3 Video-enhanced light microscopy analysis (VELM)

Video-enhanced light microscopy (VELM) results from the combination of optical microscopic techniques with advanced video and digital image-processing technology. In video-enhanced light microscopy, in particular video-enhanced contrast microscopy (VECM), a high-resolution high-light-level video camera receives its input from an unconventionally adjusted light microscope, usually employing Nomarski optics (differential interference contrast, DIC). Both analogue and digital contrast-enhancement procedures and background image subtraction are used to produce major gains of image quality. VECM involves a video-based monochrome imaging technique designed to visualize sub-resolution structures and to follow their dynamics in living systems in real time (Shotton, 1988).

For high-contrast imaging, under DIC mode, of aqueous dispersions of gemini surfactants (2.5-3.0 wt%), of gemini surfactant/DNA complexes (56 mM in gemini surfactant), and of gemini surfactant/DNA/helper lipids (200 μM in gemini surfactant), samples were prepared by dispersion of the solid surfactant in high purity Milli-Q water (gemini surfactant sample) and by using method B, as described above (section 3.2.1.1) to obtain the complexes of gemini surfactant/DNA and gemini

surfactant/DNA/helper lipids. For the thermal study of the dispersions, carefully sealed slide/coverslip preparations were made and temperature was controlled using a Linkam THMS600 heating stage (±0.1 °C). VELM images were obtained with an Olympus BX51 light microscope, under DIC mode. Images were acquired with an Olympus C5060 video camera and software CellA.

3.2.3.4 PicoGreen intercalation assay

PicoGreen is a fluorescent intercalating probe whose fluorescence is dramatically enhanced upon binding to nucleic acids (DNA or siRNAs). The accessibility of the probe to the nucleic acids in the delivery system is hence reflected by an increase in fluorescence and reports indirectly the efficiency of the protection conferred by the vector to the carried molecules. A SPECTRAmax Gemini EM fluorimeter (Molecular Devices, Union City, CA) was used to measure PicoGreen fluorescence. Complexes containing 0.2 µg of plasmid DNA or 14 pmol of siRNA, prepared in a total volume of 100 µL of HBS, were transferred to a 96-well (blackwalled) plate (Corning, NY, USA) followed by 15 min of incubation at 37 °C. Hundred microliters of PicoGreen (Molecular Probes, Eugene, OR), diluted according to the manufacturer's instructions (1:200 dilution in HBS buffer from a stock solution provided by Molecular Probes), were added to each sample. The fluorescence intensity of PicoGreen, directly proportional to the amount of accessible/free nucleic acid, was monitored at 25 °C (surfactant-, CPP- and polymer-based complexes) and at 37 °C (polymer-based complexes) for determining the extent of nucleic acid complexation. The excitation and emission wavelengths were set at 485 and 520 nm, respectively. For each formulation, the degree of nucleic acid protection conferred by the complexes was calculated by subtracting the values of residual fluorescence (PicoGreen in the absence of nucleic acid) from those obtained for each measurement, and expressed as a percentage of the control consisting of naked nucleic acid only, according to:

$$P_{nucleic\ \ acid} = 1 - \frac{F - F_{100}}{F_0 - F_{100}} \times 100$$

where F is the fluorescence intensity measured after adding the PicoGreen solution to the complexes, F_0 (corresponding to 0% of nucleic acid protection) was obtained by using free nucleic acid in the same amount as that associated with the complexes, F_{100}

(corresponding to 100% of nucleic acid protection) is the residual fluorescence intensity of a negative control obtained by using a PicoGreen solution without nucleic acid, which mimics a situation of 0% of nucleic acid available to the PicoGreen solution.

The potential destabilization of the complexes was assessed by monitoring the fluctuations of PicoGreen fluorescence intensity upon complex incubation for 15 min with SUV of DOPC or of a mixture of DOPE:DOPC:POPS (2:1:1 molar ratio), prepared from a suspension of MLV in HBS buffer by 19 times extrusion through two stacked polycarbonate filters of 50 nm pore diameter. Vesicle lipid-induced DNA deprotection was taken as the difference between the protection obtained for complexes in absence of the lipid vesicles and that obtained in their presence.

3.2.3.5 Förster resonance energy transfer (FRET)

Förster resonance energy transfer, a technique generally referred to by the acronym FRET, was used to monitor lipid mixing between two populations of vesicles induced by carrier molecules or mixing of lipids from a population of vesicles with the components of nucleic acid complexes (containing surfactants and helper lipids). This approach is based on the use of two fluorophores previously selected so that the emission band of one (the "energy donor") overlaps (at least partially) the excitation band of the other (the "energy acceptor"). When the two probes are in close proximity (approximately 10 nm of distance), the energy from a photon absorbed by the "energy donor" can be transferred non-radiatively to the "energy acceptor", which will then fluoresce as if it had been excited directly. Since the efficiency of fluorescence energy transfer between two given fluorophores is dependent upon their spatial separation, this technique provides a means to monitor the mixing of the lipids from vesicles labeled with adequated fluorophores (Struck et al., 1981). For this purpose, the fluorophores N-(7-nitro-2,1,3-benzoxadiazol-4-yl) (NBD), the "energy donor", and rhodamine (Rho), the "energy acceptor", are commonly used, being covalently coupled to the free amino group of phosphatidylethanolamine to provide lipid analogues, which should be incorporated into lipid bilayers at appropriate surface densities (ratio of fluorescent lipid to total lipid of 1 mol%). When labeled vesicles are added to non-labeled vesicles or other structures, at such conditions that

the mixing of components from both structures is induced, the surface density of the probes decreases and the distance between the "energy donor" and "energy acceptor" increases, resulting in a decreased efficiency of resonance energy transfer, which can be measured experimentally by an increase in the fluorescence of the "energy donor" or a decrease in the fluorescence of the "energy acceptor" (**Figure 3.5**). Alternatively, a population of vesicles can be labeled with the "energy donor" and the other with the "energy acceptor". In this case, lipid mixing between the two vesicle populations promotes the proximity of the fluorescent probes with an increase in FRET.

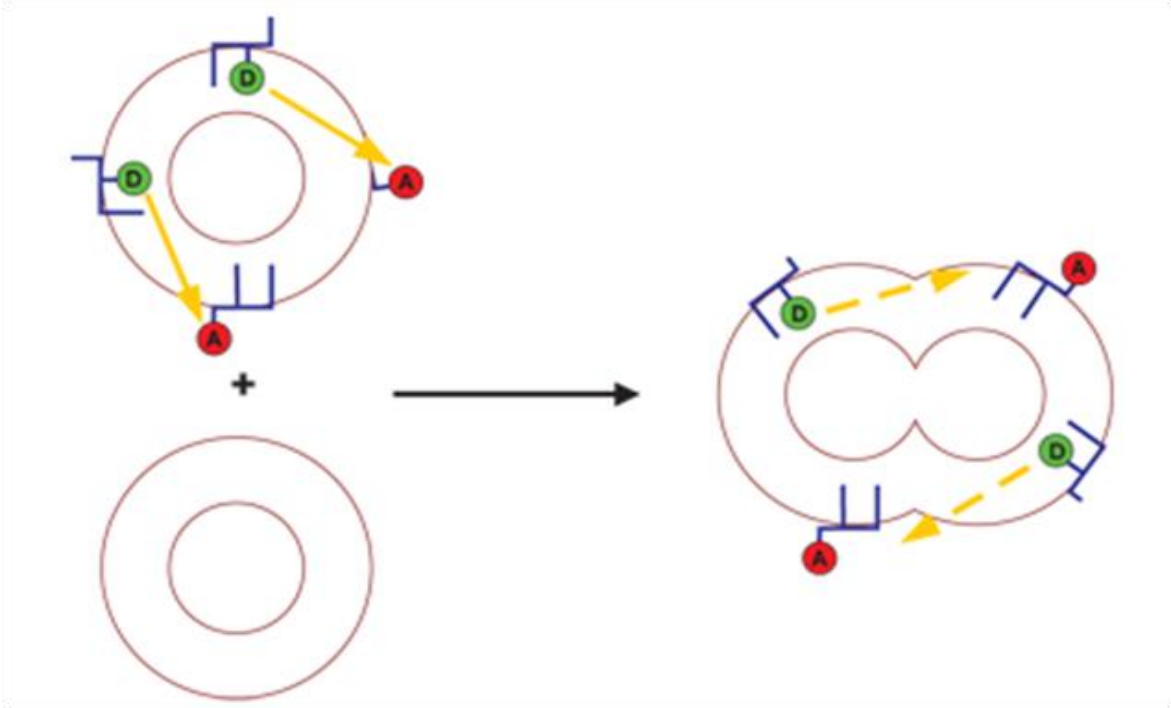

Figure 3.5 Representation of a component-mixing assay based on Förster resonance energy transfer (FRET). The average spatial separation of the donor (D) and acceptor (A) lipid probes increases upon mixture of labeled membranes with unlabeled membranes, resulting in decreased efficiency of proximity-dependent FRET. Decreased FRET efficiency is registered by increased donor fluorescence intensity and decreased acceptor fluorescence intensity (from www.probes.com/handbook/boxes/0432.html).

In the present work, FRET experiments were performed in order to assess the extent of the interaction between components of the cationic surfactant-based vectors and vesicles mimicking the lipid composition of different membranes and different membrane regions as follows: non-raft regions of the cytoplasmic membrane (POPC:DOPE at 2:1 molar ratio), lipid-rafts (SM:DMPC:Chol at 1:1:1 molar ratio), late

endosomal membrane (POPC:DOPE:SM:BMP at 5:2:1:2 molar ratio) and mitochondrial membrane (DOPC:DOPE:TOCL at 1:1:1 molar ratio). Lipid vesicles were labeled with 1% N-(7-nitrobenz-2-oxa-1, 3-diazol-4-yl)-phosphatidylethanolamine (NBD-PE) and 1% rhodamine-phosphatidylethanolamine (Rho-PE) (Molecular Probes, Eugene, OR). Aliquots of chloroform solutions of both probes were added to the lipid mixtures in chloroform. This solvent was removed by evaporation in a rotatory evaporator and the dried lipid films were hydrated in HBS saline buffer (pH 7.4). The resulting MLV were then sonicated for 3 min and extruded 15 times through two stacked polycarbonate filters of 100 nm pore diameter using a Liposofast device (Avestin, Toronto, Canada) to obtain LUV. Phospholipid content was determined by measuring the inorganic phosphate (Murphy & Riley 1962) released after hydrolysis of dried phospholipids, at 180 °C, in 70% HClO4 (Bottcher et al. 1961). Component mixing assays were performed in a 96-well black-walled plate, using 400 µM of labeled lipid vesicles and 100 µM of the different surfactant-based complexes. Component mixing was measured at 37 °C, after an incubation period of 15 min at the same temperature, by monitoring fluorescence intensity alterations in a SPECTRAmax Gemini EM fluorimeter (Molecular Devices, Union City, CA), using the excitation and emission wavelengths of 470 and 535 nm, respectively. At the concentration at which the probes were incorporated in the vesicles (1%), Rho-PE efficiently suppressed the emission of NBD-PE at 535 nm, when the excitation wavelength was set at 470 nm. Due to the energy transfer dependence on the distance between the donor and acceptor probes, the mixing of components of the complexes with lipids of the fluorescently-labeled preparations generated an increase of NBD-fluorescence, reflecting an increase in the average distance between probes in the lipid environment. The percentage of component mixing was calculated according to the equation:

$$Component\ mixing = \frac{F - F_0}{F_{100} - F_0} \times 100$$

where F corresponds to the fluorescence detected after 15 minutes of complex incubation with the vesicles, F_0 corresponds to the initial vesicle fluorescence in the absence of the complexes, and F_{100} corresponds to the maximal fluorescence, which was obtained after complete lysis of the vesicles with octaethylene glycol

monododecyl ether ($C_{12}E_8$) (0.5% v/v). For each complex formulation, three independent experiments were carried out at pH 7.4. Experiments with vesicles mimicking the composition of the late endosome were also performed at pH 5.2. Briefly, after incubation of the complexes with the vesicles at 37 °C for 15 min at pH 7.4, the pH was lowered to 5.2 by the addition of HCl (1 M) and NBD-PE fluorescence was measured (F). The percentage of component mixing at pH 5.2 was calculated according to the above equation, where F_0 and F_{100} correspond to the minimum fluorescence obtained with the labeled vesicles at pH 7.4 and to the maximum fluorescence, obtained with $C_{12}E_8$ at pH 7.4, respectively.

3.2.3.6 Calcein release

Calcein fluorescence dequenching is commonly used to assess vesicle membrane destabilization by monitoring the release of their aqueous content. Calcein fluorescence dequenching is observed when the fluorophore encapsulated inside the vesicles at a self-quenching concentration leaks out and dilutes in the surrounding buffer upon membrane destabilization. The relief of self-quenching of encapsulated calcein measures the leakage of vesicle contents and, hence, the stability of the vesicles under given conditions.

Calcein release experiments were performed in order to assess the ability of cationic surfactant-based gene delivery systems to destabilize vesicles (LUV) mimicking the lipid composition of non-raft regions of the cytoplasmic membrane (POPC:DOPE at 2:1 molar ratio), lipid-rafts (SM:DMPC:Chol at 1:1:1 molar ratio), late endosomal membrane (POPC:DOPE:SM:BMP at 5:2:1:2 molar ratio) and mitochondrial membrane (DOPC:DOPE:TOCL at 1:1:1 molar ratio), which were prepared as described in the previous section, but using 80 mM calcein (Sigma, St. Louis, MO) in 50 mM HEPES and 1 mM EDTA (pH 8.4) to resuspend the dried films of lipid mixtures. Free calcein was separated from the dye-containing LUV by size exclusion chromatography on a Sephadex G-75 column, using a buffer (20 mM HEPES, 140 mM NaCl and 1 mM EDTA, pH 7.4) with the same osmolarity (300 mOsm) of the calcein solution. Phospholipid content was determined as previously described. Vesicle leakage assays were performed on a 96-well black-walled plate, using labeled lipid vesicles (400 μM) and surfactant-based complexes (100 μM in surfactant). After

incubation of the vesicles with the complexes at 37 °C for a period of 15 min, calcein release was measured at the same temperature by monitoring fluorescence intensity in a SPECTRAmax Gemini EM fluorimeter (Molecular Devices, Union City, CA), using the excitation and emission wavelengths of 494 and 517 nm, respectively. The percentage of complex-induced leakage from the vesicles was calculated according to the equation:

$$Calcein\ release = \frac{I - I_0}{I_{100} - I_0} \times 100$$

where I corresponds to the fluorescence detected after 15 min incubation of the surfactant-based complexes with the vesicles, I_0 corresponds to the vesicle fluorescence in the absence of complexes, and I_{100} corresponds to the maximum fluorescence, which was obtained after the complete lysis of the vesicles with $C_{12}E_8$ (0.5% v/v). For each condition, three independent assays were performed.

3.2.4 Cell culture and maintenance

All cells lines were maintained at 37 °C in the appropriate medium and humidified atmosphere containing 5% CO_2. HeLa cells (human epithelial cervical carcinoma cell line) and A549 cells (human epithelial lung adenocarcinoma) were maintained in culture in Dulbecco's modified Eagle's medium–high glucose (DMEM–HG; Sigma, St. Louis, MO, USA), supplemented with heat inactivated fetal bovine serum (FBS; Sigma, St. Louis, MO, USA) (10% v/v), penicillin (100 U/mL) and streptomycin (100 µg/mL). HT1080 cells (human fibrosarcoma, stably transfected in order to permanently express GFP) were maintained in Dulbecco's modified Eagle's low glucose medium (DMEM-LG; Sigma, St. Louis, MO, USA) supplemented with heat-inactivated FBS (10% v/v), penicillin (100 U/mL) and streptomycin (100 µg/mL). The cells were grown in monolayer and detached by treatment with 0.25% trypsin solution (Sigma, St. Louis, MO, USA).

3.2.5 Transfection

Cells plated at a density of 25 000 cells/cm^2 were incubated for 24 h at 37 °C, under 5% CO_2, in complete medium supplemented with FBS (10% v/v) and antibiotics before transfection. Immediately before addition of plain or ternary complexes, cells

were washed and the medium was replaced with fresh medium. Surfactant-, peptide- and polymer-based complexes, prepared at different (+/-) charge ratios as described above (section 3.2.1), were added to the cells in a total volume of 100 µL in order to obtain a final concentration of 1µg/mL for DNA (pEGFP-C1) and 50 nM for siRNA. Lipofectamine 2000 (Invitrogen, Carlsbad, CA) diluted in OptiMEM was used, according to the manufacturer's instructions, as a positive control for DNA and siRNA delivery. Parallel gene silencing studies employing a nonsilencing siRNA sequence (Mut sequence) were performed, to ensure the specificity of the selected siRNA and the absence of off-target effects. Following 4 h of incubation, the medium was replaced with fresh medium containing FBS (10% v/v) and antibiotics, and the cells were further incubated for 44 h to allow gene expression/silencing.
Flow cytometry, QRT-PCR and Western blot were used as complementary techniques, for an accurate evaluation of transfection efficiency.

3.2.5.1 Analysis of GFP expression by flow cytometry

Multiple physical characteristics of cells, such as relative hydrodynamic diameter, relative granularity or internal complexity, and relative fluorescence intensity, can be evaluated by flow cytometry as cells pass through a laser beam. The mode of scattering of the incident laser light and emitting fluorescence by cells were recorded and used to determine the different properties of the cells. Flow cytometry measures the fluorescence per cell, which constitutes an advantage with respect to other techniques, in which light absorption and emission at specific wavelengths are measured for an entire population of cells (Cardoso et al. 2009).
In the present work, the transfection efficiency mediated by the different complexes was evaluated through analysis of the expression of green fluorescent protein (GFP) by flow cytometry. Briefly, 48 h after transfection, cells (HeLa, A549 or HT1080) were washed once with PBS and detached with trypsin at 0.25% (10 min at 37 °C). Cells were further washed three times by centrifugation (200 g, 4 °C, 5 min) in ice-cold PBS. The resulting pellet was resuspended in ice-cold PBS, and the samples were immediately analyzed. Flow cytometry analysis was performed in live cells using a Becton Dickinson FACSCalibur flow cytometer (BD Biosciences, San Jose, CA, USA). Data were collected and analyzed using CellQuest software. To discriminate between

viable and dead cells and to exclude doublets, cells were appropriately gated by forward/side scatter and pulse width from a total of 10,000 events. The fluorescein isothiocyanate (FITC) bandpass filter was used in emission detection. GFP expression was evaluated through the analysis of the percentage of transfected cells and of the geometric mean fluorescence intensity with respect to control cells (non-transfected cells). GFP silencing was evaluated through the analysis of the fluorescence intensity with respect to cells treated with mut siRNA (scrambled sequence) complexes. The analysis of the percentage of transfected cells (transfection efficiency) gives information on the number of cells expressing detectable GFP with respect to the total number of live cells, whereas the analysis of fluorescence intensity (transfection activity) indicates the average amount of reporter gene expression in the cells.

3.2.5.2 Determination of mRNA levels by quantitative real time polymerase chain reaction (QRT-PCR)

QRT-PCR is a useful tool to quantify the levels of mRNA of a given target protein upon cell transfection. Following 24 h of cell incubation with target or mut siRNAs, total RNA was extracted from cells using the MasterPure RNA Purification Kit (Epicenter Biotechnologies, Madison, WI, USA), according to the manufacturer's recommendations for cultured cells. RNA conversion into cDNA was performed using the Superscript III First Strand Synthesis Kit (Invitrogen, Karlsruhe, Germany), according to the manufacturer's instructions. For each sample, cDNA was produced from 0.5 μg of total RNA in an iQ5 thermocycler (Bio-Rad), by applying the following protocol: 10 min at 25 °C (stabilization of the primers and template), 30 min at 55 °C (cDNA synthesis), and 5 min at 85 °C (reaction termination with inactivation of the reverse transcriptase). After cDNA synthesis, 30 min incubation with RNase H at 37 °C was performed to remove any remaining RNA contamination. Finally, the cDNA was diluted 1:3 with RNase-free water prior to quantification by QRT-PCR (Cardoso et al., 2007). Quantitative PCR was performed in an iQ5 thermocycler using 96-well microtiter plates and the iQ SYBR Green Supermix Kit (Bio-Rad). Primers for the selected target (survivin) and reference genes (HPRT) were acquired from Qiagen (QuantiTect Primer). As expected, the expression of the reference gene did not vary

between samples. Target gene expression was normalized to the amount of total RNA, by comparison of the target gene with the endogenous reference gene.

A master mix was prepared for each primer set, containing a fixed volume of SYBR Green Supermix and the appropriate amount of each primer to yield a final concentration of 150 nM. For each reaction, 20 µL of master mix were added to 5 µL of template cDNA. All reactions were performed at least in duplicate (two cDNA reactions per RNA sample) at a final volume of 25 µL per well, using the iQ5 Optical System Software (Bio-Rad). The reaction conditions consisted of enzyme activation and well-factor determination at 95 °C for 1 min and 30 s, followed by 40 cycles at 95 °C for 10 s (denaturation), 30 s at 55 °C (annealing), and 30 s at 72 °C (elongation). The melting curve protocol started immediately after amplification and consisted of 1 min heating at 55 °C followed by eighty 10 s steps, with an increase in temperature of 0.5 °C at each step. This protocol allows to evaluate the efficiency of sample amplification and to determine the integrity and purity of the cDNA. Threshold values for threshold cycle (Ct) determination were generated automatically by the iQ5 Optical System Software (Cardoso et al. 2007).

Target gene expression in cells transfected with the target siRNAs was compared with that in cells treated with mut siRNAs to determine gene knockdown. Differences in gene expression between nontransfected cells and cells transfected with the mut siRNAs indicate the presence of nonspecific effects. The percentage of gene knockdown was determined by the ΔΔCt method, using one of the reference genes (HPRT gene), according to the equations:

$$\Delta C_{t(target\ \ siRNA)} = C_{t(target\ \ gene)} - C_{t(HPRT\ gene)}$$

$$\Delta C_{t(mut\ siRNA)} = C_{t(target\ \ gene)} - C_{t(HPRT\ gene)}$$

$$\Delta\Delta C_t = \Delta C_{t(target\ siRNA)} - \Delta C_{t(mut\ siRNA)}$$

$$\%\ knockdown = 100\% - (2^{-\Delta\Delta C_t} \times 100)$$

The ΔΔCt value indicates the changes in RNA transcription caused by treatment with target siRNAs. A positive ΔΔCt value indicates downregulation of the target mRNA. The selected housekeeping genes should have amplification efficiencies similar to the target gene. The amplification efficiencies can be determined according to:

$$E = 10^{-1/S} - 1$$

where S is the slope of the standard curve obtained for each gene. To compare the amplification efficiencies of the target and reference genes, the Ct values of the target gene are subtracted from the Ct values of the reference gene. The difference in Ct values is then plotted against the logarithm of the total RNA amount. If the slope of the resulting straight line is less than 0.1, amplification efficiencies are comparable.

3.2.5.3 Determination of GFP levels by Western blot analysis

Western blot experiments were performed 72 h after transfection to detect the maximum protein knockdown. Briefly, protein extracts were obtained from cells transfected in 6-well microplates using a lysis buffer (50 mM NaCl, 50 mM EDTA, 1% Triton X-100) containing a protease inhibitor cocktail (Sigma), DTT (10 mg/ml), and PMSF (1 mM). During this procedure, all samples were maintained at 4 °C to minimize protein degradation. Protein content was determined using the Bio-Rad protein quantification kit, and 20 µg of total protein were resuspended in protein loading buffer (20% glycerol, 10% SDS, and 0.1% bromophenol blue), incubated for 2 min at 95 °C, and loaded onto a 15% polyacrylamide gel. After electrophoresis, the proteins were blotted onto a PVDF membrane according to standard protocols. After blocking in 5% nonfat milk, the membrane was incubated with the appropriate primary antibody (anti-survivin 1:200, Santa Cruz) overnight at 4 °C, and with the appropriate secondary antibody (1:10,000, Sigma) for 2 h at room temperature. Equal protein loading was shown by reprobing the membrane with an anti-α-tubulin antibody (1:10,000, Sigma) and with the appropriate secondary antibody. After this incubation period, the membrane was washed several times with saline buffer (TBS/T: 25 mM Tris–HCl, 150 mM NaCl, 0.1% Tween, and 5 mg/mL nonfat powder milk), and incubated with ECF (alkaline phosphatase substrate; 20 mL of ECF/cm^2 of membrane) for 5 min at room temperature. The membrane was then submitted to fluorescence detection at 570 nm using a Storm-860 (Molecular Dynamics, CA). The analysis of band intensity was performed using the Image J software (Wayne Rasband National Institutes of Health, USA). Target band intensity of all samples was normalized for individual α-tubulin band intensities to correct for variation in total protein content, and any differences in sample handling. Results were expressed as percentage of protein levels with respect to nontransfected controls.

3.2.6 Evaluation of cell viability

The delivery systems used to transfect cells may lead to toxicity, which can be a limitation to their application *in vitro* and *in vivo*. Therefore, evaluation of the biological activity of DNA and siRNA complexes should be accompanied by studies on their cytotoxicity. Cell viability under the different experimental conditions was assessed by a modified Alamar Blue assay (Simões et al. 1999). This assay is simple, involving the use of a sole reagent and limited manipulation. Alamar Blue is nontoxic to the cells and to the user and, because no cell lysis is required, the cells can still be used for other experiments or submitted to further analysis. This assay measures the extent of the conversion of a dye (resazurin) in its metabolite (resorufin), thus reflecting the redox activity of viable cells (Konopka et al., 1996).

Briefly, 48 h (for flow cytometry and QRT-PCR analysis) or 72 h (for Western blot analysis) after transfection, 0.3 mL of resazurin (10% v/v) dye in complete DMEM–HG (HeLa and A549 cells) or DMEM-LG (HT1080 cells) medium were added to each well. After color development (45 min to 1 h of incubation at 37 °C), 150 µL of the supernatant were collected from each well and transferred to 96-well plates. The absorbance at 570 and 600 nm (information provided by the supplier) was measured in a SPECTRAmax PLUS 384 spectrophotometer (Molecular Devices, Union City, CA) and cell viability was calculated according to the equation:

$$Cell\ viability\ (\%\ of\ the\ control) = \frac{A_{570} - A_{600}}{A'_{570} - A'_{600}} \times 100$$

where A_{570} and A_{600} are the absorbances of the samples, and A'_{570} and A'_{600} are those of the control (non-treated cells), at the indicated wavelengths.

3.2.7 Assessment of complex-cell interactions

Different experiments were performed to examine the mechanisms by which complexes delivered genetic material into cells. Standard protocols to assess the relative contribution of membrane interaction or of endocytosis to the process of intracellular nucleic acid delivery mediated by complexes were carried out.

3.2.7.1 Cell association

Cell association experiments were performed at 37 °C under the same experimental conditions described for transfection. Briefly, HeLa cells were incubated for 4 h with the complexes containing the fluorescent probe Rh-PE (Avanti Polar Lipids, Alabaster, AL) at 5 mol%, in a final volume of 0.5 mL of serum-free OptiMEM. The medium containing the complexes that did not associate to cells was then collected and the fluorescence was measured at 37 °C following the addition of $C_{12}E_8$ (Sigma, St. Louis, MO), at a final concentration of 0.5% (v/v). To assess the fluorescence of complexes associated with the cells, cells were rinsed with serum-free OptiMEM, detached from the culture plates and then suspended in 0.5 mL of medium. The fluorescence of the cell suspension was measured at 37 °C in the presence of $C_{12}E_8$, as described above. The extent of cell association was determined according to the equation:

$$Cell\ association = \frac{F_{cells}}{F_{nonassociated} + F_{cells}} \times 100$$

where F_{cells} is the value of fluorescence of the complexes associated with the cells and $F_{nonassociated}$ is the value of fluorescence of nonassociated complexes (supernatant) (Pedroso de Lima et al. 2003).

3.2.7.2 Cellular internalization pathways

To address the mechanisms through which surfactant-based complexes were internalized by cells, transfection experiments were performed both at low temperature (4 °C) and in the presence of inhibitors for different endocytic pathways. For this purpose, plated HeLa cells were washed with PBS and incubated (37 °C, 30 min) in serum-free OptiMEM with the following inhibitors of endocytosis (from Sigma): (i) chlorpromazine (30 μM); (ii) fillipin III (5 μg/mL) or (iii) amiloride hydrochloride (5 mM). Parallel experiments were performed by incubating HeLa cells (not treated with these inhibitors) at 4 °C for 30 min. Thereafter, cells either inhibitor-treated or maintained at 4 °C were incubated with the complexes for 1 h. To confirm that the endocytosis inhibitors tested compromised selectively different endocytic pathways, their effects on the cellular uptake of fluorescently labeled markers (transferrin as a known marker of clathrin-mediated endocytosis, and lactosylceramide as a marker of raft/caveolae-dependent endocytosis) were

analyzed. Cytotoxicity was assessed following cell treatment with each of the drugs by the Alamar blue assay, as described above (section 3.2.6). Flow cytometry analysis was performed as described above (section 3.2.5.1) to evaluate transfection efficiency of the complexes in cells pre-incubated at 4 °C (a condition that impairs any energy-dependent endocytic pathway) or at 37 °C with each of the endocytosis inhibitors (Pedroso de Lima et al. 2003).

3.2.7.3 Analysis of siRNA internalization and intracellular distribution by confocal microscopy

The efficiency of siRNA entry into the cell and its intracellular distribution is usually performed employing fluorescently labeled siRNAs. In the present work, HT1080 cells (0.2×10^5 cells/well) were plated onto 8-well chambered coverslips (Lab-Tek II, Thermo, Waltham, MA) and incubated for 24 h before addition of siRNA delivery systems. Following incubation for 4 h with naked or complex-formulated Cy3-labeled siRNAs, or following further 20 h of incubation in serum-containing medium, cells were rinsed twice with PBS and incubated with Hoechst 33342 dye (1 μg/mL, Molecular Probes, Eugene, OR) and immediately visualized by confocal microscopy in a Zeiss Axiovert confocal scanning microscope (Zeiss, Jena, Germany), under the 60× oil immersion objective.

3.2.8 Statistical analysis

Data are presented as mean ± SD of at least three independent experiments. The significance of the results was statistically analyzed by a one-way analysis of variance (ANOVA) with Tukey's multiple pairwise comparison, unless stated otherwise. Statistical significance was set at $p < 0.05$.

Chapter 4

Bis-Quaternary Gemini Surfactants as Components of Nonviral Gene Delivery Systems: a Comprehensive Study from Physicochemical Properties to Membrane Interactions

A.M. Cardoso, C.M. Morais, S.G. Silva, E.F. Marques, M.C. Pedroso de Lima and A.S. Jurado, "*Bis-Quaternary Gemini Surfactants as Components of Nonviral Gene Delivery Systems: a Comprehensive Study from Physicochemical Properties to Membrane Interactions*" Accepted for publication in the International Journal of Pharmaceutics.

4.1 Abstract

Gemini surfactants have been successfully used as components of gene delivery systems. In the present work, a family of gemini surfactants, represented by the general structure $[C_mH_{2m+1}(CH_3)_2N^+(CH_2)_sN^+(CH_3)_2C_mH_{2m+1}]2Br^-$, or simply m-s-m, was used to prepare cationic gene carriers, aiming at their application in transfection studies. An extensive characterization of the gemini surfactant-based complexes, produced with and without the helper lipids cholesterol and DOPE, was carried out in order to correlate their physico-chemical properties with transfection efficiency. The most efficient complexes were those containing helper lipids, which, combining amphiphiles with propensity to form structures with different intrinsic curvatures, displayed a morphologically labile architecture, putatively implicated in the efficient DNA release upon complex interaction with membranes. While complexes lacking helper lipids were translocated directly across the lipid bilayer, complexes containing helper lipids were taken up by cells also by macropinocytosis. This study contributes to shed light on the relationship between important physico-chemical properties of surfactant-based DNA vectors and their efficiency to promote gene transfer, which may represent a step forward to the rational design of gene delivery systems.

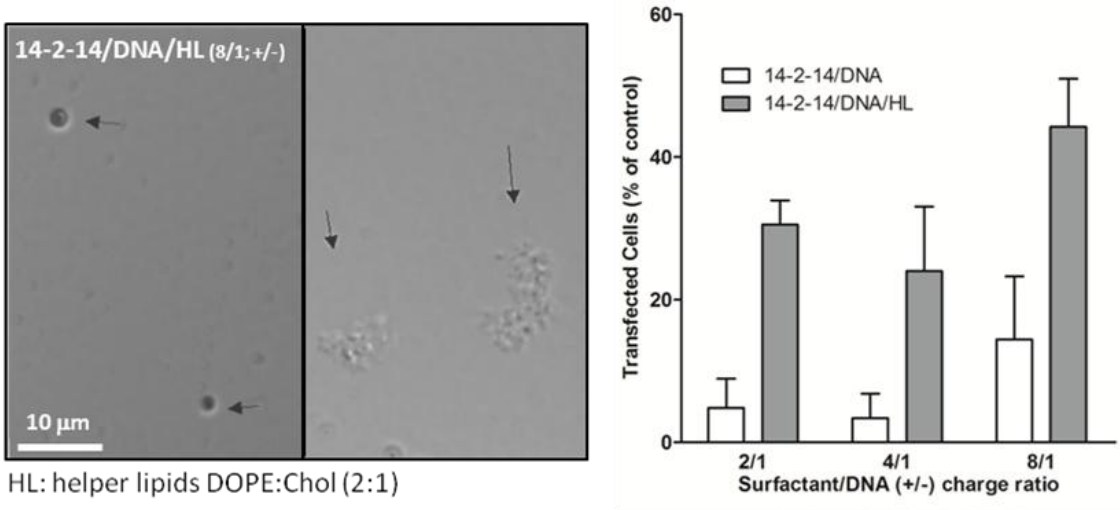

Gemini-based complexes containing the helper lipids (HL) DOPE and cholesterol form vesicular and multivesicular structures, which are able to efficiently transfect HeLa cells.

4.2 INTRODUCTION

Gemini surfactants are amphiphilic molecules composed of two sets of a polar head group plus an hydrocarbon chain, linked by a spacer at the level or close to the head group (Menger & Littau 1991). Interest in these molecules originally sparkled from the work of Menger and Littau in 1991 (Menger & Littau 1991), and, over the last twenty years, several families of gemini surfactants were produced and extensively studied in terms of their aggregation and surface properties (Alami et al. 1993; Buijnsters et al. 2002; Silva et al. 2012). Gemini surfactants have been shown to present several relevant biological activities, namely as antimicrobial (Murguía et al. 2008; Badr et al. 2010; Colomer et al. 2011; Hoque et al. 2012; Obłąk et al. 2014) and antifungal (Murguía et al. 2008; Obłąk et al. 2013) agents. Their application in drug delivery has also been reported as a promising approach. In fact, recent studies have shown that gemini surfactants are able to facilitate drug delivery by enhancing the drug load and the cellular entry of a peptide-based drug delivery system (Ding et al. 2011), and a cyclodextrin-modified gemini surfactant was used to successfully deliver anticancer drugs (Singh et al. 2012). However, the most extensively studied application of cationic gemini surfactants regards their use as nucleic acid delivery systems (Rosenzweig et al. 2001; Bombelli et al. 2005a; Badea et al. 2005; Badea et al. 2007; Wang & Wettig 2011; Damen et al. 2010; Donkuru et al. 2010; Cardoso et al. 2011; Mohammed-Saeid et al. 2012; Grigoriev et al. 2012; Wang et al. 2013).

The therapeutic potential of DNA depends on the development of efficient and safe vehicles that can overcome the potential bottle-neck for intracellular gene delivery. Due to the propensity of gemini surfactants for structure modulation (Menger & Littau 1991; Rosenzweig et al. 2001; Wang et al. 2007) these compounds have been designed in order to promote low toxicity and immunogenicity, high stability in biological fluids and biodegradability, which are essential requirements for safe gene delivery systems (Kirby et al. 2003).

In the case of *bis-quat* gemini surfactants, the presence of two quaternary ammonium groups per surfactant molecule, which increases their strength of interaction with DNA (Rosenzweig et al. 2001), as well as the hydrophobic contribution from the spacer, which increases surfactant tendency to self-assemble (Menger & Keiper

2000), contribute to enhance the formation of stable gemini surfactant-DNA complexes (Karlsson et al. 2002; Bombelli et al. 2005b), when compared to the monomeric counterparts of the gemini. The length and corresponding conformational flexibility of the spacer (Luciani et al. 2007), and the hydrophobicity of the two main hydrocarbon chains (Wang et al. 2007), influence the type of self-assembled structures formed *a priori*, as well as their complexation with DNA. Thus, gemini surfactants present a rich mesomorphism in aqueous solution, with the ability to form *inter alia* non-lamellar structures (Zana 2002a; In & Zana 2007), regarded as an important feature for transfection competence (Zuhorn et al. 2002; Wasungu et al. 2006a; Koynova et al. 2006). In this context, cationic gemini surfactants exhibit suitable features for the design of promising gene delivery systems.

In several cases, however, gemini surfactants were found to be unable to efficiently mediate gene delivery *per se*, benefiting from the addition of other components, such as helper lipids, to perform this task (Badea et al. 2005). The lipid 1,2-dioleoyl-sn-glycero-3-phosphoethanolamine (DOPE) has been reported to enhance transfection efficiency (Hui et al. 1996; Cardoso et al. 2011) by facilitating the formation of non-bilayer structures (Siegel & Epand 1997), and the enhancing effect of cholesterol on transfection has been assigned to its ability tostabilize a fluid, yet ordered, lamellar phase (liquid-ordered phase, Lo) (Feigenson 2006), which may guide a lipid/DNA arrangement that combines stability with lability, two essential features of an efficient gene delivery system. The incorporation of helper lipids in the surfactant-based system has the potential to promote structural alterations and increase the susceptibility for DNA exposure in the presence of model membranes containing anionic lipids (Cardoso et al. 2011).On the other hand, in complexes formulated with three components—gemini surfactant, helper lipids and DNA—the order of component addition is decisive to the achievement of the maximal performance of the systems (Badea et al. 2005), as has been described for other types of gene delivery vectors, such as those formulated with cationic lipids (Penacho et al. 2008) or cell-penetrating peptides (Trabulo et al. 2008; Cardoso et al. 2013).

In the present study, the main purpose is to unveil the properties of gemini surfactant-based delivery systems that promote high transfection efficiency, in parallel with low cytotoxicity, with the ultimate goal of paving the way to a more

rational design of DNA delivery systems. In a previous work (Cardoso et al. 2011), a gemini surfactant of the alkanediyl-α,ω-bis(alkyldimethylammonium bromide) family, or m-s-m (**Figure 4.1**), containing 14 carbon atoms-long hydrocarbon chains and a two carbon atom-long spacer (14-2-14) showed that, in the presence of helper lipids, was able to protect DNA from degradation and to efficiently transfect cultured mouse mammary adenocarcinoma cells. In the present work, we aimed at further investigating this approach, by broadening the study to five *bis-quaternary* gemini surfactants of the m-s-m family differing in the length of their spacer or main hydrocarbon chains. These surfactants were used to assess their ability to mediate transfection, either *per se* or in a mixture with the helper lipids DOPE and cholesterol, kept at constant molar ratio and hence treated here as single helper lipid component. Efforts have thus been made to unveil the properties that underlie the most suitable gene delivery systems. With this purpose, an extensive characterization of gemini-based complexes was performed in terms of their physicochemical properties (size, surface charge, and colloidal stability), surfactant/lipid mesomorphic behavior and protection conferred to the carried nucleic acids. Complex-membrane interaction, membrane association/binding and cellular internalization, regarded as major events for an effective gene delivery, were also addressed.

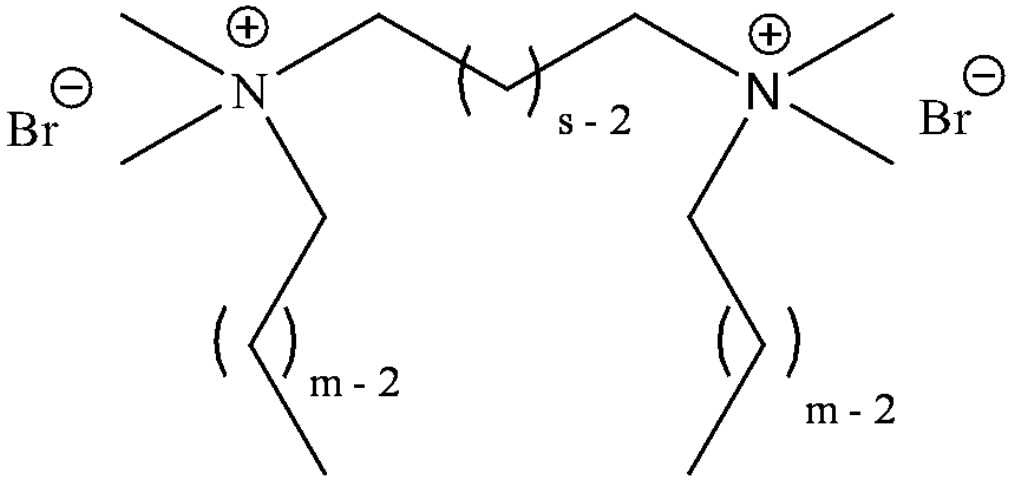

Figure 4.1 Schematic representation of the general structure of the *bis-quaternary* gemini surfactants used in this work (s = 2, 5 or 10 and m = 12, 14 or 16).

4.3 MATERIALS AND METHODS

Materials

The gemini surfactants were synthesized by the method reported by Menger (Menger & Littau 1993) and purified by recrystallization. The purity of the compounds was evaluated by NMR and mass spectrometry and further confirmed by the *cmc* values, obtained by surface tension measurements, which were all in very good agreement with those already reported in the literature (Burrows et al. 2007; Zana 1997). The lipids 1,2-dioleoyl-sn-glycero-3-phosphoethanolamine (DOPE), cholesterol, 1,2-dioleoyl-sn-glycero-3-phosphocholine (DOPC) and 1-palmitoyl-2-oleoyl-sn-glycero-3-phospho-L-serine (POPS) were purchased from Avanti Polar Lipids (Alabaster, AL). All the other chemicals were of the highest grade.

Cells

HeLa cells (human epithelial cervical carcinoma cell line) were maintained in culture at 37 °C, under 5% CO_2, in Dulbecco's modified Eagle's medium–high glucose (DMEM–HG; Sigma, St. Louis, MO, USA), supplemented with 10% (v/v) heat inactivated fetal bovine serum (FBS; Sigma, St. Louis, MO, USA), penicillin (100 U/mL) and streptomycin (100 µg/mL). The cells were grown in monolayer and detached by treatment with 0.25% trypsin solution (Sigma, St. Louis, MO, USA).

Complex Preparation

Plain complexes of surfactant/DNA or ternary complexes of surfactant/helper lipid/DNA were prepared using two different methods (A and B). Method A was previously reported (Cardoso et al. 2011) and consisted of dissolving gemini surfactants or their mixture with DOPE and cholesterol in chloroform, at the desired molar ratios (3:2:1 and 3:4:2). Solutions were then dried under vacuum in a rotatory evaporator and the resulting lipid films were hydrated with deionised water to a final lipid concentration of 2 mM. Surfactant or surfactant plus lipid dispersions were then sonicated for 3 min, extruded 21 times through two stacked polycarbonate filters of 50 nm pore diameter, using a Liposofast device (Avestin, Toronto, Canada), and after

a three-fold dilution with deionised water, they were filter-sterilized utilizing 0.22 μm pore-diameter filters (Schleicher & Schuell, BioScience, Germany). Plain complexes (surfactant/DNA) and ternary complexes (surfactant/DNA/lipid) were prepared by mixing 100 μL of a HEPES-buffered saline solution (HBS; 100 mM NaCl, 20 mM HEPES, pH 7.4) containing 0.5 μg of pEGFP-C1 plasmid DNA encoding GFP (Clontech, CA, USA) with a volume of the previously prepared surfactant suspensions (without or with lipids), to obtain surfactant/DNA (+/-) charge ratios in the range of 2/1 to 8/1. The resulting mixtures were then incubated for 15 min at room temperature.

Method B consisted of an adaptation of the method described by Badea and coworkers (Badea et al. 2005). Briefly, aqueous solutions (0.5 mM) of gemini surfactants were filtered through 0.22 μm pore-diameter filters (Schleicher & Schuell, BioScience, Germany), and a solution of DOPE and cholesterol (2:1 molar ratio) in chloroform was dried under vacuum in a rotatory evaporator, the resulting lipid film being hydrated with HBS (pH 9.0) to a final lipid concentration of 0.5 mM. The resulting multilamellar vesicles (MLV) of DOPE plus cholesterol were then sonicated for 3 min and filtered through 0.22 μm pore-diameter filters (Schleicher & Schuell, BioScience, Germany). Complexes were prepared by mixing 100 μl of HBS containing 0.5 μg of pEGFP-C1 plasmid DNA encoding GFP with aliquots of the aqueous gemini surfactant solution, to obtain surfactant/DNA (+/-) charge ratios in the range of 2/1 to 8/1 thereafter incubated at room temperature for 15 min. To produce the ternary complexes, a volume of DOPE:Chol liposomes was added to surfactant/DNA complexes to obtain surfactant/lipid molar ratios in the range of 1/1 to 1/2, followed by 30 min incubation at room temperature.

The two methods are depicted in **Figure 3.1** in Chapter 3 (Materials and Methods).

Differential Scanning Calorimetry Measurements

Aqueous solutions of gemini surfactants were incubated with DNA which, in the case of ternary complexes, was followed by incubation with a DOPE:Chol MLV suspension. In parallel, equivalent formulations lacking DNA were also prepared. The preparations with gemini surfactants (2.5 to 3.0 wt%) were let to stabilize at room temperature for 15 min and for an extra period of 30 min when they also contained helper lipids. The mixtures were then centrifuged at 45,000 g for 45 min at 4 °C. The

pellets were sealed into aluminum pans, and heating scans were performed over an appropriate temperature range in a Perkin–Elmer Pyris 1 differential scanning calorimeter at a scan rate of 5 °C/min. To check the reproducibility of data, three heating scans were recorded for each sample. Two distinct temperatures were automatically defined in the thermotropic profiles: the temperature of the onset (T_{on}) and the temperature at the endothermic peak (T_m).

Data acquisition and analysis were performed using the software provided by Perkin–Elmer.

Video-Enhanced Light Microscopy Analysis (VELM)

High-contrast imaging of aqueous dispersions of gemini surfactants (2.5-3.0 wt%), of gemini surfactant/DNA complexes (56 mM in gemini surfactant) and of gemini surfactant/DNA/helper lipids (200 μM in gemini surfactant) was carried out with an Olympus BX51 light microscope, under differential interference contrast (DIC) mode. Images were acquired with an Olympus C5060 video camera and software CellA. Samples of gemini surfactant for microscopic observations were prepared by dispersion of the solid surfactant in high purity Milli-Q water. Complexes of gemini surfactant/DNA and gemini surfactant/DNA/helper lipids were prepared using the Method B, as described above. For the thermal study of the dispersions, carefully sealed slide/coverslip preparations were made, and temperature was controlled using a Linkam THMS600 heating stage (±0.1 °C).

Physical Properties (Zeta Potential, Particle Size and Colloidal Stability)

The zeta potential of the surfactant-containing structures was measured using a zeta sizer Nano ZS, ZN 3500, with a 532 nm laser (Malvern Instruments, UK). The measurements were performed in the aqueous buffer HBS, at 25 °C, using DTS 1060C disposable zeta cells and the protocol for general purposes (medium viscosity 0.89 cP, medium refractive index 1.33, sample viscosity 0.89 cP, particle refractive index 1.45 and equilibration time 3 min). Values of dielectric constant of 78.5 and beam mode F(Ka) of 1.5 (Smoluchowsky) were used for zeta potential determination.

The size of the surfactant-containing particles complexed with DNA was assessed using a Submicron Particle Size Analyzer, Beckman Coulter N4 Plus. The colloidal

suspensions were diluted with HBS, and particle size analysis was carried out at a scattering angle of 90º and a temperature of 25 °C.

The turbidity of gemini surfactants and complex dispersions, providing a measure of their colloidal stability, was monitored as a function of time in a SPECTRAmax PLUS 384 spectrophotometer (Molecular Devices, Union City, CA) at a wavelength of 550 nm. The final concentration of lipid plus gemini surfactant was 0.1 mM in HBS buffer, pH 7.4 and the turbidity values were registered over a period of 48 h.

PicoGreen Fluorescence Assay

Complexes containing 0.2 μg of plasmid DNA, prepared in a total volume of 100 μL of HBS, were allowed to incubate for further 15 min at 37 °C and were then transferred to a 96-well (blackwalled) plate (Corning, NY, USA). Hundred microliters of PicoGreen (Molecular Probes, Eugene, OR), diluted according to the manufacturer's instructions (1:200 dilution in HBS buffer), were added to each sample. The fluorescence intensity of PicoGreen, directly proportional to the amount of accessible/free plasmid DNA, was monitored in a SpexFluorolog Spectrometer for determining the extent of gemini surfactant-DNA complexation. The excitation and emission wavelengths were set at 485 and 520 nm, respectively. The degree of plasmid DNA protection conferred by the complexes, taken as proportional to the surfactant/DNA complexation, was calculated as follows:

$$P_{DNA} = 1- [(F-F_{100})/(F_0-F_{100})]$$

where F is the fluorescence intensity measured after adding the PicoGreen solution to the complexes, F_0 (corresponding to 0% of plasmid DNA protection) was obtained by using free plasmid DNA in the same amount as that associated with the complexes, F_{100} (corresponding to 100% of plasmid DNA protection) is the residual fluorescence intensity of a negative control obtained by using a PicoGreen solution without plasmid DNA, which mimicked a situation of 0% of DNA available to the PicoGreen solution.

Destabilization of the complexes was accomplished by incubating them for 15 min with small unilamellar vesicles (SUV) of DOPC or of a mixture of DOPE:DOPC:POPS (2:1:1 molar ratio) and evaluated through PicoGreen fluorescence intensity as the difference between the protection obtained for complexes in absence of the lipid vesicles and that obtained in their presence.

Cell Viability

Cell viability was assessed by a modified Alamar Blue assay (Simões et al. 1999). This assay takes into account the redox capacity of cells and measures the extent of the produced metabolites (resorufin) as a result of cell growth (Konopka et al. 1996). Briefly, 48 h after transfection 0.3 ml of 10% (v/v) resazurin dye in complete DMEM–HG medium was added to each well. After 45 min of incubation at 37 °C, 150 μL of the supernatant was collected from each well and transferred to 96-well plates. The absorbance at 570 and 600 nm (information provided by the supplier) was measured in a SPECTRAmax PLUS 384 spectrophotometer (Molecular Devices, Union City, CA) and cell viability was calculated according to the equation:

$$\text{Cell viability (\% of control)} = [(A_{570} - A_{600})/(A'_{570} - A'_{600})] \times 100$$

where A_{570} and A_{600} are the absorbances of the samples, and A'_{570} and A'_{600} are those of the control (non-treated cells), at the indicated wavelengths.

Transfection Efficiency

HeLa cells (0.8×10^5 cells/well) were seeded onto 12-well plates. Following overnight culture, cells were incubated with the different DNA complexes (0.5 μg of pEGFP-C1 per well) at 37 °C, under 5% CO_2, for 4 h, in OptiMEM medium. After this period, the medium was replaced with fresh medium containing 10% (v/v) FBS and antibiotics, and the cells were further incubated for 44 h to allow gene expression. The transfection efficiency mediated by the different complexes was evaluated through analysis of the expression of green fluorescent protein (GFP) by flow cytometry. Briefly, 48 h after transfection, cells were washed once with PBS and detached with 0.25% trypsin (10 min at 37 °C). Cells were further washed three times by centrifugation (200g, 4 °C, 5 min) in ice-cold PBS. The resulting pellet was resuspended in ice-cold PBS, and the samples were immediately analyzed. Flow cytometry analysis was performed in live cells using a Becton Dickinson (NJ, USA) FACSCalibur flow cytometer. Data were collected and analyzed using CellQuest software. Live cells were gated by forward/side scattering from a total of 10,000 events.

Cell Association

Cell association experiments were performed at 37 °C under the same experimental conditions described for transfection. Briefly, HeLa cells were incubated for 4 h with the complexes containing 5 mol% of the fluorescent probe rhodamine-phosphoethanolamine (Rh-PE; Avanti Polar Lipids, Alabaster, AL), in a final volume of 0.5 ml of serum-free OptiMEM. The medium containing the nonassociated complexes was then collected and the fluorescence was measured at 37 °C following the addition of octaethylene glycol monododecyl ether ($C_{12}E_8$; Sigma, St. Louis, MO), at a final concentration of 0.5% (v/v). To assess the fluorescence associated with the cells, cells were rinsed with serum-free OptiMEM, detached from the culture plates and then suspended in 0.5 ml of medium. The fluorescence of the cell suspension was measured at 37 °C in the presence of $C_{12}E_8$, as described above. The extent of cell association was determined according to the following equation:

$$\% \text{ cell association} = [F_{cells}/(F_{nonassociated} + F_{cells})] \times 100$$

where F_{cells} is the value of fluorescence of the complexes associated with the cells and $F_{nonassociated}$ is the value of fluorescence of nonassociated complexes (supernatant).

Cellular Internalization Pathways

To address the mechanisms through which surfactant-based complexes are internalized by cells, recognized inhibitors of different endocytic pathways were used. For this purpose, plated HeLa cells washed with PBS were pre-treated for 30 min, at 37 °C, in serum-free OptiMEM, with the following endocytosis inhibitors (from Sigma): (i) chlorpromazine (30 μM); (ii) fillipin III (5 μg/mL) or (iii) amiloride hydrochloride (5 mM). The cells were then incubated with the complexes in the presence of each drug, for 1 h, at 37 °C, in serum-free OptiMEM. In order to confirm that these drugs compromise selectively different endocytic pathways, the effect of the drugs on the cellular uptake of the fluorescently labeled markers, transferrin, a known marker of clathrin-mediated endocytosis, and lactosylceramide, a marker of raft/caveolae-dependent endocytosis, was analyzed. Cytotoxicity was assessed following cell treatment with each of the drugs by the Alamar Blue assay, as described above. Flow cytometry analysis was performed as described above (Transfection

Efficiency section) to evaluate transfection efficiency of the complexes in cells pre-incubated with each of the drugs.

Statistical Analysis

Data are presented as mean ± SD. The significance of the results was statistically analyzed by a one-way analysis of variance (ANOVA) with Tukey's multiple pairwise comparison. Statistical significance was set at $p < 0.05$.

4.4 RESULTS

4.4.1 SELECTION OF THE METHOD OF PREPARATION OF GEMINI-BASED DNA COMPLEXES

Two methods of preparation of gemini surfactant/DNA complexes were tested in order to select the one that originates the most effective and less cytotoxic complexes (see **Figure 3.1** in Chapter 3). **Figure 4.2** illustrates the cell viability (a) and the percentage of transfected cells (b) obtained with complexes composed of the surfactants 12-2-12 and 16-2-16 with DNA, at different (+/-) charge ratios, produced by the two methods. As shown in **Figure 4.2**, complexes prepared by the method A revealed higher cytotoxicity, mainly for the highest (+/-) charge ratios tested (**Figure 4.2a**), and lower transfection efficiency (**Figure 4.2b**) than complexes prepared by the method B. It is particularly relevant the striking increase of the transfection ability of 16-2-16-based complexes, when prepared by the method B as compared to the method A.

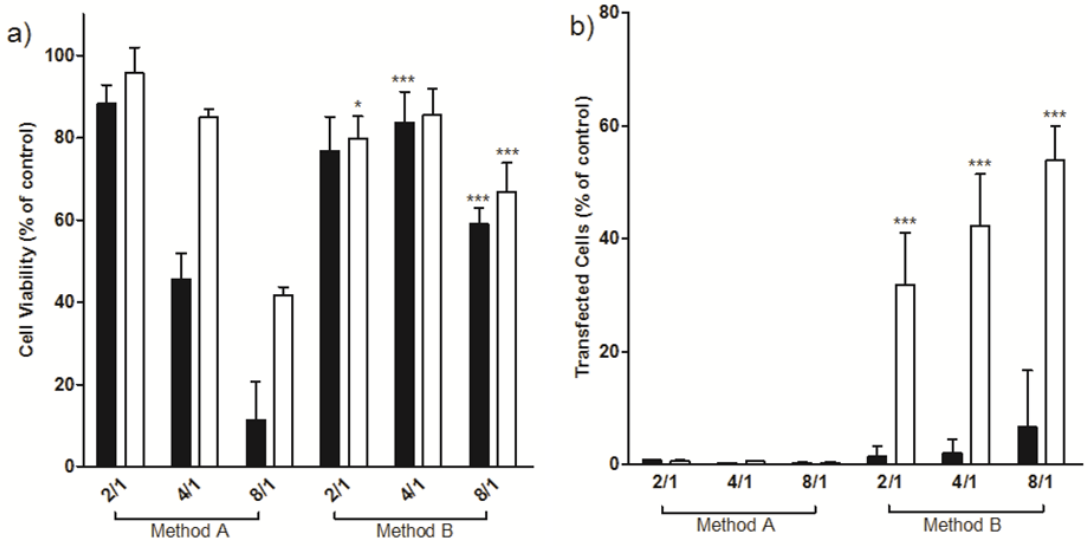

Figure 4.2 Cell viability (a) and transfection efficiency (b) of 12-2-12- (■) and 16-2-16-based (□) complexes prepared by the two methods described in the experimental section and illustrated in **Figure 3.1**. Cell viability and transfection efficiency were evaluated by the Alamar blue assay and flow cytometry analysis, respectively. Pairwise data comparisons were performed for the complexes produced by the method A vs. the same complex formulations produced by the method B (*$p < 0.05$, ***$p < 0.001$).

Noteworthy, at the 4/1 (+/-) charge ratio, these complexes prepared by the method B exhibited also a relatively low cytotoxicity. The cytotoxicity and transfection competence of 14-2-14-based complexes (**Figure 4.3**), with or without the helper lipids DOPE:Chol (2:1), were not affected by the method of complex preparation. On the basis of these data, the surfactant-based complexes used in the present study were formulated following the method B, since besides being advantageous for complexes prepared with 12-2-12 and 16-2-16 surfactants, this method is simpler and less time consuming than method A.

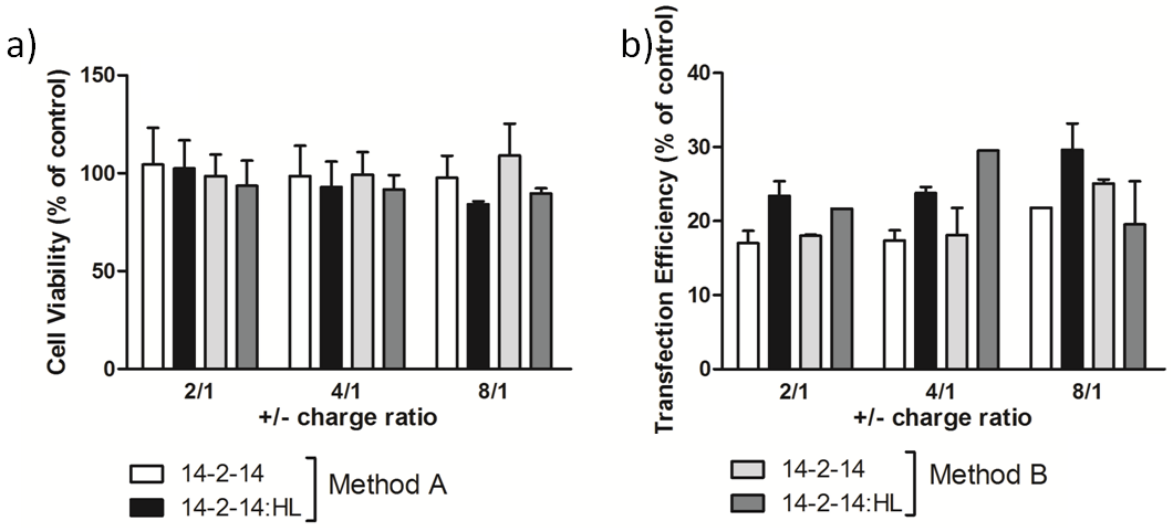

Figure 4.3 Cell viability (a) and transfection efficiency (b) of 14-2-14-based complexes formulated without (white and light grey bars) or with the helper lipids (HL) DOPE and cholesterol (black and dark grey bars), prepared by method A (white and black bars) and method B (light grey and dark grey bars), as indicated. Data comparisons were performed for each formulation prepared by the methods A and B (*$p < 0.5$).

4.4.2 Evaluation of the Thermal Behavior of Gemini Surfactants and Corresponding Complexes with DNA

In order to characterize the structures formed by gemini surfactants or mixtures of gemini surfactants plus helper lipids and the corresponding complexes with DNA, DSC and VELM experiments were performed. **Figure 4.4** shows the thermal profiles of surfactants containing a spacer with two carbon atoms and hydrocarbon chains with increasing length (**Figure 4.4a**), as well as profiles of14-2-14 and 16-2-16 surfactants as compared to those of the respective complexes with DNA (**Figure 4.4b** and **c**). Both 14-2-14 and 16-2-16, but not 12-2-12, presented an endothermic peak, denoting the presence of a phase transition. Taking into account that the endotherms

observed for these surfactants occurred at temperatures close to those reported for their Krafft temperatures, assessed by conductimetry (Zhao et al. 1998), they should represent a transition from an aqueous dispersion of surfactant crystallites to a micellar solution.

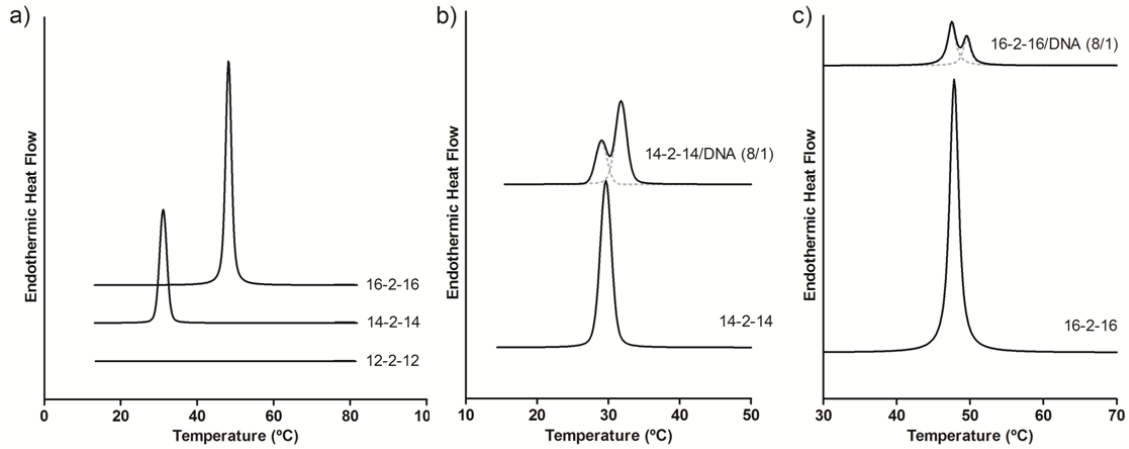

Figure 4.4 DSC thermograms of 12-2-12, 14-2-14 and 16-2-16 pure gemini surfactant structures (a), of complexes of 14-2-14 with DNA (b) and of complexes of 16-2-16 with DNA (c) at the 8/1 (+/-) charge ratio. The DSC profiles are heating scans. The thermograms are typical of at least three independent experiments. The DSC profiles of 14-2-14 and 16-2-16 pure surfactant structures are also represented in the panels b and c to facilitate comparison with the respective DNA complexes.

Observations by VELM (**Figure 4.5**) in fact confirm the presence of dispersed crystallites that disappear to yield an isotropic solution at about the same temperature as that of the DSC endothermic peaks. The temperature range of the phase transition of 16-2-16 surfactant structures detected by DSC and VELM was shifted to higher values as compared to that of 14-2-14 surfactant structures.

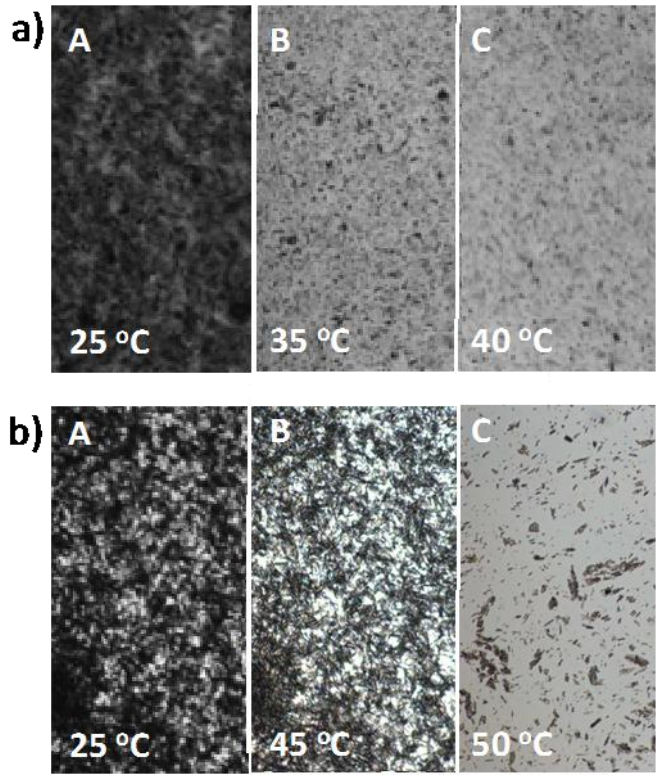

Figure 4.5 VELM micrographs of gemini surfactant dispersions prepared at 3.0 wt% (the same concentration as that used in DSC), namely: a) 14-2-14 and b) 16-2-16. For 14-2-14, the crystals started disappearing at ≈ 35 °C and full solubilization proceed until about 40 °C. For 16-2-16, crystallites solubilize within the range 45-50 °C, consistently with the Krafft temperature obtained in the present work by DSC, and in other works by conductimetry (Zhao et al., 1998).

The complexation of 14-2-14 and 16-2-16 surfactants with DNA resulted in a split of the endotherm (**Figure 4.4b** and **c**). As clearly seen by VELM (**Figure 4.6**), these complexes form solid-like aggregates of large dimensions (typically > 25 μm), which remain insoluble upon heating to 80 °C. However, the heating probably induced the solubilization of surfactant crystallites that are not associated to DNA, giving rise to DSC peaks (**Figure 4.4b** and **c**) centered at the temperature of the corresponding DNA-free surfactants. On the other hand, the decrease of the enthalpy (ΔH) of complex transitions as compared to that of free surfactant transitions (data not shown) may reflect the presence of most of the surfactant in the insoluble form (DNA-surfactant complex). The shoulder of the peaks, shifted to slightly higher temperatures, can be explained by the presence of surfactant molecules establishing weak interactions with DNA. VELM observations clearly show that these peaks cannot be attributed to the solubilization of the large DNA-surfactant aggregates formed, since they remain noticeable at temperatures up to 80 °C (**Figure 4.6**).

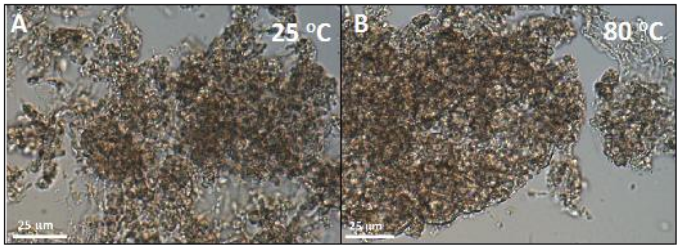

Figure 4.6 VELM micrographs of plain complex dispersions (14-2-14 plus DNA, at a +/- charge ratio of 8/1) observed upon heating. The flocs appear to be solid in nature and remain insoluble from room to high temperature (80 °C). Bars: 25 µm.

The addition of helper lipids to the previous systems completely abolished their phase transitions (data not shown).

4.4.3 Physicochemical and Morphological Characterization of Gemini Surfactant-based Complexes with DNA in the Absence or Presence of Helper Lipids

The surface charge density and hydrodynamic diameter were determined for the complexes formulated with gemini surfactants and their mixtures with helper lipids, at the (+/-) charge ratios of 2/1, 4/1 and 8/1.

As expected, in the absence of helper lipids, addition of DNA to the gemini surfactants, which exhibit a high positive surface charge, resulted in a decrease of the Zeta potential (**Table 4.1**). The only exception was observed for the 16-2-16-based complexes, which did not undergo a zeta potential change, with respect to the pure gemini, over the range of charge ratios tested (2/1, 4/1 and 8/1). The addition of DOPE and cholesterol to the gemini surfactants decreased consistently the zeta potential displayed by the pure surfactants. In the case of lipid mixtures with the 12-2-12 and 12-10-12 surfactants, the surface charge decreased to negative values, despite the positive charge of surfactants and the zwitterionic character of helper lipids.

Although the addition of the helper lipids to surfactant-DNA complexes, prepared at the 8/1 and 4/1 (+/-) charge ratios has in general resulted in a decrease of the Zeta potential, complexes at the 2/1 (+/-) charge ratio showed high variability regarding that effect.

Table 4.1 Zeta potential of HBS buffer dispersions of the surfactants or surfactants plus helper lipids (no DNA) and of the respective complexes with DNA at 8/1, 4/1 and 2/1 (+/-) theoretical charge ratios.

	ζ-potential (mV)*			
	no DNA	plus DNA		
		8/1 (+/-)	4/1 (+/-)	2/1 (+/-)
DOPE:Chol	-26.0 (±0.1)	-	-	-
12-2-12	+89.0 (±12.5)	+4.3 (±5.0)	-3.6 (±3.3)	+12.4 (±3.9)
12-2-12: DOPE:Chol	-25.9 (±4.7)	-32.4 (±0.7)	-34.0 (±2.3)	+30.4 (±1.7)
14-2-14	+43.3 (±0.8)	+16.9 (±2.3)	+12.9 (±3.4)	+7.8 (±3.6)
14-2-14: DOPE:Chol	+30.4 (±6.9)	-10.5 (±5.7)	+13.0 (±6.4)	+1.6 (±8.3)
16-2-16	+22.2 (±3.2)	+23.7 (±7.4)	+22.8 (±4.8)	+15.4 (±6.6)
16-2-16: DOPE:Chol	+3.9 (±9.9)	-4.8 (±6.9)	-13.9 (±6.6)	+21.1 (±7.7)
12-5-12	+14.3 (±2.9)	+6.5 (±1.6)	-0.3 (±1.4)	+3.8 (±2.0)
12-5-12: DOPE:Chol	+7.6 (±1.9)	-2.8 (±7.1)	-3.2 (±4.5)	+2.8 (±1.8)
12-10-12	+39.1 (±9.6)	+6.0 (±1.5)	+5.2 (±1.4)	+1.2 (±1.6)
12-10-12: DOPE:Chol	-18.6 (±2.4)	-19.7 (±1.9)	-10.5 (±0.4)	+12.0 (±1.7)

*The values represented are means ± standard deviation, obtained for triplicates, in three independent experiments.

Size distribution of the complexes was evaluated as monomodal or as polydisperse, when the polydispersity index (PI) was found to be lower or higher than 0.3, respectively. Although, the polydisperse complex suspensions displayed more than one population, most of them presented a predominant population with an average size above 3 μm (**Table 4.2**).

Table 4.2 Size of HBS buffer dispersions of DNA complexes composed of surfactants or surfactants plus helper lipids at 2/1, 4/1 and 8/1 (+/-) theoretical charge ratios.

	Hydrodynamic diameter (nm)[a)]		
	2/1 (+/-)	4/1 (+/-)	8/1 (+/-)
12-2-12	269 ± 72 ~42% 2243 ± 460 ~57%	>3000	590 ± 83
12-2-12: DOPE:Chol	2425 ± 427	294 ±99 ~15% >3000 ~81%	481 ± 70
14-2-14	>3000	402 ± 92 ~63% 1953 ± 782 ~37%	153 ± 76 ~35% 858 ± 125 ~50%
14-2-14: DOPE:Chol	>3000	225 ± 74 ~10% >3000 ~89%	212 ± 62 ~21% 2152 ± 685 ~78%
16-2-16	243 ± 85 ~10% >3000 ~80%	>3000	>3000
16-2-16: DOPE:Chol	273 ± 106 ~23% >3000 ~76%	>3000	1441 ± 47 ~9% >3000 ~91%
12-5-12	324 ± 70 ~8% >3000 ~91%	322 ± 40 ~43% 2632 ± 583 ~56%	198 ± 40 ~43% 1628 ± 561 ~56%
12-5-12: DOPE:Chol	>3000	236 ± 60 ~30% 1973 ± 895 ~70%	421 ± 91
12-10-12	>3000	320 ± 67 ~32% >3000 ~68%	282 ± 79 ~44% 2468 ± 356 ~55%
12-10-12: DOPE:Chol	>3000	224 ± 83 ~34% >3000 ~67%	210 ± 48 ~37% 1910 ± 500 ~63%

[a)] The values represented are means ± standard deviation, obtained for triplicates, in three independent experiments.

Observation of gemini surfactant-based complexes containing 12-2-12, 14-2-14 or 16-2-16 and helper lipids, by VELM, confirmed the presence of a rich variety of self-assembled aggregates, in particular giant vesicles of diameters between 1-6 μm (**Figure 4.7a-c**). It was also possible to observe vesicles with a fine inner structure (**Figure 4.7a**, right-hand side) and irregularly-shaped aggregates of larger dimensions, which appear to be composed by flocculated vesicles of smaller size (**Figure 4.7b**, right-hand side; **Figure 4.7c**, left-hand side). On the other hand, under polarized light some vesicles displayed birefringence, which unequivocally indicates their multilamellar structure (**Figure 4.7a**, left-hand side, inset).

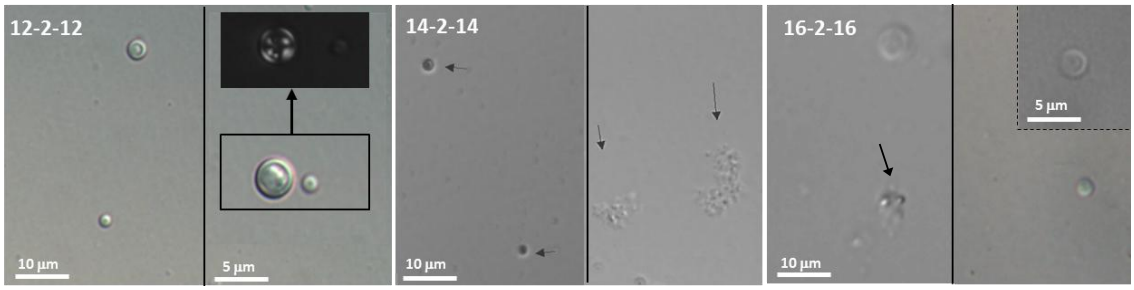

Figure 4.7 VELM micrographs of ternary complex dispersions (gemini/helper lipids plus DNA, at a +/- charge ratio of 8/1) containing: a) 12-2-12; b) 14-2- 14; c) 16-2-16. Arrows point to some of the morphologies described in the text: birefringent multilamellar vesicles (a, right-hand side), smaller vesicles (b, left-hand side) and flocs of presumably vesicular aggregates (b, right-hand side; c, left-hand-side).

All complexes were found to be extremely stable over a period of at least 24 h, as assessed by monitoring the absorbance at 550 nm over a period of 48 h (data not shown).

4.4.4 Evaluation of the Complexation of Gemini Surfactants with DNA

The ability of gemini surfactants to complex and protect DNA was assessed by the PicoGreen fluorescence assay. PicoGreen is a DNA-intercalating agent, whose fluorescence is dramatically enhanced upon binding to DNA and quenched by condensation of the DNA structure; thus, allowing the determination of free/accessible DNA. As shown in **Figure 4.8**, for all the complexes tested, the increase in the amount of surfactant with respect to DNA (increase of (+/-) charge ratio) in the complex formulations resulted in a more extensive gemini-DNA interaction, as deduced by the reduction of PicoGreen fluorescence. With the exception of the 14-2-14 and 12-10-12 surfactants, which conferred almost full DNA protection even at the lowest (+/-) charge ratio tested, it is noticeable that the helper lipids enhanced DNA shielding, at least at the lowest (+/-) charge ratios. Interestingly, the lowest protection levels were observed for the 12-2-12 surfactant, which presents both the shortest and most flexible hydrocarbon chains and spacer, eventually supporting the weakest hydrophobic interactions with the DNA molecules.

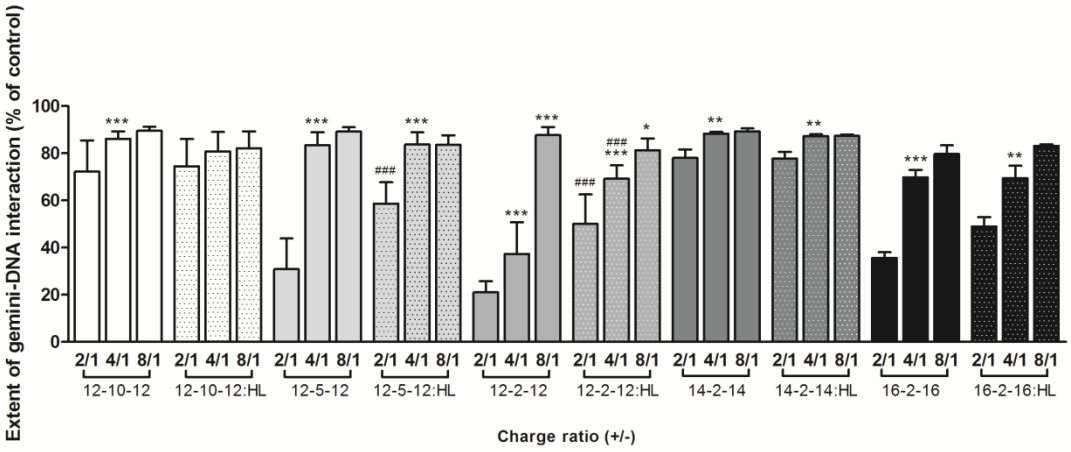

Figure 4.8 Gemini-DNA interactions, as assessed by PicoGreen accessibility to DNA complexed with gemini surfactants or gemini surfactants plus the helper lipids (HL) DOPE and Cholesterol (2:1 molar ratio) at the indicated (+/-) charge ratios. The maximum fluorescence (control) corresponds to maximum DNA accessibility. Data comparisons were performed for the complexes at different (+/−) charge ratios vs. the same complex formulations at the immediately precedent (+/−) charge ratio ($^{*}p < 0.05$, $^{**}p < 0.01$, $^{***}p < 0.001$) and for complexes formulated without helper lipids vs. complexes formulated with helper lipids ($^{\#\#\#}p < 0.001$).

4.4.5 Evaluation of the Interaction of Gemini Surfactant-Based DNA Complexes with Model Membranes

Figure 4.9 reports the destabilization of surfactant-based DNA complexes, as assessed by the PicoGreen fluorescence assay, upon interaction with zwitterionic vesicles composed of DOPC (**Figure 4.9a**) and anionic vesicles composed of DOPE:DOPC:POPS (**Figure 4.9b**). As shown, zwitterionic vesicles were unable to destabilize the complexes to a great extent. In fact, in some conditions, an increased "stabilization" of the structures was even observed, suggesting that the wrapping of the lipid vesicles around the complexes promoted a decrease of DNA exposure to the fluorescent probe. Complexes containing helper lipids were more extensively destabilized by the zwitterionic and anionic lipid vesicles than their counterparts lacking helper lipids. On the other hand, the extent of destabilization of complexes prepared with helper lipids decreased with the increase of surfactant hydrocarbon chain length. For complexes containing surfactants with spacers of different length, the lowest degree of destabilization (and, in some cases, higher degree of stabilization) was found with the surfactant presenting the intermediate spacer (5 carbon atoms). The pattern of complex destabilization regarding its dependence on surfactant characteristics was similar for both zwitterionic and anionic vesicles.

However, destabilization induced by the anionic vesicles occurred in a larger extent than that observed for zwitterionic vesicles.

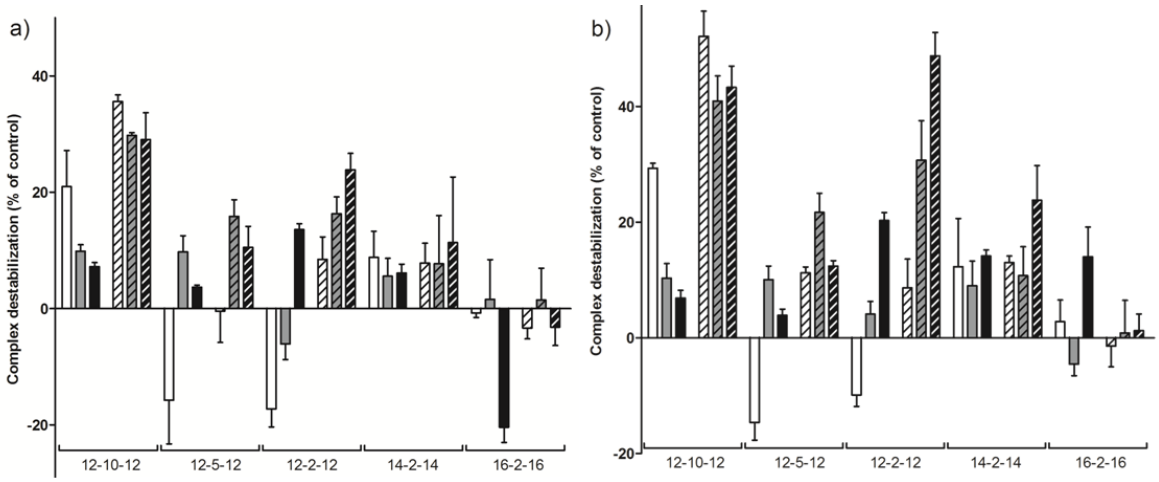

Figure 4.9 Destabilization of gemini surfactant-based DNA complexes induced by zwitterionic lipid vesicles of DOPC (a) or anionic vesicles of DOPE:DOPC:POPS at 2:1:1 molar ratio (b), as assessed by PicoGreen accessibility. The complexes containing the surfactants indicated in the figure were prepared at 2/1 (□), 4/1 (▩) and 8/1 (■) (+/-) charge ratios and with (striped bars) or without (plain bars) helper lipids. Maximum destabilization corresponds to maximum DNA accessibility.

4.4.6 Comparison of the Cytotoxicity of Different Gemini Surfactant-Based DNA Complexes

Figure 4.10 presents the results of viability observed in HeLa cells following incubation with gemini surfactant-based complexes, adding or not the helper lipids DOPE and cholesterol (2:1 molar ratio). As shown, complexes formulated with the gemini surfactants containing two carbon atom-long spacers exerted very low cytotoxicity on HeLa cells, at the lowest (+/-) charge ratios tested (2/1 and 4/1), and complexes prepared with 14-2-14 maintained a low cytotoxicity even at the highest (+/-) charge ratio tested (8/1). The addition of helper lipids to complexes composed of 12-2-12 or 16-2-16 and DNA, at the 8/1 (+/-) charge ratio, decreased their cytotoxicity. On the other hand, gemini surfactants containing longer spacers (s = 5 or 10) produced highly toxic complexes, even at the lowest charge ratios tested, which was not reverted by the addition of helper lipids. Hence, complexes formulated with surfactants owning spacers longer than two carbon atoms revealed to be unsuitable for the delivery of nucleic acids, being therefore excluded from the subsequent experiments.

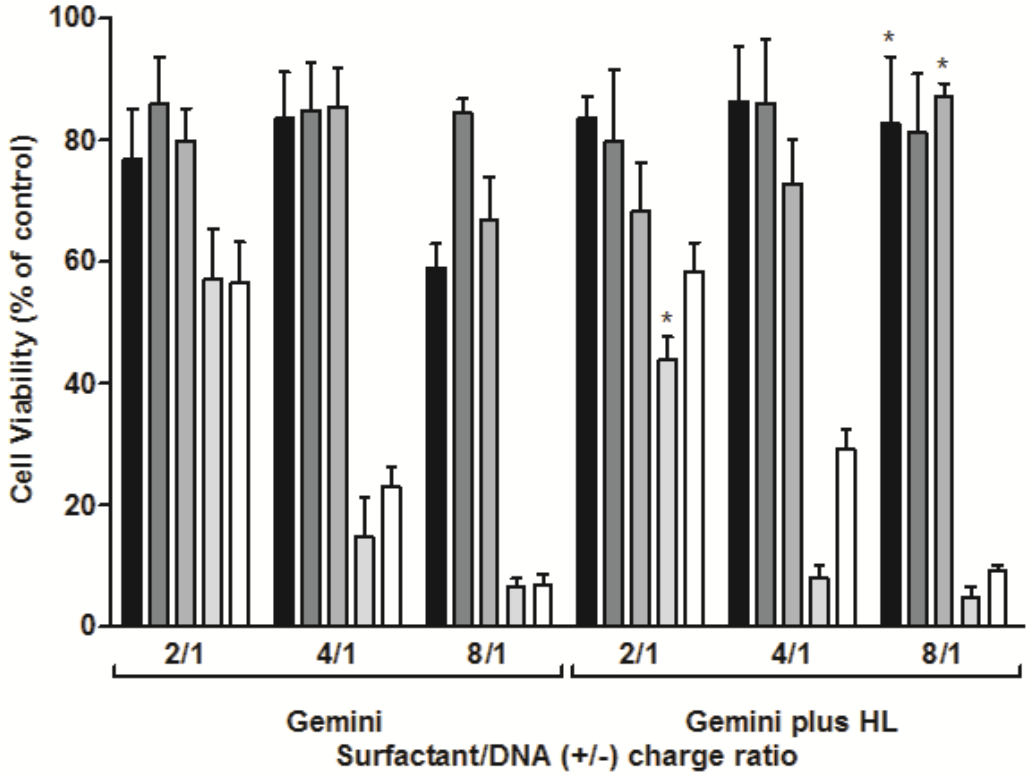

Figure 4.10 Viability of HeLa cells upon incubation with complexes composed of 12-2-12 (■), 14-2-14 (■), 16-2-16 (■), 12-5-12 (■) or 12-10-12 (□) surfactants and DNA, containing or not the helper lipids (HL) DOPE and Cholesterol (2:1 molar ratio). Cell viability is expressed as a percentage of a control (non-treated cells). Pairwise data comparisons were performed for the complexes produced without helper lipids vs. the same complexes containing helper lipids (*$p < 0.05$).

4.4.7 Transfection Efficiency of Non-Toxic Gemini Surfactant-Based DNA Complexes

Aiming at establishing a putative dependence of the biological activity of the non-toxic complexes and their physico-chemical properties, the ability of complexes formulated with 12-2-12, 14-2-14 and 16-2-16 gemini surfactants to transfect HeLa cells was evaluated (**Figure 4.11**). As shown in the figure, an increase of transfection competence was noticed with the increase of surfactant hydrocarbon chain length. On the other hand, the addition of helper lipids to the composition of the complexes resulted in an improvement of their ability to mediate gene expression. This effect was particularly relevant for the complexes formulated with the surfactants 12-2-12 and 14-2-14, which displayed low levels of transfection in the absence of the helper lipids (maximum transfection of 6.6 and 14.4%, respectively), that increased to a maximum of 45.7 and 44.2%, respectively, in the presence of the lipids. The gemini surfactant 16-2-16, which already displayed relatively high transfection levels

(maximum of 32.1%) in the absence of helper lipids, also showed to benefit from the addition of these lipids, mainly at the highest (+/-) charge ratio tested, with a maximum of 53.9% transfected cells.

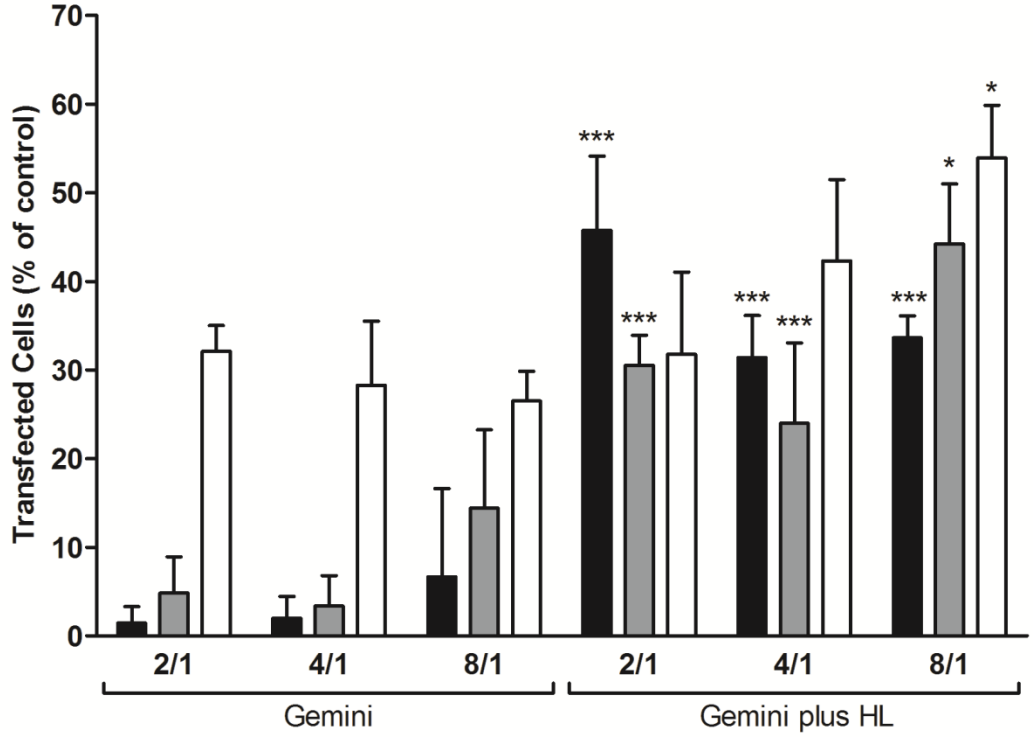

Figure 4.11 Transfection efficiency of gemini surfactant-based DNA complexes containing12-2-12 (■), 14-2-14 (■) and 16-2-16 (□) gemini surfactants with or without helper lipids (HL), prepared at the indicated (+/-) charge ratios. Data comparisons were performed for HL-containing complexes vs.the corresponding HL-free complexes at the same (+/−) charge ratio (*$p < 0.05$, ***$p < 0.001$).

4.4.8 Evaluation of the Extent of Complex-Cell Association

In order to gain insights into the mechanisms underlying the effects of gemini hydrocarbon chain length, the presence of helper lipids and the charge ratio of gemini-based complexes on transfection efficiency, the influence of those parameters on the extent of complex association with HeLa cells was evaluated. For this purpose, the gemini-based complexes, prepared without or with helper lipids at different (+/-) charge ratios and containing a rhodamine-labeled lipid, were incubated with HeLa cells at 37 °C. It is important to note that cell association encompasses the processes of binding, fusion with the plasma membrane, endocytosis and fusion with the endosomal membrane (da Cruz et al. 2001). **Figure 4.12** shows that complex-cell association was not affected by the gemini hydrocarbon chain length, whereas the

addition of helper lipids decreased the extent of cell-association for all the complexes. The (+/-) charge ratio of surfactant-based complexes did not influence cell association in the absence of helper lipids. However, for complexes containing helper lipids the increase of (+/-) charge ratio promoted a reduction of cell-association.

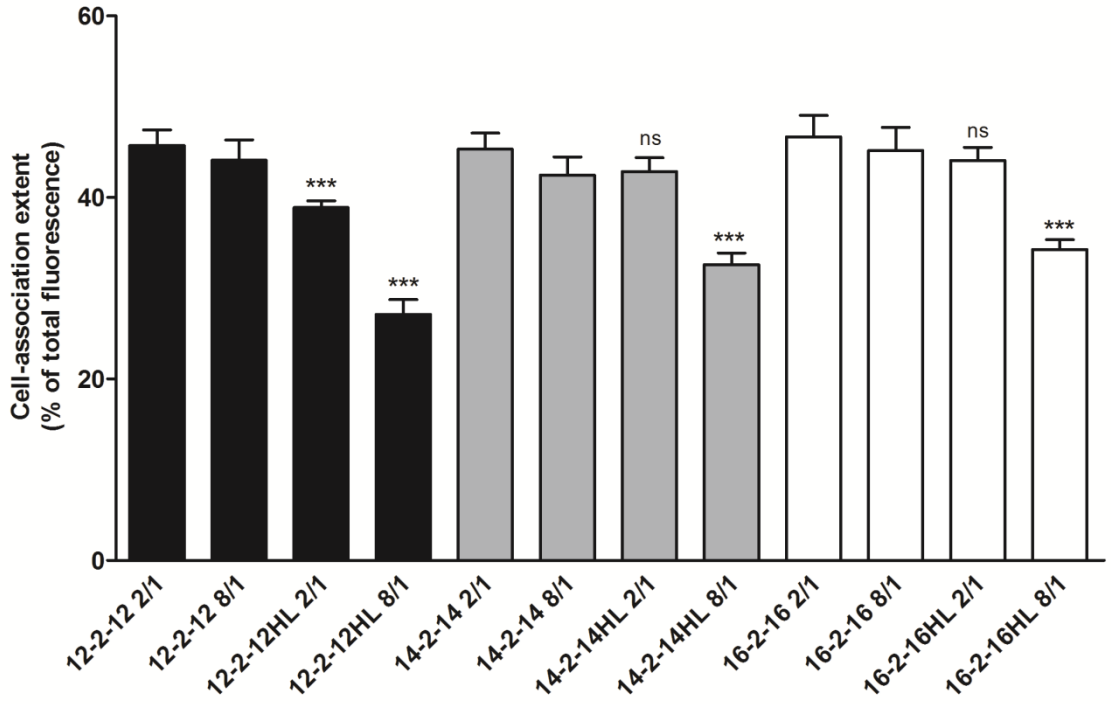

Figure 4.12 Effects of surfactant chain length, surfactant/DNA (+/-) charge ratio and presence of helper lipids on the extent of association of gemini surfactant-based complexes to HeLa cells at 37 °C. Extent of complex-cell association is expressed as a percentage of the total rhodamine fluorescence corresponding to the complexes associated to cells plus that of the nonassociated complexes (fluorescence of the supernatant). Data represent the mean ± SD from two independent experiments carried out in triplicate. Data comparisons were performed for complexes without helper lipids vs. the same complexes formulated with helper lipids ($^{***}p < 0.001$, ns, non-significant).

4.4.9 Cellular Internalization Pathways of Gemini Surfactant-Based DNA Complexes

Eukaryotic cells use different endocytic pathways to internalize extracellular molecules, and the selected mechanism determines their intracellular fate. Therefore, the route of internalization of DNA complexes might affect the kinetics of their intracellular processing and, consequently, transfection efficiency.

Cellular internalization mechanisms of gemini surfactant-based complexes were examined by flow cytometry by evaluating the transfection levels of cells pre-incubated with the pharmacological inhibitors of clathrin-mediated endocytosis

(chlorpromazine), macropinocytosis (amiloride hydrochloride) and endocytic processes occurring in lipid raft domains of the membrane (filipin III). It is important to note that, among these inhibitors, only chlorpromazine is currently accepted as being an inhibitor of a specific endocytosis pathway (clathrin-mediated endocytosis), by preventing clathrin-coated pit formation at the plasma membrane. Although the other inhibitors are less specific, amiloride hydrochloride inhibits the Na^+/H^+ exchanger protein, and hence, contributes to the acidification and suppression of the forming micropinosome ruffle; thus, being recognized as an inhibitor of macropinocytosis. On the other hand, filipin III binds cholesterol; therefore, making lipid rafts unavailable for both caveolae and non-caveolae mediated endocytosis.

Studies were conducted to investigate the internalization pathways of gemini surfactant-based DNA complexes composed of 16-2-16 without helper lipids (data not shown) and with helper lipids, prepared at 2/1, 4/1 and 8/1 (+/-) charge ratios, as well as complexes composed of 12-2-12 or 14-2-14 and helper lipids at the 8/1 (+/-) charge ratio (**Figure 4.13**).

Similar transfection efficiency was observed in cells that had been exposed to the endocytosis inhibitors, prior to transfection with complexes of 16-2-16 plus DNA (at 2/1, 4/1 and 8/1 +/- charge ratios) and in untreated control cells (data not shown). This indicates that the internalization of these complexes did not involve commonly reported endocytic pathways, but most likely, occurred through direct membrane translocation at non-raft domains. On the other hand, complexes produced from the gemini surfactants plus DNA and helper lipids presented a decrease in the transfection efficiency when cells were incubated with amiloride hydrochloride, indicating that, at least partially, these complexes are internalized by macropinocytosis (**Figure 4.13**).

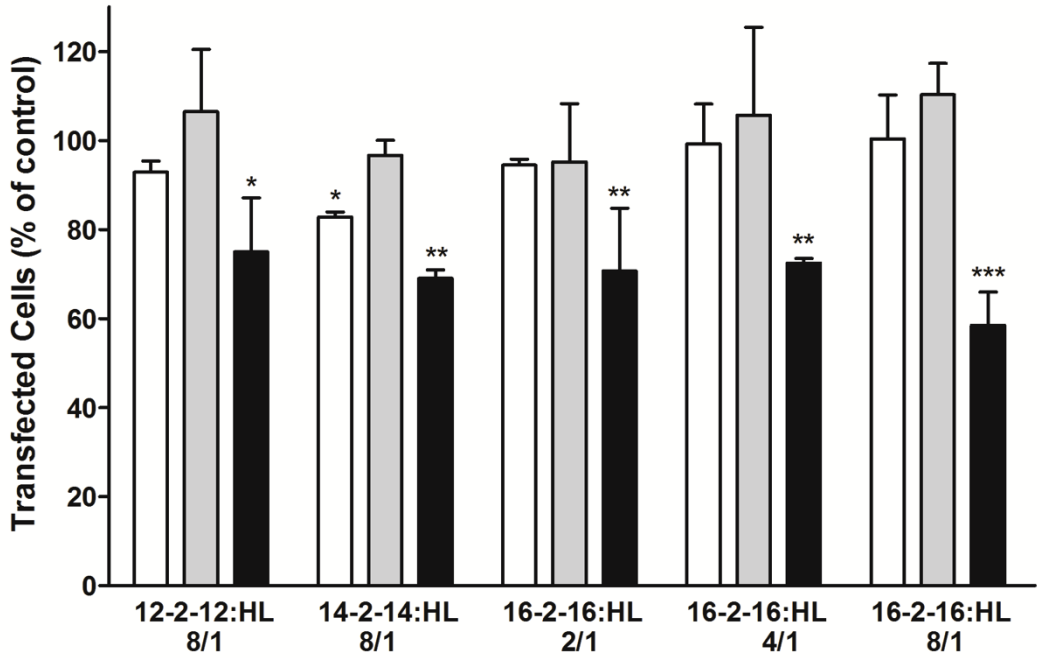

Figure 4.13 Effect of different endocytosis inhibitors on transfection mediated by gemini/DNA/lipid complexes. HeLa cells were incubated with either 30 μM of chlorpromazine (□), 5μg/ml of fillipin III (■), or 2.5 mM of amiloride hydrochloride (■) and then transfected with the complexes containing helper lipids and prepared at the indicated charge ratios. Transfection in the presence of each inhibitor is expressed as percentage of transfected cells but not treated with the drugs (control). Data is presented as mean ± standard deviation, representative of at least three independent experiments. Data comparisons were performed between each condition tested and the respective control corresponding to 100% of transfected cells (*p<0.05, **p<0.01, ***p<0.001).

4.5 DISCUSSION

A variety of molecules have been studied over the years with the ultimate goal of finding systems able to efficiently deliver their cargo to target cells without presenting the disadvantages associated with viral vectors. In parallel to the comprehensive evaluation of transfection efficiency of a multitude of nonviral delivery systems, several different approaches have been employed to correlate structure and biological activity by determining characteristics shared by the systems that are able to efficiently accomplish that task (Aleandri et al. 2013; Foldvari et al. 2006).

In the present work, we attempted to correlate the transfection efficiency of DNA complexes based on gemini surfactants from the alkanediyl-α,ω-bis(alkyldimethylammonium bromide) family with their physico-chemical properties, aiming at unraveling key features amenable to efficient gene delivery.

The method of complex preparation revealed to be determinant for the efficiency of transfection as well as for the cytotoxic profile. The main difference between the two methods tested for complex formation relied on the order of component addition, which was also shown to affect the efficiency of other delivery systems (Badea et al. 2005; Trabulo et al. 2008; Cardoso et al. 2013). Additionally, the complexes formed by the simple mixture of their components without further extrusion (method B) were larger than the ones formed by the method A, which underwent an additional step of extrusion. This fact can be deduced by comparing the size of the 14-2-14-based complexes produced here (sizes from 400 to more than 3000 nm in the absence of helper lipids and larger than 2000 nm in their presence) with that of complexes based on the same surfactant but formulated with the extrusion step (sizes from 230 to 2100 nm in the absence of helper lipids and from 170 to 1600 nm in their presence), as previously reported (Cardoso et al. 2011). *In vitro* studies have shown that complexes with a large size are often well succeeded in transfection, which has been assigned to their capacity to sediment over the adherent cultured cells, increasing the contact area between the complex and the cellular surface, and hence facilitating their internalization. Furthermore, large complexes are able to carry great amounts of DNA, which associated to a high efficiency of internalization should contribute to high transfection levels. On the other hand, although the small size of delivery systems has been described as an essential feature for *in vivo* application

involving intravenous administration, so that capillary retention of the complexes can be avoided, other *in vivo* administration routes (intraperitoneal, intramuscular or subcutaneous routes) do not exhibit the same size requirement, the retention issue being circumvented in such cases (Neves et al. 2006; Pfeiffer et al. 2006; Donkuru et al. 2010).

Interestingly, most of the complexes produced in the present study that were able to efficiently transfect cells showed sizes larger than 3 µm. The size of the complexes has been shown to affect their route of internalization (Rejman et al. 2004; Conner & Schmid 2003). In this regard, macropinocytosis has been reported to allow internalization of particles larger than 1 µm and, consistently, this pathway showed to be an important mechanism for the uptake of the large gemini-based complexes containing helper lipids. However, the cell uptake mechanism of 16-2-16/DNA complexes, apparently a direct translocation across the membrane, should depend, rather than on their size (large as well), on other characteristics of the particles, such as their ability to interact with cellular membranes, as demonstrated in the present work and evoked as being determinant for the success of transfection of nonviral delivery systems (Barenholz 2001).

Another physico-chemical property traditionally recognized as being determinant of transfection efficiency regards the Zeta potential displayed by the complexes. Although most of nonviral delivery systems present positive Zeta potential, due to the presence of excess positive charges from the cationic component, complexes presenting negative Zeta potential have also been reported in the literature as being successfully used in drug delivery (Simões et al. 1998; Faneca et al. 2004; Donkuru et al. 2010), which has been assigned to reduced interactions with negatively charged serum proteins. This finding is in accordance with our observation that DNA complexes formulated with 12-2-12, 14-2-14 or 16-2-16 gemini surfactants and helper lipids, although displaying negative Zeta potentials, were able to efficiently transfect HeLa cells. This issue will be further explored, towards a putative application of these surfactants to produce nucleic acid delivery systems to be administered *in vivo*. The negative surface charge of these complexes probably results from the different supramolecular arrangement of the molecules, which depends on the interplay of hydrophobic interactions established between surfactant hydrocarbon chains and the plasmid DNA, and electrostatic interactions between the charged surfactant polar groups and DNA phosphate groups. However, it is interesting to note that structures composed of gemini surfactants and helper lipids in the absence of DNA also present a

negative surface charge, which may result from the adsorption of inorganic anions from the medium, which might also explain the negative Zeta potential of the helper lipids *per se* (**Table 4.1**).

A relationship between the transfection efficiency of nonviral delivery systems and their ability to adopt different structures has also been described in the literature (Foldvari et al. 2006). Thus, the coexistence of distinct packing arrangements may originate structural defects, which can favor drug delivery (Barenholz 2001). The supramolecular structure adopted by the surfactants in solution depends on inherent characteristics of the molecules, such as the length of their chains and spacer, and on the concentration at which they are present in the aqueous medium (lyotropism). In this regard, it is important to mention that aqueous dispersions of 16-s-16 gemini surfactants have been shown to exhibit a richer phase behavior, presenting more phases across a concentration range, than those of 12-s-12 (Zana & In 2005; Fuller et al. 1996; Alami et al. 1993). The present study of the thermal behavior of hydrated gemini surfactant structures, by DSC and VELM, showed that structures composed of 14-2-14 and 16-2-16 gemini surfactants, but not of 12-2-12, present a phase transition in the temperature range assayed. More interesting, in the context of this study, is the finding that ternary complexes (surfactant/DNA/helper lipids) displaying transfection capacity can form a diversity of vesicle structures in solution, as revealed by VELM micrographs **(Figure 4.7**). Thus, individual vesicles of different size and structure, including multilamellar vesicles, have been observed together with irregular aggregates of large dimensions, which seem to result from the flocculation of vesicles of smaller size. In fact, DNA complexes of 16-2-16 plus DOPE were shown to present at least two coexisting phases, one lamellar phase enriched in cationic surfactant and one ambiguous structure, enriched in the helper lipid, which could correspond to a lamellar or an inverted hexagonal phase. Furthermore, these complexes were found to be compacted in a multilamellar sandwiched structure (Muñoz-Úbeda et al. 2012). Unfortunately, VELM micrographs did not reveal structural details of samples composed of plain complexes, which appeared as clear and colorless liquids, probably corresponding to dispersions of very small crystallites (smaller than 400 μm). Other systems exhibiting a lamellar-to-non-lamellar phase transition at a temperature close to the physiological temperature, have been shown to mediate transfection more efficiently than those lacking that feature (Zuhorn et al. 2007; Wasungu et al. 2006a). This fact was interpreted in terms of pH-driven interaction of the

delivery system with the endosomal membrane, after the gene-carrying particles had been endocytosed (Zuhorn et al. 2007; Wasungu et al. 2006b). Such transition from lamellar-to-non-lamellar phases could not be identified at the experimental conditions used herein. However, the rich variety of self-assembled aggregates revealed by VELM, which could result from the combination of amphiphiles which tend to form aggregates of opposite curvature — gemini with propensity to form micelles of high positive curvature and DOPE able to form inverted structures of negative curvature — allow to predict the generation of structures with high curvature strain andintermediate spontaneous curvatures, *i.e.*, bilayer structures.

In this context, it is noteworthy that the complexes used herein able to efficiently mediate transfection were internalized through direct membrane translocation with some contribution of macropinocytosis. This indicates that complex interaction with the endosomal membrane is important only for a relatively small portion of complexes that are endocytosed. On the other hand, the multiplicity of aggregates originated by gemini-surfactant-based complexes with helper lipids in aqueous dispersions, at concentrations close to those used in the preparation of complexes for the transfection studies, could provide the complexes with sufficient lability to allow DNA dissociation upon interaction with certain membrane structures. Therefore, in order to better appreciate the ability of gemini surfactant-based complexes to mediate effective delivery of the DNA cargo into the cell, assays of complex destabilization in the presence of lipid membrane models were performed. Successful transfection depends on surpassing a series of cellular barriers, including nucleic acid release from the delivery system. On the other hand, a premature release of the cargo may lead to its degradation before reaching the cell target, thus, preventing transgene expression. The studies of complex destabilization induced by lipid vesicles showed that complexes formulated with the surfactant containing the spacer of intermediate length (s = 5) were more prone to be destabilized both by zwitterionic and anionic vesicles, as compared to complexes prepared with surfactants containing the shortest and the longest spacer (**Figure 4.9**). This behavior is consistent with what has been reported in the literature, stating that a more efficient DNA compaction is promoted by gemini surfactants having either short (< 4) or long (> 10) spacers, as compared to surfactants having intermediate length spacers (Karlsson et al. 2002). In fact, surfactants containing short or long spacers induce more efficiently a Ψ-phase in DNA, which is a

tightly packed condensed form of DNA (Zuidam et al. 1999). A distance of 4.9 Å between surfactant amine groups has been reported to be ideal for their interaction with adjacent phosphate groups of DNA (Wettig et al. 2008), this distance being closer to the one measured for gemini surfactants containing < 3 carbon atom long spacers. The similar destabilization pattern obtained for complexes containing surfactants with short and long spacers might reflect the ability of the 12-10-12 surfactant to coil its spacer, originating a headgroup area resembling that of 12-2-12 surfactant, as previously reported (Almeida et al. 2011).

On the other hand, gemini surfactant-based complexes with long spacers induced high levels of cytotoxicity, which made them unsuitable for gene delivery purposes. In this regard, it was reported (Almeida et al. 2011) that the highly toxic 12-10-12 gemini surfactant was able to induce leakage of aqueous contents from lipid models formulated to mimic the composition of a cell membrane, while the less toxic 12-2-12 and 14-2-14 gemini surfactants showed only a residual percentage of membrane destabilization.

Regarding the gemini surfactant-based complexes with competence for gene delivery, it was shown that they combine low cytotoxicity with high cell association, different levels of DNA interaction and intermediate capacity to be destabilized in the presence of membrane lipid models. It was also shown that all the gemini surfactant-based complexes able to promote transfection without inducing cytotoxicity benefit from the addition of helper lipids. However, although improving transfection ability, these lipids induced a reduction of the extent to which complexes associate to cells. Therefore, other steps in the transfection process, rather than cell-association, are improved by the addition of helper lipids, such as the propensity of DNA to dissociate from the complexes, resulting from a general decrease of the positive surface charge density of the complexes, which in some cases involves an inversion of the charge from positive to negative.

Altogether, our results draw attention to the importance of conducting studies on DNA complex-membrane interactions in order to fully evaluate the physical and structural properties that a delivery system should present to enhance its performance, and contribute to establish guidelines towards the design of efficient nonviral systems for nucleic acid delivery.

Chapter 5

New Serine-derived Gemini surfactants as gene delivery systems

A.M. Cardoso, C.M. Morais, A. Rita Cruz, S.G. Silva, M.L. do Vale E.F. Marques, M.C. Pedroso de Lima and A.S. Jurado, "*New Serine-derived Gemini surfactants as gene delivery systems*" Under review in the European Journal of Pharmaceutics and Biopharmaceutics.

5.1 ABSTRACT

Gemini surfactants have been extensively used for *in vitro* gene delivery. Amino acid-derived gemini surfactants gather the special aggregation properties characteristic of the gemini surfactants allied to high biocompatibility and biodegradability. In this work, new serine-derived gemini surfactants, differing in alkyl chain lengths and in the linker group bridging the spacer to the headgroups (amine, amide and ester),were evaluated for their ability to mediate gene delivery either *per se* or in combination with helper lipids. Gemini surfactant-based DNA complexes were characterized in terms of hydrodynamic diameter, surface charge, stability in aqueous buffer and ability to protect DNA. Efficient formulations, able to transfect up to 50% of the cells without causing toxicity, were found at very low surfactant/DNA charge ratios (1/1 to 2/1). The most efficient complexes presented sizes suitable for intravenous administration and negative surface charge, a feature known to preclude potentially adverse interactions with serum components. This work brings forward a new family of gemini surfactants with great potential as gene delivery systems.

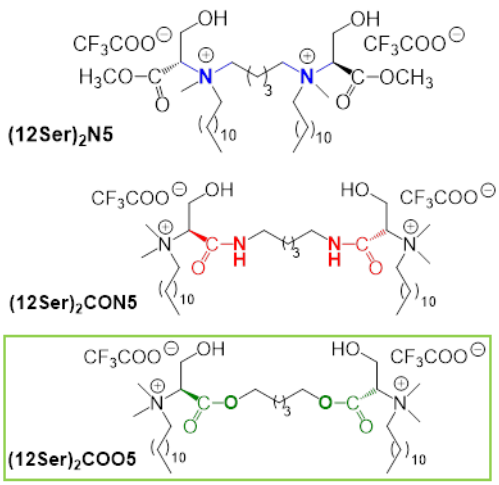

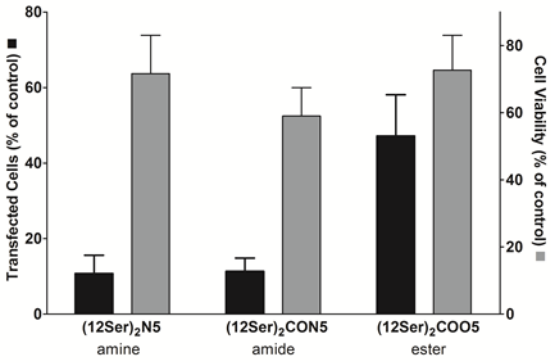

High transfection efficiency and low cytotoxicity was achieved by complexes containing the serine-derived gemini surfactant of the ester series, whose biodegradability allows for DNA release inside the cells and facilitates the clearance of complex debris.

5.2 INTRODUCTION

New biocompatible materials, such as gemini surfactants mimicking natural amphiphilic structures, featured by low toxicity and high biodegradability and thus overcoming environmental concerns and suiting pharmaceutical applications, have recently emerged (Morán et al. 2004). Gemini surfactants composed of two sets of an ionic group and an hydrocarbon chain, linked by a spacer at the level of or close to the head group (Menger & Littau 1991), have shown to exhibit special surface and aggregation properties, which allow a decrease of the concentration needed for a therapeutic effect and thus minimize their potential toxicity (Alami et al. 1993; Buijnsters et al. 2002; Silva et al. 2012). The inclusion of aminoacid moieties in these structures has shown to influence their intermolecular behavior, due to the chiral centers that allow the formation of aggregates with a variety of morphologies (Fan et al. 2008; Silva et al. 2012; Brito et al. 2013), and to enhance their biodegradability and thus their safe use in biological applications (McGregor et al. 2001; Yang et al. 2010). The presence of various functional groups in the amino acid offers the possibility of a great structural variability in the resulting surfactants that can be finely tuned in order to obtain an effective control of their aggregation properties and biological activity. For example, their sensitivity to pH, which is of the utmost relevance in biomedical applications, can be tailored through the introduction of amide/ester bonds. In particular, pH-sensitivity of surfactants used as gene delivery systems can promote DNA release inside the cells in response to the low pH of the endosomal compartment.

Serine-derived gemini surfactants have been recently synthesized for the first time (Silva et al. 2012). These surfactants are modified in two serine amino acid residues, which are polar yet uncharged, thus acquiring one positive charge at the amine functional group of each serine residue. This new family of serine-derived gemini surfactants comprises three different series of compounds, designated, according to the nature of the spacer linkage to the headgroup, as the amine series (**Figure 5.1A**), the amide (**Figure 5.1B**) and the ester series (**Figure 5.1C**). For the amine series, compounds with different alkyl chain lengths were prepared. The impact of this new family of gemini surfactants on the viability of HeLa cells has been studied aiming at their application in the pharmaceutical field (Silva et al. 2013). With respect to their

monomeric counterparts as well as to conventional *bis-quaternary* gemini surfactants with similar hydrocarbon chains and spacer length, serine derivatives show the advantage of exerting lower cytotoxic effects.

In the present work, six members of this new family of serine-derived gemini surfactants were studied towards their application as gene delivery systems in gene therapy. For this purpose, serine-derived gemini surfactants were complexed with a reporter gene and evaluated for their capacity to mediate transfection, while inducing low cytotoxicity. Complexes were characterized in terms of physico-chemical properties relevant for their *in vivo* application, such as their hydrodynamic diameter, surface charge and stability in an aqueous buffer. Furthermore, the ability of the complexes to condense and protect DNA was assessed using a DNA-intercalating agent, as an approach to predict the degree of DNA protection from nuclease degradation. However, in order to promote an efficient gene delivery, the complexes should be able to dissociate upon interaction with cell membrane structures. In this context, membrane-mimicking lipid models were used to evaluate complex cell interactions. In an attempt to unravel the intracellular traffic of the complexes (leading to the endolysosomal degradative route or bypassing this obstacle), the cellular internalization pathways used for the uptake of the complexes able to efficiently mediate transfection were also evaluated.

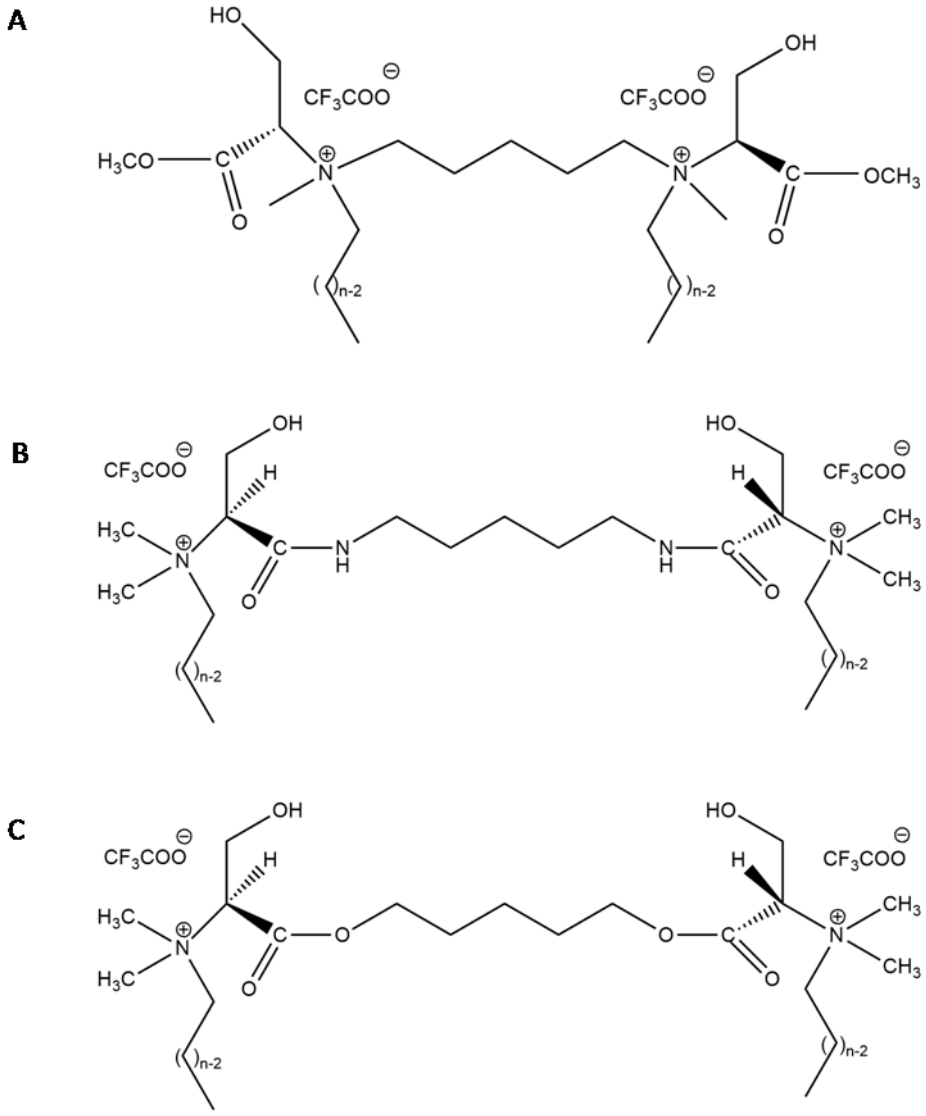

Figure 5.1 Schematic representation of serine-derived gemini surfactants: (A) amine series, herein designated $(nSer)_2Nm$, (m=5 and n=12, 14, 16 and 18); (B) amide, $(12Ser)_2CON5$, and ester, $(12Ser)_2COO5$, series (n=12). All the surfactants contain fully saturated alkyl chains.

5.3 MATERIALS AND METHODS

Materials

The gemini surfactants were synthesized by the method reported by Silva (Silva et al. 2012) and purified by column chromatography. The purity of the compounds was assessed by NMR and mass spectrometry and further confirmed by the *cmc* values, obtained by surface tension measurements, which were all in very good agreement with those already reported (Silva et al. 2012). The lipids 1,2-dioleoyl-sn-glycero-3-phosphoethanolamine (DOPE), cholesterol, 1,2-dioleoyl-sn-glycero-3-phosphocholine (DOPC) and 1-palmitoyl-2-oleoyl-sn-glycero-3-phospho-L-serine (POPS) were purchased from Avanti Polar Lipids (Alabaster, AL). All the other chemicals were of the highest grade.

Preparation of DNA complexes

Complexes were prepared using the method described by (Badea et al. 2005) with a few modifications (Cardoso et al. 2014). Briefly, aqueous solutions (0.5 mM) of gemini surfactants were filtered through 0.22 μm pore-diameter filters (Schleicher & Schuell, BioScience, Germany) and a solution of 1,2-dioleoyl-sn-glycero-3-phosphoethanolamine (DOPE) and cholesterol (Chol) (Avanti Polar Lipids, Alabaster, AL, USA) in chloroform was dried under vacuum in a rotatory evaporator, the resulting lipid films being hydrated with HBS (pH 9.0) to a final lipid concentration of 0.5 mM. The resulting multillamelar vesicles (MLV) of DOPE plus cholesterol were then sonicated for 3 min and filtered through 0.22 μm pore-diameter filters (Schleicher & Schuell, BioScience, Germany). Plain complexes were prepared by mixing 100 μL of HBS containing 0.5 μg of pEGFP-C1 plasmid DNA encoding GFP with aliquots of the aqueous gemini surfactant solution, to obtain a gemini/DNA charge ratios in the range of 1/1 to 8/1 thereafter incubated at room temperature for 15 min. To produce ternary complexes, a volume of DOPE:Chol liposomes was added to surfactant/DNA complexes to obtain surfactant/helper lipids molar ratios in the range of 1/1 to 1/4, followed by 30 min incubation at room temperature.

Cells

HeLa cells (human epithelial cervical carcinoma cell line) were maintained in culture at 37 °C, under 5% CO_2, in Dulbecco's Modified Eagle's medium-high glucose (DMEM-HG; Sigma, St Louis, MO, USA) supplemented with 10% (v/v) heat inactivated fetal bovine serum (FBS; Sigma, St. Louis, MO, USA), penicillin (100 U/mL) and streptomycin (100 µg/mL). The cells were grown in monolayer and detached by treatment with 0.25% trypsin solution (Sigma, St. Louis, MO, USA).

Cell Viability

Cell viability was assessed by a modified Alamar Blue assay (Simões et al. 1999). This assay takes into account the redox capacity of cells and measures the extent of the produced metabolites (resorufin) as a result of cell growth (Konopka et al. 1996). Briefly, 48 h after transfection 0.3 mL of 10% (v/v) resazurin dye in complete DMEM-HG medium were added to each well. After 45 min of incubation at 37 °C, 150 µL of the supernatant was collected from each well and transferred to 96-well plates. The absorbance at 570 and 600 nm (information provided by the supplier) was measured in a SPECTRAmax PLUS 384 spectrophotometer (Molecular Devices, Union City, CA) and cell viability was calculated according to the equation:

$$\text{Cell viability (\% of control)} = [(A_{570} - A_{600})/(A'_{570} - A'_{600})] \times 100$$

where A_{570} and A_{600} are the absorbances of the samples, and A'_{570} and A'_{600} are those of the control (non-treated cells), at the indicated wavelengths.

Transfection efficiency

HeLa cells (0.8×10^5 cell/well) were seeded onto 12-well plates. Following overnight culture, cells were incubated with the different DNA complexes (0.5 µg of pEGFPC1 per well) at 37 °C under 5% CO_2 for 4 h, in OptiMEM medium, or in DMEM medium containing 5 or 10% (v/v) FBS. After this period, the medium was replaced with fresh medium containing 10% (v/v) FBS and antibiotics, and the cells were further incubated for 44 h to allow gene expression. The transfection efficiency mediated by the different complexes was evaluated trough analysis of the expression of green fluorescent protein (GFP) by flow cytometry. Briefly, 48 h after transfection, cells were washed once with PBS and detached with 0.25% trypsin (10 min at 37 °C), and again washed three times by centrifugation (200g, 4 °C, 5 min) in ice-cold PBS. The

resulting pellet was resuspended in ice-cold PBS and the samples were immediately analyzed. Flow cytometry analysis was performed in live cells using a Becton Dickinson (NJ, USA) FACScalibur flow cytometer. Data were collected and analyzed using CellQuest software. Live cells were gated by forward/side scattering from a total of 10,000 events.

Cellular internalization pathways

To address the mechanisms through which surfactant-based complexes are internalized by cells, recognized inhibitors of different endocytic pathways were used. Thus, plated HeLa cells washed with PBS were pre-treated for 30 min, at 37 °C, in serum-free OptiMEM, with the following endocytosis inhibitors (from Sigma): (i) chlorpromazine (30 μM); (ii) fillipin III (5 μg/mL) or (iii) amiloride hydrochloride (5 mM). The cells were then incubated with the complexes in the presence of each inhibitor, for 1 h, at 37 °C, in serum-free OptiMEM. To confirm that inhibitors compromise selectively different endocytic pathways, their effect on the cellular uptake of the fluorescently labeled markers, transferrin, a known marker of clathrin-mediated endocytosis, and lactosylceramide, a marker of raft/caveolae-dependent endocytosis, was analyzed. Cytotoxicity was assessed following cell treatment with each of the drugs by the Alamar blue assay (as described above). Flow cytometry analysis was performed as described in the Transfection Efficiency section to evaluate transfection efficiency of the complexes in cells pre-incubated with each of the drugs.

Surfactant-DNA interactions

Complexes containing 0.2 μg of plasmid DNA, prepared in a total volume of 100 μL of HBS, were allowed to incubate for further 15 min at 37 °C and were then transferred to a 96-well (blackwalled) plate (Corning, NY, USA). Hundred microliters of PicoGreen (Molecular Probes, Eugene, OR), diluted according to the manufacturer's instructions (1:200 dilution in HBS buffer), were added to each sample. The fluorescence intensity of PicoGreen, which is directly proportional to the amount of accessible/free plasmid DNA, was monitored in a Spex Fluorolog Spectrometer for determining the extent of gemini surfactant-DNA complexation. The excitation and emission wavelengths were set at 485 and 520 nm, respectively. The degree of plasmid DNA protection conferred

by the complexes, taken as proportional to the surfactant/DNA complexation, was calculated as follows:

$$P_{DNA} = 1- [(F-F_{100})/(F_0-F_{100})]$$

where F is the fluorescence intensity measured after adding the PicoGreen solution to the complexes, F_0 (corresponding to 0% of plasmid DNA protection) was obtained by using free plasmid DNA in the same amount as that associated with the complexes, F_{100} (corresponding to 100% of plasmid DNA protection) is the residual fluorescence intensity of a negative control obtained by using a PicoGreen solution without plasmid DNA, which mimicked a situation of 0% of DNA available to the PicoGreen solution.

Destabilization of the complexes was accomplished by incubating them for 15 min with small unilamellar vesicles (SUV) of DOPC or of a mixture of DOPE:DOPC:POPS (2:1:1 molar ratio) and evaluated through PicoGreen fluorescence intensity as the difference between the protection obtained for complexes in absence of the lipid vesicles and that obtained in their presence.

Physico-Chemical Properties of the DNA complexes (Particle Size, Zeta Potential, Colloidal Stability)

The size of the surfactant-based structures was assessed using a Submicron Particle Size Analyzer, Beckman Coulter N4 Plus. The colloidal suspensions of the complexes were diluted with HBS, and the particle size analysis was carried out at a scattering angle of 90° and a temperature of 25 °C.

The zeta potential of the surfactant-based structures was measured using a zeta sizer Nano ZS, ZN 3500, with a 532 nm laser (Malvern Instruments, UK). The measurements were performed in HBS, at 25 °C, using DTS 1060C disposable zeta cells and the protocol for general purposes (medium viscosity 0.89 cP, medium refractive index 1.33, sample viscosity 0.89 cP, particle refractive index 1.45 and equilibration time 3 min).Values of dielectric constant of 78.5 and beam mode F(Ka) of 1.5 (Smoluchowsky) were used for zeta potential determination.

The turbidity of gemini surfactants and complex dispersions, providing a measure of their colloidal stability, was monitored as a function of time on a SPECTRAmax PLUS 384 spectrophotometer (Molecular Devices, Union City, CA) at a wavelength of

550 nm. The final concentration of lipid plus gemini surfactant was 0.1 mM in HBS buffer, pH 7.4. The turbidity values were registered over a period of 48 h.

Statistical analysis

Data are presented as mean ± SD. The significance of the results was statistically analyzed by a one-way analysis of variance (ANOVA) with Tukey's multiple pairwise comparison. Statistical significance was set at $p < 0.05$.

5.4 RESULTS

5.4.1 BIOLOGICAL ACTIVITY OF SERINE-DERIVED GEMINI SURFACTANT-BASED DNA COMPLEXES

At cellular level, an efficient nonviral gene delivery system has to encapsulate/complex the nucleic acids and confer protection from degradation by intracellular and extracellular nucleases, carry them into the cell, release its cargo next to the intracellular target and promote high gene expression, without causing cytotoxicity. In this regard, cytotoxicity of the plain (gemini surfactant/DNA) and ternary (gemini surfactant/DNA/helper lipids) complexes was evaluated, and those complexes that did not promote significant loss of cell viability were selected for evaluating their ability to mediate transfection. The internalization pathways used by the complexes able to efficiently mediate gene expression were also assessed.

Cytotoxicity induced by serine-derived gemini surfactant-based DNA complexes

Figure 5.2 shows the results obtained for the toxicity of surfactant-based DNA complexes in HeLa cells. As observed, the cytotoxic effect was dependent on the (+/-) charge ratio of the complexes, increasing for the highest charge ratios tested. The complexes that induced the highest loss of cell viability were those formulated with $(12Ser)_2CON5$ and $(18Ser)_2N5$ at the 8/1 (+/-) charge ratio, both in the absence and presence of helper lipids. On the other hand, complexes prepared with $(12Ser)_2COO5$ and $(16Ser)_2N5$ were the least toxic, particularly at the lowest charge ratios assayed. Furthermore, at the highest charge ratio, cytotoxicity was found to decrease with increasing hydrocarbon chain length of the surfactant, for alkyl chains from 12 to 16 carbon atoms-long. However, this trend was reverted by $(18Ser)_2N5$-based complexes, which induced the highest cytotoxicity among the complexes containing surfactants of the amine series. Concerning the effect of the nature of the spacer linkage on cell viability, comparison of the analogous compounds of each series shows that complexes containing surfactants of the ester series are the least cytotoxic, followed by complexes containing surfactants of the amine series and at last those with surfactants of the amide series.

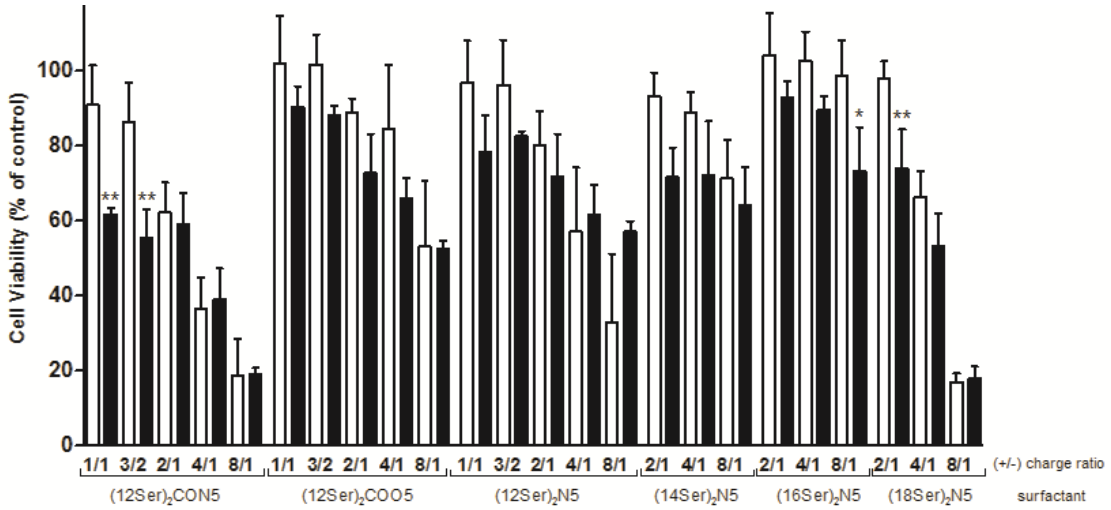

Figure 5.2 Viability of HeLa cells upon incubation with complexes composed of the surfactant (indicated in the figure), without (□) or with (■) the helper lipids DOPE and cholesterol (2:1 molar ratio), at the indicated (+/-) charge ratios. Cell viability was expressed as a percentage of a control (non-treated cells). Pairwise data comparisons were performed for the helper lipids-containing complexes *vs.* the corresponding helper lipids-free complexes at the same (+/−) charge ratio (*p < 0.05, **p< 0.01).

Transfection efficiency of serine-derived gemini surfactant-based DNA complexes

Complexes that did not cause significant toxicity to HeLa cells were selected for the evaluation of their ability to mediate gene delivery. As observed in **Figure 5.3A**, complexes prepared in the absence of helper lipids lack the ability to efficiently mediate gene expression. The only exception was found for complexes composed of $(18Ser)_2N5$ surfactant prepared at the 2/1 (+/-) charge ratio, which were able to transfect 21 and 32% of cells in the presence and absence of helper lipids, respectively, albeit no significant difference was obtained between the two formulations. Although the gemini surfactants of each series (amine, amide and ester) with 12 carbon alkyl chains (C12) were unable to efficiently mediate transfection *per se*, the corresponding complexes formulated with the helper lipids DOPE and cholesterol presented significant transfection efficiency (up to 27%, 37% and 50%, respectively for $(12Ser)_2CON5$, $(12Ser)_2N5$ and $(12Ser)_2COO5$). Interestingly, the highest levels of transfection were found for the lowest charge ratios tested (1/1 to 2/1). Comparison with the commercial reagent Lipofectamine 2000 showed that, although this reagent was able to transfect more cells than the serine-derived gemini surfactant-based complexes (74%, data not shown), it induced significantly higher levels of cytotoxicity (only 35.6% of viable cells, data not shown).

Transfection experiments in the presence of increasing amounts of serum were performed using the formulations containing the ester, the amide and the amine gemini surfactants with 12C tails and helper lipids. As illustrated in **Figure 5.3B,** transfection efficiency of complexes containing the ester gemini surfactant, prepared at the 3/2 and 2/1 (+/-) charge ratios, showed to be independent of the presence of serum.

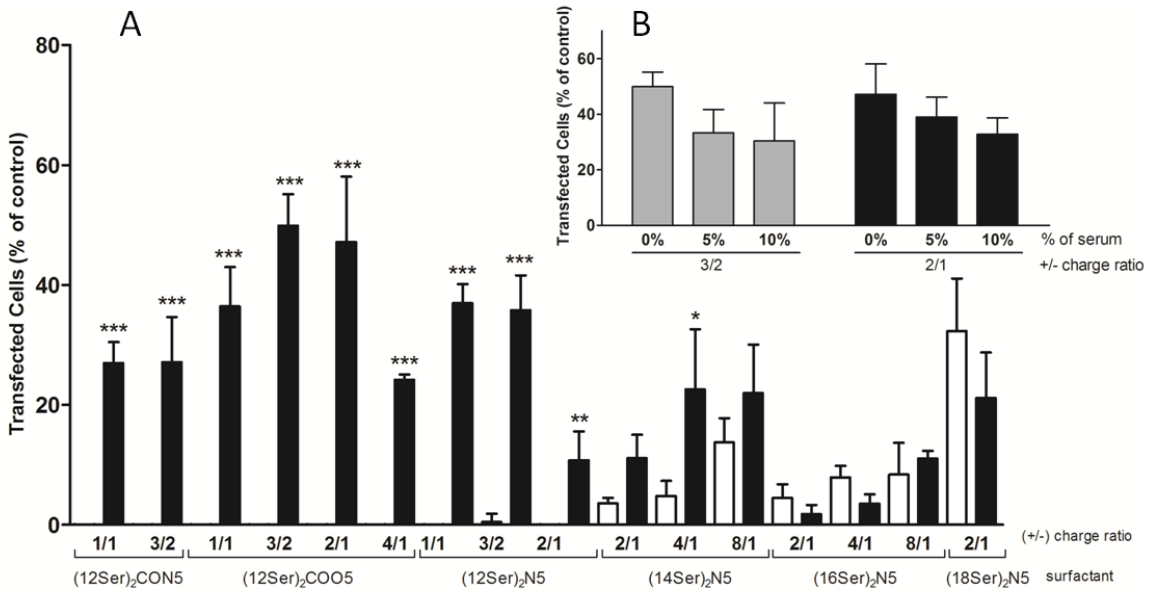

Figure 5.3 Transfection efficiency of gemini surfactant-based DNA complexes formulated without (□) or with (■) the helper lipids DOPE and cholesterol (2:1 molar ratio), at the indicated (+/-) charge ratios (A) and of $(12Ser)_2COO5$:HL-based DNA complexes prepared at 3/2 (■) and 2/1 (■) (+/-) charge ratio, performed in the absence (0%) or presence of increasing amounts of serum (5 and 10%) (B). Data comparisons were performed for helper lipid-containing complexes vs. the corresponding helper lipid-free complexes at the same (+/−) charge ratios (*$p < 0.05$, **$p < 0.005$, ***$p < 0.001$). No significant statistical differences were found between cells transfected in the presence of each percentage of serum and in absence of serum.

Cellular internalization pathways used for the uptake of serine-derived gemini surfactant-based DNA complexes

The mechanisms involved in the internalization of serine-derived gemini surfactant-based DNA complexes by HeLa cells were studied for the complexes that presented the highest transfection ability. Cells were treated with drugs that selectively inhibit endocytic processes that occur at different membrane domains, namely clathrin-mediated endocytosis, which takes place in non-lipid raft domains, macropinocytosis, which occurs in mixed raft and non-raft domains, and raft-mediated endocytosis, which includes caveolae-mediated endocytosis (El-Sayed & Harashima 2013). Cellular internalization mechanisms were identified by flow cytometry, through the evaluation of transfection efficiency of cells pre-incubated with the pharmacological inhibitors of clathrin-mediated endocytosis (chlorpromazine), macropinocytosis (amiloride hydrochloride) and endocytic processes occurring in lipid raft domains of the cell membrane (filipin III).

The complexes containing surfactants with 12 carbon alkyl chains of each of the three series and helper lipids showed to be preferentially internalized by macropinocytosis, since the lowest level of transfection was observed upon treatment of cells with amiloride hydrochloride (**Figure 5.4**). Among these complexes, those prepared with $(12Ser)_2CON5$ and $(12Ser)_2COO5$ surfactants were also internalized through cholesterol-enriched membrane domains (lipid-rafts),as concluded from the significant reduction in transfection observed in filipin III-treated cells. The clathrin-mediated endocytosis showed to have also a significant contribution to internalize complexes prepared with $(12Ser)_2N5$ and $(12Ser)_2COO5$. Complexes prepared with $(18Ser)_2N5$ in the absence and presence of helper lipids were compared in terms of the cellular internalization pathways. While the complexes devoid of helper lipids were not internalized by any of the endocytic pathways evaluated, suggesting the capacity to cross membranes through direct interaction with membrane lipids, the complexes formulated with helper lipids were partly taken up by a clathrin-mediated endocytosis process and partly by macropinocytosis.

Noteworthy, the transfection efficiency observed for all the studied complexes upon cell treatment with endocytosis inhibitors did not decay to residual values, suggesting that a membrane lipid-mediated process may be involved in their cell uptake.

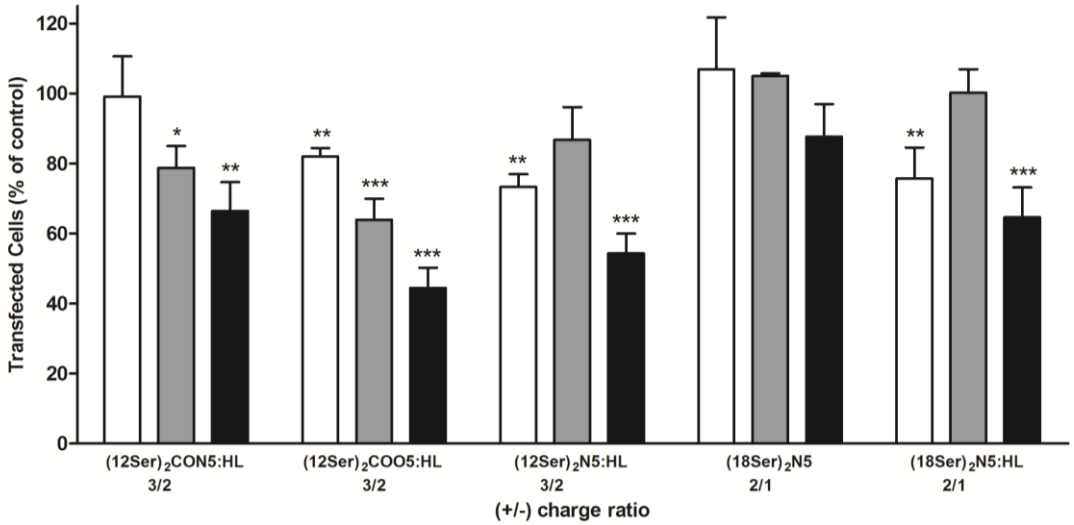

Figure 5.4 Effect of different endocytosis inhibitors on transfection mediated by surfactant-based DNA complexes. HeLa cells were incubated with either 30 μM of chlorpromazine (□), 5μg/mL of fillipin III (■), or 2.5 mM of amiloride hydrochloride (■) and transfected with the complexes indicated in the figure. Transfection in the presence of each inhibitor was expressed as percentage of transfected cells with each complex but not treated with the inhibitors of internalization pathways. Data are presented as mean ± standard deviation, representative of at least three independent experiments. Data comparisons were performed between each condition tested and the respective control corresponding to 100% of transfected cells (*p<0.05, **p<0.01, ***p<0.001).

5.4.2 Characterization of serine-derived gemini surfactant/DNA complexes

Interaction of gemini surfactants with opposing charged DNA is regarded as a key feature for the efficient nucleic acid complexation and protection from nuclease degradation. As other nonviral gene delivery systems, gemini surfactant-based DNA complexes should meet some criteria, in terms of surface charge, hydrodynamic diameter and stability, towards successful transfection. In this regard, complexes displaying high transfection efficiency as well as those unable to transfect cells were evaluated for those parameters in order to ascertain the physico-chemical properties responsible for efficiency in gene delivery.

Protection of DNA by serine-derived gemini surfactants

The ability of gemini surfactants to interact and protect DNA was evaluated using the fluorescent probe PicoGreen, which intercalates nucleic acid double strands and whose fluorescence is dramatically enhanced in this condition. **Figure 5.5** displays the percentage of DNA inaccessible to the probe, expressed in terms of DNA protection conferred by the gemini surfactants or the gemini surfactants plus the helper lipids DOPE and cholesterol. A higher degree of DNA protection was observed with increasing (+/-) charge ratio of the complexes, formulated both in the absence

and presence of helper lipids. The ester-derived surfactant showed the lowest levels of protection (**Figure 5.5A**), displaying high protection ability only at the highest (+/-) charge ratio tested (8/1). Protection promoted by $(14Ser)_2N5$ and $(18Ser)_2N5$ was very efficient even at the (+/-) charge ratio of 2/1 (more than 80%) in contrast to $(12Ser)_2N5$, which showed high protection only at the (+/-) charge ratio of 4/1 or higher, and to $(16Ser)_2N5$, which exhibited much lower protection levels at all the (+/-) charge ratios assayed. Therefore, no linear relationship between alkyl chain length and efficiency of DNA protection was found. The addition of helper lipids to the complexes decreased the degree of DNA protection conferred by the surfactants at the highest charge ratios, except in the case of the complexes containing $(14Ser)_2N5$ and $(18Ser)_2N5$, which showed similar abilities to protect DNA in the absence and presence of helper lipids over the range of charge ratios tested. On the other hand, at the lowest charge ratios, $(12Ser)_2COO5$ and $(12Ser)_2N5$ complexes exhibited higher capacity to avoid DNA-probe interactions in the presence of helper lipids. In contrast, complexes of $(16Ser)_2N5$ and helper lipids conferred lower protection to DNA than the corresponding complexes composed of neat surfactant at all the charge ratios tested.

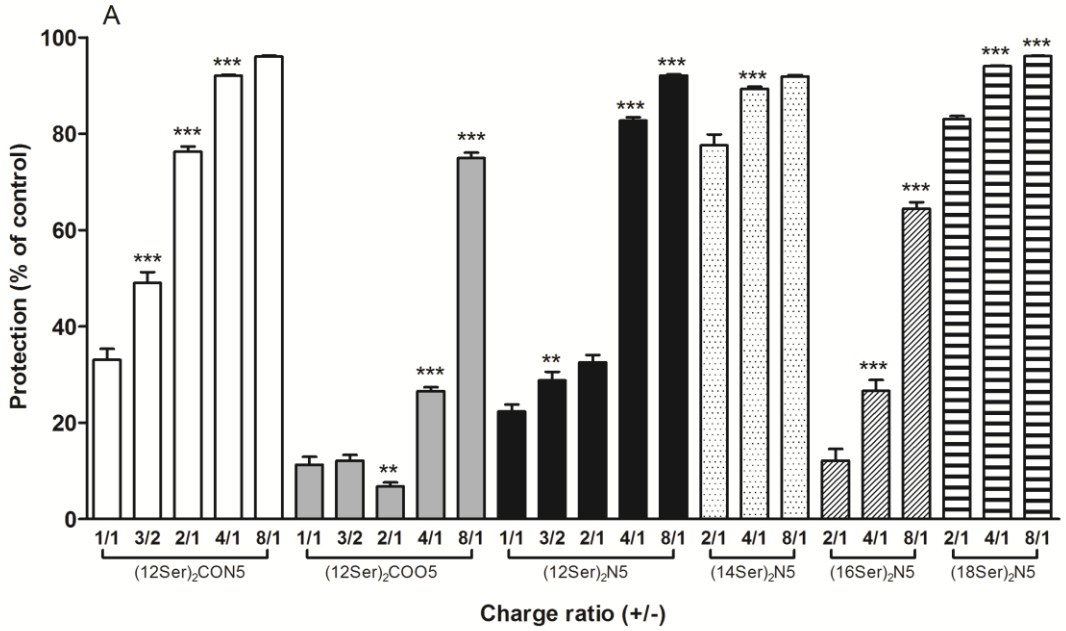

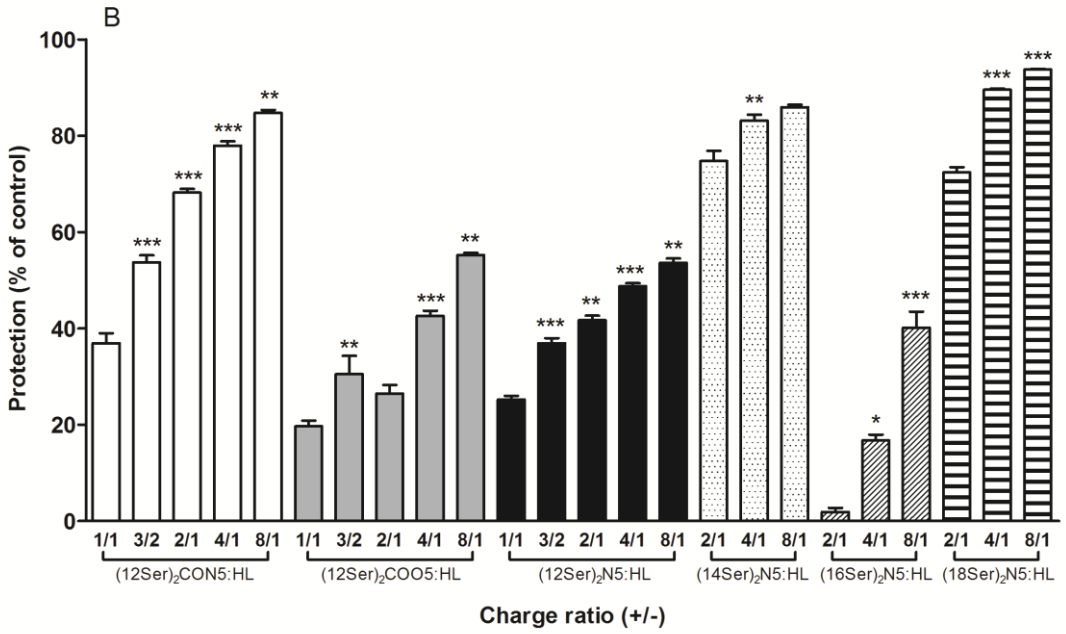

Figure 5.5 Gemini-DNA interactions, as assessed by PicoGreen accessibility to DNA complexed with gemini surfactants (A) or gemini surfactants plus the helper lipids (HL) DOPE and Cholesterol (2:1 molar ratio) (B), at the indicated (+/-) charge ratios. The maximum fluorescence (control) corresponds to maximum DNA accessibility. Data comparisons were performed for the complexes at different (+/−) charge ratios vs. the same complex formulations at the immediately precedent (+/−) charge ratio ($^{*}p < 0.05$, $^{**}p < 0.01$, $^{***}p < 0.001$).

Physico-chemical properties of surfactant-based DNA complexes

The size of the complexes was evaluated by dynamic light scattering and was found to vary depending on composition and charge ratio (**Table 5.1**). The sizes of the complexes were found to range from 163 nm to more than 3 μm, all samples showing a polydispersity index higher than 0.3, and being therefore analyzed as polydisperse samples. Complexes formulated with the surfactants having long hydrocarbon chains (16 and 18 carbon atoms) showed at all (+/-) charge ratios an increase in size promoted by the addition of the helper lipids. The complexes formulated with surfactants containing short hydrocarbon chains (C12 and C14) showed the same tendency, except at the lowest (+/-) charge ratio assayed (1/1 for the complexes of surfactants C12 and 2/1 for the $(14Ser)_2N5$-based complexes), under which condition the helper lipids induced a decrease in size.

Table 5.1 Hydrodynamic diameter of DNA complexes formulated with gemini surfactants at different (+/-) charge ratios, in the absence and in the presence of the helper lipids DOPE and cholesterol.

	Hydrodynamic Diameter /nm[1)]				
	1/1	3/2	2/1	4/1	8/1
$(12Ser)_2CON5$	970 ± 140	1741 ± 186	1662 ± 467	560 ± 140	290 ± 27
$(12Ser)_2CON5$:DOPE:Chol	933 ± 98	>3000	2221 ± 674	1032 ± 43	460 ± 45
$(12Ser)_2COO5$	490 ± 200	271 ± 63	393 ± 41	355 ± 41	2000 ± 348
$(12Ser)_2COO5$:DOPE:Chol	387 ± 13	410 ± 14	454 ± 12	960 ± 140	2413 ± 266
$(12Ser)_2N5$	810 ± 220	1232 ± 114	2239 ± 629	526 ± 65	267 ± 13
$(12Ser)_2N5$:DOPE:Chol	800 ± 170	2827 ± 376	2747 ± 362	1022 ± 95	500 ± 250
$(14Ser)_2N5$	-	-	2389 ± 692	312 ± 43	163 ± 9
$(14Ser)_2N5$:DOPE:Chol	-	-	1624 ± 399	1582 ± 151	919 ± 36
$(16Ser)_2N5$	-	-	233 ± 25	497 ± 85	1374 ± 102
$(16Ser)_2N5$:DOPE:Chol	-	-	607 ± 42	780 ± 190	1824 ± 399
$(18Ser)_2N5$	-	-	850 ± 120	196 ± 14	166 ± 9
$(18Ser)_2N5$:DOPE:Chol	-	-	2527 ± 478	304 ± 31	222 ±10

[1)] Results represent mean ± SD of at least three independent experiments. All samples were polydisperse.

The surface charge of the complexes composed of gemini surfactant/DNA and gemini surfactant/DNA/helper lipids was assessed by Zeta potential measurements (**Table 5.2**). The surface charge of the structures formed by gemini surfactants and gemini surfactants plus helper lipids in aqueous suspensions, in the absence of DNA, was also measured for comparison. As observed in **Table 5.2**, the particles composed of surfactants exhibited a positive surface charge. The complexation of DNA by the surfactants containing C12 alkyl chains led to a change in the Zeta potential to negative values, although for complexes of $(12Ser)_2CON5$ the signal inversion occurred only at the lowest (+/-) charge ratios assayed (1/1 and 3/2). Surfactants with longer hydrocarbon chains maintained the positive Zeta potential upon complexation with DNA, at least at (+/-) charge ratios higher or equal to 2/1. In the absence of DNA, the addition of helper lipids to the surfactants containing 12 carbon alkyl chains did not alter the sign of the surface charge. However, for surfactants with longer hydrocarbon chains, the helper lipids inverted the Zeta potential value, from positive to negative. Complexes of $(12Ser)_2CON5$ prepared with helper lipids showed a highly positive charge over the range of (+/-) charge ratios tested. The incorporation of helper lipids into the complexes of surfactants $(12Ser)_2N5$ and

$(12Ser)_2COO5$ produced structures with positive Zeta potential at high surfactant/DNA charge ratio and with negative Zeta potential at low surfactant/DNA charge ratio. The opposite occurred for complexes of surfactants containing longer hydrocarbon chains and formulated with helper lipids. Complexes of $(14Ser)_2N5$ and $(16Ser)_2N5$ displayed negative Zeta potential at the highest (+/-) charge ratio (8/1) and positive surface charge at the other (+/-) charge ratios. Furthermore, $(18Ser)_2N5$-containing complexes formulated with helper lipids presented a highly negative Zeta potential in the range of charge ratios assayed.

Table 5.2 Zeta potential of DNA complexes formulated with gemini surfactants at different (+/-) charge ratios, in the absence or in the presence of the helper lipids DOPE and cholesterol.

	ζ-potential /mV[1)]					
	1/1	3/2	2/1	4/1	8/1	no DNA
$(12Ser)_2CON5$	-14 ± 11	-5 ± 12	+18 ± 8	+18 ± 6	+14 ± 5	+6 ± 8
$(12Ser)_2CON5$:DOPE:Chol	+21 ± 8	+28 ± 7	+30 ± 9	+36 ± 8	+32 ± 10	+30 ± 8
$(12Ser)_2COO5$	-16 ± 11	-26 ± 7	-27 ± 8	-23 ± 10	-10 ± 10	+2 ± 9
$(12Ser)_2COO5$:DOPE:Chol	-35 ± 7	-38 ± 7	-37 ± 7	-21 ± 10	+4 ± 13	+14 ± 8
$(12Ser)_2N5$	-21 ± 8	-23 ± 9	-21 ± 7	-7 ± 14	-3 ± 11	+17 ± 9
$(12Ser)_2N5$:DOPE:Chol	-38 ± 7	-28 ± 8	-13 ± 10	+13 ± 7	+19 ± 5	+17 ± 9
$(14Ser)_2N5$	-	-	+13 ± 10	+9 ± 3	+13 ± 7	+6 ± 2
$(14Ser)_2N5$:DOPE:Chol	-	-	+27 ± 2	+25 ± 3	-35 ± 2	-40 ± 3
$(16Ser)_2N5$	-	-	+22 ± 5	+31 ± 2	+23 ± 2	+52 ± 9
$(16Ser)_2N5$:DOPE:Chol	-	-	+18 ± 2	+16 ± 1	-39 ± 2	-42 ± 3
$(18Ser)_2N5$	-	-	+31 ± 3	+29 ± 5	+34 ± 4	+46 ± 5
$(18Ser)_2N5$:DOPE:Chol	-	-	-35 ± 4	-43 ± 2	-44 ± 2	-49 ± 3

[1)] Results represent mean ± SD of at least three independent experiments. All samples were monodisperse.

Evaluation of the colloidal stability of the surfactant-based DNA complexes, by monitoring the absorbance at 550 nm over a period of 48 h, revealed that all complexes were extremely stable over a period of at least 24 h (data not shown). This aspect is particularly important for intravenous administration of freshly prepared complexes, in order to ensure their prolonged blood circulation.

5.4.3 Interaction of surfactant/DNA complexes with lipid membrane models

Destabilization of DNA complexes upon interaction with cellular membranes is essential for nucleic acid release in or close to their intracellular target, in order to allow gene expression.

Destabilization of the serine-derived gemini surfactant-based DNA complexes was evaluated upon interaction with lipid vesicles with different composition (neutral DOPC vesicles, and negatively charged DOPE:DOPC:POPS (2:1:1) vesicles). **Figure 5.6** shows the effects exerted by the two lipid membrane models on complex stability, reflected by the exposure of the DNA to the fluorescent probe (PicoGreen). Complexes prepared at high (+/-) charge ratios were more extensively destabilized than those prepared at lower charge ratios. Among the complexes formulated with surfactants containing 12 carbon alkyl chains, those possessing an ester bond presented the lowest level of destabilization and their stability did not show to be affected by the presence of helper lipids. In contrast, the addition of helper lipids to complexes formulated with $(12Ser)_2N5$ and $(12Ser)_2CON5$ surfactants led to a decrease in the susceptibility to destabilization induced by both types of membranes. Differences in the destabilizing effects exerted by the zwitterionic and the anionic vesicles were noticeable for complexes formulated with surfactants containing hydrocarbon chains with 14 or more carbon atoms. Whereas complexes containing surfactants with 14 and 16 carbon alkyl chains were less destabilized by anionic lipid vesicles than by the zwitterionic vesicles, complexes formulated with $(18Ser)_2N5$ were not destabilized by DOPC vesicles but presented a high degree of destabilization in the presence of the anionic lipid mixture, especially those complexes containing helper lipids.

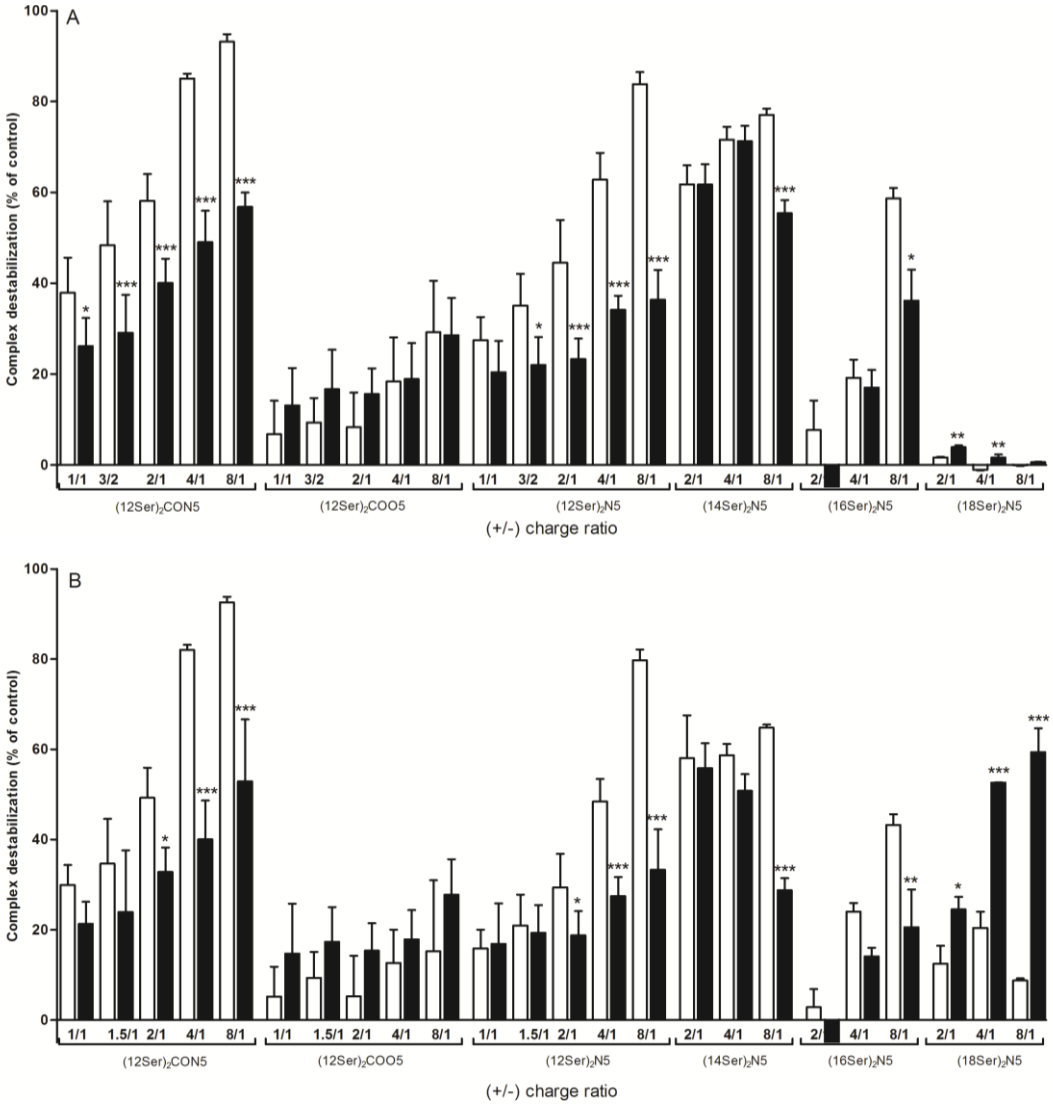

Figure 5.6 Destabilization of surfactant-based complexes upon interaction with lipid vesicles of DOPC (A) or of a mixture of DOPE:DOPC:POPS (2:1:1 molar ratio) (B), evaluated in terms of PicoGreen (fluorescent probe) access to DNA. The surfactant/DNA (white bars) or surfactant/DNA/helper lipids (black bars) complexes, at the indicated (+/-) charge ratios, were incubated with a PicoGreen solution (dilution 1:200) and lipid vesicles were then added in a two-fold excess over the surfactant concentration. Data are presented as percentage of maximum complex destabilization obtained with a control prepared with PicoGreen and free DNA (in the same amount as that associated with the complexes), corresponding to maximum PicoGreen accessibility to DNA. The results represent the mean ± standard deviation obtained from three independent experiments. Data comparisons were performed between formulations prepared with and without helper lipids (*$p<0.05$, **$p<0.005$, ***$p<0.001$).

5.5 DISCUSSION

A systematic comparative study of the ability of six members of a new family of serine-derived gemini surfactants to safely mediate gene delivery and transfection has been conducted in the present work. The gemini surfactants of this family were selected in order to examine the influence of i) the length of the hydrocarbon chains (C12, C14, C16 and C18), specifically in the amine series, and ii) the nature of the linkage between the cationic headgroup and the spacer (amine, amide and ester) on the transfection efficiency. For this purpose, plain gemini surfactant/DNA complexes and ternary complexes of gemini surfactant/DNA/helper lipids, resulting from the addition of DOPE and cholesterol liposomes (2/1 molar ratio) to plain complexes, were evaluated as safe gene delivery systems and characterized in terms of their physico-chemical properties. Destabilization of the gemini surfactant-based complexes was monitored upon the addition of membrane mimicking lipid vesicles in order to shed light on the importance of complex-membrane interactions in their ability to mediate gene delivery. For the sake of clarity, these data will be discussed from two perspectives: a) the influence of the hydrocarbon chain length and b) the importance of the nature of the headgroup/spacer linkage in the biological activity of serine-derived gemini surfactants.

Influence of the hydrocarbon chain length on the biological activity of serine-derived gemini surfactants

Concerning the surfactants of the amine series (effect of alkyl chain length), in the presence of helper lipids, all the surfactants studied were able to mediate gene delivery to some extent. There was no linear relationship between alkyl chain length and transfection efficiency, the surfactant containing the 16 carbon alkyl chain, $(16Ser)_2N5$, being the least efficient. This relationship seems to contrast with that observed for complexes of conventional *bis-quaternary* gemini surfactants, for which the surfactant containing 16 carbon alkyl chains exhibited the highest transfection efficiency (Cardoso et al. 2014). However, care must be taken before a direct comparison is made. The different behavior of the conventional *versus* the serine-derived gemini surfactants in terms of transfection can be assigned either to the nature of their headgroups (simple alkyl ammonium vs. serine-derived ammonium), or to the length of the spacers (2 methylene vs. 5 methylene groups). In fact, the

volume occupied by the cationic headgroup of serine-derived gemini surfactants is much larger than that of the conventional *bis-quat* gemini surfactants, whose headgroups are composed of simple dimethyl quaternary ammonium groups instead of the larger serine residues. On the other hand, the spacer length is important in governing gemini surfactant interactions with other molecules. According to Wettig *et al*. (Wettig et al. 2007), surfactant ammonium groups should be 4.9 Å apart in order to better interact with adjacent phosphate groups of DNA. This distance has been reported to be equivalent to the trimethylene spacing in spermine, which is closest to that determined for gemini surfactants containing a two (Karlsson et al. 2002) to three methylene spacer (Wettig et al. 2007). However, the presence of large headgroups, such as those of the serine-derived gemini surfactants, can result in an efficient accommodation of the DNA phosphate groups due to the flexibility of the surfactant chemical structure, namely at the level of the number of rotatable C-C bonds (Karlsson et al. 2002).

DNA protection provided by the complexes prepared with serine-derived gemini surfactants with different hydrocarbon chain lengths followed a trend similar to that observed for the transfection efficiency, *i.e*. the $(16Ser)_2N5$-based complexes were those that confer the lowest protection to DNA and exhibit the lowest transfection efficiency. Interestingly, these complexes showed also the lowest cytotoxicity. Taking into consideration the effects on cytotoxicity and DNA protection exerted by plain complexes prepared with gemini surfactants containing 14, 16 and 18 carbon alkyl chains at the 8/1 (+/-) charge ratio, the following sequence $(18Ser)_2N5 \geq (14Ser)_2N5 > (16Ser)_2N5$ can be established. This turning point has been already found in terms of the cytotoxicity of this series of serine-derived surfactants (Silva et al. 2013), an event that we interpreted in light of the cutoff-effect described for the interaction of alcohols of increasing chain length with lipid membranes (Peoples et al. 1996). However, the cytotoxicity of the surfactants *per se* was found to vary with the hydrocarbon chain length inversely to the corresponding complexes, i.e. $(16Ser)_2N5 > (14Ser)_2N5 > (18Ser)_2N5$.

In order to improve the transfection efficiency of serine-derived gemini surfactants, the helper lipids DOPE and cholesterol were used in combination. The helper lipid DOPE confers the system the ability to escape lysosomal degradation, while cholesterol was found to be a more biocompatible lipid and less prone to interact

with serum proteins (Faneca et al. 2002; Liu et al. 1997; Templeton et al. 1997). The addition of helper lipids to complexes containing serine-derived gemini surfactants with 14 to 18 carbon atom alkyl chains increased their cytotoxicity. Apparently, helper lipid-induced cytotoxicity had only a negative impact on the transfection efficiency in the case of complexes prepared with $(18Ser)_2N5$. Despite the increase of cytotoxicity, the addition of helper lipids promoted increased transfection levels for complexes containing $(14Ser)_2N5$ and did not significantly affect transfection induced by complexes containing $(16Ser)_2N5$. In view of the disparity of effects exerted by helper lipids on the transfection efficiency of complexes containing gemini surfactants with hydrocarbon chains of different length, it is expected that those lipids induce the formation of structurally different aggregates, depending on the incorporated surfactants.

Regarding the interaction of the complexes with lipid vesicles, it is interesting to observe that the plain complexes containing the surfactants with the shortest hydrocarbon chains were more extensively destabilized than those containing surfactants with longer hydrocarbon chains, and that only the $(18Ser)_2N5$ surfactant-containing complexes were preferentially destabilized by anionic lipid vesicles. Curiously, the addition of helper lipids to $(18Ser)_2N5$-containing complexes significantly increased their destabilization, specially by the anionic lipid vesicles, in contrast to what occurred with the other complexes. The negative impact that helper lipids exhibited on the transfection efficiency of $(18Ser)_2N5$-based complexes may be attributed not only to the increased cytotoxicity, but also to a detrimental lack of DNA protection upon interaction with membranes.

Importance of the nature of the headgroup/spacer linkage in the biological activity of serine-derived gemini surfactants

Regarding the influence of the nature of the headgroup/spacer linkage on the biological behavior of gemini surfactants, it has been shown that the incorporation of chemical bonds susceptible of being enzymatically cleaved, such as ester and amide, in the molecular structure of delivery system components, reduces their cytotoxicity and enhances their ability to produce efficient complexes with DNA (Ilies et al. 2006). Consistent with this finding, data obtained with complexes prepared with surfactants of each of the three series (amine, amide and ester) possessing C12 alkyl chains

showed low cytotoxicity and high transfection efficiency, although the latter was observed only when complexes were formulated with helper lipids. The lowest cytotoxicity and the highest transfection efficiency were displayed by complexes containing the surfactant of the ester series.

It is worth noting that the ester gemini surfactant presents two more rotatable bonds than the amine and amide derivatives with the same hydrocarbon chain length. On the other hand, the effective length of the spacer for the gemini surfactants of the ester and amide series, i.e. the distance separating the two quaternary ammonium groups, corresponds to 11 methylene groups, because the linkage of the spacer to the serine residue is made through the α-carboxylate group of the aminoacid, rather than directly to the charged nitrogen atom. Therefore, these gemini surfactants should have the ability to coil their flexible spacer in order to place the charged headgroups at the ideal distance to interact with the phosphate groups of DNA molecules (Karlsson et al. 2002). This ability to refine the interaction with DNA molecules is likely higher in the ester series since the amide linkage, in contrast with the ester linkage, has a high double bond character that constrains free rotation of this bond, thus reducing the flexibility of the spacer. This could explain the higher transfection efficiency of complexes formulated with surfactant of the ester series in the presence of helper lipids as compared to those incorporating the other 12 carbon alkyl chain-containing surfactants with amide or amine linkages to the headgroup. However, the transfection efficiency of complexes composed of $(12Ser)_2COO5$ plus helper lipids does not seem to be related with the DNA protection afforded by these components. Indeed, the ester derivative gemini surfactant formulated with helper lipids conferred lower protection to DNA than the amide derivative and similar to that conferred by the amine derivative, both also formulated with helper lipids. Considering the plain complexes (without helper lipids), it is probable that the interaction of the least flexible surfactant molecules (amine and amide derivatives) with DNA originates more steric hindrance with consequent higher protection levels, as compared to those afforded by the surfactant of the ester series. Furthermore, addition of helper lipids to these systems leveled the protection conferred to DNA, which implicates a new structural arrangement of the surfactant molecules around DNA, at least at the highest charge ratios tested at which the protection levels decreased upon addition of the helper lipids. A possible explanation for this could be the existence of liposomes in

suspension that do not take part in the complex formation but displace some surfactant molecules from the DNA complex to partition in the lipid bilayer, whenever this process is thermodynamically favorable. The interaction between DOPE and gemini surfactants was described as antagonistic in nature, due to their differences regarding the preferred curvature of the aggregates (Akbar et al. 2012). In light of these data, we would expect the serine-derived gemini surfactants, which aggregate into micelles in aqueous environment, to interact with DOPE in an antagonistic manner. However, the serine-derived gemini surfactants are pre-complexed with DNA, which most likely alters the suppramolecular aggregates formed. Moreover, DOPE, mixed with cholesterol, is prepared at basic pH, and added to the surfactant/DNA complexes in the form of vesicles.

For those formulations able to efficiently mediate transfection, a compromise should exist between the ability to complex and protect DNA and to release it inside the cell. The eventual intracellular degradation of the labile amide and ester bonds may lead to the disaggregation of the complexes and consequent nucleic acid release. In fact, although the complexes incorporating $(12Ser)_2COO5$,containing or not helper lipids, showed to be less efficient in releasing DNA upon interaction with membranes, as compared to complexes prepared with the amide, $(12Ser)_2CON5$, or amine, $(12Ser)_2N5$, homologues, they presented the highest transfection efficiency. Thus, DNA release should occur inside the cell, where acidification of the endosomal compartment could trigger structural changes in the surfactant molecules (e.g. hydrolysis of the ester bond), leading to complex destabilization and nucleic acid release into the cytoplasm.

Regardless of what has been described for lipoplexes about the relationship between size and transfection efficiency (Simões et al. 2005), large complexes containing the gemini surfactants were found not to be those presenting the highest transfection ability. In fact, the complexes that induced the highest transfection levels (formed by the ester derivative, DNA and helper lipids at low (+/-) charge ratios) displayed rather small sizes (387 to 454 nm). Interestingly, complexes of serine-derived gemini surfactants showed to be generally smaller than those of conventional 12-5-12 gemini surfactant, using the same methodology for preparation of both types of complexes. Furthermore, 12-5-12 surfactant produced complexes which, besides exhibiting very low transfection efficiency, they revealed to be highly cytotoxic, even

when formulated with helper lipids, thus being unsuitable for gene delivery purposes (Cardoso et al. 2014). The small sizes of the complexes are important for intravenous administration to circumvent capillary retention. Noteworthy, the hydrodynamic diameter of the most efficient complexes described here is similar to that reported for branched PEI-based DNA complexes, which have been used for intravenous administration in Balb/c mice (Tripathi et al. 2013), indicating that serine-derived surfactant-based formulations possess dimensions suitable for use *in vivo*. However, other routes for *in vivo* administration of DNA complexes that are not constrained by their size have been applied (Neves et al. 2006; Pfeiffer et al. 2006; Donkuru et al. 2010). Therefore, the potential of large DNA complexes such as those based on $(12Ser)_2N5$ for *in vivo* application should not be excluded.

Another relevant feature presented by the complexes containing the ester-derived surfactant is their negative Zeta potential at all charge ratios tested (except at the highest charge ratio, in the presence of helper lipids). Complexes containing the C12 amine-derived surfactant shared this feature in most conditions. Such negatively charged complexes should escape from the unspecific electrostatic interaction with serum proteins, a drawback associated with the use of highly positive charged particles for gene delivery *in vivo*. In fact, these complexes were also those which showed ability to transfect HeLa cells in the presence of serum, with no significant efficiency reduction with respect to that obtained in the absence of serum.

Noteworthy, the high transfection efficiency of DNA complexes formulated with the ester derivative was observed at low surfactant/DNA charge ratios (1/1 to 2/1). This is particularly relevant for a potential application *in vivo*, since a decrease in surfactant dose ensures a decrease in toxicity, thus reducing the safety concerns regarding the fate of the complex debris into the organism and in the environment.

5.6 Conclusion

The most efficient complexes were those prepared with C12 surfactants and helper lipids, reaching 50% of transfected cells without causing cytotoxicity. These complexes have the particularity of being most efficient at low surfactant/DNA charge ratios, which is advantageous in terms of cell, organism and environmental toxicity. Some of the most efficient complexes were found to have sizes compatible with intravenous administration, as well as negative surface charge, which increases the likelihood of reaching the desired target cells, and were shown to mediate transfection even in the presence of serum. The most efficient and least cytotoxic complexes were produced from the biodegradable ester derivative, which supports the concept that cleavable chemical bonds would facilitate the release of DNA inside the cells.

Chapter 6

Gemini Surfactants Mediate Efficient Mitochondrial Gene Delivery and Expression

A.M. Cardoso, C.M. Morais, A.R. Cruz, S.G. Silva, M.L. do Vale E.F. Marques, M.C. Pedroso de Lima and A.S. Jurado, "*Gemini Surfactants Mediate Efficient Mitochondrial Gene Delivery and Expression*" Under review in Molecular Pharmaceutics.

6.1 ABSTRACT

Gene delivery targeting mitochondria has the potential to transform the therapeutic landscape of mitochondrial genetic diseases. Taking advantage of the non-universal genetic code used by mitochondria, a plasmid DNA construct was designed with the ability to be specifically expressed in these organelles. In the present work, gemini surfactants were shown to successfully deliver plasmid DNA to mitochondria. Gemini surfactant-based DNA complexes were taken up by cells through a variety of routes, including endocytic pathways, and showed propensity for inducing membrane destabilization under acidic conditions, thus facilitating cytoplasmic release of DNA. Furthermore, the complexes interacted extensively with lipid membrane models mimicking the composition of the mitochondrial membrane, which predicts a favored interaction of the complexes with mitochondria in the intracellular environment. This work unravels new possibilities for gene therapy towards mitochondrial diseases.

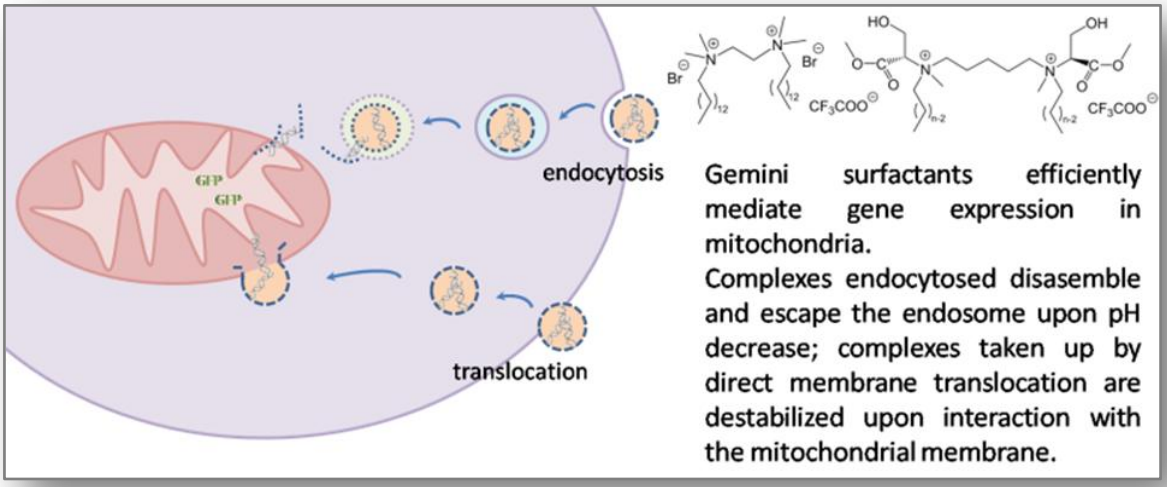

6.2 INTRODUCTION

Along evolution, most of the genes coding for proteins engaged in mitochondrial function were transferred to the nuclear DNA. Indeed, mitochondrial DNA encodes only 2 rRNAs, 22 tRNAs and 13 subunits of the mitochondrial respiratory chain (Howell 1999). However, since the mitochondrial DNA (mtDNA) nucleotide sequence was first reported by Anderson *et al.* (Anderson et al. 1981), more than 100 pathogenic mutations related with mitochondrial disorders have been described (DiMauro & Schon 2001; Yoon et al. 2010). The high rate of mutation that occurs in mtDNA has been related both with the lack of histones and effective DNA repair mechanisms, as well as with the large amount of reactive oxygen species (ROS) generated in the mitochondrial matrix where mtDNA is located.

Mitochondrial pathologies with origin in mtDNA are diverse and encompass encephalomiopathies, such as mitochondrial encephalopathy with lactic acidosis and strokelike episodes (MELAS) and myoclonic epilepsy with ragged-red fibers (MERRF), and neuropathies, such as Leber hereditary optic neuropathy (LHON).(Howell 1999; Mukhopadhyay & Weiner 2007) Abnormal mitochondrial function plays a role in the pathogenesis of many other diseases, including Huntington's disease (Panov et al. 2002), Alzheimer's disease (Castellani et al. 2002), Parkinson's disease (Arduíno et al. 2012), cancer (Clark et al. 2002), obesity and diabetes (Boddapati et al. 2005). Current therapies targeting mitochondrial disorders are mostly based on ROS scavenging and antioxidants (Scarpelli et al. 2010). Allotopic expression of mitochondrial proteins has also been explored, but all human mtDNA-expressed proteins contain hydrophobic transmembrane-spanning regions, which compromise the protein configuration during mitochondrial import through the TOM/TIM protein import complexes (Doyle & Chan 2008). Mitochondrial gene therapy, through delivery of a plasmid DNA targeting mitochondria, has therefore emerged as a promising strategy to correct mtDNA mutations responsible for several mitochondrial diseases (Weissig & Torchilin 2001b).

Each mitochondrion contains between 1000 and 5000 DNA copies, and a certain threshold of mutated copies must be reached for a mitochondrial pathology to display its phenotype, the exact threshold for a given disorder being highly dependent on the particular mutation (Doyle & Chan 2008). Therefore, mitochondrial transfection able to correct some of the mutated copies of mtDNA could be sufficient for the successful gene therapy of mitochondrial diseases with origin in mtDNA mutations. Several

studies have reported the use of different vehicles for the delivery of molecules to mitochondria, including fluorescent probes (Yasuzaki et al. 2010), proteins (Shokolenko et al. 2010), nucleic acids (D'Souza et al. 2003; Weissig & Torchilin 2001c; Lee et al. 2008), and peptide nucleic acids (PNA) (Chinnery et al. 1999; Muratovska et al. 2001). Lyrawati *et al.* (Lyrawati et al. 2011) were the pioneers to demonstrate the expression in mitochondria of a synthetic mitochondrial plasmid DNA (mpDNA)-encoded protein, but, to the best of our knowledge, no further work aiming at exploring this approach has been reported. These researchers designed a plasmid DNA encoding GFP to be translated exclusively in mitochondria, taking advantage of the fact that the genetic code used by mitochondria is different from that used in the nucleus, by four codons (Wallace 1999; Wallace 2007; Yoon et al. 2010). One of these codons (uga), which functions as a stop codon if recognized by the cytosolic ribosomal machinery, but codes for a tryptophan if read by the mitochondrial ribosomes, was included in mpDNA for GFP (Lyrawati et al. 2011). In order to promote the plasmid DNA delivery to mitochondria, Lyrawati and coworkers used DQAsomes produced according to the method described by Weissig *et al.* (Weissig et al. 1998). This delivery system was based on the use of dequalinium, an amphiphile with delocalized cationic charge and exhibiting the ability to preferentially accumulate near mitochondria and fuse with the outer membrane of this organelle (Weissig & Torchilin 2001b,c; D'Souza et al. 2003). However, transfection efficiency of complexes of dequalinium with mpDNA, designated DQAsomes, in a mouse macrophage cell line was found to be very low (Lyrawati et al. 2011). Traditionally, mitochondriotropic molecules have been described as cationic amphiphiles with delocalized charge (Weissig & Torchilin 2001d). However, a thorough revision work on mitochondriotropic agents carried out by Horobin and coworkers (Horobin et al. 2007), involving a systematic characterization of a large number of molecules previously described in literature as accumulating at or near mitochondria, showed that they exhibited interesting features that comprise electric potential, ion-trapping and complex formation with cardiolipin (Horobin et al. 2007). In addition, it has been shown that liposomes taken up by cells can selectively target mitochondria if they are properly modified to present known mitochondriotropic residues, such as stearyl-triphenylphosphonium bromide (TPP) (Boddapati et al. 2005), or the mitochondrial signaling peptide(Lee et al. 2008).

In the present work, the ability of gemini surfactants to mediate mitochondrial delivery and expression of the mpDNA produced by Lyrawati and coworkers

(Lyrawati et al. 2011) was assessed in HeLa cells. Two families of cationic gemini surfactants, conventional and serine-derived *bis-quaternary (bis*-quat) ammonium salts, previously shown to efficiently mediate nuclear transfection (unpublished work), were used to target mitochondria (**Figure 6.1**). Gemini surfactants have been extensively used as nuclear transfection agents due to their particular aggregation properties (low *cmc*), which allows the use of small amounts of surfactants, therefore reducing their potential cytotoxicity (Alami et al. 1993; Buijnsters et al. 2002; Silva et al. 2012). They have also been shown to efficiently condense and protect DNA (Bombelli et al. 2005; Karlsson et al. 2002), a requirement for successful gene delivery, either targeting the nucleus or mitochondria. Protonable groups can be introduced in the structure of gemini surfactants, conferring them an additional advantage to enhance gene delivery upon internalization of their DNA complexes endocytosis, since the conformational change upon pH decrease at the endolysosomal route can contribute to the nucleic acid release in the cytoplasm (Wettig et al. 2007). Furthermore, the versatility of gemini surfactants for structural modulation allows for improvement of their efficiency as gene delivery systems.

In this work, gemini-based gene delivery systems were found to exhibit high ability to mediate gene expression in mitochondria without causing significant cytotoxicity. Moreover, these systems were shown to be internalized into cells by different routes, including endocytic and non-endocytic (direct membrane translocation) pathways. The interaction of the complexes with lipid membrane models mimicking the cytoplasmic and the mitochondrial membranes occurred in great extent, supporting the relevance of such interactions for efficient mitochondrial targeting and gene delivery.

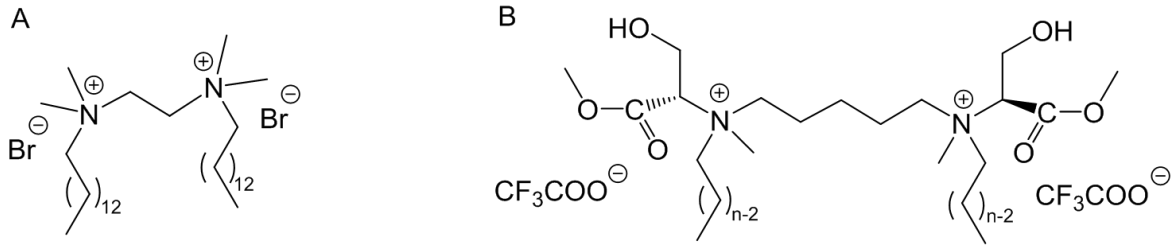

Figure 6.1 Schematic representation of the gemini surfactants used in this work. Conventional *bis*-quat gemini surfactant 14-2-14 (A) and serine-derived *bis*-quat gemini surfactants $(nSer)_2N5$ (n=14 and 16) (B).

6.3 MATERIALS AND METHODS

Materials

The conventional gemini surfactant 14-2-14 was synthesized by a previously established method (Menger & Littau 1991) and the serine-derived gemini surfactants were synthesized by using the method recently reported by Silva (Silva et al. 2012). The surfactants were purified either by recrystallization (conventional *bis-quat* gemini surfactants) or by column chromatography (serine-based gemini surfactants). Purities were confirmed by NMR and high resolution mass spectroscopy, and further confirmed by the *cmc* values obtained by surface tension, all in good agreement with values previously reported (Silva et al. 2012). The lipids 1,2-dioleoyl-sn-glycero-3-phosphoethanolamine (DOPE), cholesterol (Chol), 1-palmitoyl-2-oleoyl-sn-glycero-3- phosphocholine (POPC), bovine brain sphingomieline (SM), 1,2-dimyristoyl-sn-glycero-3-phosphocholine (DMPC), bis(monooleoylglycero)phosphate (18:1 BMP), 1,2-dioleoyl-sn-glycero-3-phosphocholine (DOPC) and 1',1',2,2'-tetraoleoyl cardiolipin (TOCL) were purchased from Avanti Polar Lipids (Alabaster, AL). The fluorescent lipids N-(7-nitrobenz-2-oxa-1, 3-diazol-4-yl)-Phosphatidylethanolamine (NBD-PE) and 1% rhodamine-phosphatidylethanolamine (Rho-PE) were acquired from Molecular Probes (Eugene, OR). All the other chemicals were of the highest grade.

Preparation of mpDNA complexes

Surfactant-based complexes were prepared using a GFP-coding plasmid DNA, designed to be specifically expressed in mitochondria (mpDNA, kindly provided by Dr. Diana Lyrawati) (Lyrawati et al. 2011), by employing the method described by Badea and coworkers (Badea et al. 2005) with a few modifications. Briefly, aqueous solutions (0.5 mM) of gemini surfactants were prepared and filtered through 0.2 μm pore diameter filters (Schleicher & Schuell). 1,2-dioleoyl-sn-glycero-3-phosphoethanolamine (DOPE) and cholesterol (Chol) (Avanti Polar Lipids, Alabaster, AL, USA) were dissolved in chloroform, mixed at a 2:1 molar ratio and dried under vacuum in a rotatory evaporator. The dried lipid films were hydrated with HBS, pH

9.0, to obtain multilamellar lipid vesicles (MLV) at a final lipid concentration of 0.5 mM, which were then filtered through 0.2 μm pore diameter filters. Plain complexes (gemini surfactant/mpDNA) were prepared as follows: plasmid DNA encoding mitochondrial GFP (mpGFP) was mixed with aliquots of gemini surfactant solution to obtain gemini surfactant/mpDNA charge ratios of 8/1, 10/1 and 12/1 and incubated at room temperature for 15 min. Ternary complexes (surfactant/mpDNA/helper lipids) were prepared at a 1/1 surfactant/helper lipid molar ratio, by adding DOPE:chol MLV (HL) to plain complexes. All the complexes (plain and ternary complexes) were allowed to incubate for further 30 min at room temperature for full stabilization.

Cells

HeLa cells (human epithelial cervical carcinoma) were maintained at 37 °C, under 5% CO_2, in Dulbecco's Modified Eagle's medium-high glucose (DMEM; Sigma, St Louis, MO, USA) supplemented with 10% (v/v) heat inactivated fetal bovine serum (FBS), and with 100 units of penicillin and 100 μg of streptomycin (Sigma) per mL.

For cell viability determination and flow cytometry experiments (see next sections), 0.8×10^5 HeLa cells/well were seeded onto 12-well plates, 24 h prior to incubation with gemini surfactant-based complexes.

Cell viability

Cell viability was assessed by a modified Alamar Blue assay (Simões et al. 1999). Briefly, 0.4 mL of 10% (v/v) resazurin dye in complete DMEM medium were added to each well, 48 h after the addition of the complexes. After 45 min of incubation at 37 °C, 180 μL of the supernatant were collected from each well and transferred to 96-well plates. The absorbance at 570 and 600 nm (as indicated by the supplier) was measured in a SPECTRAmax PLUS 384 spectrophotometer (Molecular Devices, Union City, CA). Cell viability was calculated, as a percentage of control cells (i.e. non-treated cells), according to the equation:

$$\text{Cell viability (\% of control)} = [(A_{570} - A_{600})/(A'_{570} - A'_{600})] \times 100 \qquad \text{(Equation 1)}$$

where A_{570} and A_{600} are the absorbances of the samples, and A'_{570} and A'_{600} are those of the control (non-treated cells), at the indicated wavelengths.

Transfection efficiency

The transfection mediated by the different complexes was evaluated by analyzing GFP expression by flow cytometry. HeLa cells were incubated with the different complexes (0.5 μg of mpDNA per well) in serum-free OptiMEM medium at 37 ^{o}C under 5% CO_2 for 4 h. The medium was then replaced with complete DMEM medium, and cells were further incubated for 44 h to allow gene expression. Cells were washed once with PBS and detached upon incubation with 0.25% trypsin solution (Sigma, St. Louis, MO, USA) at 37 °C for 10 min. Cells were further washed three times by centrifugation (950 rpm, 4 °C, 5 min) in ice-cold PBS, being then resuspended in ice-cold PBS and immediately analyzed. Flow cytometry was performed in a FACScalibur flow cytometer (BD Biosciences, San Jose, CA) and data were obtained and analyzed using CellQuest software. Live cells were gated by forward/side scattering from a total of 10,000 events. Transfection efficiency was determined in terms of the percentage of transfected cells.

Cellular internalization pathways

To address the mechanisms through which surfactant-based complexes were internalized by cells, transfection experiments were performed both at low temperature (4 °C) and in the presence of inhibitors of different endocytic pathways. For this purpose, plated HeLa cells washed with PBS were incubated (37 °C, 30 min) in serum-free OptiMEM, with the following inhibitors of endocytosis (from Sigma): (i) chlorpromazine (30 μM); (ii) fillipin III (5 μg/mL) or (iii) amiloride hydrochloride (5 mM). Parallel experiments were performed by incubating HeLa cells (not treated with these inhibitors) at 4 °C for 30 min. Thereafter, cells either inhibitor-treated or maintained at 4 °C were incubated with the complexes for 1 h. To confirm that the endocytosis inhibitors tested compromised selectively different endocytic pathways, their effects on cellular uptake of the fluorescently labeled markers, transferrin, a known marker of clathrin-mediated endocytosis, and lactosylceramide, a marker of raft/caveolae-dependent endocytosis, were analyzed. Cytotoxicity was assessed following cell treatment with each of the drugs by the Alamar blue assay, as described above. Flow cytometry analysis was performed as described above to evaluate

transfection efficiency of the complexes in cells pre-incubated at 4 °C (a condition that impairs any energy-dependent endocytic pathway) or with each of the endocytosis inhibitors.

Surfactant-mpDNA interactions

Surfactant-based complexes containing 0.2 μg of mpDNA, prepared in a total volume of 100 μL of HBS (pH 7.4) or MES buffer (pH 6.4 and 5.2), were incubated at 37 °C for 15 min, and then transferred to a 96-well (blackwalled) plate (Corning, NY, USA). Hundred microliters of PicoGreen (Molecular Probes, Eugene, OR), diluted according to the manufacturer's instructions (1:200 dilution in HBS buffer), were added to each sample. The fluorescence intensity of PicoGreen, which is directly proportional to the amount of accessible/free mpDNA, was monitored in a Spex Fluorolog Spectrometer for determining the extent of gemini surfactant-mpDNA complexation. The excitation and emission wavelengths were set at 485 and 520 nm, respectively. The degree of mpDNA protection conferred by the complexes (P_{mpDNA}), taken as proportional to the surfactant/mpDNA complexation, was calculated as follows:

$$P_{mpDNA} = 1- [(F-F_{100})/(F_0-F_{100})] \quad \text{(Equation 2)}$$

where F is the fluorescence measured after adding the PicoGreen solution to the complexes, F_0 (corresponding to 0% of plasmid mpDNA protection) was obtained by using free mpDNA in the same amount as that associated with the complexes, F_{100} (corresponding to 100% of mpDNA protection) is the residual fluorescence of a negative control obtained by using a PicoGreen solution without mpDNA, which mimicked a situation of 0% of mpDNA available to PicoGreen.

Physical properties of surfactant-based mpDNA complexes (particle size and Zeta potential)

The size of the surfactant-based complexes was assessed using a Submicron Particle Size Analyzer, Beckman Coulter N4 Plus. The colloidal suspension of the complexes was diluted with HBS, and the particle size analysis was carried out at a scattering angle of 90° and at 25 °C.

The Zeta potential of the surfactant-based complexes was measured using a Zeta sizer Nano ZS, ZN 3500, with a 532 nm laser (Malvern Instruments, UK). The

measurements were performed in HBS, at 25 °C, using DTS 1060C disposable Zeta cells and the protocol for general purposes (medium viscosity 0.89 cP, medium refractive index 1.33, sample viscosity 0.89 cP, particle refractive index 1.45 and equilibration time 3 min). Values for the dielectric constant of 78.5 and beam mode F(Ka) of 1.5 (Smoluchowsky) were used for Zeta potential determination.

Fluorescence polarization measurements

The probes 1,6-diphenyl-1,3,5-hexatriene (DPH) and 3-(p-(6-phenyl)-1,3,5-hexatrienyl)phenylpropionic acid (DPH-PA) in dimethylformamide were injected (a few microliters) into the surfactant or surfactant:lipid mixture, or the respective complexes in aqueous dispersions (final surfactant:lipid concentration of 200 μM), in order to obtain a final surfactant or surfactant plus lipid/probe molar ratio of about 200/1, as previously described (Jurado et al. 1991). Probe addition was performed at 55 °C and the mixture was incubated at room temperature, in the dark for probe protection, for a period of 15 h to reach equilibrium. In order to correct fluorescence measurements for the contribution of light scattering, appropriate blanks with equivalent volumes of dimethylformamide were prepared, although these corrections were found to be negligible. The fluorimetric measurements of DPH- or DPH-PA-labelled surfactant:lipid systems, in the absence or presence of mpDNA at different cationic surfactant/mpDNA charge ratios, were performed in a Perkin Elmer LS 55B fluorescence spectrophotometer (Perkin Elmer, U.S.A), equipped with polarization filters. The excitation and emission wavelengths were set at 336 and 450 nm, respectively (5 nm excitation and 6 nm emission band pass). The fluorescence polarization (P) was calculated according to Shinitzky and Barenholz (Shinitzky & Barenholz 1978), using the equation:

$$P = (I_{\parallel} - GI_{\perp})/(I_{\parallel} + GI_{\perp}) \qquad \text{(Equation 3)}$$

where $I_{\parallel}$ and $I_{\perp}$ are the intensities of the light emitted with its polarization plan parallel and perpendicular to that of the exciting beam, respectively. G, the instrumental grating factor, is given by the ratio of vertically to horizontally polarized emission components where the excitation light is polarized in the horizontal plane.

Interaction of surfactant-based mpDNA complexes with lipid vesicles (component mixing)

Förster Resonance Energy Transfer (FRET) experiments were performed in order to assess the extent of the interaction between components of the cationic surfactant-based complexes and vesicles mimicking the lipid composition of non-raft regions of the cytoplasmic membrane (POPC:DOPE at a 2:1 molar ratio), lipid-rafts (SM:DMPC:Chol at a 1:1:1 molar ratio), late endosomal membrane (POPC:DOPE:SM:BMP at a 5:2:1:2 molar ratio) and mitochondrial membrane (DOPC:DOPE:TOCL at a 1:1:1 molar ratio). For this purpose, the vesicles were labeled with 1% *N*-(7-nitrobenz-2-oxa-1, 3-diazol-4-yl)phosphatidylethanolamine (NBD-PE) and 1% rhodamine-phosphatidylethanolamine (Rho-PE) (Molecular Probes, Eugene, OR), upon addition to the lipid mixtures in chloroform. The solvent was removed by evaporation in a rotatory evaporator and the dried lipid films were hydrated in HBS saline buffer (pH 7.4). The resulting MLV were then sonicated for 3 min and extruded 15 times through two stacked polycarbonate filters of 100 nm pore diameter using a Liposofast device (Avestin, Toronto, Canada) to obtain large unilamellar vesicles (LUV). Phospholipid content was determined by measuring the inorganic phosphate (Murphy & Riley 1962) released after hydrolysis of dried phospholipids, at 180 °C, in 70% $HClO_4$ (Bottcher et al. 1961). Component mixing assays were performed in a 96-well black-walled plate, using 400 μM of lipid vesicles and 100 μM of the different surfactant-based complexes, prepared as previously described. Component mixing was measured at 37 °C, after an incubation period of 15 min at the same temperature, in a SPECTRAmax Gemini EM fluorimeter (Molecular Devices, Union City, CA), using the excitation and emission wavelengths of 470 and 535 nm, respectively. At the concentration at which the probes were incorporated into the vesicles (1%), Rho-PE efficiently suppresses the emission of NBD-PE at 535 nm, when the excitation wavelength is set at 470 nm. Due to the energy transfer dependence on the distance between the donor and acceptor probes, the mixing of components of the complexes with lipids of the fluorescently-labeled preparations generates an increase of NBD-fluorescence, which reflects alterations in the distribution of probes in the lipid environment. The percentage of component mixing, taken as proportional to FRET reduction, was calculated according to equation 4:

$$\text{Component mixing (\%)} = (F-F_0)/(F_{100}-F_0)x100, \qquad \text{(Equation 4)}$$

where F corresponds to the fluorescence detected after 15 minutes of complex incubation with the vesicles, F_0 corresponds to the initial vesicle fluorescence in the absence of the complexes, and F_{100} corresponds to the maximal fluorescence, which was obtained after complete lysis of the vesicles with 0.5% (v/v) octaethylene glycol monododecyl ether ($C_{12}E_8$). For each complex, three independent experiments were carried out at pH 7.4. Parallel experiments with vesicles mimicking the composition of the late endosome were also performed at pH 5.2. Briefly, after incubation of the complexes with the vesicles at 37 °C for 15 min at pH 7.4, the pH was lowered to 5.2 upon addition of HCl (1 M) and NBD-PE fluorescence was measured (F). The percentage of component mixing at pH 5.2 was calculated according to Equation 4, where F_0 and F_{100} corresponded to the minimum fluorescence obtained with the labeled vesicles at pH 7.4 and to the maximum fluorescence, obtained with $C_{12}E_8$ at pH 7.4, respectively.

Destabilization of lipid vesicles induced by surfactant-based mpDNA complexes (calcein release)

Calcein release experiments were performed in order to assess the ability of cationic surfactant-based gene delivery systems to destabilize vesicles mimicking the lipid composition of non-raft regions of the cytoplasmic membrane (POPC:DOPE at a 2:1 molar ratio), lipid-rafts (SM:DMPC:Chol at a 1:1:1 molar ratio), late endosomal membrane (POPC:DOPE:SM:BMP at a 5:2:1:2 molar ratio) and mitochondrial membrane (DOPC:DOPE:TOCL at a 1:1:1 molar ratio). Lipid mixtures at the indicated molar ratios were dissolved in chloroform and dried under vacuum in a rotatory evaporator. The dried lipid films were hydrated with 80 mM calcein solution (Sigma, St. Louis, MO) in 50 mM HEPES and 1 mM EDTA (pH 8.4), submitted to 3 minutes of sonication, and then extruded 15 times through two stacked polycarbonate membranes of 100 nm pore diameter, using a Liposofast device (Avestin, Toronto, Canada), to obtain LUV. Free calcein was removed from the probe-containing LUV by size exclusion chromatography on a Sephadex G-75 column, using a buffer solution (20 mM HEPES, 140 mM NaCl and 1 mM EDTA, pH 7.4) with the same osmolarity as that of the calcein solution. Vesicle phosphate content was determined by the Murphy

and Riley method (Murphy & Riley 1962) and leakage assays were performed on a 96-well black-walled plate, using 400 μM of lipid vesicles and 100 μM of surfactant-based complexes. After incubation of labeled vesicles with surfactant-based complexes, at 37 °C for a period of 15 min, calcein release was measured in a SPECTRAmax Gemini EM fluorimeter (Molecular Devices, Union City, CA), using the excitation and emission wavelengths of 494 and 517 nm, respectively. The percentage of vesicle leakage, taken as percentage of calcein release, was calculated according to equation 5:

$$\text{Calcein release (\%)} = [(I-I_0)/(I_{100}-I_0)]x100\%, \qquad \text{(Equation 5)}$$

where I corresponds to the fluorescence detected after 15 min of incubation of the surfactant-based complexes with the vesicles, I_0 corresponds to the vesicle fluorescence in the absence of the complexes, and I_{100} corresponds to the maximum fluorescence, obtained after the complete lysis of the vesicles with 0.5% (v/v) $C_{12}E_8$. For each surfactant concentration, three independent experiments were performed.

Statistical analysis

Results from all experiments are represented as mean ± SD. Data were analyzed using GraphPad Software, Inc., CA, USA. Statistical significances of differences between data were evaluated using ANOVA Tukey's multiple comparison test when comparing all experimental means.

6.4 RESULTS

6.4.1 CYTOTOXICITY AND TRANSFECTION EFFICIENCY OF GEMINI SURFACTANT-BASED COMPLEXES CONTAINING MPDNA

Gemini surfactants from two different families, conventional and serine-derived *bis*-quat ammonium salts, were used to prepare complexes with mpDNA, in order to evaluate their ability to mediate mitochondrial GFP expression. The surfactants selected for this purpose, namely conventional *bis*-quat 14-2-14 and serine-derived *bis*-quats $(14Ser)_2N5$ and $(16Ser)_2N5$, were those displaying the lowest cytotoxicity when complexed with a nuclear DNA plasmid coding for GFP, as evaluated in previous studies performed in our laboratory (unpublished work). **Figure 6.2** shows the percentage of transfected cells (A) and of viable cells (B) obtained with mpDNA complexes prepared with the abovementioned gemini surfactants, at different gemini surfactant/DNA (+/-) charge ratios, in the absence or presence of the helper lipids (HL) DOPE and cholesterol (at a 2:1 molar ratio). As observed, for all the complexes, the transfection efficiency showed an increase with increasing complex (+/-) charge ratios. The enhancement of transfection efficiency was most notorious for complexes prepared with conventional *bis*-quat 14-2-14, when the (+/-) charge ratio increased from 8/1 to 10/1. Although the transfection efficiency of complexes prepared from serine-derived surfactants was not significantly different for the various charge ratios, the tendency for an increase of transfection with an increase of (+/-) charge ratio is clear, except for complexes of $(16Ser)_2N5$ prepared with helper lipids, which showed low levels of transfection regardless the (+/-) charge ratio (**Figure 6.2A**). In contrast, cell viability decreased with increasing (+/-) charge ratios of the complexes, except for complexes of $(16Ser)_2N5$ containing helper lipids, which exhibited low cytotoxicity for all the (+/-) charge ratios assayed (**Figure 6.2B**). The most promising formulations for gene delivery were gemini surfactant-based mpDNA complexes containing 14-2-14 and 14-2-14 plus helper lipids at the 10/1 (+/-) charge ratio, $(14Ser)_2N5$ plus helper lipids at the 10/1 (+/-) charge ratio and $(16Ser)_2N5$ at the 12/1 (+/-) charge ratio, which present a suitable conjugation of high transfection efficiency with low cytotoxicity.

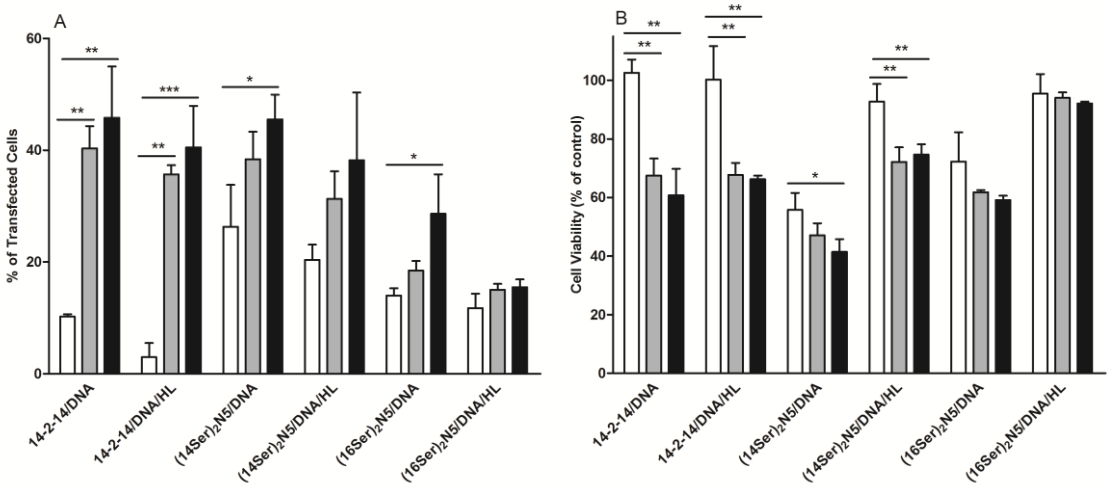

Figure 6.2 Transfection efficiency (A) and cytotoxicity (B) of gemini surfactant-based complexes (indicated in the figure), at 8/1 (□), 10/1 (■) and 12/1 (■) (+/-) charge ratios. Transfection efficiency was deduced from the percentage of transfected cells, from a total of 10,000 events, and cytotoxicity from the percentage of viable cells with respect to a control (non-treated cells). Pairwise data comparisons were performed as indicated in the figure (*$p < 0.05$, **$p < 0.01$, ***$p < 0.001$).

6.4.2 Cellular internalization pathways of gemini surfactant-based mpDNA complexes

The mechanisms of cellular internalization were evaluated for the complexes that showed to be the most promising gene delivery systems for mitochondrial targeting. For this purpose, HeLa cells were incubated at 4 °C, in order to prevent uptake of the complexes by endocytosis, or treated with drugs that selectively inhibit different endocytic pathways, namely clathrin-mediated endocytosis (chlorpromazine), raft-mediated endocytosis (filipin III) and macropinocytosis (amiloride hydrochloride), and transfected with the complexes. Transfection efficiency was evaluated by flow cytometry analysis of GFP expression and the results are presented in **Figure 6.3** as percentages of the maximum transfection obtained with the same complexes in untreated cells. As observed, more than one pathway showed to be relevant for the internalization of the studied complexes and all of them led to transfection. Endocytosis showed to be important for the uptake of 14-2-14-based complexes containing or not helper lipids, as concluded by the significant decrease in transfection observed upon cell incubation at 4 °C. The mechanisms involved in the internalization of the complexes are raft-mediated endocytosis and macropinocytosis (but not clathrin-mediated endocytosis). In contrast, transfection efficiency mediated by $(14Ser)_2N5$:HL-based complexes was not affected by incubation at low

temperature or cell pre-treatment with the different endocytosis inhibitors, thus suggesting an energy-independent mechanism for their internalization. Concerning complexes prepared with the $(16Ser)_2N5$ surfactant, internalization occurred by clathrin-mediated and raft-mediated endocytosis, but not by macropinocytosis. Since the transfection efficiency of the complexes did not decay to residual values upon cell incubation at low temperature or after cell pre-treatment with endocytosis inhibitors, it is fair to deduce that all of them can be partly (or entirely in the case of $(14Ser)_2N5$/mpDNA/HL complexes) translocated across the cell membrane, by a non-endocytic pathway.

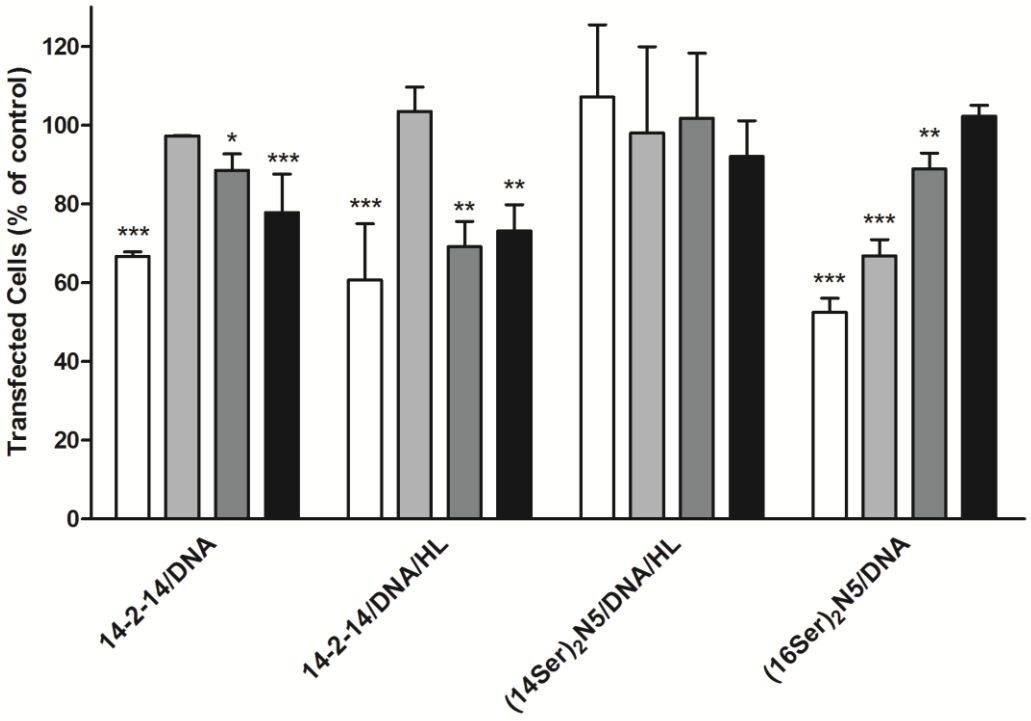

Figure 6.3 Effect of different endocytosis inhibitors on transfection mediated by surfactant-based DNA complexes. HeLa cells were incubated at 4 °C (□), or treated at 37 °C with either 30 μM of chlorpromazine (▫), 5μg/ml of fillipin III (■), or 2.5 mM of amiloride hydrochloride (■), and transfected with the complexes indicated in the figure. Transfection efficiency in the presence of each inhibitor was expressed as percentage of control (untreated) cells transfected with the corresponding complex. Data are presented as mean ± standard deviation, representative of at least three independent experiments. Data comparisons were performed between each condition tested and the respective control corresponding to 100% of transfected cells (*p<0.05, **p<0.01, ***p<0.001).

6.4.3 Physico-chemical properties of gemini surfactant-based complexes (hydrodynamic diameter and Zeta potential)

The hydrodynamic diameter and Zeta potential of gemini surfactant-based complexes were found to depend on their composition (**Table 6.1**). Regarding complex size, all samples showed to be polydisperse. The complexes 14-2-14/DNA and $(16Ser)_2N5$/DNA, formulated in the absence of helper lipids, presented very similar diameters, centered at ca. 550 nm, while in the presence of helper lipids, 14-2-14/DNA complexes underwent a significant size increase to 800 nm. The complexes of $(14Ser)_2N5$/DNA/HL showed to be the smallest (ca. 270 nm).

Regarding the complex surface charge, assessed in terms of Zeta potential, 14-2-14/DNA complexes were found to be neutral, while the same complexes formulated with helper lipids showed a high positive charge; $(16Ser)_2N5$/DNA complexes also showed a high positive Zeta potential. On the other hand, $(14Ser)_2N5$/DNA/HL complexes presented a highly negative Zeta potential. Taking into account that all the complexes were formulated at high (+/-) charge ratios (10/1 and 12/1), the results obtained indicate that a specific arrangement of the molecules or a different degree of particle hydration could be on the origin of the differences observed for the size and surface charge of the complexes. In particular, the highly negative Zeta potential of the $(14Ser)_2N5$/DNA/HL complexes probably results from the adsorption of inorganic anions from the medium.

Table 6.1 Hydrodynamic diameter and Zeta potential of DNA complexes formulated with gemini surfactants or gemini surfactants plus helper lipids (HL) at the indicated (+/-) charge ratios.

Complexes	(+/-) charge ratio	Hydrodynamic Diameter (nm)[1)]	Zeta potential (mV) [1)]
14-2-14/DNA	10/1	555 ± 77	+3.8 ± 1.9
14-2-14/DNA/HL	10/1	802 ± 47	+32.2 ± 2.7
$(14Ser)_2N5$/DNA/HL	10/1	274 ± 12	-34.3 ± 4.1
$(16Ser)_2N5$/DNA	12/1	528 ± 56	+35.1 ± 3.0

[1)] Results represent mean ± SD of at least three independent experiments. All samples were polydisperse with relation to size and monodisperse with relation to Zeta potential.

6.4.4 DPH AND DPH-PA FLUORESCENCE POLARIZATION IN GEMINI SURFACTANT-BASED STRUCTURES AND IN THEIR COMPLEXES WITH DNA

Fluorescence polarization of the probes DPH and DPH-PA embedded in structures of 14-2-14, 14-2-14 plus helper lipids, $(14Ser)_2N5$ plus helper lipids and $(16Ser)_2N5$, as well as in the respective complexes with DNA, was determined at 37 °C. As observed in **Figure 6.4**, for formulations prepared in the absence of DNA, fluorescence polarization (P) values registered for DPH distributed over the wide range from 0.105 to 0.174, which was dramatically narrowed, from 0.141 to 0.166 upon addition of mpDNA (**Figure 6.4A**). The fluorescence polarization values observed when DPH-PA was embedded in DNA-devoid formulations ranged from 0.167 to 0.209. These values are higher than those observed with DPH and did not follow the same trend as that observed with this probe (**Figure 6.4B**). Based on DPH-PA fluorescence polarization measurements, two groups of complexes should be considered, plain complexes (surfactant plus DNA) presenting lower P values (0.170-0.174) and complexes containing helper lipids, presenting higher P values (0.212-0.224).

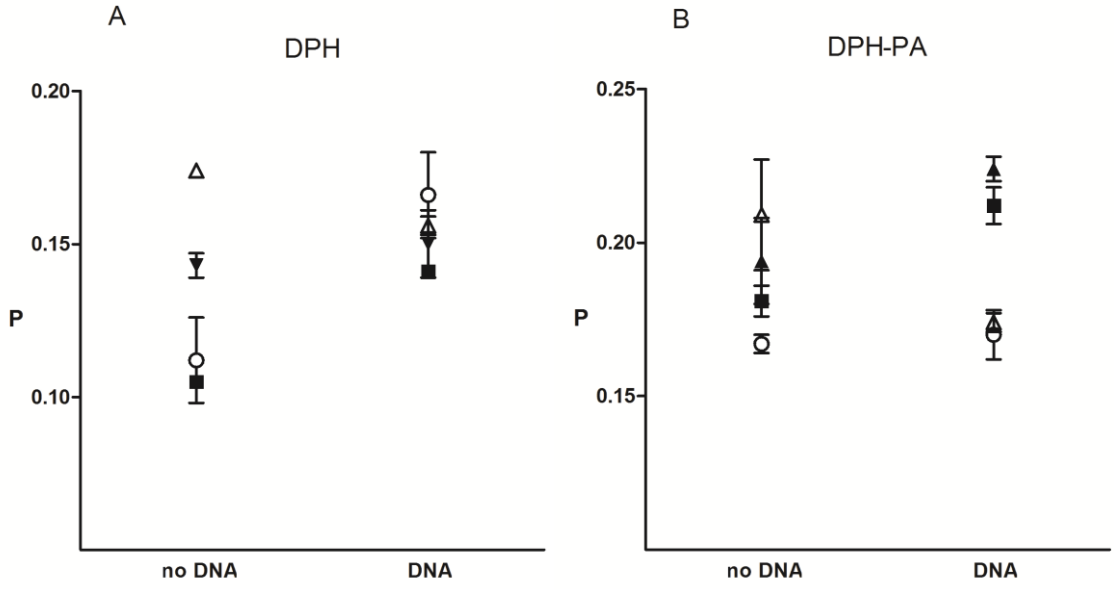

Figure 6.4 Fluorescence polarization values (P) of DPH (A) and DPH-PA (B) incorporated in 14-2-14 (○), 14-2-14:HL (■), $(14Ser)_2N5$:HL (▲) and $(16Ser)_2N5$ (△) structures complexed (DNA) or not (no DNA) with mpDNA. DNA was added to obtain complexes of 14-2-14 and of $(14Ser)_2N5$ at the 10/1 (+/-) charge ratio and complexes of $(16Ser)_2N5$ at the 12/1 (+/-) charge ratio.

6.4.5 Effect of pH on mpDNA protection conferred by gemini surfactant-based complexes

The ability of gemini surfactants to complex and protect mpDNA from access to other molecules was evaluated using the fluorescent probe PicoGreen, whose fluorescence dramatically increases when it intercalates nucleic acid double strands. mpDNA protection was evaluated at conditions that reflect those observed when i) complexes were prepared (25 °C and pH 7.4, dotted bars), ii) complexes interacted with cells (37 °C and pH 7.4, white bars), and iii) complexes were internalized by cells through a endolysosomal pathway (37 °C and pH 6.4, grey bars, or pH 5.2, black bars). As **Figure 6.5** shows, mpDNA complexation was found to be highly efficient at room temperature, with a minimum mpDNA complexation of approximately 80% for complexes of $(14Ser)_2N5$/DNA/HL. Upon temperature increase, no disassembly of the complexes was observed, as the mpDNA protection levels remained constant at 37 °C (pH 7.4). At this temperature (37 °C), lowering the pH led, in most cases, to a decrease in DNA protection. Indeed, complexes of $(16Ser)_2N5$ started to disassemble at pH 6.4, as indicated by the 20.2% of DNA protection observed at this pH. At pH 5.2, for all the complexes devoid of helper lipids, total dissociation of DNA from the cationic surfactant was achieved. Complexes containing helper lipids underwent a much lower destabilization upon pH decrease. However, for complexes of 14-2-14/DNA/HL, 31.8% of the associated DNA became free at the lowest pH assayed. Only $(14Ser)_2N5$-based complexes were capable of conferring mpDNA protection in a pH-independent manner.

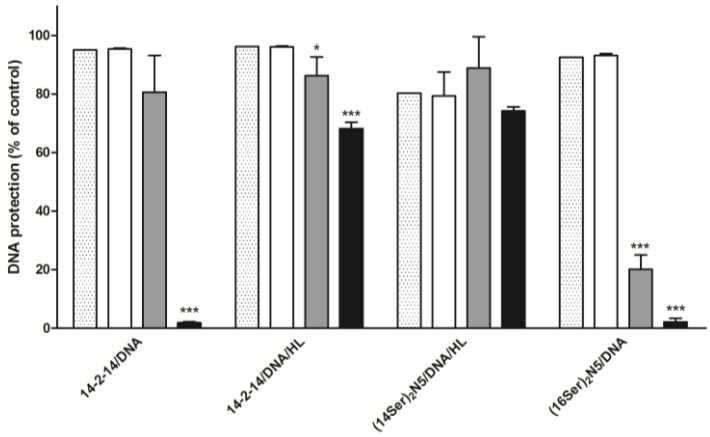

Figure 6.5 Protection conferred to DNA by the gemini-based complexes, as assessed by PicoGreen accessibility to the nucleic acid, at 25 °C, pH 7.4 (dotted bars), 37 °C, pH 7.4 (□), 37 °C, pH 6.4 (■) and 37 °C, pH 5.2 (■). Maximum DNA accessibility (0% DNA protection) was taken as the maximum fluorescence obtained using the same amount of DNA as that used for the preparation of the complexes in the presence of PicoGreen, and maximum DNA protection corresponded to the minimum fluorescence, taken from the residual PicoGreen fluorescence in the absence of DNA. Data comparisons were performed for the protection conferred by each complex at 25 °C and pH 7.4 vs. that conferred by the same complex at 37 °C and pH 7.4 (not significant) and for the protection conferred by each complex at 37 °C and pH 7.4 vs. that conferred by the same complex at 37 °C and pH 6.4 and 5.2 ($^{*}p < 0.05$, $^{***}p < 0.001$).

6.4.6 Interaction of gemini surfactant-based complexes with lipid membrane models

Interaction of gemini surfactant-based complexes with lipid membrane models mimicking different cell membrane structures was evaluated by FRET and calcein release assays. The lipid models used in this study were designed to resemble the lipid composition of raft and non-raft regions of the cytoplasmic membrane, and late endosome and mitochondria membranes. FRET between the fluorescent lipids NBD-PE (donor) and Rho-PE (acceptor) incorporated in the same vesicle population was evaluated upon addition of surfactant-based complexes, by monitoring the fluorescence increase of the donor probe (NBD-PE) (**Figure 6.6A**). All the complexes showed to interfere with FRET between NBD-PE and Rho-PE incorporated in vesicles mimicking non-raft and raft portions of the cytoplasmic membrane, and the mitochondrial membrane, but did not extensively impair FRET in vesicles mimicking the late endosomal membrane (maximum of 22% of FRET decrease promoted by ($14Ser_2$)N5/DNA/HL complexes, **Figure 6.6A**). Interestingly, upon reduction of pH (in order to resemble the acidification of endosomes), a small increase in the interaction between complexes of 14-2-14 plus helper lipids and the late endosome membrane model was observed. However, for the other complexes studied,

interaction with this model membrane was not enhanced under these conditions. Regarding leakage of vesicle contents, evaluated in terms of fluorescence increase of calcein encapsulated in the vesicles at a self quenching concentration, all the complexes induced calcein release from vesicles mimicking non-raft regions of the cytoplasmic membrane. However, complexes based on the serine-derived surfactants were less efficient in promoting vesicle leakage than those composed of the conventional gemini surfactant (14-2-14). Vesicles mimicking the mitochondrial membrane also showed an extensive leakage with all the complexes assayed, whereas vesicles mimicking the composition of lipid-rafts and of the late endosomal membrane were only slightly destabilized by gemini surfactant-based complexes (maximum of 17 and 26% of calcein release, both promoted by 14-2-14/DNA complexes, **Figure 6.6B**).

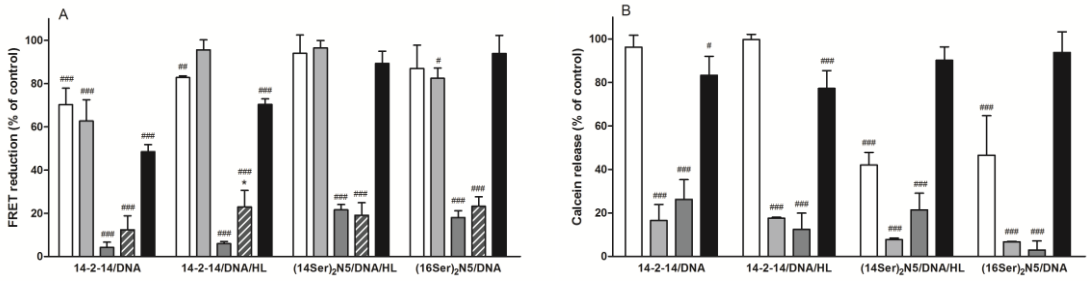

Figure 6.6 FRET (A) and calcein release (B) assays performed in lipid vesicles mimicking the lipid composition of non-raft domains of the cytoplasmic membrane (□), lipid-rafts (▫), late endosomal membrane at pH 7.4 (■) or pH 5.2 (striped bars) and mitochondrial membrane (■), induced by the surfactant-based complexes indicated in the figure. The surfactant-based DNA complexes were added to vesicles containing two fluorescent lipids NBD-PE and Rho-PE (FRET) or to vesicles loaded with calcein (calcein release) at a 1:4 complex:vesicle molar ratio. FRET reduction and calcein release induced by the complexes are presented as percentage of maximum FRET reduction or maximum calcein release obtained with a control prepared with each type of vesicle to which the detergent $C_{12}E_8$ (0.5% v/v) was added. The results represent the mean ± standard deviation obtained from three independent experiments. Pairwise data comparisons were performed between complex-induced FRET reduction in the late endosome membrane model at pH 7.4 and in the same model at pH 5.2 ($^{*}p < 0.05$) and between maximum FRET reduction or maximum calcein release (controls) and complex-induced FRET reduction or calcein release, respectively ($^{\#}p < 0.05$, $^{\#\#}p < 0.005$, $^{\#\#\#}p < 0.001$).

6.5 DISCUSSION

In this work, the ability of gemini surfactants to mediate gene delivery to mitochondria using intact cells was studied, employing a plasmid specifically designed to be expressed in these organelles. Although a number of studies have focused on nucleic acid delivery to mitochondria (Weissig & Torchilin 2001a; Weissig & Torchilin 2001d; D'Souza et al. 2003; Boddapati et al. 2005; Lee et al. 2008; Yasuzaki et al. 2010), to the best of our knowledge, only one study evaluated the expression in mitochondria of a transgene, which revealed to occur at a limited extent (1-5%) (Lyrawati et al. 2011).

In the present study, conventional and serine-derived *bis*-quat gemini surfactants showed to be able to efficiently mediate gene delivery to mitochondria in HeLa cells and to promote gene expression, either *per se*, or in combination with the helper lipids DOPE and cholesterol. Transfection of up to 40.4% of the cells was achieved, which is almost twice that attained with Lipofectamine 2000™ (25.1%, data not shown). The most promising systems, i. e. those combining high transfection efficiency and low cytotoxicity, were selected for subsequent physico-chemical characterization in order to disclose the properties shared by delivery systems able to efficiently target mitochondria.

The selected complexes, 14-2-14/mpDNA, 14-2-14/mpDNA/HL, $(14Ser)_2$N5/mpDNA/HL and $(16Ser)_2$N5/mpDNA, presented sizes from 273.7 nm to 801.9 nm and significantly different surface charges, from highly positive to highly negative. It is worth mentioning that the complexes displaying the smallest size (presumably compatible with intravenous administration), i.e. those consisting of $(14Ser)_2$N5/mpDNA/HL, exhibited negative Zeta potential, which can prevent undesired interactions with serum proteins (Faneca et al. 2002; Templeton et al. 1997; Liu et al. 1997). Therefore, the $(14Ser)_2$N5-based complexes display a combination of features that render them promising for *in vivo* studies.

The four selected gemini surfactants showed a convergence of the values of fluorescence polarization of DPH and DPH-PA upon addition of DNA. These fluorescent probes are expected to monitor the structural order of the

surfactant/mpDNA or surfactant/mpDNA/HL systems in the hydrophobic core, i.e., far from the aqueous medium, the preferred DPH environment, and closer to the water/lipid interface, where electrostatic interactions dominate and DPH-PA is located. In the case of the structures containing $(16Ser)_2N5$ gemini surfactant, DNA addition promoted a decrease in molecular packing (taking this as proportional to P values) in both the core and close to the surface region. However, for all other complexes, DNA addition promoted an increase in the packing reported by each of the fluorescent probes, similarly to what was described previously (Cardoso et al. 2011). Therefore, a given range of molecular packing seems to be ideal for most of the transfection-competent complexes, probably by optimizing complex-membrane interactions, regarding either the cytoplasmic or intracellular membranes. FRET assays conducted with lipid vesicles mimicking different cellular membrane structures allowed to estimate the extent of complex-membrane interactions. Interestingly, all the studied complexes seemed to interact efficiently with lipid-raft and non-raft regions of the cytoplasmic membrane, which could be responsible for the pathway taken by the complexes to be internalized into the cells. In fact, with the exception of (14Ser)2N5-based complexes, all complexes were taken up through endocytic routes taking place in raft (those inhibited by filipin III) or non-raft (clathrin-mediated endocytosis) regions of the cytoplasmic membrane or in mixed raft and non-raft domains, in the case of macropinocytosis (El-Sayed & Harashima 2013). Interestingly, the studies of aqueous contents leakage in models resembling the cytoplasmic membrane lipid composition showed that gemini surfactant-based complexes were able to induce destabilization of non-raft domains but not of lipid-rafts. Lipid-rafts are cholesterol-enriched membrane regions, which are found to be detergent-resistant at low temperatures (Simons & Gerl 2010). Therefore, it is not surprising that vesicles composed of SM:DMPC:Chol (1:1:1), such as those used in this work to mimic lipid-rafts, were not easily disrupted by gemini surfactants, as has been previously shown for other surface-active agents (Chen et al. 2009). The low extent of aqueous content release from lipid-raft-mimicking vesicles in the presence of gemini surfactant-based complexes indicates that the uptake of these complexes (inhibited by cell treatment with filipin III) should be driven by an energy-dependent process, involving one or several proteins that mediate cellular internalization in

these domains. On the other hand, the extensive calcein release induced by the complexes in the non-raft membrane model, allied to the observed extensive reduction of FRET, suggests that gemini surfactant-based complexes, whose internalization was shown not to be affected by the endocytosis inhibitors assayed, could be internalized by passive translocation across non-raft domains of the cytoplasmic membrane.

Taking into account FRET and calcein release assays, the interaction of the complexes with the late endosomal membrane model seemed to occur at a very low extent, even at acidic pH (5.2), a condition mimicking the environment found in the endosomal lumen. However, it is expected that three of the four complexes studied travel through the endolysosomal route, according to their internalization by energy-dependent endocytic pathways. Although these complexes were able to efficiently release the mpDNA in the acidic endosome milieu (as deduced from the PicoGreen assay conducted at low pH), the transfection efficiency should be counteracted by their inability to destabilize the endosomal membrane. Therefore, although a significant portion of the complexes appear to be internalized independently of endocytosis, the complexes that are endocytosed seem to be, at least partially, trapped in this degradative pathway. Hence, it is expected that the performance of the complexes studied herein can be further improved, by facilitating their escape from the endolysosomal route. This can be accomplished by including in their composition molecules that undergo protonation under acidic conditions, thus leading to endosomal membrane destabilization and thereby promoting cytoplasmic release of the carried DNA (Wettig et al. 2007). Interestingly, the $(14Ser)_2N5$-based complexes, which showed to be apparently internalized through direct membrane translocation, were those that, in contrast to the others, did not dissociate upon pH decrease (**Figure 6.5**). Since this fact did not interfere with their transfection efficiency, other factors may contribute to the release of nucleic acids from the complexes during their intracellular trafficking to mitochondria, which did not involve transport through the endolysosomal pathway.

On the other hand, DNA delivery to mitochondria has been described to be a passive process, as long as the complexes accumulate in the surroundings of this organelle (Koulintchenko et al. 2006). DNA entry into mitochondria involves translocation

across two membranes. The outer membrane has been considered relatively permeable, due to the presence of the voltage-dependent anion channel (VDAC) (Koulintchenko et al. 2006; Weber-Lotfi et al. 2009). This channel was shown to allow the uptake of nucleic acids with up to 4 kb regardless of their sequence (Ibrahim et al. 2011), and, therefore, mpDNA should be internalized through this pathway (Lyrawati et al. 2011). On the other hand, the complexes are expected to cross the cardiolipin-enriched inner membrane, considering the extensive degree of interaction observed between the complexes and the mitochondrial membrane model, as assessed by FRET and calcein release. Interestingly, selective mitochondrial accumulation of DNA has been described to involve, not only electric potential and ion-trapping, but also complex formation with cardiolipin (Horobin et al. 2007). According to the studies of Rashid and coworkers (Rashid & Horobin 1990), using cationic fluorescent probes, only moderately lipophylic molecules are able to passively penetrate mitochondrial membranes and the cationic molecules would form insoluble salts with cardiolipin (Rashid & Horobin 1990; Horobin et al. 2007). It is possible that the cationic amphiphilic gemini surfactant-based complexes used herein could also strongly interact with the cardiolipin-enriched mitochondrial inner membrane, favoring mpDNA translocation into mitochondria.

In summary, in this work gemini surfactant-based complexes have been shown to be able to efficiently deliver plasmid DNA to mitochondria and to promote gene expression through the machinery of this organelle. These complexes presented variable sizes, from those suitable for intravenous administration (smaller than 300 nm) to larger ones (up to 800 nm), variable surface charge (from positive to negative), and high ability to efficiently protect the nucleic acids. Complexes internalized by cells through endocytosis should undergo structural changes upon pH decrease so that they can release the DNA at the endosomal level, while those internalized through direct membrane translocation, which showed no ability to release the nucleic acids at low pH, should deliver the mpDNA upon interaction with mitochondrial membranes. All the complexes revealed the capacity to strongly interact with vesicles mimicking the mitochondrial membrane composition, suggesting that DNA could be passively taken up by mitochondria. Although a high yield of accumulation of the gemini surfactant-based complexes used in the

surroundings of mitochondria is deduced from the observation of significant levels of gene expression, improved transfection could be achieved by modulation of the vehicle gemini surfactants, namely by using a mitochondrial leader peptide (Lee et al. 2008), to increase mitochondrial tropism, or by conferring pH-sensitivity to the gene delivery system to enhance endosomal escape (Abes et al. 2006a,b). On the other hand, a decrease of the cytotoxicity of the most efficient complexes to mediate transfection (e.g. those including helper lipids) could be obtained by addition of an antioxidant molecule to the gemini surfactant formulation, as suggested by other authors (Lee et al. 2013).

6.6 CONCLUSION

In this work, we approached mitochondrial gene delivery from a functional perspective, using a GFP-encoding plasmid DNA designed for specific mitochondrial expression. Gemini surfactant-based mpDNA complexes showed significant efficiency to mediate gene expression in this organelle. This work paves the way to a new era of mitochondrial gene delivery, bringing new therapeutic possibilities to patients suffering from mitochondrial diseases originated in mitochondrial DNA.

Chapter 7

S4(13)-PV cell-penetrating peptide induces physical and morphological changes in membrane-mimetic lipid systems and cell membranes: Implications for cell internalization

A.M.S. Cardoso, S. Trabulo, A.L. Cardoso, A. Lorents, C.M. Morais, P. Gomes, C. Nunes, M. Lúcio, S. Reis, K. Padari, M. Pooga, M.C. Pedroso de Lima, A.S. Jurado, "*S4(13)-PV cell-penetrating peptide induces physical and morphological changes in membrane-mimetic lipid systems and cell membranes: Implications for cell internalization*" Published in the Biochimica et Biophysica Acta – Biomembranes, **2012**; 1818: 877–888.

7.1 ABSTRACT

The present work aims to gain insights into the role of peptide-lipid interactions in the mechanisms of cellular internalization and endosomal escape of the S4(13)-PV cell-penetrating peptide, which has been successfully used in our laboratory as a nucleic acid delivery system. A S4(13)-PV analogue, S4(13)-PV_{scr}, displaying a scrambled amino acid sequence, deficient cell internalization and drug delivery inability, was used in this study for comparative purposes. DSC, fluorescence polarization and SAXS/WAXS techniques showed that both peptides interacted with anionic membranes composed of phosphatidylglycerol or a mixture of this lipid with phosphatidylethanolamine, increasing the lipid order, shifting the phase transition to higher temperatures and raising the correlation length between the bilayers. However, S4(13)-PV_{scr}, in contrast to the wild-type peptide, did not promote lipid domain segregation and induced the formation of an inverted hexagonal lipid phase instead of a cubic phase in the lipid systems assayed. Electron microscopy showed that, as opposed to S4(13)-PV_{scr}, the wild-type peptide induced the formation of a non-lamellar organization in membranes of HeLa cells. We concluded that lateral phase separation and destabilization of membrane lamellar structure without compromising membrane integrity are on the basis of the lipid-driven and receptor-independent mechanism of cell entry of S4(13)-PV peptide.
Overall, our results can contribute to a better understanding of the role of peptide-lipid interactions in the mechanisms of CPP membrane translocation, helping in the future design of more efficient CPP-based drug delivery systems.

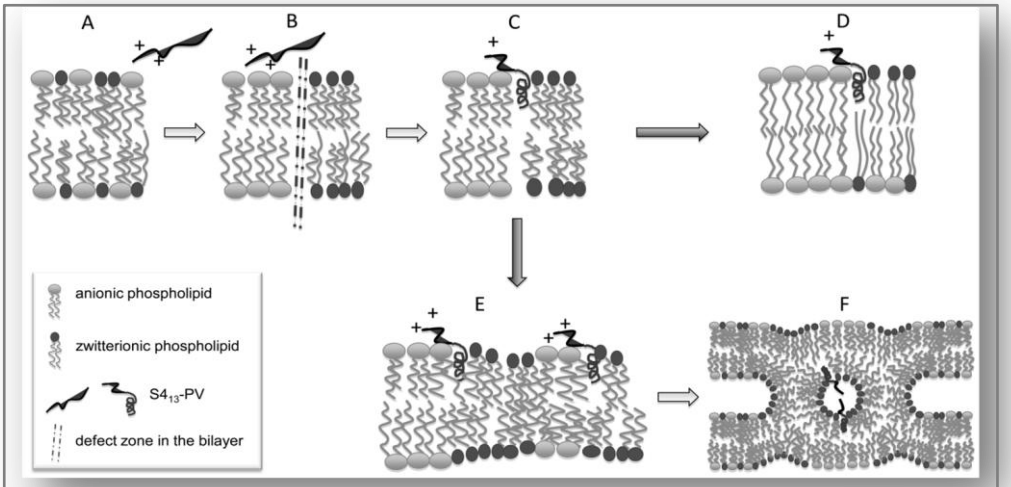

Structural changes induced by S4(13)-PV interactions with a membrane lipid model, containing differently charged lipids. In a membrane composed of anionic and zwitterionic phospholipids, a random distribution of lipid molecules is expected (A). Upon interaction with the peptide, ionic bonds are formed between the positive charges of the peptide and the anionic phospholipids. Subsequently, lateral phase separation occurs with the appearance of defects at the boundaries of domains with different lipid composition (B). The peptide will be embedded in the membrane, adopting an amphipathic α-helix conformation (C). In the case of highly ordered domains, the hydrophobic mismatch will promote fatty acid chain interdigitation with an additional increase of order (D). In the case of liquid-disordered domains, the insertion of the peptide may afford a higher separation and mobility of the hydrocarbon chains, leading to an increase of the curvature stress with destabilization of the bilayer (E) and eventual formation of inverted micelles (F), which could create conditions for the peptide translocation across the membrane thickness.

7.2 INTRODUCTION

Cell-penetrating peptides (CPPs) constitute an expanding peptide family whose members share the ability to cross biological membranes and gain access into living cells (Morris et al. 2008; Trabulo et al. 2010). Although biomembranes are generally impermeable to large or highly charged molecules, accumulating evidences have demonstrated the capacity of CPPs to mediate intracellular delivery of a wide variety of exogenous charged molecules, especially peptides and proteins (Morris et al. 2008; Tunnemann et al. 2006) and nucleic acids, such as splice correcting oligonucleotides (Trabulo et al. 2010a), siRNA (Morris et al. 2008; Crombez et al. 2009) and plasmid DNA (Trabulo et al. 2008). Thus, CPPs opened new possibilities in biomedical research and therapy, offering new tools for intracellular delivery of drugs or genetic cargo as an alternative to the conventional pharmaceutical approaches involving viral vectors (Pfeifer & Verma 2001), lipid-based carriers (Simões et al. 2005) and physical methods to enhance internalization of therapeutic molecules into cells (Niidome & Huang 2002).

Although CPPs have been widely used to deliver cargo molecules into cells, the mechanisms underlying CPP cellular uptake are far from being fully understood. Several endocytotic and non-endocytotic pathways for CPP internalization have been proposed depending on CPP own features, the carried cargo, the cell type and the membrane lipid composition (Morris et al. 2008; Trabulo et al. 2010a). In this context, the interactions between CPPs and membrane lipids have been suggested to play a major role in CPP membrane translocation (Morris et al. 2008). With respect to the membrane, the transverse as well as the lateral structure of the membrane lipid bilayer assume high relevance. Membrane outer regions, with a high density of negative charges mainly conferred by membrane-associated glycosaminoglycan (GAG)-linked proteins (proteoglycans) or neuraminic acid-containing oligosaccharides attached to membrane embedded glycoproteins and gangliosides, may establish electrostatic interactions with the positively charged regions of CPPs resulting from the high density of basic amino acid residues (e.g. Arg and Lys) (Morris et al. 2008). On the other hand, the hydrophilic-hydrophobic interface of the lipid bilayer interacts with the amphiphilic portions of the peptides, modulating their

folding/unfolding and hence their membrane penetration. The heterogeneous lateral structure of the lipid bilayer and the lipid-microdomain organization are not less important in terms of membrane transposition by CPP molecules, since domain boundaries enhance bilayer permeability and may favor the insertion of those foreign molecules (Vereb et al. 2003).

In order to study the role of CPP-lipid interactions in translocation of CPP-conjugated drug delivery systems through the cell membrane, different biophysical approaches have been adopted, most of them using membrane models (Peetla et al. 2009; Alves et al. 2008; Alves et al. 2009; Dennison et al. 2007). These simple experimental systems have allowed addressing the influence of structural and physical features of CPPs and their conjugates in the efficiency of the delivery process. In this regard, the amino acid composition and sequence, as well as the peptide conformation, have been shown to be important features of CPPs towards the success of cargo delivery (Trabulo et al. 2010b). Moreover, the size, the interfacial properties of CPP-based drug delivery systems and other physical characteristics, such as hydrophobicity/hydrophilicity and surface charge of the vectors or their components, can significantly influence their interactions with membrane lipids, and hence the efficiency of vector internalization (Morris el al. 2008; Guterstam et al. 2009; Mano et al. 2006). On the other hand, studies of CPP-lipid interactions in membrane models manipulated to mimic biomembranes have shown the importance of the degree of lipid saturation, the cholesterol content and the membrane local charge on the ability of the peptide to interact, disturb and penetrate model membranes (Arsov et al. 2008; Hallock et al. 2002; Mano et al. 2007).

The peptide S4(13)-PV, a chimeric CPP containing a cell-penetrating sequence of 13 amino acids derived from dermaseptin S4 peptide and the nuclear localization signal of the simian virus 40 (SV40) large T antigen (Trabulo et al. 2010b), has shown to be efficiently taken up by cells through an apparently receptor- and energy-independent process and, less efficiently, through clathrin-mediated endocytosis (Mano et al. 2006; Mano et al. 2005). The high translocation ability of S4(13)-PV peptide across cell membranes is reflected in its competence to generate nucleic acid carrier systems with great potential to deliver plasmid DNA (Trabulo et al. 2008), splice switching oligonucleotides (Trabulo et al. 2010a) and siRNA (unpublished data). However,

these features are not fully shared by its analogue [S4(13)-PV_{scr}], which displays a scrambled sequence and was herein used for comparison, hence reflecting the relevance of the cell penetrating amino acid sequence and resulting α-helical conformation upon membrane interaction for translocation and biological activity (Mano et al. 2006).

In the present study, biophysical and ultrastructural studies were performed to characterize membrane interactions of the wild type S4(13)-PV peptide [S4(13)-PV_{wt}] and its scrambled analogue in order to uncover the mechanisms underlying their membrane translocation and ability for nucleic acid delivery, hence, contributing to the advance in the application of this CPP for therapeutic purposes.

7.3 MATERIALS AND METHODS

Chemicals

The lipids 1,2-dioleoyl-sn-glycero-3-phosphoethanolamine (DOPE), 1,2-dioleoyl-sn-glycero-3-phospho-(1'-rac-glycerol) (DOPG), 1,2-dipalmitoyl-sn-glycero-3-phosphoethanolamine (DPPE), 1,2-dipalmitoyl-sn-glycero-3-phosphocholine (DPPC), 1,2-dipalmitoyl-sn-glycero-3-phospho-(1'-rac-glycerol) (DPPG) and 1-palmitoyl-2-oleoyl-sn-glycero-3-phospho-(1'-rac-glycerol) (POPG) were purchased from Avanti Polar Lipids, Alabaster, AL. The fluorescent probes 3-(p-(6-phenyl)-1,3,5-hexatrienyl)phenylpropionic acid (DPH-PA), 2-(9-anthroyloxy) stearic acid (2-AS), 6-(9-anthroyloxy) stearic acid (6-AS), 12-(9-anthroyloxy) stearic acid (12-AS) and 16-(9-anthroyloxy) palmitic acid (16-AP) were obtained from Molecular Probes Inc. (Eugene, OR).

Peptides

Peptide S4(13)-PV [S4(13)-PV_{wt}, **Table 7.1**] was prepared as a C-terminal amide by solid-phase methodologies based on classical Fmoc (1-(9H-fluoren-9-yl)-methoxycarbonyl)/tert-Butyl chemistry (Fields & Noble 1990), as previously described (Trabulo et al. 2008). The scrambled peptide [S4(13)-PV_{scr}, **Table 7.1**] was generated on the basis of S4(13)-PV peptide sequence, so that the resulting peptide had the same amino acid composition and overall charge, but a distinct primary sequence. Both peptides were acetylated at their N-terminus and isolated in high purity level (>95%). Freeze-dried peptides were reconstituted in ultra-pure water. Concentration of S4(13)-PV peptides was determined by amino acid analysis and light absorption at 280 nm. Amino acid analysis was performed in a Beckman 6300 automatic analyzer, (CA, USA), following acid hydrolysis of the peptide.

Table 7.1 Amino acid sequences of the S4(13)-PV_{wt} and a scrambled analogue, S4(13)-PV_{scr} used in the present study.

Peptide	Sequence
S4(13)-PV_{wt}	ALWKTLLKKVLKAPKKKRKVC-NH_2
S4(13)-PV_{scr}	KTCKVAKWLKKAKPLRKLVKC-NH_2

Lipid Preparations

Liposomes were prepared by hydration of lipid films as previously described (Jurado et al. 1991). Briefly, lipid films, resulting from the evaporation to dryness of aliquots of lipid solutions in chloroform (DPPC, DMPG, DPPG or a mixture of POPG/DPPE at 3/7 molar ratio) were hydrated with an appropriate volume of 50 mM KCl, 10 mM Tris–maleate buffer (pH 7.4) and liposome dispersions were obtained by handshaking in a water bath set 7–10 °C above the transition temperature of the phospholipids. Then, the suspensions of multilamellar vesicles were vortexed for 1 min to disperse aggregates. For DSC experiments, liposomal samples (75 mM in phospholipid) were used immediately after preparation. However, for spectrofluorimetric techniques, liposomes (200 µM in phospholipid) were subsequently sonicated in a low energy water sonifier for a few seconds to decrease the light scattered by the multilamellar vesicle (MLV) suspensions. For fluorescence polarization measurements, the probes (DPH-PA, 2-AS, 6-AS, 12-AS or 16-AP) were then incorporated in liposomes, by injecting a few microliters of the concentrated probe solution in dimethylformamide into liposome suspensions to obtain a lipid/probe molar ratio of 200/1. Thereafter, the liposome suspensions were incubated for 30 minutes in a water bath set 7-10 °C above the transition temperature of the phospholipids and let to stabilize overnight at room temperature, in the dark. Blank samples were prepared with equivalent volumes of the probe solvent.

For SAXS and WAXS measurements, lipid films obtained as described above were dried under a stream of N_2 and left overnight under reduced pressure to remove all traces of the organic solvents. The lipid films were hydrated with 50 mM KCl, 10 mM Tris–maleate buffer (pH 7.4) or buffered solutions of S4(13)-PV peptides (wt and scr) added to obtain lipid/peptide molar ratios from 50/1 to 100/1. Lipid suspensions were then heated above the lipid phase transition temperature in a water bath, mixed by vortexing for about 5 min and centrifuged for 30 s at 2000 g. This procedure was repeated three times. Finally, the samples were aged overnight at 4 °C and shaken under vortex at room temperature for 5 min. The dispersions were transferred into glass capillaries, transparent to X-rays, of 1.5 mm diameter (Hilgenberg, Malsfeld, Germany). The flame-sealed capillaries were stored at 4 °C until the time of the measurements.

DSC Scans

The MLV suspensions incubated with peptide (peptide/lipid molar ratios in the range of 20/1 to 80/1) were sealed into aluminum pans. Heating scans were performed over an appropriate temperature range in a Perkin–Elmer Pyris 1 differential scanning calorimeter, at a scan rate of 5 °C.min^{-1}. To check the reproducibility of data, three heating scans were recorded for each sample. Data acquisition and analysis were performed using the software provided by Perkin–Elmer. Two distinct temperatures were automatically defined in the thermotropic profiles: the temperature of the onset (T_{on}) and the temperature at the endothermic peak (T_m). To define the range of the phase transition or lateral phase separation (T_f–T_{on}), a third temperature corresponding to the completion of the phase transition (T_f) was determined by extrapolating to the baseline a tangent to the descendent slope of the endothermic peak. These critical transition temperatures were estimated as the mean value of heating scans obtained, at least, from three different samples of the same lipid preparation. To determine the total amount of phospholipid contained in the pans, these were carefully opened at the end of the DSC assay and the lipid was dissolved in chloroform/methanol (3:1) and dried with N_2 flow. Phospholipid content was determined by measuring the inorganic phosphate (Bartlett 1958) released after hydrolysis of dried phospholipids, at 180 °C, in 70 % $HClO_4$ (Bottcher et al. 1961). The calorimetric enthalpy changes (ΔH) of the thermotropic events, expressed in kcal/mol, were normalized to the exact phospholipid content in each pan.

SAXS and WAXS

SAXS and WAXS experiments were performed at the beamline A2 of Doris III at HASYLAB (DESY, Hamburg, Germany) with a monochromatic radiation of wavelength 0.15 nm. The SAXS detector was calibrated with rat-tail tendon and the WAXS detector by polyethyleneterephthalat (PET). Heating and cooling scans were performed at a rate of 1 K.min^{-1} in the range of 10 °C to 70 °C. Data was recorded for 10 s every min. Static exposures were also taken below and above the main transition temperature of the lipids DPPC and DPPG and only above the main transition temperature of DOPE or the lipid mixture DOPG:DOPE (3:7), and compared at the same temperatures in heating/cooling cycles to check for possible radiation damage.

In order to minimize sample exposure to X-ray, a shutter mounted before the sample was kept closed when no data were acquired.

Lamellar lattice distances, *d*, were calculated from the small angle Bragg reflections using $s = n/d$, where *s* is the lamellar spacing and *n* the order of the reflection (n = 1, 2…). To obtain a more precise position for *s*, the diffraction peaks were fitted with Lorentzians and the positions of maximal intensities and peak half-widths at one half of the maximal intensity were determined.

Fluorescence Polarization Measurements

The fluorescence polarization measurements of MLV suspensions were performed with a Perkin Elmer LS 55B fluorescence spectrophotometer (Perkin Elmer, U.S.A), equipped with polarization filters and a thermostated cell holder. The excitation wavelength was set at 336 nm and the emission wavelength at 450 nm (5 nm excitation and 6 nm emission band pass) for DPH-PA and at 365 nm and 450 nm for the 2-AS, 6-AS, 12-AS and 16-AP. The fluorescence polarization (*P*) was calculated according to the equation

$$P = \frac{I_{II} - GI_{\perp}}{I_{II} + GI_{\perp}}$$

where I_{II} and $I_{\perp}$ are the intensities of the emitted light when the polarizer and analyzer are in the vertical position (I_{II}) or the polarizer is in the vertical and the analyzer in the horizontal position ($I_{\perp}$). The instrumental grating correction factor for the optical system (G) is given by the ratio of the vertically to the horizontally polarized emission components when the excitation light is polarized in the horizontal plane. All fluorescence measurements were corrected for the contribution of light scattering by using appropriate blanks without added fluorescent probes.

The degree of fluorescence polarization reflects probe rotational diffusion and, therefore, reports the structural order or membrane fluidity in the bilayer lipid environments where the probes are embedded. Thus, the term fluidity is operationally used in this work as being inversely proportional to the polarization parameter, and it essentially reflects the rate and the range of motion of phospholipid acyl chains (Lentz 1989).

Labeling of peptides with nanogold cluster and treatment of cells with peptides

Peptides were tagged with nanogold (Monomaleimido Nanogold, Nanoprobes, NY, d 1.4 nm) as described earlier (Palm-Apergi et al. 2009). A covalent bond was formed between the thiol group of peptide and the maleimide group of label by incubation at a molar ratio 2.5:1 in 50 % methanol at 30 °C for 90 min. Methanol was removed and the conjugate concentrated by speed-vac to reach 50-100 μM concentration of labeled peptide. The conjugate with 1:1 peptide/nanogold ratio was purified to homogeneity by size-exclusion chromatography and concentrated.

HeLa cells cultured under standard conditions were seeded onto glass coverslips in 24-well plates, grown to 80-90% confluence and incubated with culture medium containing 1 or 3 μM gold-labeled peptides at 37 °C for 1 h or 4 h. After incubation, the cells were washed twice with cell culture medium and processed for electron microscopy as described earlier (Padari et al. 2010).

Statistical Analysis of Data

The results of DSC and fluorescence polarization are presented as mean ± standard deviation of at least three independent experiments. Multiple comparisons are performed using one-way analysis of variance (ANOVA) with Tukey's multiple pairwise comparison. Statistical significance was set at $P < 0.05$. Errors in experimental values of x-ray diffraction in the determination of d and ξ were assessed based on error estimates of the partial molecular volumes of lipids and water.

7.4 RESULTS

7.4.1 PEPTIDES S4(13)-PV_{WT} AND S4(13)-PV_{SCR} DIFFERENTLY AFFECT THE THERMODYNAMIC PROPERTIES OF ZWITTERIONIC (DPPC) AND ANIONIC (DPPG) LIPID SYSTEMS

In order to evaluate the effect of the peptides S4(13)-PV_{wt} and S4(13)-PV_{scr} on the thermodynamic properties of lipid bilayers, DSC studies were performed using, as a first approach, liposomes prepared from a single synthetic lipid. A zwitterionic (DPPC) and an anionic phospholipid (DPPG) were used for this purpose and several lipid/peptide molar ratios were assayed, as depicted in **Figures 7.1** and **7.2**.

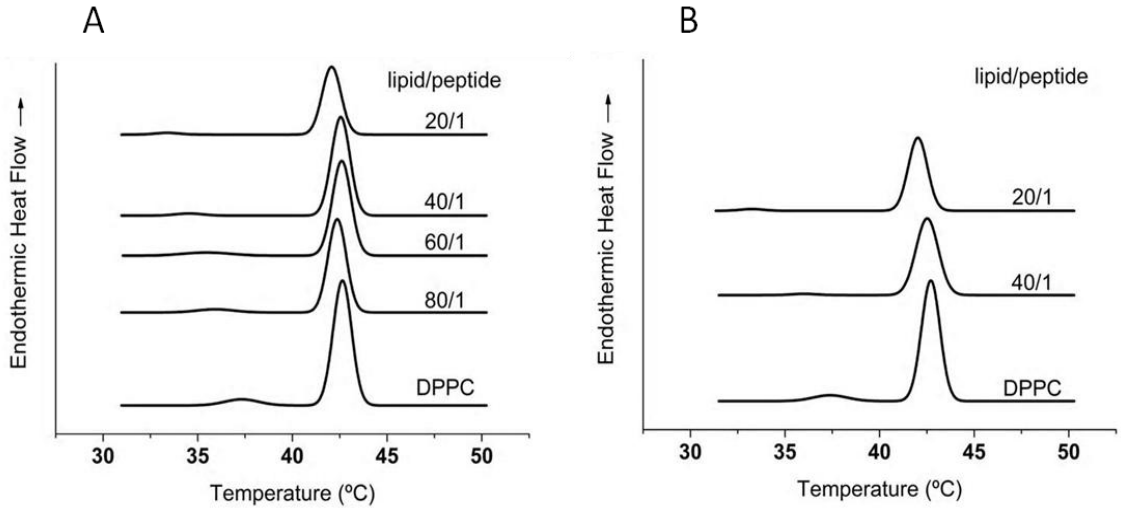

Figure 7.1 DSC profiles (heating scans) of DPPC bilayers in the presence of different concentrations of the peptides S4(13)-PV_{wt} (A) and S4(13)-PV_{scr} (B). The lipid/peptide molar ratios are indicated on the scans, which are representative of at least three independent experiments.

According to what has been extensively documented in literature (Gennis 1989), aqueous dispersions of DPPC exhibited two endothermic events (**Figure 7.1**): a pre-transition near 36 °C and a more energetic main transition at around 42 °C. The first endotherm is due to a transition between two gel phases: $L_{\beta'}$, characterized by tightly packed molecules with tilted acyl chains in the *all-trans* conformation and $P_{\beta'}$ phase, where acyl chains are still highly ordered and tilted, but the lipid hydration is enhanced and the bilayer forms periodic membrane ripples (Gennis 1989). The main transition, whose enthalpy reflects the disruption of van der Waals interactions between the hydrocarbon chains, arises from the conversion of the $P_{\beta'}$ gel phase to a

fluid L_α phase, where the fatty acid chains are highly disordered due to conformational changes (*trans-gauche* isomerization), the headgroups undergo extensive rotational motion and the whole molecules display lateral diffusion rates of the order of 10^{-8} cm^2 s^{-1}.

In the presence of S4(13)-PV_{wt} or S4(13)-PV_{scr} (**Figure 7.1** and **Table 7.2**), the main phase transition of DPPC liposomes did not show significant alterations. However, the wild-type peptide (**Figure 7.1A** and **Table 7.2**) induced a shift of the pre-transition to lower temperatures (from 35.8 °C in the absence of peptide to 33.2 °C at the maximum peptide concentration tested) and a decrease in enthalpy (from 1.14 kcal/mol to 0.24 kcal/mol, in the same conditions). The scrambled peptide (**Figure 7.1B** and **Table 7.2**), at a peptide/lipid molar ratio of 1/40, also promoted an enthalpy decrease of the pre-transition of DPPC membranes (to 0.23 Kcal/mol). Since the enthalpy of the main transition was not significantly altered (**Table 7.2**), these findings suggest that both peptides did not deeply penetrate the hydrophobic core of DPPC bilayers. However, some interactions might be established between the cationic peptides and the negatively charged phosphate groups of the phospholipids, stabilizing, in the case of the S4(13)-PV_{wt}, the ripple phase, as indicated by the decrease of the pre-transition midpoint.

Table 7.2 Characterization of the phase transitions detected by DSC (temperature of the endothermic peaks, T_p and T_m, and enthalpy change, ΔH) in liposomes of DPPC in the absence and presence of the peptides S4(13)-PV_{wt} or S4(13)-PV_{scr}, at the lipid/peptide molar ratios indicated in the table.

		Pre-transition		Main transition	
Peptide type	**DPPC/peptide molar ratio**	**T_p (°C)[1)]**	**Δ*H* (kcal/mol)[1)]**	**T_m (°C)[1)]**	**Δ*H* (kcal/mol)[1)]**
no peptide		35.76 ± 0.20	2.4 ± 0.50	42.24 ± 0.34	19.37 ± 1.16
S4(13)-PV_{wt}	80/1	35.70 ± 0.14	0.98 ± 0.34	42.22 ± 0.09	12.28 ± 1.35
	60/1	34.93 ± 0.12	0.97 ± 0.68	42.31 ± 0.20	15.54 ± 2.06
	40/1	34.04 ± 0.42***	0.90 ± 0.33*	42.30 ± 0.20	15.48 ± 3.06
	20/1	33.18 ± 0.12***	0.51 ± 0.32*	42.24 ± 0.25	12.97 ± 2.43
S4(13)-PV_{scr}	40/1	36.49 ± 1.40	0.48 ± 0.40	42.55 ± 0.51	12.99 ± 2.25

[1)] These values (means ± standard deviation) were obtained from three DSC experiments. Comparisons were performed in the presence *vs.* absence of the peptide (*p<0.01, ***p<0.0001).

A distinct scenario resulted from peptide interactions with DPPG membranes displaying a net negative charge (**Figure 7.2**). A pre-transition of DPPG vesicles in media with low ionic strength has been referred in the literature (Wilkinson & McIntosh 1986). However, this was not observed with the liposome samples we used for DSC assays, most likely because they were prepared in a salt-containing buffer, reducing the repulsive electrostatic interactions between the phosphate groups and then decreasing the area required for the phospholipid headgroups. In fact, the pre-transition has been registered only with lipids featured by a large area requirement for the polar groups (Gennis 1989). Therefore, a single endothermic event was observed in our assays, corresponding to the main transition centered at around 41 °C, in agreement with what has been reported in the literature (Wilkinson & McIntosh 1986). The wild-type peptide induced a split of this endotherm in two components (**Figure 7.2A**, **Table 7.3**), suggesting a non-homogeneous distribution of the peptide within the membrane. The lower temperature component, which is preserved in the lipid/peptide range of 80/1 to 40/1, centered at the temperature of the pure lipid transition, is assigned to less disturbed lipid molecules, which remain in peptide-poor regions. In contrast, the higher temperature component is assigned to lipids residing in peptide-rich domains or those being in closer proximity to peptides, undergoing high perturbation. With increasing concentrations of the peptide, the second peak was progressively favored, leading to a situation (with the higher concentration of peptide tested, 20/1) where the splitting was vanished and only one peak was detected at the highest temperature (42 °C), probably due to a homogeneous lipid population, which is under the influence of peptide molecular interactions. Interestingly, the enthalpy of the main transition of DPPG liposomes in the absence of peptide (ΔH = 5.9 Kcal/mol) was approximately equivalent to the sum of the enthalpies of the two endotherms obtained in peptide-containing preparations at peptide/lipid molar ratios from 80/1 to 60/1 (**Table 7.3**). At a peptide/lipid molar ratio of 40/1, the enthalpy of the lower temperature endotherm further decreased, but that of the higher temperature endotherm stopped increasing and, at the maximal peptide/lipid ratio tested (20/1), the enthalpy of the single endotherm was much lower (approximately one half) than that observed in the absence of the peptide. This probably indicates that a fraction of DPPG molecules were somehow “sequestered” by

tight interaction with the peptide, being inhibited to participate in the bulk phase transition.

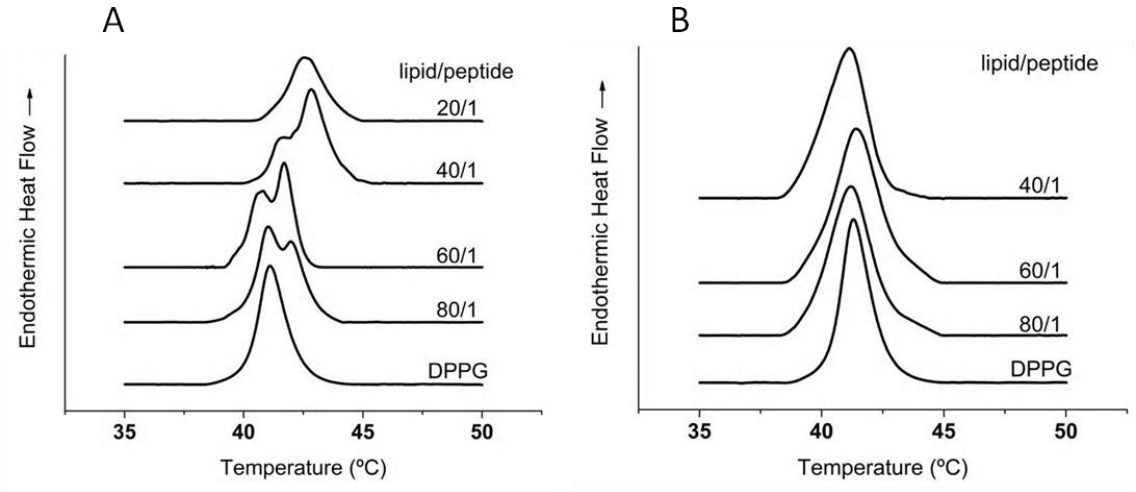

Figure 7.2 DSC profiles (heating scans) of DPPG bilayers in the presence of different concentrations of the peptides S4(13)-PV_{wt} (A) and S4(13)-PV_{scr} (B). The lipid/peptide molar ratios are indicated on the scans, which are representative of at least three independent experiments.

Table 7.3 Characterization of the phase transitions detected by DSC (temperature of the endothermic peak, T_m and enthalpy change, ΔH) in liposomes of DPPG in the absence and presence of the peptides S4(13)-PV_{wt} or S4(13)-PV_{scr}, at the lipid/peptide molar ratios indicated in the table.

		Main transition			
Peptide type	**DPPG/ peptide molar ratio**	**T_m (°C)[1)]**		**ΔH (kcal/mol)[1)]**	
no peptide		41.28 ± 0.56	-	5.92 ± 0.17	-
S4(13)-PV_{wt}	80/1	41.22 ± 0.20	42.07 ± 0.13	2.35 ± 3.7	3.03 ± 0.33
	60/1	41.05 ± 0.40	41.82 ± 0.15	2.15 ± 1.70	3.65 ± 1.73
	40/1	41.54 ± 0.30	42.45 ± 0.36	1.65 ± 1.91	3.05 ± 0.74
	20/1	-	42.24 ± 0.32**	-	3.11 ± 1.26
S4(13)-PV_{scr}	80/1	41.48 ± 0.36		4.14 ± 1.20	
	60/1	40.36 ± 1.43		2.68 ± 0.10*	
	40/1	41.38 ± 0.32		2.35 ± 0.17*	

[1)] These values (means ± standard deviation) were obtained from three DSC experiments. Comparisons were performed in the presence *vs* absence of the peptide (*p<0.05, **p<0.01).

Despite having similar physico-chemical properties (length of the primary sequence, charge and amino acid composition), the scrambled peptide differently affected DPPG model membranes, its action being limited to a concentration-dependent decrease in the enthalpy of the main transition (**Figure 7.2B** and **Table 7.3**), which reinforces its different ability to interact and disturb the lipid bilayer.

7.4.2 Peptides S4(13)-PV$_{WT}$ and S4(13)-PV$_{SCR}$ induce structural changes in zwitterionic (DPPC) or anionic (DPPG) lipid systems

The degree of peptide-induced perturbation of the different DPPC phases ($L_{\beta'}$, $P_{\beta'}$ and L_{α}) at a peptide/lipid molar ratio of 1/50 was evaluated by X-ray diffraction patterns at small and wide angles (SAXS and WAXS), which provide information on the long-range bilayer organization and the hydrocarbon chain packing, respectively.

SAXS (data not shown) and WAXS patterns (**Figure 7.3A**) taken at different temperatures in heating scans allowed the determination of the pre-transition ($L_{\beta'} \rightarrow P_{\beta'}$) and the main transition ($P_{\beta'} \rightarrow L_{\alpha}$) temperatures of DPPC bilayers (≈35 °C and 42 °C, respectively), which are in agreement with the results obtained by DSC and previously published data (Lúcio et al. 2008). Thus, the WAXS patterns of DPPC, showing two WAXS reflection peaks at 28, 32 and 34 °C (**Figure 7.3A**), are typical of a $L_{\beta'}$ phase with orthorhombic hydrocarbon chain packing. At 36 °C, a broad single Bragg peak was observed, indicating a transition to the $P_{\beta'}$ phase, and the main phase transition occurred at 42 °C, where a defined WAXS peak is no longer visible.

As shown in **Figure 7.3B** and **C**, the peptides did not alter the main phase transition temperature of DPPC, but promoted some perturbation of the chain packing regarding the $L_{\beta'}$ phase, shifting DPPC pre-transition to lower temperatures (34 °C). This effect, which is particularly evident for the S4(13)-PV$_{wt}$ peptide, corroborates DSC data.

Deconvolution of the WAXS patterns in the $L_{\beta'}$ phase (20 °C) gives the lattice distances of the orthorhombic lattice of the DPPC chain packing, i.e., 4.12 ± 0.05 Å and 4.04 ± 0.05 Å (data not shown), which are also in good agreement with the literature (Lúcio et al. 2008). Neither this chain packing nor the correlation length (ξ) between the bilayers (data not shown) was affected by the presence of the peptides.

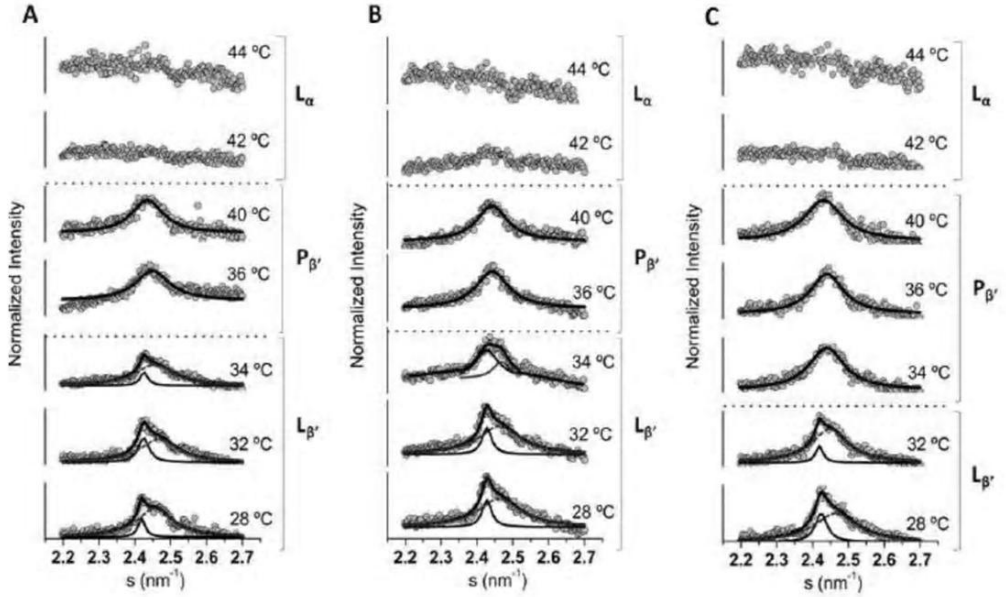

Figure 7.3 WAXS patterns of (A) DPPC; (B) DPPC/S4(13)-PV_{scr} (50/1 molar ratio) and (C) DPPC/S4(13)-PV_{wt} (50/1 molar ratio), at different temperatures. Solid lines give the best fit of the Lorentzian's analysis model to the scattered intensities. Dotted lines represent the transition points observed between $L_{\beta'}$ and $P_{\beta'}$ phases (pre-transition) and between $P_{\beta'}$ and L_α phases (main transition).

A very different scenario was provided by SAXS and WAXS studies with DPPG membranes. It should be emphasized that in these lipid preparations (much more concentrated than those used in DSC assays), it was possible to detect the pre-transition by SAXS and WAXS. The SAXS patterns of DPPG exhibited very diffuse scattering especially at higher temperatures, which results in broad Bragg peaks with low correlation length between the bilayers (ξ). This has been previously observed (Danner et al. 2008; Pabst et al. 2007; Prossnigg et al. 2010) and explained because of the electrostatic repulsion, which leads to the formation of uncorrelated bilayers. DPPG lamellar distances (d) determined in each lipid phase are displayed in **Table 7.4**. In the $L_{\beta'}$ gel phase, the DPPG bilayer including the water layer showed to be 5.02 ± 0.07 nm thick. Along a heating scan, the spacing increased to 5.76 ± 0.07 nm in the ripple gel phase $P_{\beta'}$, and decreased again to 5.40 ± 0.07 nm in the L_α phase, in a similar fashion to what has been described in the literature (Pabst et al. 2007).

In the presence of S4(13)-PV peptides, no significant effects were denoted in the L_α and $P_{\beta'}$ phases of DPPG bilayers (**Table 7.4**). Thus, the position of the Bragg peaks was not altered and d values show only a very small increase as compared with pure DPPG bilayers.

However, the addition of peptides led to a lipid phase separation in the $L_{\beta'}$ phase. Hence, the coexistence of a non-affected DPPG gel phase, showing *d* values (≈ 5.0 nm) not significantly different from those of pure DPPG bilayers, and a phase with much smaller *d* values (≈ 3.0 nm), characteristic of a $L_{\beta I}$ interdigitated phase (**Table 7.4**), indicates a non-homogeneous distribution of peptides in the most ordered phase ($L_{\beta'}$) of DPPG membranes.

Table 7.4 Long range distances (d) and correlation length (ξ) determined from SAXS patterns in DPPG bilayers in the absence and in the presence of the peptides S4(13)-PV_{wt} or S4(13)-PV_{scr} (100/1 or 50/1 lipid/peptide molar ratio), at 20, 38 and 50 °C and physiological pH.

Sample	T (°C) / expected lipid phase	d_{SAXS} (Å)		ξ (Å)	
DPPG	20 ($L_{\beta'}$)	50.2 ± 0.7		187 ± 10	
	38 ($P_{\beta'}$)	57.6 ± 0.7		32 ± 15	
	50 (L_{α})	54.1 ± 0.7		33 ± 15	
DPPG:S4(13)-PV_{scr} (100/1)	20 ($L_{\beta'}$)	50.4 ± 0.7	36.8 ± 0.7	180 ± 10	140 ± 10
	38 ($P_{\beta'}$)	57.9 ± 0.7		34 ± 15	
	50 (L_{α})	54.2 ± 0.7		23 ± 15	
DPPG:S4(13)-PV_{scr} (50/1)	20 ($L_{\beta'}$)	50.4 ± 0.7	36.5 ± 0.7	5 ± 3	18 ± 15
	38 ($P_{\beta'}$)	57.6 ± 0.7		32 ± 15	
	50 (L_{α})	54.7 ± 0.7		22 ± 10	
DPPG:S4(13)-PV_{wt} (100/1)	20 ($L_{\beta'}$)	50.7 ± 0.7	37.5 ± 0.7	22 ± 15	105 ± 15
	38 ($P_{\beta'}$)	59.0 ± 0.7		34 ± 15	
	50 (L_{α})	54.8 ± 0.7		23 ± 15	
DPPG:S4(13)-PV_{wt} (50/1)	20 ($L_{\beta'}$)	51.7 ± 0.7	37.2 ± 0.7	38 ± 15	114 ± 15
	38 ($P_{\beta'}$)	58.9 ± 0.7		30 ± 15	
	50 (L_{α})	54.9 ± 0.7		32 ± 15	

The interdigitated phase visible in the SAXS regime was confirmed in the corresponding WAXS patterns (**Figure 7.4**), which exhibit sharp peaks (gray lines at 10 and 20 °C) in addition to the β' pattern assigned to an orthorhombic packing of hydrocarbon chains (dashed black lines at 10 and 20 °C). At 38 °C, a single phase was observed again, which is assigned to a ripple phase as indicated by the broad peak, similarly to what was observed in pure DPPG bilayers.

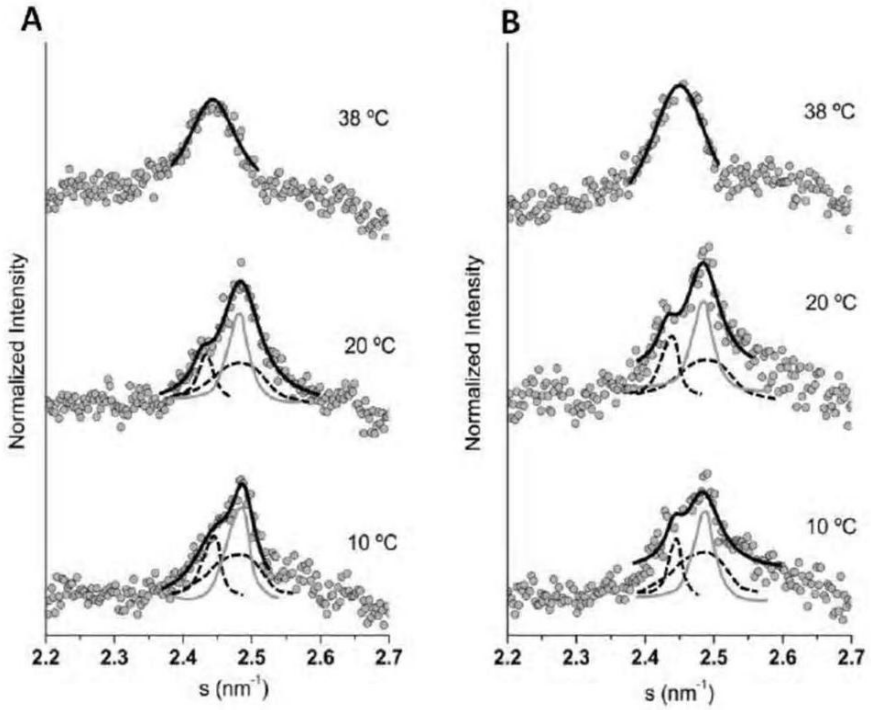

Figure 7.4 WAXS patterns of (A) DPPG/S4(13)-PV_{scr} (50/1 molar ratio) and (B) DPPG/S4(13)-PV_{wt} (50/1 molar ratio) at different temperatures. Solid lines give the best fit of the Lorentzian's analysis model to the scattered intensities. At the temperatures of 10 and 20 °C the fitting can be described as the superimposition of three peaks corresponding to the orthorhombically packed acyl chains (dashed black lines) and interdigitated acyl chains (gray line).

Besides studying the influence of the peptides on each lipid phase, WAXS heating scans were taken at different temperatures to determine the effect of the peptides on the main phase transition temperature ($P_{\beta'} \rightarrow L_{\alpha}$). Both peptides shifted DPPG main transition to higher temperatures (data not shown), from an ordered to a disordered phase where a defined WAXS peak is no longer visible. Probably peptide-induced broadening of this transition impeded the detection of the temperature upshift in DSC scans in the case of the scrambled peptide (**Figure 7.2B** and **Table 7.3**).

7.4.3 Peptides S4(13)-PV_{WT} and S4(13)-PV_{SCR} alter membrane order parameters monitored at different depths of an anionic lipid (DPPG) system

Fluorescence polarization measurements using fluorescent probes that intercalate at different depths of the lipid bilayer were performed in order to uncover how the S4(13)-PV peptides affect the lateral pressure profile across the thickness of a DPPG membrane. As a first approach, a fluorescence polarization thermogram in DPPG liposomes was obtained with the probe DPH-PA, which monitors the hydrophobic

region of the bilayer closer to the surface, at which this molecule is anchored by its negatively charged group (Trotter & Storch 1988). The fluidity-related spectroscopic parameter (P) in DPPG bilayers undergoes, as expected, an abrupt decrease within a relatively narrow temperature range (**Figure 7.5A**), reflecting a sharp phase transition with a temperature midpoint (T_m) at 42 °C, as indicated by the peak of the fluorescence polarization derivative curve (inset in **Figure 7.5A**), in accordance with the above results obtained by DSC and X-ray diffraction. Also consistent with DSC data, both peptides, at a 40/1 lipid/peptide molar ratio, broaden DPPG transition profile, affecting its cooperativity. Additionally, an increase of the order parameter over all the transition temperature range and in the fluid phase was observed (**Figure 7.5A**), this effect being more pronounced for the scrambled peptide. The peptide-induced increase of lipid order may result from the electrostatic interaction between the peptides and the lipid membranes, with a consequent shielding of the surface net charge that might decrease the repulsive forces between the lipid headgroups.

In order to further characterize peptide-induced perturbation across the bilayer thickness, fluorescence polarization studies were performed with n-(9-anthroyloxy) stearic acid (n = 2, 6 and 12) and 16-(9-anthroyloxy) palmitic acid, at lipid/peptide molar ratios of 80/1 and 40/1 and at two different temperatures, one below (12 °C) and other above (60 °C) the DPPG main phase transition (**Figure 7.5B**). For both temperatures, peptide-induced ordering effect was more pronounced in the extremes of the hydrocarbon chains (at the level of carbons 2 and 16 of the stearoyl and palmitoyl chains, respectively). This effect was shown to be dependent on peptide concentration and more evident at 12 °C, temperature at which the coexistence of a $L_{\beta'}$ phase and a $L_{\beta I}$ interdigitated phase was demonstrated by the SAXS and WAXS patterns. Peptide-induced broadening of phase transition, as detected by DPH-PA, is also indicative of lateral phase separation.

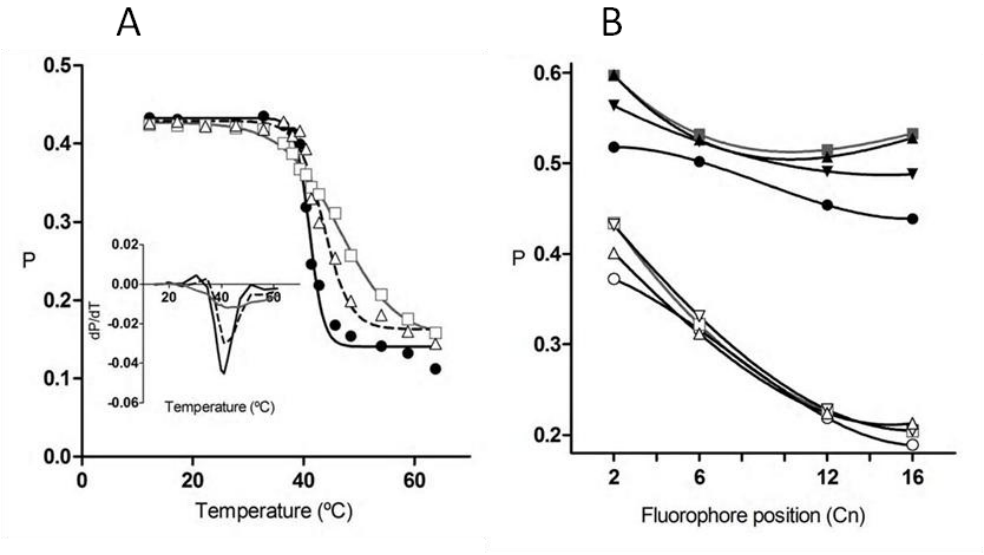

Figure 7.5 Fluorescence polarization (P) of DPH-PA (A) or 2-AS, 6-AS, 12-AS and 16-AP (B) in DPPG bilayers in the absence and in the presence of S4(13)-PV_{wt} or S4(13)-PV_{scr}. In A, thermograms were obtained in the absence (●) and in the presence of S4(13)-PV_{wt} (△) or S4(13)-PV_{scr} (□), at a lipid/peptide molar ratio of 40/1. The inset shows the first derivative of the polarization curves. In B, the fluorescence polarization of 2-AS, 6-AS, 12-AS and 16-AP (the carbon number of the stearic or palmitic chain where the 9-anthroyloxy group is attached being represented in the x axis) was measured at 12 ºC (filled symbols) and 60 ºC (open symbols), in the absence (●, ○) or the presence of S4(13)-PV_{wt} at a lipid/peptide molar ratio of 40/1 (▲, △) and 80/1 (▼, ▽) or S4(13)-PV_{scr} at a lipid/peptide molar ratio of 40/1 (■, □). The results shown are representative of at least three independent experiments.

It should be noted that the interpretation of fluorescence polarization data in these conditions is complicated by the uncertainty of the localization of the fluorescent probes in the plane of the membrane and their preferential distribution between the different coexisting domains. Taking into account these limitations, the increase of fluorescence polarization of 2-AS at temperatures below and above the main phase transition may be a consequence of the interaction of the cationic peptide with the overall negative charges of DPPG headgroups, thus reducing electrostatic repulsion. A tighter packing of lipid molecules would be hence favored in the segment of the hydrocarbon chains closer to the phospholipid polar groups. This effect was not however detected by DPH-PA at 12 °C, probably because this probe monitors the lipid order in a deeper region of the lipid bilayer. On the other hand, the ordering effect induced by the peptide in the hydrophobic core of the bilayer, as monitored by 16-AP, might result from the interdigitation of phospholipid hydrocarbon chains, thus increasing van der Waals interactions.

7.4.4 THE S4(13)-PV_{WT} PEPTIDE PROMOTES LIPID DOMAIN SEGREGATION IN A POPG/DPPE LIPID SYSTEM

To further characterize peptide-membrane interactions, a binary lipid system containing a partially unsaturated anionic lipid (POPG) and a saturated zwitterionic lipid (DPPE) was used to mimic a physiologically more relevant membrane. The mixture of POPG/DPPE at a molar ratio of 3/7 constitutes a useful model system for DSC studies, since, in spite of the different transition temperatures of its lipid components (-2 °C for POPG and 63 °C for DPPE), it gives rise to a single, yet broad and assymetric peak, which reflects a certain lateral phase separation.

The incorporation of the S4(13)-PV_{wt} peptide into this membrane system produced significant changes in the thermotropic behavior of the lipid mixture (**Figure 7.6**). Relatively low peptide concentrations (lipid/peptide molar ratio of 80/1) promoted an alteration of the DSC profile, giving rise to a shoulder and a peak, which can be assigned to different lipid domains. The peptide apparently induced a displacement of the minor lipid (POPG) to segregated domains, corresponding to the lower melting temperature component (shoulder in the DSC profile). As a consequence, DPPE-enriched domains then exhibit a more cooperative transition, at higher temperatures (the peak in the DSC scan). The lower temperature component seems to shift to higher temperatures as the peptide concentration increased, from 80/1 to 40/1 lipid/peptide molar ratio, suggesting a peptide-induced increase of lipid order. At the highest peptide concentration assayed (20/1), the endotherm became more symmetric, although still comprising two distinct components. Thus, the deconvolution of this peak reflects an effective lateral phase separation between a higher temperature component, assigned to the DPPE-enriched and peptide-poor domains, and a low temperature component, representing the more disordered domains of the anionic lipid POPG to which the peptide preferentially interacts.

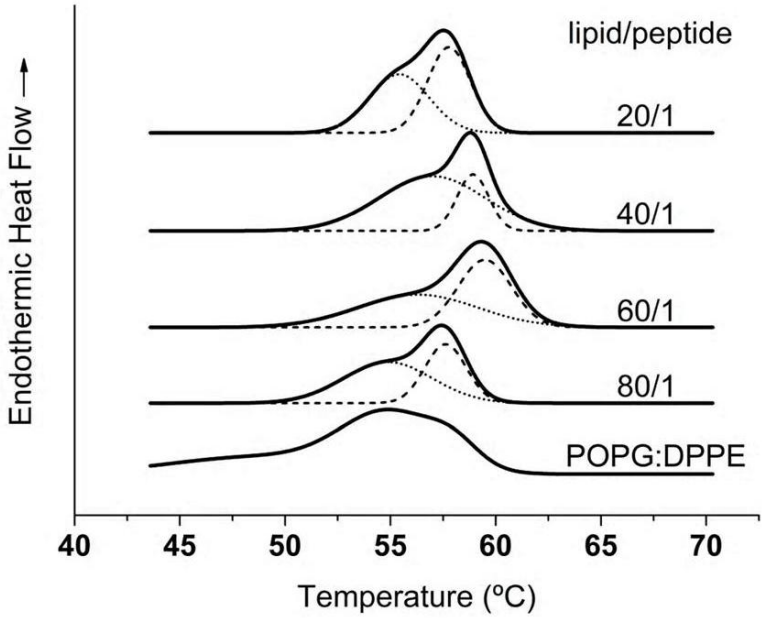

Figure 7.6 DSC profiles (heating scans) of POPG/DPPE (3/7 molar ratio) bilayers in the presence of different concentrations of the peptide S4(13)-PV_{wt}. The lipid/peptide molar ratios are indicated on the scans, which are representative of at least three independent experiments.

7.4.5 PEPTIDES S4(13)-PVWT AND S4(13)-PVSCR AFFECT THE PHASE BEHAVIOR OF A DOPG/DOPE LIPID SYSTEM

To evaluate the effect of the peptides S4(13)-PV_{wt} and S4(13)-PV_{scr} on lipid mesomorphism, a mixture of DOPG and DOPE (3/7 molar ratio) was chosen as a model system, since it undergoes a lamellar-to-inverted hexagonal phase ($L_\alpha \rightarrow H_{II}$) transition at temperatures easily available in laboratory (Morein et al. 2000). In this context, the ability of the peptides used in this work to induce non-lamellar phases was studied by evaluating their capacity to lower the temperature at which the above lipid mixture undergoes a transition from the lamellar to a non-lamellar phase. As reported in the literature, the L_α phase of DOPG/DOPE mixture (3/7 molar ratio) is stable up to 50 °C, an isotropic phase (I) having been detected by ^{31}P NMR only at temperatures above 60 °C (Prossnigg et al. 2010). SAXS studies at 65 ºC showed reflections consistent with the formation of a cubic phase (belonging to the space group *Pn3m*) and a small amount of H_{II} phase (Morein et al. 2000).

In the present work, SAXS measurements were performed at two different temperatures: 20 and 50 °C, where only lamellar phases (L_α) are expected. At the temperatures tested, several small angle diffraction peaks were detected in the

DOPG/DOPE mixture. The observed reflections in the absence of the peptides are consistent with the coexistence of two lamellar phases: a remaining $L_{\beta'}$ corresponding to the peaks positioned at lower lattice spacings (higher lattice distances in **Table 7.5**) and a L_{α} phase corresponding to the peaks positioned at higher lattice spacings (lower lattice distances in **Table 7.5**). The first and second order Bragg peaks of each of these lipid phases presented an indexed ratio of 1:2, which indicates the lamellar nature of these phases.

Table 7.5 Long range distances (*d*) and correlation length (ξ) determined from SAXS patterns for DOPE:DOPG (7:3) bilayers in the presence of the peptides S4(13)-PV_{wt} or S4(13)-PV_{scr} (50/1 lipid/peptide molar ratio), at 20 and 50 °C and physiological pH.

Sample	T (°C) / expected lipid phase	d_{SAXS} (Å)					ξ (Å)
		1st Order Diffraction Peak			2nd Order Diffraction Peak		
Lipid mixture	20 (L_{α})	61.3 ± 0.5	47.5 ± 0.5		29.6 ± 0.5	25.6 ± 0.5	33 ± 10
DOPE:DOPG (7:3)	50 (L_{α})	61.3 ± 0.5	50.2 ± 0.5		29.8 ± 0.5	27.1 ± 0.5	43 ± 10
Lipid mixture:	20 (L_{α})	61.3 ± 0.5	51.4 ± 0.5		29.7 ± 0.5	26.6 ± 0.5	99 ± 10
S4(13)-PV_{scr} (50:1)	50 (L_{α})	59.8 ± 0.5	50.6 ± 0.5	46.5 ± 0.5	29.7 ± 0.5	26.3 ± 0.5	136 ± 10
Lipid mixture:	20 (L_{α})	61.0 ± 0.5	57.1 ± 0.5		29.9 ± 0.5	28.5 ± 0.5	539 ± 10
S4(13)-PV_{wt} (50:1)	50 (L_{α})	65.5 ± 0.5	54.2 ± 0.5	46.5 ± 0.5	29.8 ± 0.5	27.3 ± 0.5	522 ± 10

Concentration-dependent effects were detected upon interaction of either of the two peptides with the lipid mixture. For sake of clarity, only the results obtained with the highest peptide/lipid molar ratio (1/50) are shown. Both peptides showed a significant effect on the lipid mixture phase behavior at this concentration, promoting the formation of more defined Bragg peaks (data not shown) and rising the correlation length (ξ) between the bilayers (**Table 7.5**), thus indicating an increase of the lipid order. Moreover, both peptides promoted the formation of non-lamellar phases at lower temperatures (50 °C) than those at which these phases have been reported in this lipid mixture (about 65 °C (Morein et al. 2000)). In the presence of S4(13)-PV_{scr}, several small angle reflections were observed at 50 °C (**Table 7.5**). The first order reflection at 5.06 ± 0.05 nm and the second order reflection at 2.63 ± 0.05 nm were assigned to the lamellar phase (indexed ratio of 1:2), whereas

the first order reflections at 4.65 ± 0.05 nm and 5.98 ± 0.05 nm and the second order reflections at 2.63 ± 0.05 nm and 2.97 ± 0.05 nm were assigned to an inverted hexagonal (H_{II}) phase (indexed ratio of 1:√3:2). S4(13)-PV_{wt} peptide also proved to be able to promote the formation of non-lamellar phases, identified in this case as a cubic phase and a small amount of H_{II} phase. Thus, the first order reflections at 4.65 ± 0.05 nm, 5.42 ± 0.05 nm and 6.55 ± 0.05 nm, and the second order reflections at 2.73 ± 0.05 nm and 2.98 ± 0.05 nm (**Table 7.5**) were assigned to the cubic phase (indexed ratio of 1:√3:√4:√5) and a H_{II} phase (indexed ratio of 1:√3:2).

7.4.6 Peptide S4(13)-PVwt induces formation of quasi-hexagonal domains in membranes of HeLa cells

The observation that S4(13)-PV_{wt} peptide was able to affect the phase behavior in a model lipid system prompted us to analyze the interaction of the peptide with the plasma membrane of cells at the ultrastructural level by using transmission electron microscopy. The peptide was tagged for better visualization with nanogold label as described earlier (Padari et al. 2010) and the electron microscopy studies were performed at peptide concentrations, which would enable a non-endocytotic uptake to occur (Mano et al. 2005) and could favor lipid transition from a lamellar to a non-lamellar phase. Incubation of HeLa cells with 3 μM labeled wild-type peptide resulted in formation of peptide-containing particles at/on the cell surface (**Figure 7.7A, B**). Analogous structures were not observed with the scrambled peptide (not shown). A closer inspection revealed that the formed particles were not random aggregates but multi-layered and well-structured (**Figure 7.7A a', a'' and 7.7B b'**) with an average distance between layers of 9.5-10 nm. The nanogold label on S4(13)-PV peptide locates between the layers and is detectable as black dots of a non-uniform size with a diameter in the range of 5-15 nm (**Figure 7.7A a', a'' and 7.7B b'**). These findings suggest that the peptide has induced and stabilized the non-lamellar organization of cellular membranes, which is reminiscent of quasi-hexagonal domains (Siegel & Epand 1997; Siegel 1993). The plasma membrane, which is usually very well distinguishable in its lamellar organization in electron micrographs, becomes undetectable (**Figure 7.7A**). However, in some regions of the plasma membrane the

formation of non-lamellar lipid phase did not interfere markedly with its regular organization (**Figure 7.7B**).

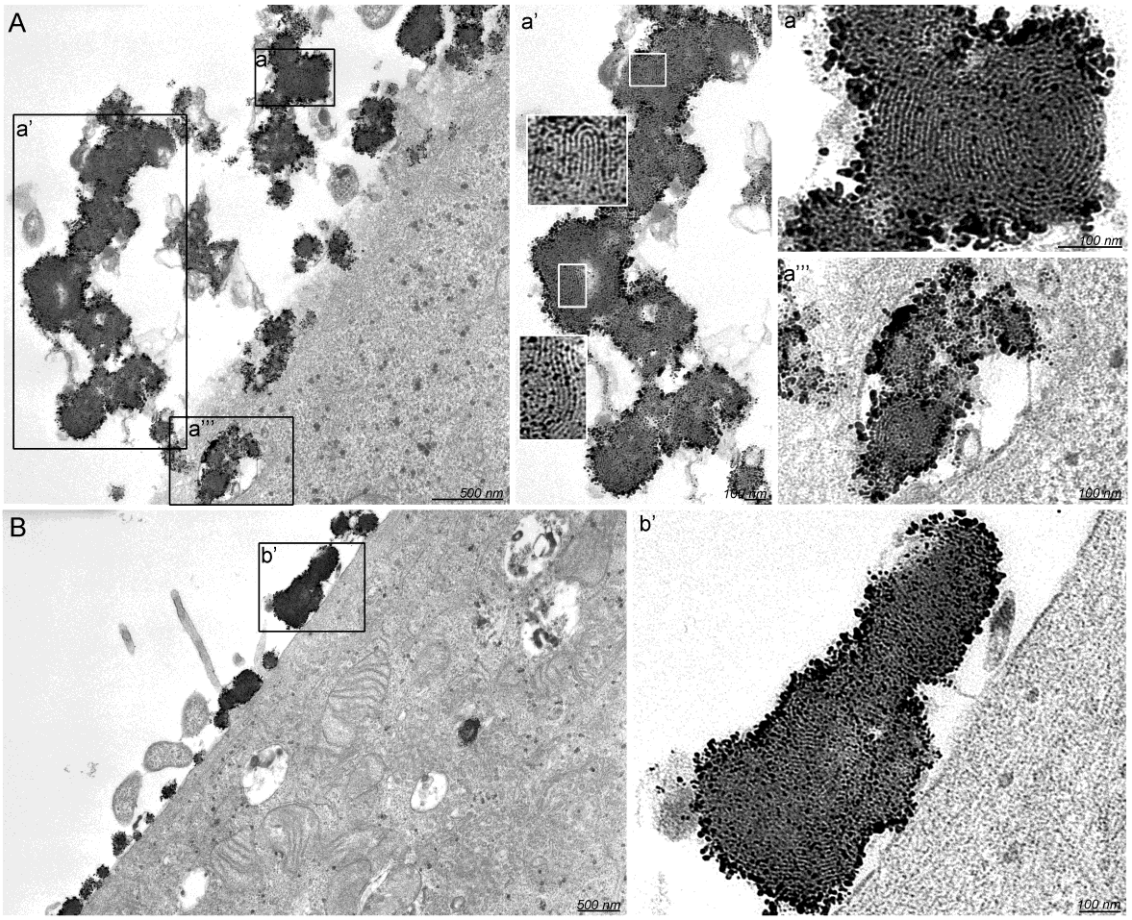

Figure 7.7 Transmission electron micrographs showing the interaction of S4(13)-PV_{wt} peptide with plasma membrane of HeLa cells and peptide translocation into the cells. HeLa cells were incubated with 3 μM S4(13)-PV_{wt} during 1 h at 37 °C. Black dots correspond to the nanogold label, visualized by silver enhancement to ~10 nm. S4(13)-PV peptide-containing quasi-hexagonal structures are observed at the surface of HeLa cells (A, B) and their fingerprint pattern is evidenced in enlarged sections (a', a'', a''' for image A and b' for image B).

The peptide-containing structures that resembled quasi-hexagonal domains were very rarely detected on the cell surface at 1 μM S4(13)-PV concentration in parallel with peptide nanoparticles (Padari et al. 2010). Whereas the latter were typical and abundant at 1 μM concentration of S4(13)-PV, the former were very seldom found. In addition, the non-lamellar formations detected at 1 μM concentration were always markedly smaller and less organized than those observed at the high peptide concentration. Furthermore, the appearance of quasi-hexagonal domains was a time-dependent process, since such structures were only detected upon 1 h or longer

incubation at the physiological temperature, suggesting the recruitment of specific lipids or slow separation of particular phases in the plasma membrane.

In addition to their presence at the cell surface, the putative non-lamellar structures were found in the membrane of intracellular vesicles, at 3 μM concentration of S4(13)-PV peptide (**Figure 7.7A a'''**). Such peptide-induced arrangements were somewhat surprisingly also observed after incubation of HeLa cells with 1 μM S4(13)-PV (**Figure 7.8**), although the respective structures were markedly smaller and their organization was not as typical as that seen with the peptide at 3 μM concentration. At the low peptide concentration, quasi-hexagonal domains were detected in intracellular vesicles after 4 h incubation (**Figure 7.8A**), although occasionally such structures could also be observed after 1 h (**Figure 7.8B**). Although the SAXS assay demonstrated the induction of the cubic phase in the membrane-mimicking system by the S4(13)-PV peptide, characteristic structures were not detected by electron microscopy after peptide incubation with HeLa cells.

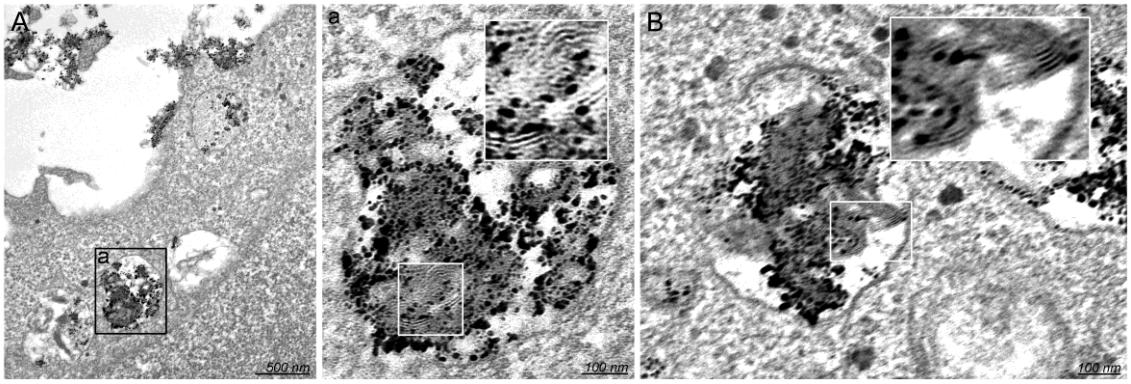

Figure 7.8 Transmission electron micrographs showing the interaction of S4(13)-PV_{wt} peptide with the endosomal membrane of HeLa cells. The cells were incubated with 1 μM S4(13)-PV_{wt} for 4 h (A) or 1 h (B), at 37 °C. Black dots correspond to the nanogold label, visualized by silver enhancement to ~10 nm. Quasi-hexagonal domains are detected in endocytotic vesicles after 1 h or 4 h incubation and evidenced in enlarged section (a for A image).

7.5 DISCUSSION

In the field of CPP pharmacological application, the characterization of peptide-membrane interactions has assumed a high relevance to clarify the molecular mechanisms underlying CPP ability to transpose membranes and induce a desirable biological response. In the present work, we focused on the S4(13)-PV peptide and its scrambled analogue, which have been studied in our laboratory showing different capacities to translocate across cell membranes (Mano et al. 2006) and, accordingly, different competences for nucleic acid delivery (Trabulo et al. 2010b). These studies have shown a good correlation between the extent of cellular uptake and the conformational behavior of the peptides upon interaction with negatively charged membrane models (Mano et al. 2006; Mano et al. 2007). In this regard, more efficient internalization of the wild-type peptide has been attributed to its ability to adopt an amphipathic α-helical conformation, whose content increased with the negative charge density of the membrane model. In contrast, the scrambled peptide showed less significant conformational changes, suggesting that the sequence derived from the Dermaseptin S4 peptide [1-13 amino acid residues of the S4(13)-PV_{wt}] is required for the formation of α-helical structures in the presence of negatively charged membranes (Mano et al. 2007).

Aiming at gaining further insight into the molecular mechanisms responsible for the distinct internalization properties of S4(13)-PV_{wt} and S4(13)-PV_{scr} peptides, we attempted herein to unveil the other side of peptide/membrane interactions, that is, how the physical properties of membrane lipids are affected by each of the peptides.

For reasons of simplicity, we chose as a primary approach membrane models composed of a single synthetic phospholipid, DPPC, because of the relevance of phosphatidylcholine species in eukaryotic plasma membranes, typically found in the outer monolayer of these membranes, or DPPG, which, although rare in mammalian cell membranes, allows to model an anionic membrane mimicking the outer surface of cellular membranes whose negative charges are mainly conferred by gangliosides and proteoglycans.

The minor effects exerted by both peptides on the thermodynamic and structural properties of the neutrally charged DPPC bilayers, in contrast to our observations for the anionic DPPG membranes, as monitored by DSC, fluorescence polarization and X-ray diffraction, evidenced the importance of the electrostatic interactions between the cationic peptide and the lipid headgroups in terms of membrane physical alterations. Therefore, this type of interactions is equally important both from the peptide and the lipid perspective. As mentioned above, the secondary structure of the S4(13)-PV peptide is significantly affected in the presence of vesicles containing negatively charged phospholipids but no conformational changes were observed when neutral membranes are added to the peptide solution in buffer (Mano et al. 2006). Moreover, POPC vesicles did not affect the peptide fluorescence emission spectrum, but a blue-shift occurred when the vesicles included increasing amounts of the anionic lipid POPG (Mano et al. 2007). Consistently, the intrinsic fluorescence of the S4(13)-PV peptide was efficiently quenched by acrylamide in the presence of neutral lipid vesicles consisting of POPC, in a similar way to that occurring in buffer, but the quenching significantly decreased when increasing amounts of POPG were added to the binary system (Mano et al. 2006; Mano et al. 2007). Overall, these results indicate that electrostatic interactions between the S4(13)-PV peptide and the lipid bilayer are required to trigger a sequence of events: conformational alterations in the peptide followed by its incorporation into the lipid bilayer and, finally, disturbance of membrane physical properties. However, the possibility for perturbations of the membrane structure to occur upon a first contact of the peptide with the membrane surface, due to electrostatic interactions, should not be excluded. In this case, alterations of the lipid environment would be responsible for peptide conformational changes and its insertion into the lipid bilayer. The similar dependence on the presence of negative charges in model membranes observed for the S4(13)-PV_{wt} behavior regarding, on the one hand, its conformational preference and incorporation into the membrane (Mano et al. 2006; Mano et al. 2007), and on the other hand, its impact on the physical properties of the bilayer structure, strongly suggests a phenomenological correlation between these two types of events. An identical preference for interacting with anionic versus zwitterionic lipids, affecting the physical properties of the former in a larger extent than the latter, was demonstrated

for penetratin (Alves et al. 2009), an extensively studied CPP, which similarly to the S4(13)-PV_{wt} peptide adopts a helical structure upon interaction with anionic membranes (Alves et al. 2008). According to the same authors (Alves et al. 2009), the electrostatic interaction of the positive charges of penetratin with the anionic lipid headgroups might trigger peptide conformational changes, creating hydrophobic patches in its structure, which prompt the peptide to partially insert into the lipid bilayer.

From the analysis of the differential effects exerted by the wild-type peptide and its scrambled analogue on membranes containing exclusively an anionic lipid (DPPG) or prepared from a mixture of an anionic (POPG or DOPG) and a zwitterionic (DPPE or DOPE) lipid, new insights are gained to explain the mechanisms of cellular uptake for both peptides.

In the simplest model, we emphasize the capacity of the wild-type peptide, not shared by the scrambled analogue, to promote lateral phase separation. This effect denoted in DSC scans, associated to the appearance of an interdigitated phase ($L_{\beta I}$) coexisting with the gel phase characteristic of DPPG pure systems, as revealed by SAXS and WAXS patterns, reflects the capacity of the S4(13)-PV_{wt} peptide to induce heterogeneities in the lipid matrix of the membrane. As a consequence, defect lines and discontinuities in the boundary of adjacent lipid domains displaying different physical properties may favor peptide insertion into the bilayer and eventual translocation across the bilayer thickness. In contrast, the scrambled peptide, being less efficient in the creation of heterogeneities in the membrane, may have more limited capacity to be taken up by this process. The preferential peptide insertion into defect regions in the bilayer has been demonstrated by atomic force microscopy with an acylated peptide (Pedersen et al. 2005) and a mechanism of peptide membrane translocation involving phospholipid segregation has been proposed for penetratin (Lamazière et al. 2010).

Data obtained with the binary lipid systems, besides confirming the capacity of the S4(13)-PV_{wt} peptide to promote lipid domain segregation (**Figure 7.6**) also showed peptide capacity to induce non-lamellar phases (**Table 7.5**). The isotropic phase detected in the DOPG/DOPE (7:3) mixture at high temperatures has been reported by other authors (Morein et al. 2000) as corresponding to a cubic phase belonging to the

space group Pn3m, with characteristics (hysteretic phase behavior and optical transparency) pointing to a bicontinuous cubic structure. In fact, mixtures composed of a non-bilayer lipid (DOPE in the present case) and a bilayer stabilizer lipid (DOPG in the considered mixture) commonly form this type of structure. Studies with WALP model peptides (Lamazière et al. 2010) showed that the formation of the isotropic phase in this lipid system, which is by itself able to form this kind of structure at adequate temperature and water content, is afforded by very low peptide concentrations if an even slight hydrophobic mismatch occurs. This process to induce the lamellar to non-lamellar transition involving reduction of the bilayer rupture tension (Evans & Needham 1987) might be involved in the case of S4(13)-PV_{wt} peptide. Although the precise hydrophobic length of this peptide is not known, the detection of a $L_{\beta I}$ interdigitated phase in DPPG bilayers in the presence of high peptide/lipid ratios makes the hypothesis of hydrophobic mismatch a reasonable assumption. In fact, the interdigitated phase is commonly triggered to counteract the void volume created in the hydrophobic core of the bilayer as a consequence of the intercalation of molecules featuring a polar group and a short hydrophobic chain (for instance drugs such as ethanol), which does not extend along the full length of the fatty acid chains of phospholipids (Nambi et al. 1988). Therefore, the interdigitated phase is a solution in conditions where the acyl chains assume the extended (*all-trans*) conformation. However, at higher temperatures, the free space created in the core of the bilayer may induce a higher disorder in the acyl chains leading to an unbalance in the lateral pressure profile across the membrane thickness prone to the formation of non-lamellar phases.

Taking into account that non-lamellar phases have been extensively reported in the literature as being involved in destabilization of the bilayer, increase of membrane permeability and phenomena of membrane fusion and fission (Lewis et al. 1997), it will be easy to infer the impact of these structures, transiently formed in the membrane and at localized regions of the bilayer, on the entry of the S4(13)-PV peptides into the cell. The formation of a non-lamellar phase in DMPG liposomes and the induction of a negative lipid curvature in different lipid systems were also demonstrated in the presence of penetratin (Alves et al. 2008; Alves et al. 2009), supporting a mechanism proposed for its translocation (Derossi et al. 1998) which

involves inverted micelles entrapping the peptide, crossing the bilayer thickness and releasing it inside the cell.

The current study revealed that besides inducing a non-lamellar organization of lipids in membrane mimicking systems, the S4(13)-PV peptide can propagate and stabilize analogous lipid arrangements (quasi-hexagonal structures) in membranes of HeLa cells, as detected by transmission electron microscopy. In analogy with membrane-mimetic lipid systems, the quasi-hexagonal structures appeared in cell membranes at high peptide to lipid ratios, although not being the prevalent structure. To the best of our knowledge, the formation of non-lamellar structures in cellular membranes upon cell incubation with cell-penetrating peptides has not been reported yet. The inability of the scrambled analogue to promote such membrane alterations would consistently justify its incompetence for delivery. The distinct behavior between the S4(13)-PV wild-type peptide and its scrambled analogue corroborates previous ultrastructural studies (Padari et al. 2010) which showed that the S4(13)-PV_{wt} peptide assembled in small nanoparticle-like spherical structures upon interaction with the plasma membrane of HeLa cells, whereas the scrambled analogue gave rise to larger irregular aggregates. Although the formation of nanoparticle-regular structures seemed to firstly involve peptide association with the cell surface anionic glycosaminoglycans (GAG), it was observed that nanoparticles were formed even on the surface of a mutant cell line derived from CHO-K1 (pgs A-745), which lacks the capacity to synthesize proteoglycans, due to a deficiency in xylosyltransferase I, involved in GAG biosynthesis. Consistently, previous studies with this cell line and the corresponding wild type (CHO-K1) using flow cytometry and confocal microscopy (Mano et al. 2005) showed that the peptide concentration was determinant for the role played by proteoglycans in S4(13)-PV cellular internalization. Thus, while at low peptide concentrations (≤ 1μM) the cellular uptake was significantly decreased in cells lacking proteoglycans (pgs A-745), at higher concentrations (2.0 μM) peptide uptake by these cells was not significantly different from that observed in the wild-type cells. In the present work, the mechanisms underlying the successful cell internalization of the S4(13)-PV peptide, as opposed to the scrambled analogue, were investigated in conditions (high peptide concentrations) at which the peptide is taken up by an

energy-independent pathway and a GAG-non-requiring process, focusing in particular on the membrane lipid component and peptide effects on its mesomorphic behavior.

Considering the whole set of our results, describing the S4(13)-PV peptide interactions with lipid membranes in terms of the consequences for both the peptide and the lipid component, we propose that electrostatic interactions with negatively charged phospholipid headgroups should trigger two kinds of events: change in peptide conformation, adopting an amphipathic α-helix, and lateral separation of lipid domains with different physical properties, creating conditions for generating non-lamellar lipid phases. Non-bilayer phases could be favored by an eventual mismatch between the hydrophobic lipid matrix and the hydrophobic peptide length.

At the cell surface, the negative charges should be provided by proteoglycans or gangliosides, which with other lipids (saturated phospholipids and cholesterol) form specific domains in the plasma membrane (lipid rafts) of a liquid-ordered phase characterized by a high conformational order but relatively low constraints in molecular lateral diffusion. Lateral phase separation and rearrangement of lipid organization and distribution in the plane of the membrane, as a consequence of peptide-lipid interactions, are also predictable and peptide incorporation through defect zones in the interfacial boundaries of lipid domains will be easily achieved. Subsequent alterations of bilayer thickness, undulations and changes in membrane curvature may also occur and have been proposed to be involved in the translocation of other CPPs (Lamazière et al. 2010).

7.6 CONCLUSION

In conclusion, data obtained so far with S4(13)-PV peptides provide important details on the mechanism of action of these CPPs and may be useful for other amphipathic peptides. It should be emphasized that insights gained by the use of complementary biophysical techniques and transmission electron microscopy could be helpful for understanding the molecular mechanisms of membrane physical modulation by external agents, and can constitute a successful approach to clarify the specificity of biological responses triggered by apparently similar molecules. In terms of cell-penetrating peptides, it should be stressed that peptide interactions with the phospholipid matrix play a determinant role in the success of their pharmacological application and should be taken into account in the design of novel molecules.

Chapter 8

Comparison of the efficiency of complexes based on S4(13)-PV cell-penetrating peptides in plasmid DNA and siRNA delivery

A.M. Cardoso, S. Trabulo, A.L. Cardoso, S. Maia, P. Gomes, A.S. Jurado and M.C. Pedroso de Lima, "*Comparison of the efficiency of complexes based on S4(13)-PV cell-penetrating peptides in plasmid DNA and siRNA delivery*" Published in the Molecular Pharmaceutics, *10*, **2013**, 2653−2666.

8.1 ABSTRACT

The successful application of gene therapy approaches is highly dependent on the efficient delivery of nucleic acids into target cells. In the present study, new peptide-based non-viral systems were developed to enhance plasmid DNA and siRNA delivery, aiming at generating appropriate gene delivery and gene silencing tools for pre-clinical and clinical application. For this purpose, a new cell-penetrating peptide derived from the wild-type S4(13)-PV peptide was synthesized through the addition of a five-histidine tail to its *N*-terminus, H_5-S4(13)-PV, and its ability to mediate gene expression and gene silencing was evaluated and compared to that of the wild-type peptide. Plasmid delivery systems involving S4(13)-PV, H_5-S4(13)-PV or the combination of each of these peptides with cationic liposomes displayed different levels of transfection efficiency and cytotoxicity. The histidine-enriched peptide, H_5-S4(13)-PV, proved to be generally more efficient and less toxic than the wild-type peptide. In addition, complexes of H_5-S4(13)-PV with siRNAs, but not of S4(13)-PV, were efficiently internalized by cells and presented high knockdown activity. The association of cationic liposomes to binary complexes of S4(13)-PV with siRNAs enhanced silencing efficiency, although such enhancement was not enough to reach the efficiency levels observed in H_5-S4(13)-PV/siRNA complexes. For the latter complexes, the addition of cationic liposomes did not result in a further improvement of gene silencing. Interestingly, systems containing the S4(13)-PV or the H_5-S4(13)-PV peptide exhibited superior biological activity when compared to those containing the reverse NLS or scrambled peptides, suggesting that both the cell-penetrating sequence and the NLS of the S4(13)-PV peptide influence the competence of binary and ternary complexes to accomplish nucleic acid delivery. In order to unravel the cancer therapeutic potential of formulations with the histidine-enriched peptide, their efficiency to mediate silencing of the oncogenic protein survivin was evaluated. As opposed to complexes with the wild type peptide, H_5-S4(13)-PV complexes showed to be able to promote a high survivin knockdown at the level of both protein and mRNA, in HT1080 cells.

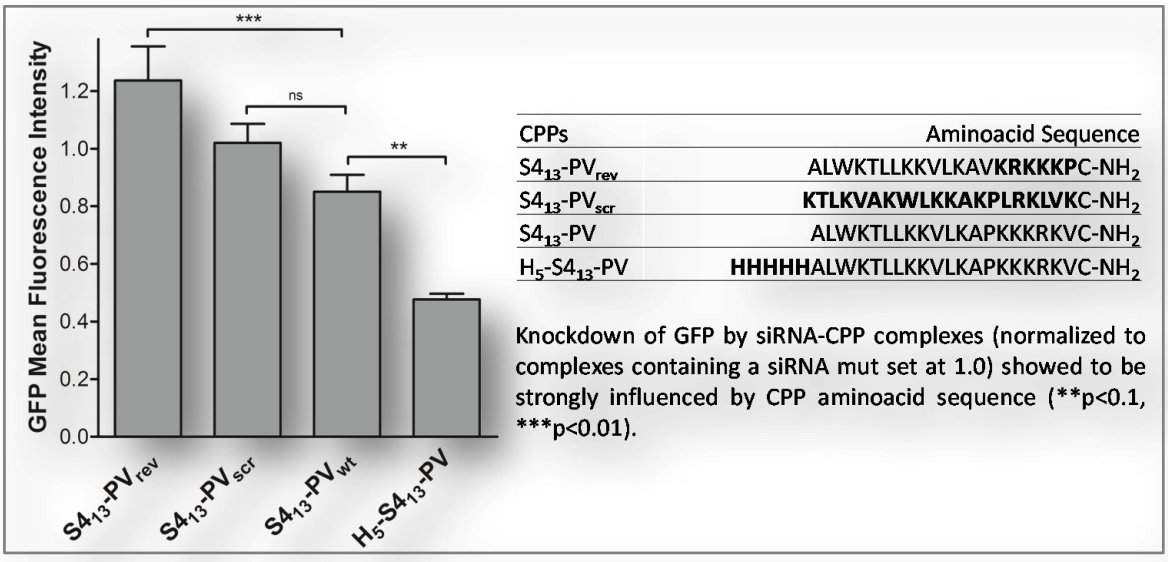

CPPs	Aminoacid Sequence
$S4_{13}$-PV_{rev}	ALWKTLLKKVLKAV**KRKKKP**C-NH_2
$S4_{13}$-PV_{scr}	**KTLKVAKWLKKAKPLRKLVK**C-NH_2
$S4_{13}$-PV	ALWKTLLKKVLKAPKKKRKVC-NH_2
H_5-$S4_{13}$-PV	**HHHHH**ALWKTLLKKVLKAPKKKRKVC-NH_2

Knockdown of GFP by siRNA-CPP complexes (normalized to complexes containing a siRNA mut set at 1.0) showed to be strongly influenced by CPP aminoacid sequence (**p<0.1, ***p<0.01).

8.2 INTRODUCTION

In order to improve the clinical efficacy of gene-based therapeutic strategies, a great deal of efforts has been expended on the discovery of potent therapeutic genes or gene-modulating molecules and on the enhancement of the efficiency of gene delivery systems. Viral and non-viral systems have been developed to mediate the delivery of plasmid DNA and siRNAs to target cells. However, gene therapy approaches that are both highly efficient and clinically viable are still scarce (Fonseca et al. 2009; de Fougerolles et al. 2007; Eguchi & Dowdy 2009). Cell-penetrating peptides (CPPs) have been extensively applied for nucleic acid delivery, using both covalent and non-covalent association strategies (Heitz et al. 2009). While the covalent linkage of CPPs to nucleic acids allows the formation of small, monomeric conjugates of known stoichiometry with high reproducibility, the preparation of non-covalent complexes is technically simpler, originates nanoparticles with a net positive charge, and decreases the risk of altering the biological activity of the cargo (Heitz et al. 2009; Meade & Dowdy 2008).

Many CPPs are derived from transduction domains of proteins, which are known for their remarkable properties of cell penetration, although model and designed CPPs have also been generated. Several modifications of natural occurring sequences have been introduced in CPPs in order to achieve higher transfection efficiencies mediated by CPP-based delivery systems. Among others, a new HIV-1 Tat peptide-based gene delivery system was designed by fusing the original Tat with histidine and cysteine residues (Lo & Wang 2008). The rationale behind these modifications was based on the features of these amino acids. The specific pKa of the histidine imidazole group, being close to the endosomal pH, allows protonation and leads to osmotic swelling, mimicking the proton-sponge effect observed with polyethyleneimine (PEI), thus facilitating nucleic acid release (Lo & Wang 2008; Midoux & Monsigny 1999). On the other hand, the cysteine residue disulfide interactions allow the stabilization and protection of the CPP-nucleic acid complexes in the extracellular medium, while their lability in the endosomal reducing environment contributes to nucleic acid release (Lo & Wang 2008).

Motivated by the improvements observed for the Tat peptide following these modifications, a similar approach was tested with the S4(13)-PV peptide, a

Dermaseptin derived peptide fused to the nuclear localization sequence of the SV40 large T antigen (Hariton-Gazal et al. 2002), which has been extensively studied in our laboratory. For this purpose, a S4(13)-PV analogue with a five-histidine tail at the *N*-terminus was synthesized, originating a new peptide called herein H_5-S4(13)-PV. Following our previous work on the development of S4(13)-PV peptide-based vectors for nucleic acid delivery (Trabulo et al. 2008; Trabulo et al. 2010a), and aiming at identifying the molecular features responsible for efficient nucleic acid delivery, the new peptide was here compared with the wild-type, S4(13)-PV, and its scrambled, S4(13)-PV_{scr}, and reverse NLS, S4(13)-PV_{rev}, analogues (**Table 8.1**), in terms of its ability to efficiently deliver plasmid DNA and siRNA to different cell lines. Ternary systems produced through the addition of dioleoyltrimethylammoniumpropane: dioleoylphosphatidylethanolamine (DOTAP:DOPE) liposomes to the CPP-nucleic acid complexes were also assayed, since previous work had revealed that the association of these vesicles with CPP complexes led to the formation of more efficient plasmid delivery systems (Trabulo et al. 2008).

Our results showed that the histidine tail preserves or improves the S4(13)-PV peptide ability to efficiently deliver reporter plasmid DNA and siRNAs to different cell lines. In order to test the efficiency of the new CPP-based delivery systems to silence endogenous genes, the survivin gene was selected as a target. Survivin is a member of the IAP family, playing an important role in cell proliferation and inhibition of apoptosis (Ryan et al. 2009; Mesri et al. 2001; Tamm et al. 1998; Li et al. 1998; Hoffman et al. 2002; Beltrami et al. 2004; Dohi et al. 2004; Li et al. 1999; Uchida et al. 2004; Liu et al. 2006). Due to its overexpression in cancer cells, while no expression or very low levels of expression are detected in normal cells, survivin constitutes a particularly promising target for cancer therapy. Moreover, survivin renders malignant cells resistant to conventional anti-tumoral treatments, by counteracting pro-apoptotic stimuli and, therefore, enhancing cancer cell survival (Ryan et al. 2009; Yonesaka et al. 2006; Kappler et al. 2005; Olie et al. 2000).

Altogether, the present findings open a new window to extend the use of CPPs, including the S4(13)-PV peptide and its histidine derivative, as appropriate tools for nucleic acid delivery, with potential for clinical applications in different pathologies, such as cancer.

8.3 MATERIALS AND METHODS

Materials

The cationic lipid 1,2-dioleoyl-3-trimethylammonium-propane (DOTAP) and 1,2-dioleoyl-*sn*-glycero-3-phosphoethanolamine (DOPE) were purchased from Avanti Polar Lipids (Alabaster, AL, USA). The primers for survivin and for HPRT-1 genes were pre-designed by Qiagen (QuantiTect Primer, Qiagen). The antibody anti-survivin was purchased from Santa Cruz (Santa Cruz Biotechnology, Inc., Heidelberg, Germany) and the remaining antibodies were obtained from Sigma (St. Louis, MO, USA). The anti-GFP siRNA (5'-GCAAGCUGACCCUGAAGUUCAU-3') and Cy3-labeled non-specific siRNA sequence were purchased from Ambion (Austin, TX, USA). The anti-survivin siRNA (5'-GGACCACCGCAUCUCUACAdTdT-3') and the non-silencing siRNA used as control were obtained from Dharmacon (Lafayette, CO, USA). Fmoc-protected amino acids, Fmoc-Rink Amide-MBHA LL resin (0.36 mmol/g) and coupling reagent *O*-(benzotriazol-1-yl)-*N,N,N',N'*-tetramethyluronium-hexaflurophosphate (HBTU) were provided by Novabiochem (VWR International, Portugal). All the other chemicals were of the highest grade.

Peptide synthesis

Peptide synthesis was performed using a Liberty Microwave Peptide Synthesizer (CEM Corporation, Mathews, NC, USA). Peptide analysis by HPLC was done using a Hitachi-Merck LaChrom Elite system equipped with a quaternary pump, a thermostatted (Peltier effect) automated sampler and a diode-array detector (DAD). An LCQ-DecaXP LC-MS system from ThermoFinnigan, equipped with both a DAD detector and an electrospray ionization-ion trap mass spectrometer (ESI/IT MS), was also used for peptide analysis. Peptide quantitation was performed by measuring the absorbance at 280 nm in a spectrophotometer Helios Gama (Spectronic Unicam).

The peptide (*C*-terminal amide) was assembled by Fmoc/tBu solid-phase peptide synthesis (SPPS) methodologies assisted with microwave (MW) energy (Collins & Leadbeater 2007). The resin was pre-conditioned for 15 min in *N,N*-dimethylformamide (DMF) and then transferred into the MW-reaction vessel. The

initial Fmoc deprotection step was carried out using 20% piperidine in DMF containing 0.1 M of 1-hydroxybenzotriazole (HOBt) in two MW irradiation pulses: 30 sec at 24 W plus 3 min at 28 W, in both cases temperature being no higher than 75 °C. The *C*-terminal amino acid was then coupled to the deprotected Rink amide resin, using 5 molar equivalents (eq) of the Fmoc-protected amino acid in DMF (0.2 M), 5 eq of 0.5 M HBTU/HOBt in DMF and 10 eq of 2 M *N*-ethyl-*N,N*-diisopropylamine (DIPEA) in *N*-methylpyrrolidone (NMP); the coupling step was carried out for 5 min at 35 W MW irradiation, with maximum temperature reaching 75 °C. The remaining amino acids were sequentially coupled in the C→N direction by means of similar deprotection and coupling cycles, except for incorporation of: (i) Fmoc-Arg(Pbf)-OH, whose coupling was done in two steps, 25 min with no MW irradiation (room temperature) followed by 5 min coupling at 25 W; (ii) Fmoc-Cys(Trt)-OH, Fmoc-Trp(Boc)-OH and Fmoc-His(Trt)-OH, all coupled also in two steps, firstly with 2 min coupling without MW irradiation (room temperature), then followed by 4 min coupling at 25 W, with maximum temperature reaching 50 °C. Double-coupling was employed to all lysines in the sequence (residues 5, 6, 7, 10 and 14), incorporated as Fmoc-Lys(Boc)-OH. Following completion of sequence assembly, the peptide was released from the resin with concomitant removal of side-chain protecting groups, by a 3 h-acidolysis at room temperature using a trifluoroacetic acid (TFA)-based cocktail (Fields & Noble 1990; Carpino et al. 2003) containing thioanisole, 1,2-ethanedithiol and anisole as scavengers (TFA/thioanisole/1,2-ethanedithiol/anisole 90:5:3:2 v/v/v/v). Crude product was purified by reverse-phase liquid chromatography to give the target peptide, as confirmed by HPLC, LC-ESI/IT MS and aminoacid analysis.

Table 8.1 Sequences of the S4(13)-PV and derived peptides used in the present study.

S4(13)-PV	ALWKTLLKKVLKAPKKKRKVC-NH_2
H_5-S4(13)-PV	HHHHHALWKTLLKKVLKAPKKKRKVC-NH_2
S4(13)-PV_{scr}	KTLKVAKWLKKAKPLRKLVKC-NH_2
S4(13)-PV_{rev}	ALWKTLLKKVLKAVKRKKKPC-NH_2

Cells

HeLa cells (human epithelial cervical carcinoma) and A549 cells (human epithelial lung adenocarcinoma) were maintained at 37 °C, under 5% CO_2, in Dulbecco Modified Eagle medium-high glucose (DMEM; Sigma) supplemented with 10% (v/v) heat-inactivated fetal bovine serum (FBS; Biochrom KG) and 100 units penicillin and 100 μg streptomycin (Sigma) per ml. HT1080 cells (human fibrosarcoma) were maintained at 37 °C, under 5% CO_2, in Dulbecco Modified Eagle low glucose (DMEM-LG; Sigma) supplemented with 10% (v/v) heat-inactivated fetal bovine serum (FBS; Biochrom KG) and 100 units penicillin and 100 μg streptomycin (Sigma) per mL.

For flow cytometry and cell viability experiments, 1.0×10^5 HeLa, A549 or HT1080 cells/well were seeded onto 12-well plates; for fluorescence microscopy studies, 0.2×10^5 HT1080 cells/well were plated onto 8-well chambered coverslips (Lab-Tek™ II Chamber Slide™ System Nunc™). For QRT-PCR and Western blot experiments, 1.0×10^5 HeLa, A549 and HT1080 cells/well were plated onto 6-well plates. Cells were plated twenty-four hours prior to incubation with the complexes.

Cationic liposome preparation

Small unilamellar vesicles (SUV) were prepared by extrusion of multilamellar vesicles composed of the cationic lipid DOTAP and DOPE at a 1:2 molar ratio. Briefly, lipid solutions in chloroform were mixed at the desired molar ratio, and dried under vacuum, at room temperature, using a rotary evaporator. The dried lipid films were then hydrated with 1.0 ml high purity water, and the obtained multilamellar vesicles were briefly sonicated and extruded 21 times through two stacked polycarbonate filters (50 nm pore diameter) using a Liposofast device (Avestin). The lipid concentration of the resulting SUV was determined by the Bartlett method (Bartlett 1958), which measures the inorganic phosphate released after the hydrolysis of dried phospholipids, at 180 °C, in 70% $HClO_4$ (Bottcher et al. 1961).

Complex preparation

The complexes (binary and ternary) were prepared in HEPES-buffered saline solution (HBS; 140 mM NaCl, 10 mM HEPES, pH 7.4). Binary complexes were produced by gently mixing the plasmid DNA or the siRNA with each of the CPPs, at the desired

charge ratio, followed by 15 min (plasmid DNA complexes) or 30 min (siRNA complexes) incubation at room temperature. Ternary plasmid DNA complexes were obtained by gently mixing peptide/pDNA complexes, prepared at the desired charge ratio, with DOTAP:DOPE liposomes. Mixtures were then incubated for 15 min, at room temperature. SiRNA formulations containing both CPP and cationic liposomes were prepared following two different protocols, which involved the addition of each CPP to the siRNAs, followed by the addition of the cationic liposomes (termed herein CPP/siRNA/DOTAP:DOPE complexes), or the mixing of the CPPs with the cationic liposomes, before the addition of the siRNAs (termed herein CPP/DOTAP:DOPE/siRNA complexes). After the addition of each component, the mixtures were gently mixed and incubated for 30 min at room temperature to allow formation of the complexes exhibiting the desired charge ratios.

Cell transfection

Twenty-four hours after plating, cells were incubated in antibiotic- and serum-free OptiMEM (Invitrogen, CA, USA) with the complexes (binary and ternary) containing plasmid DNA (1 μg/mL) or siRNA (50 nM), for 4 h at 37 °C. After this incubation period, the transfection medium was replaced with fresh medium containing 10% (v/v) FBS plus antibiotics, and the cells were further incubated for 44 h to allow gene expression/silencing. The efficiency of transfection and knockdown mediated by the different complexes was evaluated by analyzing GFP expression by flow cytometry, as described below.

Analysis of GFP expression by flow cytometry

Flow cytometry analysis of GFP expression was performed in live cells using a Becton Dickinson FACSCalibur flow cytometer (BD Biosciences, San Jose, CA, USA). Data were obtained and analyzed using CellQuest software. Forty-eight hours after transfection, the cells (HeLa, A549 or HT1080) were washed once with PBS and detached with trypsin (10 min at 37 °C). The cells were then further washed, resuspended in cold PBS and immediately analysed. To discriminate between viable and dead cells and to exclude doublets, cells were appropriately gated by forward/side scatter and pulse width from a total of 10,000 events. The FITC bandpass filter was used in emission

detection. GFP expression was evaluated through the analysis of the percentage of transfected cells and of the geometric mean fluorescence intensity with respect to control cells (non-transfected cells). GFP silencing was evaluated through the analysis of the fluorescence intensity with respect to cells treated with siRNA mut (scrambled sequence) complexes.

Analysis of siRNA internalization and intracellular distribution by confocal microscopy

HT1080 cells (0.2×10^5 cells/well) were plated onto 8-well chambered coverslips. Following overnight culture, the cells were treated for 4 h with the different delivery systems, formulated with Cy3-labelled siRNAs (50 nM), in OptiMEM medium. After this period, or following further 20 h incubation in serum-containing medium, cells were rinsed twice with PBS and incubated with Hoechst 33342 dye (1 µg/mL, Molecular Probes, Eugene, OR). Cells were then rinsed twice with PBS and directly observed in the chambers in 0.5 mL of OptiMEM. Fluorescence distribution inside live cells was analyzed under a Zeiss Axiovert 200 M fluorescence microscope (Carl Zeiss, Oberk), using the 60 × oil immersion objective.

Extraction of RNA and cDNA synthesis

RNA was recovered from A549, HeLa and HT1080 cells, 48 h after cell transfection, using the MasterPure™ RNA Purification Kit (Epicentre® Biotechnologies, Madison, WI, USA), according to the manufacturer's instructions, and then treated with DNase I. Briefly, cells were lysed using the Tissue and Cell Lysis Solution from the MasterPure™ RNA Purification Kit containing Proteinase K, and cell lysates were collected to microcentrifuge tubes. MPC Protein Precipitation Reagent was added to protein extract from the lysates. Then, 500 µL of isopropanol were added to the recovered supernatant to promote total nucleic acid precipitation, which was pelleted by centrifugation. Removal of contaminating DNA from the RNA was then performed by addition of a DNase I solution and carrying out another step of protein removal using MPC Protein Precipitation Reagent. RNA was finally pelleted by centrifugation, rinsed twice with 70% ethanol, and resuspended in TE buffer. After quantification, RNA was converted to cDNA using the Superscript III First Strand Synthesis Kit (Invitrogen, Karlsruhe, Germany), according to the manufacturer's instructions.

Quantitative real time polymerase chain reaction (QRT-PCR)

Quantitative PCR was performed in an iQ 5 thermocycler using 96-well microtitre plates and the iQ SYBR Green Supermix Kit, as described before (Cardoso et al. 2008). The primers for the target gene (survivin) and the reference gene (HPRT-1) were pre-designed by Qiagen (QuantiTect Primer, Qiagen). Survivin mRNA fold decrease with respect to control samples was determined by the Pfaffl method (Cardoso et al. 2012), taking into consideration the different amplification efficiencies of both genes in all experiments. The amplification efficiency for each target or reference gene was determined according to the equation: $E = 10^{-1/S}-1$, where S is the slope of the obtained standard curve.

Western blot analysis

Seventy-two hours after transfection of cells (HeLa, A549 or HT1080 cells) with the siRNA complexes, total protein extracts were obtained using a lysis buffer (50 mM NaCl, 50 mM EDTA, 1% Triton X-100) supplemented with a protease inhibitor cocktail (Sigma), 10 µg/mL DTT and 1 mM PMSF. Protein content was determined using the Bio-Rad DC protein assay (Bio-Rad). For each sample, 20 µg of total protein was resuspended in loading buffer (20% glycerol, 10% SDS, 0.1% bromophenol blue), incubated for 5 min at 95 °C and loaded onto a 15% polyacrylamide gel. After electrophoresis, the proteins were blotted onto a PVDF membrane according to standard protocols. After blocking in 5% non-fat milk, the membrane was incubated overnight at 4 °C with the appropriate primary antibody (anti-survivin 1:200, Santa-Cruz), and thereafter with the appropriate secondary antibody (1:10,000, Sigma) for 2 h at room temperature. Equal protein loading was shown by reprobing the membrane with an anti-α-tubulin antibody (1:10,000, Sigma) and with the appropriate secondary antibody. After this incubation period, the membrane was washed several times with saline buffer (TBS/T containing 25 mM Tris–HCl, 150 mM NaCl, 0.1% Tween and 5 mg/mL non-fat powder milk), incubated with ECF (alkaline phosphatase substrate; 20 µL of ECF/cm^2 of membrane) for 5 min at room temperature and submitted to fluorescence detection at 570 nm using a VersaDoc Imaging System Model 3000 (Bio-Rad). For each membrane, the analysis of band

intensity was performed using the Image J software (Wayne Rasband National Institutes of Health, USA).

Evaluation of cell viability

Cell viability was assessed under the different experimental conditions by a modified Alamar Blue assay, as described previously (Simões et al. 1999). Briefly, 48 h (for flow cytometry and QRT-PCR analysis) or 72 h (for Western blot analysis) after transfection, the cells were incubated with DMEM (HeLa and A549 cells) or DMEM-LG (HT1080 cells) containing 10% (v/v) resazurin dye. After 1 h of incubation at 37 °C, the absorbance of the medium was measured at 570 nm and 600 nm. Cell viability was calculated as a percentage of control cells (non-transfected cells), according to the equation:

$$\text{Cell viability (\% of control)} = [(A_{570}-A_{600})/(A'_{570}-A'_{600})] \times 100$$

where A_{570} and A_{600} are the absorbances of the samples, and A'_{570} and A'_{600} are the absorbances of control cells, at the indicated wavelengths.

8.4 RESULTS

8.4.1 PLASMID DNA DELIVERY MEDIATED BY S4(13)-PV- AND H_5-S4(13)-PV-BASED VECTORS

In order to comparatively evaluate the biological activity of the S4(13)-PV peptide, previously used as a component in plasmid DNA delivery systems (Trabulo et al. 2008), and that of a new histidine-enriched derivative (H_5-S4(13)-PV), transfection and cell viability experiments were performed in two tumoral cell lines (HeLa and A549). Complexes of each peptide with a plasmid DNA encoding the GFP gene were prepared, either *per se* or in combination with DOTAP:DOPE (1:2 molar ratio) liposomes, using the order of component addition that was previously shown to originate complexes with the highest transfection ability (Trabulo et al. 2012).

The ability of peptide-based binary complexes, S4(13)-PV/pDNA or H_5-S4(13)-PV/pDNA, and ternary complexes, S4(13)-PV/pDNA/DOTAP:DOPE or H_5-S4(13)-PV/pDNA/DOTAP:DOPE, as well as of DOTAP:DOPE/pDNA and Lipofectamine/pDNA lipoplexes (used as positive controls) to transfect HeLa and A549 cells was assessed by flow cytometry analysis. **Figure 8.1** presents the percentage of transfected cells (**A** and **C**) and the mean GFP fluorescence intensity (**B**) obtained with CPP-based complexes in both cells lines. Regarding HeLa cells, a highly transfectable cell line, the highest number of transfected cells was achieved with the binary (80.1%) and ternary (77.7%) complexes containing the wild-type CPP, prepared at 10/1 and 10/1/1 (+/-) charge ratios, respectively. Both values were higher than that obtained with Lipofectamine™ 2000 (74.0% of transfected cells). As observed, the H_5-S4(13)-PV peptide, although unable to efficiently deliver plasmid DNA to HeLa cells when formulated in a binary complex (achieving only approximately 11% of transfected cells), was able to transfect a considerable number of cells (approximately 60%) when present in ternary complexes at 5/1/1 and 10/1/1 peptide/pDNA/lipid charge ratios. Regarding the mean fluorescence intensity, which represents the average amount of DNA copies delivered to each cell, the results indicated that the binary complexes containing the S4(13)-PV or H_5-S4(13)-PV peptide delivered a low amount of plasmid copies per cell (**Figure 8.1B**). On the other hand, ternary complexes containing the H_5-S4(13)-PV peptide, prepared

at the 5/1/1 and 10/1/1 charge ratios, delivered a higher number of plasmid copies (reflected by a 8-11 fold fluorescence increase relative to the non-treated control cells) than the same formulations containing the wild-type CPP (3-4 fold increase relative to the non-treated control cells). These results indicate that the delivery ability of the complexes was increased upon addition of DOTAP:DOPE (2:1 molar ratio) liposomes, this increase being significantly more pronounced in H_5-S4(13)-PV/pDNA formulations than in S4(13)-PV/pDNA formulations.

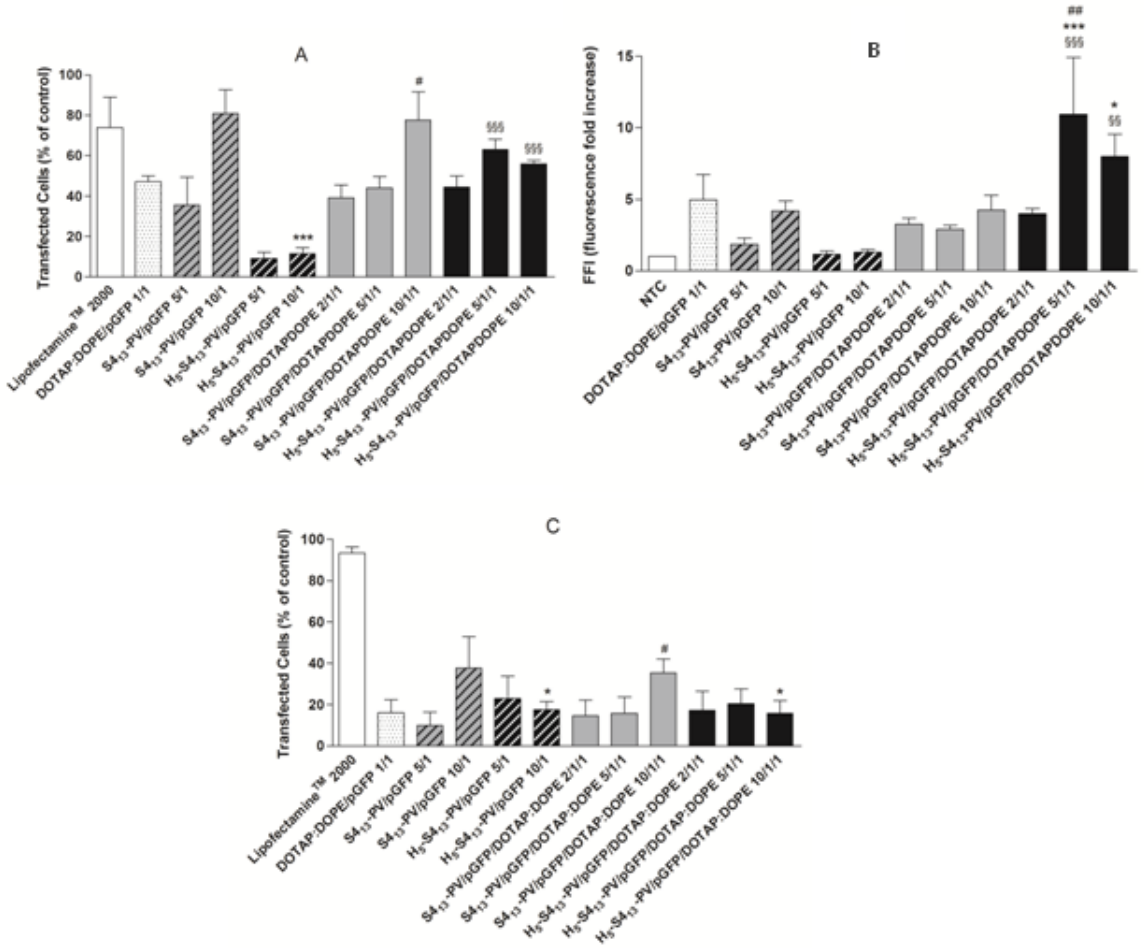

Figure 8.1 Transfection efficiency mediated by different CPP-based systems in HeLa (A and B) and A549 (C) cells. Cells were incubated with the different complexes containing 1 μg/ml of GFP-encoding plasmid DNA for 4 h at 37 ºC, as described in Materials and Methods. Flow cytometry analysis of live cells was performed 48 h after transfection to determine the percentage of transfected cells (A and C) and the increase in cell green fluorescence (B) with respect to control, non-treated cells (NTC). Complexes of DNA with DOTAP:DOPE liposomes or LipofectamineTM 2000 were used for comparison. All results are presented as mean ± SD of at least three independent experiments. Data comparisons were performed between formulations containing S4(13)-PV and H_5-S4(13)-PV (*$p < 0.05$, ***$p < 0.001$), between DOTAP:DOPE/pDNA lipoplexes and the same lipoplexes containing S4(13)-PV or H_5-S4(13)-PV ($^{\#}p < 0.05$, $^{\#\#}p < 0.01$) and between S4(13)-PV/pDNA or H_5-S4(13)-PV/pDNA and the corresponding ternary complexes containing DOTAP:DOPE ($^{\S\S}p < 0.01$, $^{\S\S\S}p < 0.001$).

Concerning A549 cells, S4(13)-PV peptide-containing binary and ternary complexes were able to transfect a considerable number of cells, only surpassed by Lipofectamine™ 2000 (**Figure 8.1C**). H_5-S4(13)-PV-based plasmid vectors, at the different charge ratios assayed, showed similar or lower transfection efficiencies as compared to the corresponding S4(13)-PV/pDNA complexes. For the transfection of these cells, both S4(13)-PV- and H_5-S4(13)-PV-based formulations did not benefit from the addition of the lipid component. The fluorescence fold increase relative to the non-treated control cells showed values lower than 1.6 for all tested conditions, being only significant for the binary complexes composed of the histidine-enriched CPP at the 10/1 charge ratio (data not shown).

The viability of A549 and HeLa cells (**Figure 8.2**) was determined following exposure to the formulations assayed for transfection, as described in Materials and Methods. HeLa cells (**Figure 8.2A**) showed to be more susceptible to complex-mediated cytotoxicity than A549 cells (**Figure 2B**), particularly at the highest peptide/DNA (+/-) charge ratios. The tested formulations did not significantly affect the viability of A549 cells (**Figure 8.2B**), especially when compared to that of the commercially available transfection reagent Lipofectamine™ 2000. In HeLa cells, the wild-type CPP, S4(13)-PV, showed to be more toxic than its histidine derivative, when formulated both in binary and ternary complexes. This cytotoxic effect was mostly significant for the formulations with high peptide amounts, i.e. CPP/pDNA at a 10/1 charge ratio and CPP/pDNA/DOTAP:DOPE at a 10/1/1 charge ratio. In these cases, the cell viability in the presence of complexes containing the wild-type peptide was about 30% of that observed in the presence of complexes prepared with the new histidine-enriched peptide, although the former complexes were more efficient in transfecting HeLa cells (**Figure 8.1A**) than the corresponding complexes prepared with H_5-S4(13)-PV peptide.

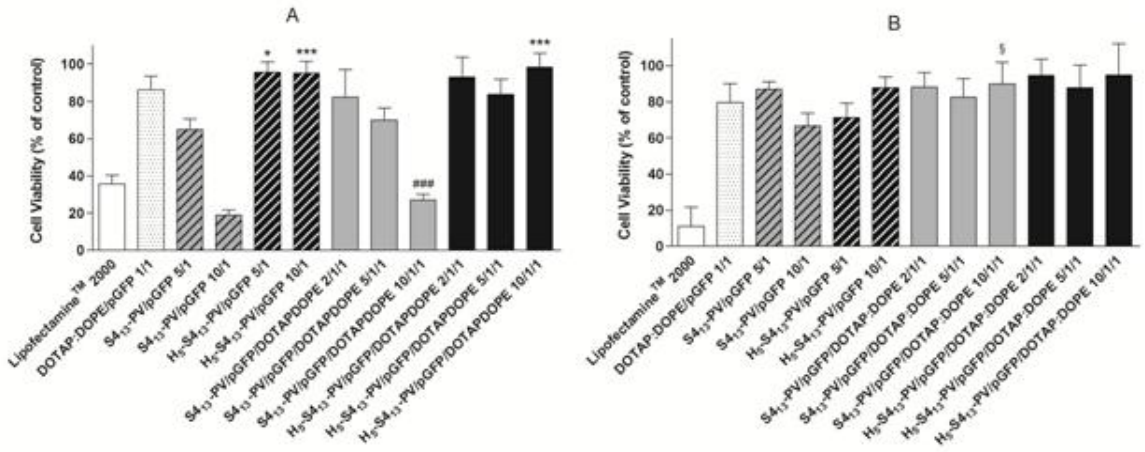

Figure 8.2 Cell viability in the presence of different CPP-based gene delivery systems. HeLa (A) and A549 (B) cells were incubated with the different complexes containing 1 μg/ml of GFP-encoding plasmid DNA for 4 h, following additional 44 h of incubation with complete medium. After this period, cell viability was determined by a modified Alamar Blue assay as described in Materials and Methods. Complexes of DNA with DOTAP:DOPE and with Lipofectamine™ 2000 were used for comparison. Cell viability is expressed as percentage of the control (non-transfected cells). All results are presented as mean ± SD of at least three independent experiments. Data comparisons were performed between formulations containing S4(13)-PV and H_5-S4(13)-PV (*$p < 0.05$, ***$p < 0.001$), between DOTAP:DOPE/pDNA lipoplexes and the same lipoplexes containing S4(13)-PV or H_5-S4(13)-PV (###$p < 0.001$) and between S4(13)-PV/pDNA or H_5-S4(13)-PV/pDNA and the corresponding ternary complexes containing DOTAP:DOPE (§$p < 0.05$).

8.4.2 SiRNA DELIVERY MEDIATED BY S4(13)-PV- AND H_5-S4(13)-PV-BASED VECTORS

In order to select the peptides owing the most suitable features to be used in a gene silencing approach, the cytotoxic effects of siRNA delivery systems generated by complexation of the S4(13)-PV peptide or one of its derivatives, H_5-S4(13)-PV, reverse NLS and scrambled, with a siRNA targeting GFP were evaluated in HT1080 GFP expressing cells (**Figure 8.3**).

Significant differences were observed in the cytotoxicity levels induced by binary complexes prepared with the different peptides. The formulations containing S4(13)-PV or its histidine analogue displayed no relevant toxicity (89% and 100% cell viability, respectively). However, cell viability decreased to 61.9% and 5.3% in the presence of complexes containing the scrambled, S4(13)-PV_{scr}, and the reverse NLS, S4(13)-PV_{rev}, peptides, respectively. Therefore, these complexes were discarded for the experiments of gene silencing and only the binary complexes that presented low toxicity profiles were evaluated concerning their ability to deliver siRNA (using confocal microscopy) and to induce GFP silencing (using flow cytometry) in HT1080 cells.

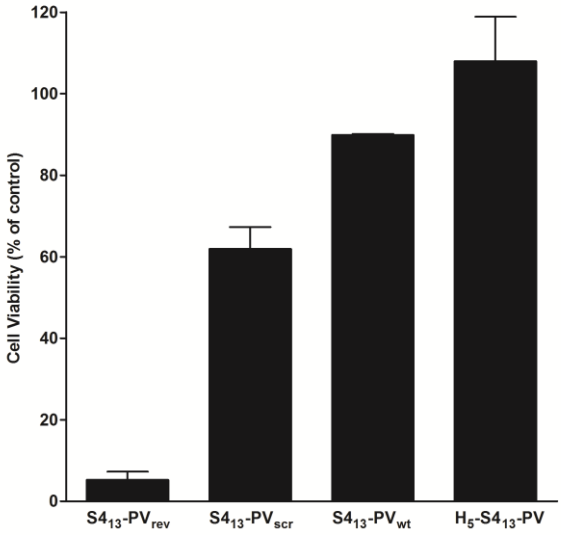

Figure 8.3 Cell viability in the presence of S4(13)-PV, S4(13)-PV$_{scr}$, S4(13)-PV$_{rev}$ and H$_5$-S4(13)-PV peptide-based complexes at a peptide/siRNA charge ratio of 3/2. HT1080 cells were incubated with the different complexes containing 50 nM of anti-GFP siRNA and, after 4 h incubation, the medium was replaced and the cells were further incubated for 44 h before analysis of cell viability by a modified Alamar Blue assay, as described in Materials and Methods. All results are presented as mean ± SD of at least three independent experiments.

Figure 8.4 displays the internalization pattern of Cy-3-labelled siRNAs delivered to HT1080 cells through complexation with S4(13)-PV or H$_5$-S4(13)-PV, after 4 (**A-C**) or 24 (**D-F**) hours of incubation. Representative flow cytometry histograms (**G-I**) reflecting GFP silencing upon transfection with the same complexes are presented in parallel. **Figure 8.4J** summarizes the silencing efficiency of the binary formulations prepared with each of the four studied peptides, at the 3/2 (+/-) charge ratio, as assessed by flow cytometry.

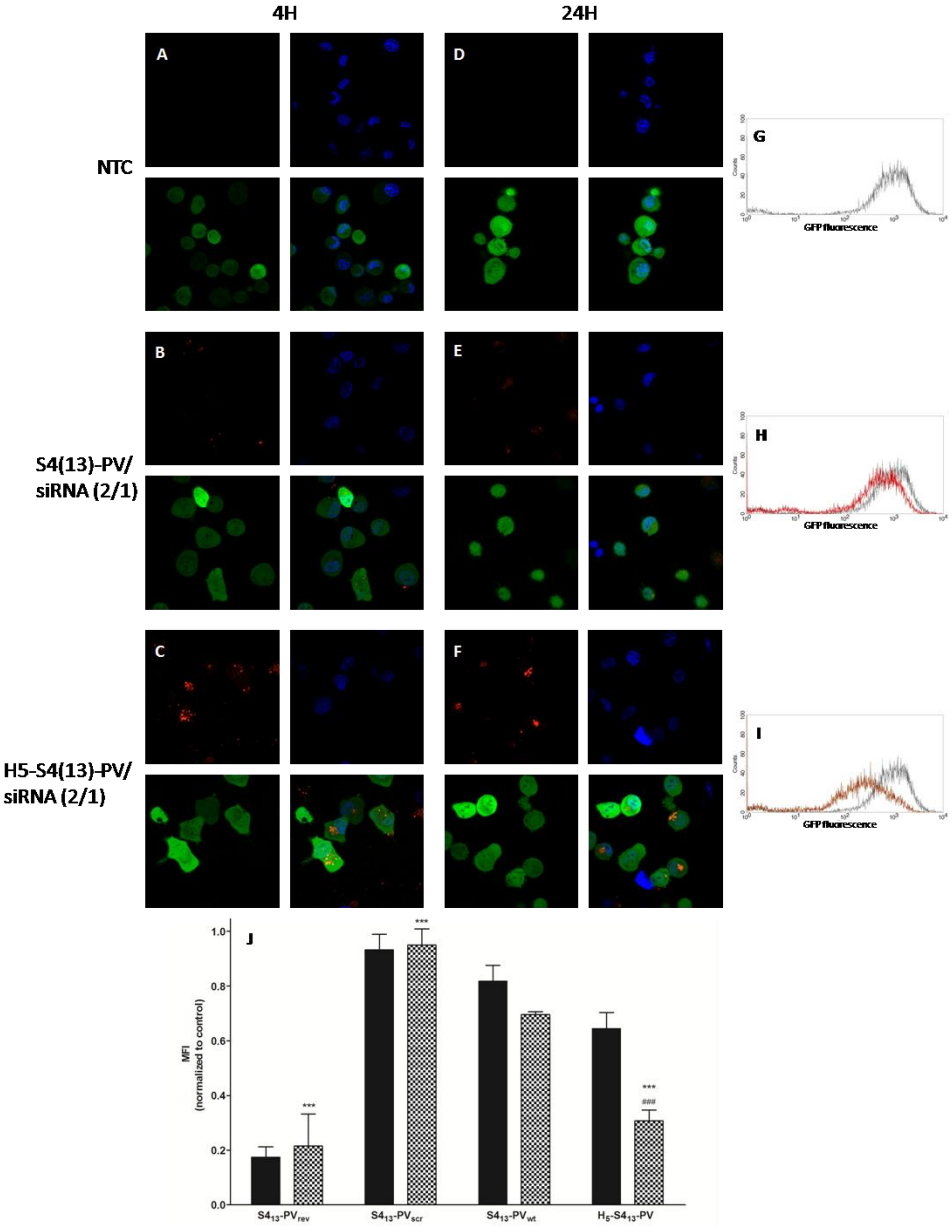

Figure 8.4 SiRNA internalization (A-F) and gene silencing efficiency (G-J) evaluated *in vitro* with different CPP-based systems. For cellular internalization experiments, HT1080 cells (green) were incubated with S4(13)-PV- or H_5-S4(13)-PV-based complexes containing 50 nM of mut Cy3-labelled siRNA (red) at the 3/2 charge ratio. Cell nuclei were labeled with Hoechst 33342 dye (blue). Representative confocal microscopy images of each experimental condition (630 ×), taken upon 4 (A-C) and 24 h (D-F) cell incubation, are presented. Representative histograms of GFP knockdown obtained by flow cytometry for the same formulations at 48 h post-transfection are also presented (G-I). Results for non-transfected cells (NTC) are shown as a control. GFP knockdown mediated by S4(13)-PV, S4(13)-PV_{scr}, S4(13)-PV_{rev} or H_5-S4(13)-PV peptide-based complexes at a peptide/siRNA charge ratio of 3/2 was quantified (J). HT1080 cells were incubated with the different complexes containing 50 nM of mut siRNA (■) or anti-GFP siRNA (■). After 4 h incubation, the medium was replaced and the cells were further incubated for 44 h before flow cytometry analysis. Data presented in (J) are mean ± SD of at least three independent experiments. Pairwise comparisons were performed between formulations containing the anti-GFP siRNA and those containing the mut siRNA ($^{###}p < 0.001$) and between S4(13)-PVscr, S4(13)-PVrev or H_5-S4(13)-PV formulations containing the anti-GFP siRNA and the S4(13)-PV formulation containing the same siRNA ($^{***}p < 0.001$). Results for non-treated cells (NTC) were used as a control.

Confocal studies revealed that siRNA internalization occurred at a similar extent for complexes containing the S4(13)-PV peptide and for those containing Lipofectamine™ 2000 (data not shown), although a more uniform distribution pattern could be observed when the delivery system included the CPP. However, the superior efficiency of S4(13)-PV binary complexes to mediate siRNA intracellular delivery was not accompanied by an improved GFP knockdown (**Figure 8.4H**). In fact, only low levels of biological activity were detected for siRNA/S4(13)-PV complexes. In contrast, the histidine-derivative peptide (H_5-S4(13)-PV) was able to promote efficient intracellular siRNA delivery (**Figure 4C, F**), while simultaneously mediating significant GFP knockdown (**Figure 4I**). Complexes formulated with this peptide promoted a 69% reduction of GFP levels, while the other peptides did not induce significant silencing or (in the case of S4(13)-PV) induced a non-specific silencing (**Figure 8.4J**).

Following the same strategy previously employed to improve S4(13)-PV-mediated pDNA (Trabulo et al. 2008) and oligonucleotide (Trabulo et al. 2010a) delivery, DOTAP:DOPE (1:2 molar ratio) liposomes were added to the formulations containing S4(13)-PV peptide and siRNA, in an attempt to enhance the RNA interference activity of these peptides. Parallel experiments were performed with both the scrambled and reverse NLS peptides in order to determine whether the sequence and structure of this CPP would be involved in the gene silencing activity of the complexes. All possible orders of addition of the components of the ternary complexes were tested, aiming at clarifying the importance of the siRNA "wrapping" by the CPP or by the liposomes to the biological activity of the CPP formulations. **Figure 8.5** (panels **A** and **B**) shows typical results obtained for GFP knockdown mediated by the different generated systems. As observed, the differences found in GFP expression when comparing equivalent systems, containing either anti-GFP siRNAs or mut siRNAs, were only significant for DOTAP:DOPE/siRNA and S4(13)-PV-containing systems (**Figure 8.5A** and **B**). It is also possible to note that the protocol of preparation of the ternary complexes did not play a crucial role in gene silencing efficiency. In fact, either the addition of cationic liposomes to pre-formed CPP/siRNA complexes (**Figure 8.5A**) or the addition of siRNAs to a mixture of cationic liposomes and CPPs (**Figure 8.5B**) resulted in the formation of efficient systems, with the latter strategy being only

slightly superior. Although a third protocol involving the addition of CPPs to pre-formed complexes of cationic liposome/siRNA was found to be less efficient (data not shown), the resulting ternary complexes still exhibited considerable biological activity.

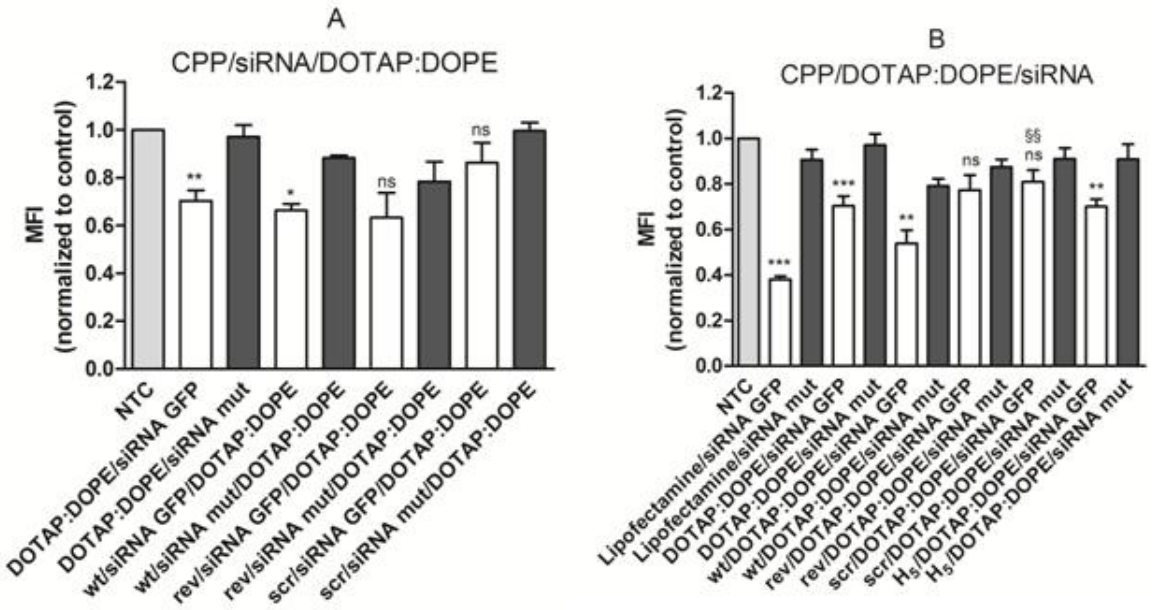

Figure 8.5 GFP knockdown mediated by siRNA complexes prepared with S4(13)-PV (wt), S4(13)-PV_{scr} (scr), S4(13)-PV_{rev} (rev) or H_5-S4(13)-PV (H_5) and DOTAP:DOPE liposomes at the peptide/lipid/siRNA 4/1/1.5 charge ratio, using two different protocols: addition of cationic liposomes to the pre-formed CPP/siRNA complexes (A) or addition of siRNAs to a mixture of cationic liposomes and CPPs (B). HT1080 cells were incubated with the different complexes containing 50 nM of anti-GFP siRNA for 4 h at 37 ºC. Parallel experiments were performed using mut siRNAs. Forty-eight hours post-transfection, the efficiency of GFP knockdown mediated by the different complexes was evaluated by flow cytometry analysis of GFP expression. All results are presented as mean ± SD of at least three independent experiments. Pairwise comparisons were performed between formulations containing the anti-GFP siRNA and the mut siRNA (*$p < 0.05$, **$p < 0.01$, ***$p < 0.001$), between the DOTAP:DOPE/anti-GFP siRNA formulation and equivalent formulations containing S4(13)-PV, S4(13)-PV_{scr}, S4(13)-PV_{rev} or H_5-S4(13)-PV ($^{\#\#}p < 0.01$), and between the Lipofectamine/anti-GFP siRNA formulation and equivalent formulations containing S4(13)-PV, S4(13)-PV_{scr}, S4(13)-PV_{rev} or H_5-S4(13)-PV ($^{\S\S}p < 0.01$). Results for non-treated cells (NTC) are shown as a control.

When comparing the various CPP-based systems, generated by addition of siRNAs to a mixture of cationic liposomes and the peptide (**Figure 8.5B**), the formulation containing the S4(13)-PV peptide was found to be the most efficient to mediate GFP knockdown. Remarkably, this system was not only significantly more efficient than DOTAP:DOPE/siRNA complexes, but also greatly superior to equivalent systems prepared with the reverse NLS, scrambled or H_5-S4(13)-PV peptides. It should be noted that no significant GFP knockdown was observed for H_5-S4(13)-PV ternary complexes containing mut siRNAs.

8.4.3 Survivin silencing in different human cancer cell lines mediated by S4(13)-PV- and H_5-S4(13)-PV-based vectors

Following the demonstration of the feasibility of CPP-based delivery systems to mediate GFP knockdown in HT1080 cells, the next step consisted of employing the developed S4(13)-PV and H_5-S4(13)-PV delivery systems to silence the endogenous gene survivin using different human tumor cell lines towards their potential application in a target gene therapy to cancer. In this context, survivin mRNA and protein levels were determined by QRT-PCR and Western blot, respectively, following the delivery of anti-survivin siRNAs by binary and ternary complexes containing S4(13)-PV or H_5-S4(13)-PV.

Figure 8.6 presents survivin mRNA levels 48 h upon cell transfection with binary complexes, composed of peptide and siRNA (**Figure 8.6A**), or with ternary complexes generated by addition of siRNA to a mixture of peptide and DOTAP:DOPE liposomes (**Figure 8.6B**). The binary delivery systems achieved variable silencing efficiencies, depending on the cell line and on the peptide incorporated in the formulation. While formulations containing the S4(13)-PV peptide were unable to efficiently decrease survivin mRNA levels in the three cell lines tested (HT1080, A549 and HeLa; **Figure 8.6A**), complexes containing the H_5-S4(13)-PV peptide presented different mRNA knockdown values, varying from 0% silencing in HeLa cells to 50% in A549 cells and 70% in HT1080 cells (**Figure 8.6A**). In an attempt to improve survivin silencing in A549 and HeLa cells, DOTAP:DOPE liposomes (1:2 molar ratio) were added to each CPP formulation by complexing the cationic liposomes with the CPP prior to the addition of the siRNA. This strategy was not tested in HT1080 cells based on the results from the experiments on GFP silencing, where its application did not result in any significant improvement (data not shown). **Figure 8.6B** shows that the ternary complexes containing the wild-type or the histidine derivative CPP decreased survivin mRNA levels in the A549 cell line, resulting in 40% and 28% knockdown, respectively. Application of this approach also led to promising results in HeLa cells, since 23% and 39% survivin knockdown were observed for the wild-type and histidine-enriched peptide-containing formulations, respectively. In both cell lines, the silencing effect obtained with lipoplexes containing exclusively the DOTAP:DOPE lipids and siRNA, but no CPP, was negligible. In A549 cells, this formulation appears even to mediate enhanced survivin expression. Therefore, our results, showing a

survivin knockdown of 23 to 40% in both cell lines with the ternary systems, S4(13)-PV/DOTAP:DOPE/siRNA and H_5-S4(13)-PV/DOTAP:DOPE/siRNA, significantly superior to that obtained with DOTAP:DOPE/siRNA complexes, suggest a clear advantage of combining the S4(13)-PV peptide or its histidine derivative with the liposome formulation towards the generation of an efficient non-viral siRNA-based anti-tumoral approach.

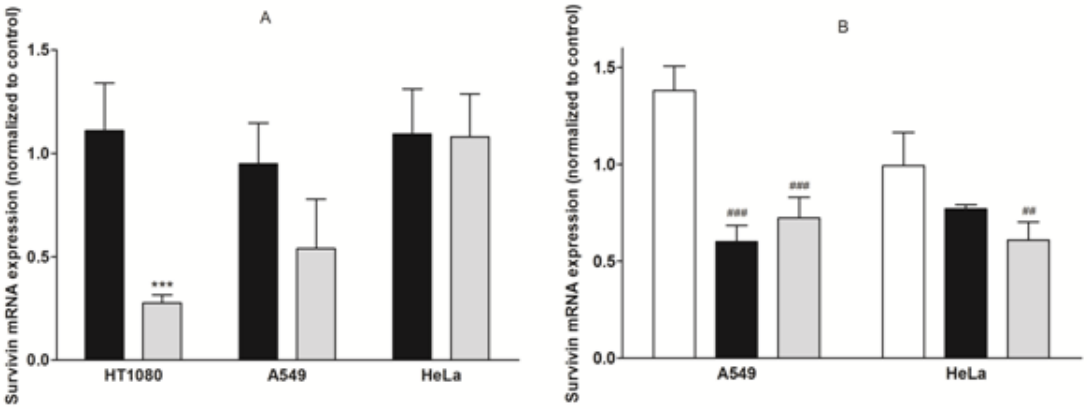

Figure 8.6 Survivin mRNA knockdown mediated by S4(13)-PV and H_5-S4(13)-PV peptide-based complexes in HT1080, A549 and HeLa cells. (A) Binary complexes of S4(13)-PV/siRNA (■) or H_5-S4(13)-PV/siRNA (■); (B) Lipoplexes of DOTAP:DOPE/siRNA (□) and ternary complexes of S4(13)-PV/DOTAP:DOPE/siRNA (■) or H_5-S4(13)-PV/DOTAP:DOPE/siRNA (■). Cells were incubated with the different complexes containing 50 nM of anti-survivin siRNA for 4 h at 37 ºC. Parallel experiments were performed using mut siRNAs. Forty-eight hours post-transfection, the efficiency of survivin knockdown mediated by the different complexes was evaluated by quantitative PCR. For determination of survivin mRNA levels, RNA was recovered from cells 48 h post-transfection and converted to cDNA, which was analyzed by quantitative PCR. Survivin mRNA expression, determined by the Pfaffl method, as described in the Materials and Methods section, is presented as the changes in RNA transcription caused by the treatment with anti-survivin siRNAs, normalized to RNA transcription changes in cells treated with mut siRNAs (set to 1). All results are presented as mean ± SD of at least three independent experiments. Data comparisons were performed for each cell line between the formulations containing S4(13)-PV and H_5-S4(13)-PV (***$p < 0.001$) and between DOTAP:DOPE/siRNA lipoplexes and the same lipoplexes containing S4(13)-PV or H_5-S4(13)-PV ($^{\#\#}p < 0.01$, $^{\#\#\#}p < 0.001$).

Figure 8.7 presents survivin protein levels, assessed by Western blot analysis and normalized with α-tubulin levels, following transfection with both binary and ternary complexes. A pattern similar to that observed for mRNA expression was apparent with binary complexes (**Figure 8.7A**). As observed, a superior knockdown of survivin was achieved with complexes containing the histidine-derivative peptide, although the results were only statistically significant for HT1080 cells, in which survivin protein levels decreased 44% (**Figure 8.7A** and **C**). Off-target effects could be observed for binary complexes containing the S4(13)-PV, since unspecific silencing

was detected following transfection with the mut siRNA, as displayed in **Figure 8.7C**. **Figure 8.7B** shows survivin protein levels upon cell transfection with ternary complexes containing the DOTAP:DOPE lipids in addition to the CPP, S4(13)-PV or H_5-S4(13)-PV, and siRNAs, prepared as previously mentioned. No decrease in the protein expression was achieved with these formulations or with the lipoplexes without CPP, although a decrease in survivin mRNA levels has been observed for the ternary complexes in both A549 and HeLa cells (**Figure 8.6B**).

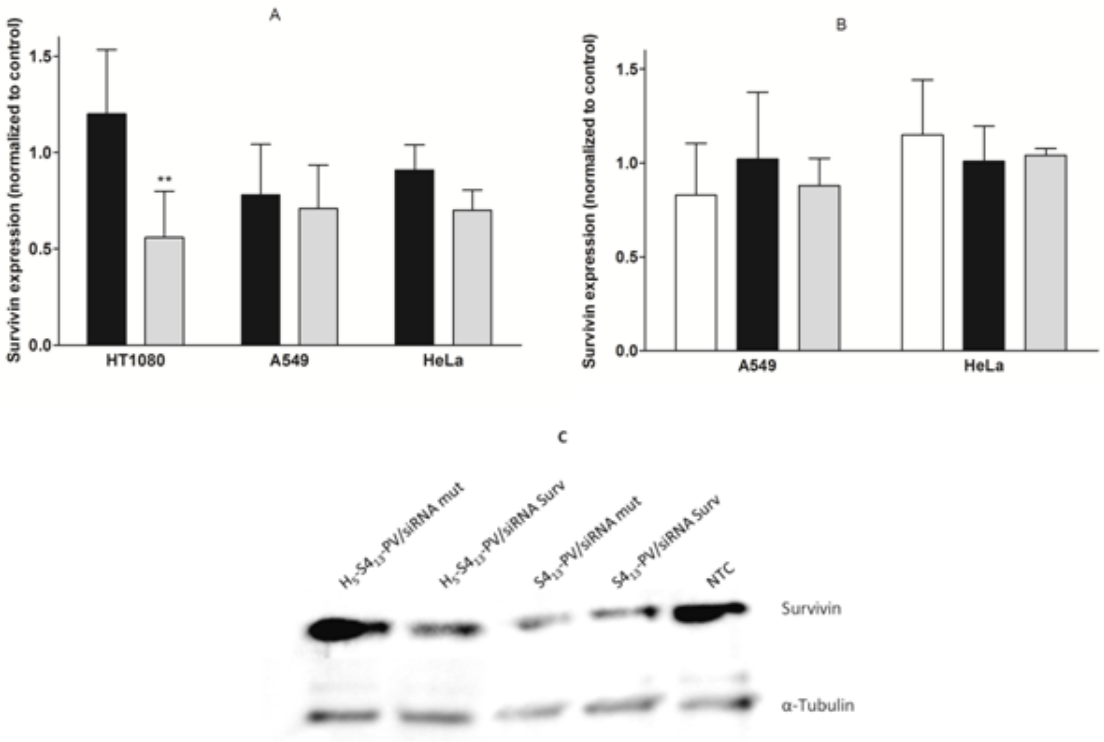

Figure 8.7 Survivin knockdown mediated by S4(13)-PV and H_5-S4(13)-PV peptide-based complexes in HT1080, A549 and HeLa cells. (A) Binary complexes of S4(13)-PV/siRNA (■) or H_5-S4(13)-PV/siRNA (■); (B) Lipoplexes of DOTAP:DOPE/siRNA (□) and ternary complexes of S4(13)-PV/DOTAP:DOPE/siRNA (■) or H_5-S4(13)-PV/DOTAP:DOPE/siRNA (■); (C) Representative Western blot images illustrating the survivin protein levels in non-treated HT1080 cells (NTC) or following siRNA (targeting survivin or siRNA mut) delivery by S4(13)-PV or H_5-S4(13)-PV. Cells were incubated for 4 h at 37 ºC, with the different complexes containing 50 nM of anti-survivin siRNA. The medium was then replaced and the cells were further incubated for 72 h before survivin and α-tubulin analysis. For each membrane, the analysis of band intensity was performed using the Image J software (Wayne Rasband National Institutes of Health, USA). Results in A and B are expressed as survivin fold change with respect to a control (cells treated with the same formulation containing siRNA mut, which was set to 1). Data comparisons were performed for each cell line between formulations containing S4(13)-PV and H_5-S4(13)-PV (**$p < 0.01$). All results are presented as mean ± SD of at least three independent experiments.

8.5 DISCUSSION

Since the 1970's, when gene therapy was first described (Carl R et al. 1971), great efforts have been expended towards the discovery of appropriate delivery systems able to surpass the cell membrane and release the different types of nucleic acid molecules, ranging from long DNA molecules to small double-stranded siRNAs, into the target intracellular compartment. Despite the recent advances concerning plasmid DNA and siRNA delivery to target cells, further work should be developed to achieve high levels of cellular uptake and long-term stability, while avoiding unspecific effects, so that nucleic acid therapeutics can reach their full potential as a clinically relevant option (de Fougerolles 2008; Pai et al. 2006; Ryther et al. 2005; Oh & Park 2009).

One of the major obstacles for a successful gene therapy strategy results from the impermeability of the cellular membranes to most charged molecules, which has, however, been surpassed by the use of vectors, including cell-penetrating peptides. CPPs constitute a relatively new branch of non-viral vectors that emerged following the description of the RNA/DNA-binding domains of the human immunodeficiency virus (HIV-1) Tat protein (Frankel & Pabo 1988) and of the *Drosophila* Antennapedia homeodomain protein (Joliot et al. 1991). Since then, several CPPs have been described and used as delivery systems for nucleic acids and other biomolecules (Heitz et al. 2009). Based on previous work from our laboratory, studies were performed in order to compare the transfection efficiency and cytotoxicity obtained with previously developed S4(13)-PV-based complexes and new complexes formulated with the S4(13)-PV analogue, H_5-S4(13)-PV peptide. This new peptide emerged as an effort to increase the intracellular bioavailability of the nucleic acids carried by CPP-based vectors, through the addition of histidine residues to the original peptide, which is expected to enhance its endosomolytic properties, favoring endosomal escape (Lo & Wang 2008), due to the protonation of histidine side chains in the endosome acidic environment.

The transfection efficiency and cell viability levels achieved following pDNA delivery by S4(13)-PV or H_5-S4(13)-PV complexes diverged between the two tested cell lines. HeLa cells proved to be more efficiently transfected than A549, although they are also more severely affected in terms of cytotoxicity exerted by the complexes. In fact, the ability to transfect a high number of cells is often associated with high cytotoxicity.

This was also observed with S4(13)-PV-based binary and ternary complexes, that transfected the largest number of HeLa cells at charge ratios at which they exerted the highest cytotoxicity, consistent with our previous results (Trabulo et al. 2008). However, the same complexes produced from the histidine-derivative peptide induced low levels of toxicity, even at high peptide concentrations (**Figure 8.2**). Noteworthy, the H_5-S4(13)-PV ternary complexes retained an elevated percentage of transfected cells and high levels of transgene expression (**Figure 8.1**). This effect is most likely linked to the endosomal escape process. The acidification of the endosomal lumen will allow the protonation of the imidazole group in the histidine residues, leading to osmotic swelling and membrane destabilization (Lo & Wang 2008; Midoux & Monsigny 1999). Moreover, it is possible that, under the acidic conditions in the endosome, the peptide undergoes conformational changes, which may enhance the interaction of the complexes with the endosomal membrane and consequent cytoplasmic release of DNA. This process might have an important outcome in the free nucleic acid yield, directly contributing to the amount of DNA that reaches the cell nucleus. An additional mechanism that might contribute to the enhanced DNA delivery by the complexes containing the histidine-enriched peptide involves favored interactions of the complexes at the cell membrane level resulting in their more efficient uptake.

On the other hand, the lower levels of protein expression in A549 cells relative to HeLa cells suggest that these cell lines have different patterns of interaction with the complexes, probably due to different proteoglycan content at the cell surface, or to the preferential use of different internalization pathways that may or may not converge in the endolysosomal route.

The potential of complexes based on S4(13)-PV peptide and its derivatives to promote siRNA delivery was also addressed in HT1080 GFP expressing cells. In this regard, we aimed at establishing the most suitable peptide structural features, which warrant efficient siRNA-mediated gene knockdown without causing cytotoxicity. Cell viability (**Figure 8.3**) indicates that the peptide primary structure plays a crucial role in terms of the cytotoxicity displayed by the corresponding peptide-based complexes. Thus, the reverse NLS peptide, whose amino acid sequence only differs from that of the original peptide in the relative position of three aminoacids of the NLS sequence, originates much more toxic complexes compared to the scrambled peptide, which preserves all

the S4(13)-PV amino acid residues, although exhibiting a random order. However, as can be observed in **Table 8.1**, the proline residue position in the scrambled peptide is maintained with respect to the wild-type and to the histidine-derivative peptides. Proline residues have been suggested to play a relevant role in membrane protein structure and dynamics (Oh & Park 2009; Frankel & Pabo 1988). Proline presents its side chain bonded to the tertiary nitrogen in a cyclic pyrrolidine ring, which makes it the only mammalian imino acid. The consequent absence of a proton in this residue impairs its participation in the formation of hydrogen bonds. This feature fixes the peptide backbone around proline residues, providing a kink or hinge that constrains the conformation of the adjacent residues (Carver, E R, Blout 1967) and leaves the neighboring carbonyl groups free to participate in alternative hydrogen bonds (Veis & Nawrot 1970). Therefore, peptide-siRNA association and interaction of the resulting complexes with the cellular membrane may be affected by the different peptide conformations, which, in the case of the reverse NLS peptide, could be caused by the change of location of the proline residue, leading to a more cytotoxic effect.

The GFP knockdown experiments also shed light on the mechanism of cytotoxicity associated with the use of complexes containing the reverse NLS peptide; the off-target effects of these complexes, reflected on the high silencing activity obtained with the mut siRNA (79%), suggest that theses complexes can strongly interfere with the cellular mechanisms involved in protein synthesis, impairing the production of proteins essential for normal cell function and thus resulting in high toxicity.

The cell internalization extent of siRNA delivered by S4(13)-PV and H_5-S4(13)-PV peptide-based complexes, observed by confocal microscopy, correlates with their silencing efficiencies (**Figure 8.4**). Furthermore, the diffuse pattern of siRNA distribution inside HT1080 cells transfected with complexes containing the histidine-derivative peptide suggests an efficient endosomal release of the complex cargo. On the other hand, cells transfected with complexes containing the wild-type peptide presented a punctuated siRNA distribution in the cytoplasm, which probably reflects endosomal entrapment. In addition, the amount of siRNAs inside the cells transfected with complexes of the wild-type peptide appears to be lower than that inside the cells transfected with histidine-derivative complexes. This observation might be explained by a putatively higher affinity of complexes containing the H_5-S4(13)-PV towards the cell surface proteoglycans.

In agreement with what has been previously observed for oligonucleotides (Trabulo et al. 2010a), S4(13)-PV peptide/siRNA complexes did not mediate significant gene silencing (**Figure 8.4J**). Also consistent with previous studies for plasmid DNA and oligonucleotides, ternary systems combining siRNAs with cationic liposomes and cell-penetrating peptides displayed higher biological activity than binary peptide/siRNA complexes (Trabulo et al. 2008; Trabulo et al. 2010a), excepting the complexes containing the H_5-S4(13)-PV peptide (**Figures 8.4J** and **8.5B**).

The results presented in **Figure 8.5** show that the protocol of preparation of the ternary complexes, specifically the order of component addition, did not play a crucial role in their gene silencing efficacy, although a small improvement in complex efficiency could be obtained when combining cationic liposomes with the cell penetrating peptide prior to siRNA addition. Most importantly, the systems containing the S4(13)-PV peptide showed superior biological activity with respect to similar formulations including the reverse NLS or scrambled peptides. This indicates that the amino acid sequence in the S4(13)-PV peptide is required to provide complexes with capacity to promote siRNA internalization and silencing of the target mRNA. The different efficiencies in GFP silencing displayed by the systems containing the S4(13)-PV and reverse NLS peptides corroborates the previous assumption that the location of the proline residue in the NLS sequence should be important for the biological activity of the S4(13)-PV-based complexes. In fact, the NLS sequence *per se* would not be required for siRNAs to accomplish their function, since these molecules do not need to reach the cell nucleus for silencing their target genes.

Since the relevance of a delivery system for potential clinical application can only be fully evaluated in a therapeutic context, we investigated the efficiency of the developed CPP-based systems to mediate silencing of an endogenous gene encoding an oncogenic protein (survivin). This protein presents a huge potential as a therapeutic target in cancer therapy due to its contribution to cancer survival, metastization and cell resistance to chemo and radiotherapy (Altieri 2008). The binary systems containing S4(13)-PV showed to be unable to decrease the messenger RNA or protein levels of survivin in any of the three cell lines tested (HT1080, A549 and HeLa). In contrast, similar complexes generated from the H_5-S4(13)-PV peptide silenced the survivin gene to different extents, depending on the cell line. The highest knockdown effect was obtained in HT1080 cells (73% decrease in mRNA and 44% decrease in protein

levels). The different ability of the H_5-S4(13)-PV peptide-based complexes to silence survivin gene in different cell lines may be explained by specific features of cells, including internalization preferred pathways, surface proteoglycans content and metabolic activity. In addition, the different levels of survivin mRNA and protein expression among various tumor cells (Li 2003) may contribute to different silencing efficiencies. Importantly, it was shown that the addition of DOTAP:DOPE liposomes, both to S4(13)-PV- and H_5-S4(13)-PV-containing systems, led to an increase in mRNA silencing efficiency (**Figure 8.6B**). Although the ability of ternary complexes to silence survivin mRNA in both A549 and HeLa cells was superior to that of DOTAP:DOPE/siRNA complexes, the levels of protein knockdown did not follow the same pattern, remaining similar to those observed in cells transfected with lipoplexes devoid of CPP (**Figure 8.7B**). This may be due to specific cellular mechanisms that regulate survivin levels in cancer cells. In this regard, some studies have reported the existence of an additional pool of survivin in mitochondria, which can exert its action whenever the levels of cytoplasmic survivin are lower than a defined threshold needed for cancer cell survival (Dohi et al. 2004; Carver & Blout 1967).

Nevertheless, a challenging finding in the present work was that siRNA complexes containing the histidine-enriched S4(13)-PV peptide showed high competence to deliver siRNA into the cells (as demonstrated in GFP-expressing HT1080 cells) and to promote specific knockdown. On the other hand, in HeLa cells, H_5-S4(13)-PV-containing formulations exhibited an efficiency in transfection with plasmid DNA comparable to those containing the wild-type peptide, with the advantage of presenting a much lower cytotoxicity.

Overall, our findings reveal that the H_5-S4(13)-PV peptide deserves to be further explored aiming at generating efficient nucleic acid delivery-based strategies in the context of therapies for cancer and other diseases. Moreover, our studies on the development of new CPP-based nucleic acid delivery systems and on the establishment of significant structure-activity relationships may open new avenues towards *in vivo* application of increasingly promising gene therapy approaches.

Chapter 9

Application of Thermoresponsive PNIPAAM-*b*-PAMPTMA Diblock Copolymers in siRNA Delivery

A.M. Cardoso, M.T. Calejo, C.M. Morais, A.L. Cardoso, A.R. Cruz, K. Zhu, M.C. Pedroso de Lima, A.S. Jurado and B. Nyström, "*Application of Thermoresponsive PNIPAAM*-b-*PAMPTMA Diblock Copolymers in siRNA Delivery*" Published in the Molecular Pharmaceutics, 11, **2014**, 819– 827.

9.1 ABSTRACT

Gene knockdown has emerged as an important tool for cancer gene therapy as well as for viral infections and dominantly inherited genetic disorders. The generation of suitable siRNA delivery systems poses some challenges, namely to avoid nuclease degradation, to surpass the cytoplasmic membrane and to release the nucleic acids into the cytosol. Aiming at evaluating the ability of thermoresponsive block copolymers formed by units of *N*-isopropylacrylamide and of (3-acrylamidopropyl)trimethyl-ammonium chloride to efficiently deliver siRNAs, an extensive study was performed with four different copolymers using a human fibrosarcoma cell line as cell model. The silencing ability and cytotoxicity of the generated copolymer-based siRNA delivery systems were found to be dependent on the cloud point of the polymer, which corresponds to the transition temperature at which the aggregation or precipitation of the polymer molecules becomes thermodynamically more favorable than their solubilization. In the present study, a system capable of delivering siRNAs efficiently, specifically and without presenting relevant cytotoxicity, even in the presence of serum, was developed. Confocal fluorescence experiments showed that the ability of the generated systems to silence the target gene is related to some extent to nucleic acid internalization, being also dependent on polymer-siRNA dissociation at 37 °C. Thus, a delicate balance between nucleic acid internalization and intracellular release must be met in order to reach an ideal knockdown efficiency.
The special features and potential for manipulation of the *N*-isopropylacrylamide-based copolymers make them suitable materials for the design and synthesis of new and promising siRNA delivery systems.

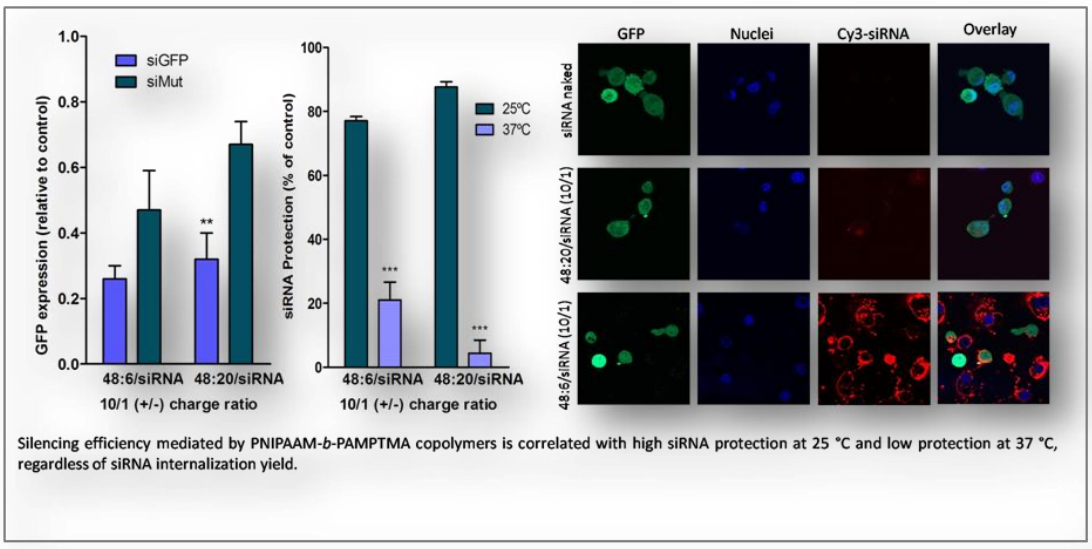

Silencing efficiency mediated by PNIPAAM-*b*-PAMPTMA copolymers is correlated with high siRNA protection at 25 °C and low protection at 37 °C, regardless of siRNA internalization yield.

9.2 INTRODUCTION

RNA interference (RNAi) is a powerful gene silencing process that holds a great therapeutic potential in several diseases, such as cancer (Brower 2010). Small interfering RNAs (siRNAs), first described in 2001 as promoting effective RNA interference in mammalian cells without inducing interferon immunological response (Elbashir et al. 2001), are short double stranded RNA (dsRNA) molecules (less than 30 nucleotides in length) that mediate post-transcriptional silencing of target genes through degradation of their mRNAs (Jinek & Doudna 2009). This process is highly efficient and sequence-dependent, thus conferring specificity to the silencing mechanism. In Nature, siRNAs are produced as an anti-viral defense, silencing mobile genetic elements resulting from viral infections. For therapeutic purposes, siRNAs have been delivered into cells using adequate carrier systems able to overcome membrane barriers and to release the nucleic acids into the cytosol, in order to allow their loading into the RNA-induced silencing complex (RISC) and the consequent specific mRNA knockdown (Jinek & Doudna 2009). Several different non-viral delivery systems, including cationic lipids, peptides and polymers, have been developed to introduce siRNAs into the cell cytoplasm, where they are active (Wu & McMillan 2009; Gavrilov & Saltzman 2012; Troiber & Wagner 2011; Meade & Dowdy 2008).

Some polymeric units, such as *N*-isopropylacrylamide (NIPAAM), are thermoresponsive and display a non-linear relationship between solubility and temperature, exhibiting a sharp thermotropic transition between a soluble and an insoluble state (Schild 1992). The phase transition temperature, known as cloud point or lower critical solution temperature (LCST), represents a transition from a hydrated form (due to the formation of water-polymer hydrogen bonds) to a non-hydrated form of the polymers, in which the disruption of the hydrogen bonds is entropically favored, leading to collapse or macroscopic phase separation of the polymers depending on the polymer concentration (Masci et al. 2012). Since the cloud point of NIPAAM was known, in 1992 (Schild 1992), homopolymers formed by NIPAAM units, or copolymers designed to exhibit different combinations and ratios between NIPAAM and other different units, have been extensively studied for biomedical applications, including

controlled delivery of therapeutic molecules and tissue engineering (Ward & Georgiou 2011). One of the reasons why the polymers containing NIPAAM have gained increasing interest in therapeutic applications resides on the possibility of modulating their thermoresponsiveness by varying several parameters, such as salt concentration, pH and composition or relative abundance of polymer components (Jain & Bates 2003; Pamies et al. 2009).

A polymer composed of several NIPAAM units, that is a poly-NIPAAM (PNIPAAM), hydrophobically aggregates at temperatures above 32 °C, depending on concentration and molecular weight (Pamies et al. 2009), and this proximity to human body temperature makes it particularly interesting for pharmaceutical and biomedical applications (Theato et al. 2013). Importantly, by copolymerization with other hydrophilic or hydrophobic blocks, one can increase or decrease the phase transition temperature of the polymer, for specific applications (Alexander 2006). For instance, copolymerization with hydrophilic blocks to produce polymers with a cloud point close to 37 °C has revealed to be particularly advantageous, since these molecules are sensitive to the physiological temperature, thus changing their structure when incorporated in the human organism. Therefore, complexes of these copolymers with nucleic acids, formed at temperatures below the polymer cloud point, are expected to display the ability to release the complexed molecule into human cells or body fluids due to a collapse of the polymeric structure at the physiological temperature (Ward & Georgiou 2011). In this context, the addition of a cationic unit, such as (3-acrylamidopropyl)trimethylammonium chloride (AMPTMA), to the NIPAAM structure was envisaged to accomplish two purposes: to increase the cloud point of the polymer (Ward & Georgiou 2011; Pamies et al. 2009) and to confer positive charges to the overall molecule (Guo et al. 2010). The addition of cationic units to hydrophobic polymers has been reported as making the polymer more prone to efficiently complex negatively charged biomolecules such as nucleic acids and to interact with negatively charged cell membranes (Guo et al. 2010). This approach has been applied to design new copolymer-based plasmid DNA delivery systems, creating molecular combinations with delivery competence that none of the individual components of the copolymer exhibit due to cytotoxicity or impairment of specific steps in the delivery process, such as cellular internalization and endosomal escape. The main objective of combining two

distinct monomers in the copolymer is to ally advantageous properties of each one and to minimize their deficiencies in order to accomplish an effective delivery (Takeda et al. 2004).

In this work, four diblock copolymers were synthesized as poly(*N*-isopropylacrylamide)$_n$-*block*-poly((3-acrylamidopropyl)trimethylammonium chloride)$_m$, abbreviated herein as PNIPAAM$_n$-*b*-PAMPTMA(+)$_m$, or n:m (n = 48 or 65 and m = 6, 10 or 20), which exhibit different cloud points and molecular weights. These block copolymers, which have already shown to be promising candidates as DNA nonviral carriers (Calejo et al. 2013b), were used in the present work to investigate their ability to efficiently deliver siRNA to HT1080 cells (a human fibrosarcoma cell line) in the absence and presence of serum. To the best of our knowledge, only one study has addressed the generation of a PNIPAAM-containing system for siRNA delivery (Kim et al. 2010), which was composed of quantum dots co-grafted with a cell penetrating peptide. Our results show that nucleic acid protection conferred by the polymers, associated with their ability to mediate cell internalization of the siRNAs and the polymer-siRNA dissociation is responsible for silencing a target protein.

These data shed light on the great variety of existing possibilities to design new and more efficient siRNA delivery systems, with the ultimate goal of developing a useful tool to modulate gene expression with implications in several fields, such as functional genomics, drug validation, and even transgenic design (Caplen 2004; Fire et al. 1998; Hannon & Rossi 2004; Napoli et al. 1990).

9.3 MATERIALS AND METHODS

Materials

The anti-GFP siRNA (5'-GCAAGCUGACCCUGAAGUUCAU-3') and Cy3-labeled non-specific siRNA sequence were purchased from Ambion (Austin, TX, USA). The non-silencing siRNA sequence used as control was obtained from Dharmacon (Lafayette, CO, USA). All the other chemicals were of the highest grade.

Charged Block Copolymers

The cationic diblock copolymers poly(*N*-isopropylacrylamide)$_n$-*block*-poly((3-acrylamidopropyl)trimethylammonium chloride)$_m$ (PNIPAAM$_n$-*b*-PAMPTMA(+)$_m$) with n = 48 or 65 and m = 6, 10 or 20 (**Figure 9.1**) were synthesized via a simple "one-pot" atom transfer radical polymerization (ATRP) procedure, as previously reported (Dedinaite et al. 2010; Kjøniksen et al. 2009). The chemical structure of the diblock copolymers used in this study is illustrated in **Figure 9.1**, and their cloud point values and molecular weights are presented in **Table 9.1**.

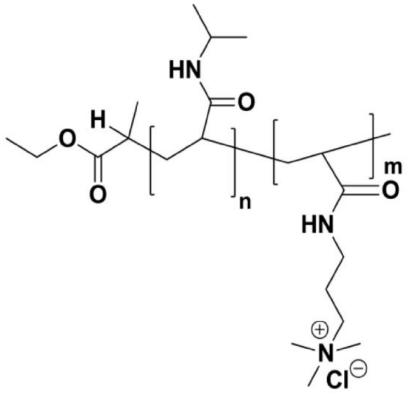

Figure 9.1 Schematic representation of the chemical structure of the PNIPAAM$_n$-*b*-PAMPTMA(+)$_m$ diblock copolymers (n = 48 or 65 and m = 6, 10 or 20).

Table 9.1 Cloud points and molecular weights of the PNIPAAM$_n$-*b*-PAMPTMA(+)$_m$ block copolymers.

Polymer (n:m)	PNIPAAM$_{48}$-*b*-PAMPTMA(+)$_6$ (48:6)	PNIPAAM$_{48}$-*b*-PAMPTMA(+)$_{10}$ (48:10)	PNIPAAM$_{48}$-*b*-PAMPTMA(+)$_{20}$ (48:20)	PNIPAAM$_{65}$-*b*-PAMPTMA(+)$_{20}$ (65:20)
Cloud Point (°C)[a]	35	36	37	34
M_w (g/mol)[a]	6770	7600	9690	11600

[a] Cloud point and molecular weight data were taken from Calejo et al. 2013b.

Cells

HT1080 cells (a human fibrosarcoma cell line that was stably transfected to express GFP endogenously) were maintained at 37 °C, under 5% CO_2, in Dulbecco Modified Eagle low glucose (DMEM-LG; Sigma) supplemented with 10% (v/v) heat-inactivated fetal bovine serum (FBS; Biochrom KG), and with 100 units penicillin and 100 µg streptomycin (Sigma) per mL.

Preparation of polymer/siRNA complexes

Polymers were dissolved in cell culture medium (OptiMEM or DMEM-LG) and gently mixed with siRNA targeting GFP (50 nM/well), at the desired polymer/siRNA (+/-) charge ratios. The mixtures were further incubated for 20 min at room temperature. Polymer/siRNA complexes were used immediately after being prepared.

Determination of the hydrodynamic diameter of polymer/siRNA complexes

Polyplexes were characterized with respect to their hydrodynamic diameter in HBS buffer, at 25 and 37 °C, by photon correlation spectroscopy-based technique (PCS) using a Coulter N4 Plus (Coulter Corporation, Miami, FL, USA). PCS uses photon correlation spectroscopy of scattered laser light to determine its time-dependent fluctuations resulting from the Brownian motion of particles in suspension. The light intensity scattered at a given angle is detected by a detector (at fixed angle of 90°) whose output current is passed to an fotocorrelator, which analyses time dependence, determining the rate of diffusion or Brownian motion of the particles and hence their hydrodynamic diameter (Cardoso et al. 2009). Complexes were prepared immediately before analysis. All complexes showed a monomodal hydrodynamic diameter distribution.

Evaluation of cell viability

Cell viability was assessed under the different experimental conditions by a modified Alamar blue assay, as described previously (Simões et al. 1999). Briefly, 48 h post-transfection, the cells were incubated with DMEM-LG (10% serum) containing 10% (v/v) resazurin dye. After 1 h incubation at 37 °C, the absorbance of the medium was

measured at 570 nm and 600 nm (supplier indication). Cell viability was calculated as a percentage of the non-transfected control cells, according to Eq. 1:

$$\text{Cell viability (\% of control)} = [(A_{570} - A_{600})/(A'_{570} - A'_{600})] \times 100 \quad (1)$$

where A_{570} and A_{600} are the absorbances of the samples, and A'_{570} and A'_{600} are those of the control (non-treated cells), at the indicated wavelengths.

Analysis of GFP silencing

HT1080 cells (1.0×10^5 cells/well) were seeded in 12-well plates. Following overnight culture, the cells were incubated with the different complexes (50 nM of siRNA per well) at 37 °C for 4 h, in OptiMEM (no serum) or DMEM-LG (10% serum) media. After this period, the medium was replaced with fresh complete medium containing 10% (v/v) FBS and antibiotics, and the cells were further incubated for 44 h to allow gene expression. Parallel experiments were performed with a control siRNA (non-target siRNA or siRNA mut). The knockdown efficiency mediated by the different complexes was evaluated by analyzing GFP silencing by flow cytometry. Briefly, 48 h after transfection, the cells were washed once with PBS and detached with trypsin (10 min at 37 °C). The cells were further washed three times by centrifugation (5 min, 1000 rpm) in ice-cold PBS and immediately analyzed, using a Becton Dickinson FACSCalibur flow cytometer (BD Biosciences, San Jose, CA, USA). Data obtained were analyzed using CellQuest software. To discriminate between viable and dead cells and to exclude doublets, cells were appropriately gated by forward/side scatter and pulse width from a total of 10,000 events. The FITC bandpass filter was used in emission detection. GFP silencing was expressed as geometric mean fluorescence intensity with respect to control (non-treated) cells.

Analysis of siRNA internalization and intracellular distribution

HT1080 cells (0.2×10^5 cells/well) were plated in 8-well chambered coverslips (Lab-Tek™ II Chamber Slide™ System Nunc™). Following overnight culture, the cells were incubated, for 4 h, with the different polymer/siRNA delivery systems formulated with non-coding Cy3-labelled siRNAs (50 nM), in OptiMEM medium. After this period, cells were washed twice with PBS and incubated with Hoechst 33342 dye (1 µg/mL, Molecular Probes, Eugene, OR). Cells were then washed twice with PBS and directly

observed in the chambers in 0.5 mL of OptiMEM. Fluorescence distribution inside cells was analyzed under a Zeiss Axiovert 200 M confocal microscope (Carl Zeiss, Oberk) without fixation, using the 60× oil immersion objective.

Analysis of siRNA protection

Complexes containing 14 pmol of siRNA prepared in a total volume of 100 µL of HBS were allowed to incubate for 20 min at room temperature and then transferred to a 96-well (blackwalled) plate (Corning, NY, USA). A total of 100 µL of PicoGreen dye (Molecular Probes, Eugene, OR), upon 1:200 dilution in HBS buffer (according to the manufacturer's instructions), was added to each well. The fluorescence of PicoGreen, directly proportional to the amount of accessible/free siRNA, was monitored in a Spex Fluorolog Spectrometer at 25 and 37 °C. The excitation and emission wavelengths were set at 485 and 520 nm, respectively. The amount of siRNA protected by the cationic polymers was calculated as a percentage of a control containing only a PicoGreen solution, according to Eq. 2:

$$P_{siRNA} = 1- [(F-F_{100})/(F_0-F_{100})] \quad (2)$$

where F is the fluorescence measured after adding the complexes to the PicoGreen solution, F_0 is the maximum fluorescence of a positive control, which accounts for 0% of siRNA protection, and F_{100}, the minimum fluorescence of a negative control taken as 100% of protection. For the positive control, free siRNA, in the same amount as that associated with the complexes, was used and a PicoGreen solution without siRNA was used as the negative control.

Statistical Analysis

Data are presented as mean ± SD. The significance of the results was statistically analyzed by a one-way analysis of variance (ANOVA) with Tukey's multiple pairwise comparison, unless stated otherwise. Statistical significance was set at $p < 0.05$.

9.4 RESULTS

9.4.1 HYDRODYNAMIC DIAMETER OF THE POLYMER/SIRNA COMPLEXES

Due to the temperature-dependent structural properties displayed by the polymers used in this study, the average diameter of their complexes with siRNA was evaluated at 25 and 37 °C. As shown in **Table 9.2**, polyplexes prepared from n:m 48:20 exhibited the largest hydrodynamic diameters at 25 °C (820 and 583 nm, when prepared at 2/1 and 10/1 (+/-) charge ratios, respectively). For the same length of polymer thermoresponsive moiety (n = 48), the increase in the number of cationic units (from 6 to 20) led to a progressive increase of polyplex hydrodynamic diameter. However, the length of the thermoresponsive component also influenced polyplex dimensions. Thus, for the same number of cationic units (m = 20), the increase of the thermoresponsive moiety length (from 48 to 65) promoted a decrease of polyplex hydrodynamic diameter.

Complexes exhibited at 37 °C the same diameter as that observed at 25 °C, except for those generated from the n:m 48:20 polymer, which showed a significant reduction in hydrodynamic diameter with increasing temperature (to 263 and 140 nm when prepared at 2/1 and 10/1 (+/-) charge ratios, respectively).

Table 9.2 Mean hydrodynamic diameter of the polymer/siRNA complexes obtained at 25 and 37 °C.

		Hydrodynamic diameter (nm)[a]	
n:m	(+/-) charge ratio	25 °C	37 °C
48:6	2/1	179 ± 34	134 ± 63
	10/1	280 ± 7	309 ± 78
48:10	2/1	306 ± 68	217 ± 38
	10/1	336 ± 12	427 ± 16
48:20	2/1	820 ± 82	264 ± 51***
	10/1	583 ± 23	140 ± 61***
65:20	2/1	299 ± 25	295 ± 68
	10/1	442 ± 67	420 ± 52

[a] Results represent the mean ± SD from three independent experiments. Data comparisons were performed between the hydrodynamic diameters of complex formulations measured at 25 and 37 °C (***$p<0.001$).

9.4.2 CYTOTOXICITY AND SILENCING EFFICIENCY

The cytotoxicity and silencing efficiency of complexes (polyplexes) composed of siRNA targeting GFP and each of four PNIPAAM$_n$-*b*-PAMPTMA(+)$_m$ block copolymers with different cloud points were evaluated in HT1080 cells, both in the absence and presence of 10% serum.

In the absence of serum, the toxicity exerted by the polyplexes showed high dependence on the polymer/siRNA (+/-) charge ratio (**Figure 9.2A**). At the lowest (+/-) charge ratio tested (2/1), only the n:m 65:20 polymer-containing complexes exhibited some toxicity, inducing a decrease of 37% in cell viability. At the polymer/siRNA (+/-) charge ratios of 5/1 and 10/1 the complexes were toxic, causing a reduction of cell viability to values between 60% [n:m 48:20 at 10/1 (+/-) charge ratio] and 30% [n:m 65:20 at 10/1 (+/-) charge ratio], except for the n:m 48:20 polymer-containing complexes at the 5/1 (+/-) charge ratio, which decreased the cell viability only to 84%. The n:m 48:20-based complexes were, therefore, the least toxic to the cells in the absence of serum. Comparatively, the cytotoxicity of the complexes in the presence of serum was in general less severe (**Figure 9.2B**). In this case, only for the highest (+/-) charge ratio tested (10/1), the complexes showed significant cytotoxicity. The most pronounced toxic effect was observed for the complexes containing the n:m 65:20 polymer, the cell viability reaching values of 46% and 32% in the presence of complexes at 5/1 and 10/1 (+/-) charge ratios, respectively.

Regarding the silencing efficiency for cells incubated with the complexes in the absence of serum (**Figure 9.2C**), only the formulations that exhibited cytotoxicity displayed unspecific silencing. As observed, complexes prepared at the lowest (+/-) charge ratios (particularly at the 2/1 charge ratio), at which they exhibited low or no toxic effects, showed high ability to specifically silence the target gene (black columns). Remarkably, the n:m 48:6 polymer/siRNA complexes, prepared at the 2/1 (+/-) charge ratio, were able to suppress gene expression in 36% in a specific manner. In the presence of serum, the silencing specificity of the complexes decreased, as deduced from the knockdown effect observed when the complexes were formulated with the non-target siRNA (white bars in **Figure 9.2D**). Despite this being the general scenario, it is important to note that complexes of the n:m 48:20 polymer and siRNA, at the 10/1 (+/-) charge ratio, presented a significantly lower unspecific silencing effect in

the presence of serum than in its absence. In this case, for complexes formulated with the non-target siRNA, GFP expression was reduced to 55% of the control in the absence of serum and to 67% in the presence of serum. On the other hand, as shown in **Figure 9.2C** and **D**, upon knockdown with the siRNA targeting GFP, protein expression was 34% and 32% of the control, in the presence and absence of serum, respectively, thus revealing an improvement of the performance of these complexes under conditions mimicking more closely those *in vivo*, regarding their specific effect on the target gene.

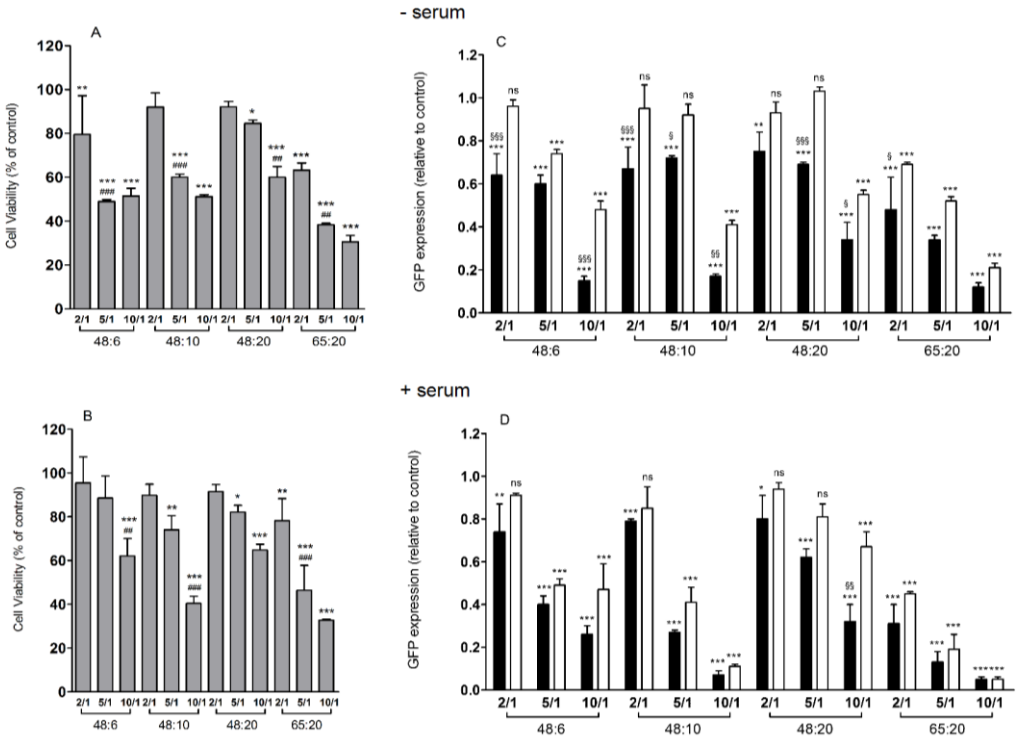

Figure 9.2 Cell viability (A and B) and GFP expression (C and D) promoted by polyplexes of PNIPAAM-*b*-PAMPTMA and siRNA in the absence (A and C) and in the presence of 10% serum (B and D) performed at 37 °C. Parallel experiments of GFP expression were performed with siRNA targeting GFP (■) and a non-target siRNA (□). The cell viability results are presented as a percentage of the control (non-treated cells, more than 98% of which are viable), taken as 100%. Results of GFP expression are presented with respect to GFP expression of a control (non-treated cells, 80% of which express GFP), taken as 1.0. The results represent the mean ± SD obtained from triplicates of three independent experiments. The following pairwise comparisons were performed: cell viability or GFP expression observed in cells treated with each complex formulation were compared to the same parameters obtained in non-treated control cells (*p<0.01, **p<0.005, ***p<0.0001, Dunnett's multiple comparison test); each complex formulation was compared to the same complex formulation at the immediately precedent (+/−) charge ratio ($^{\#}$p<0.01, $^{\#\#}$p<0.005, $^{\#\#\#}$p<0.0001); GFP expression obtained with complexes containing siRNA targeting GFP was compared with that obtained with complexes containing the non-target siRNA (§p<0.01, §§p<0.005, §§§p<0.0001, ns, non significant).

9.4.3 siRNA INTERNALIZATION AND INTRACELLULAR DISTRIBUTION

Aiming at comparing the extent of cellular internalization and distribution of siRNA molecules mediated by polyplexes displaying different levels of specific silencing, complexes containing the polymers n:m 48:6 and 48:20 at polymer/siRNA (+/-) charge ratios of 2/1 and 10/1 were selected for confocal microscopy analysis. **Figure 9.3** displays the siRNA internalization patterns obtained in HT1080 cells, in the absence of serum, for the different conditions tested. Both untreated cells (data not shown) and cells treated with naked siRNA (**Figure 9.3A**) were used as negative controls. In these two cases, no siRNA red fluorescence was noticeable, which is in accordance with the inability of the siRNA *per se* to enter the cells. Lipofectamine siRNAmax™ was used as a positive control (**Figure 9.3B**). As observed, this commercially available reagent was able to deliver siRNA to cells, which displayed some punctuated red fluorescence (round and intense red dots), most likely reflecting siRNA entrapment inside vesicles. However, some degree of siRNA dispersion throughout the cells could also be deduced from the observed diffuse red fluorescence. The n:m 48:20 copolymer showed a poor ability to mediate the entry of siRNA into the cells after 4 h of cell incubation with the polyplexes, both at the 2/1 and 10/1 (+/-) charge ratios (**Figure 9.3C** and **D**). However, the pattern of distribution of siRNAs delivered by the 10/1 (+/-) charge ratio complexes was more diffuse than that of siRNAs delivered by Lipofectamine siRNAmax™, indicating that siRNA internalization mediated by the polymer-based complexes was followed by its release from intracellular vesicles into the cytosol. On the other hand, complexes containing the n:m 48:6 copolymer were able to overload the cells with siRNA, at both charge ratios tested, as deduced from the intense and widely distributed red fluorescence observed throughout the cytoplasm (**Figure 9.3E** and **F**), thus showing their efficacy to promote both siRNA cellular uptake and cytoplasmic delivery.

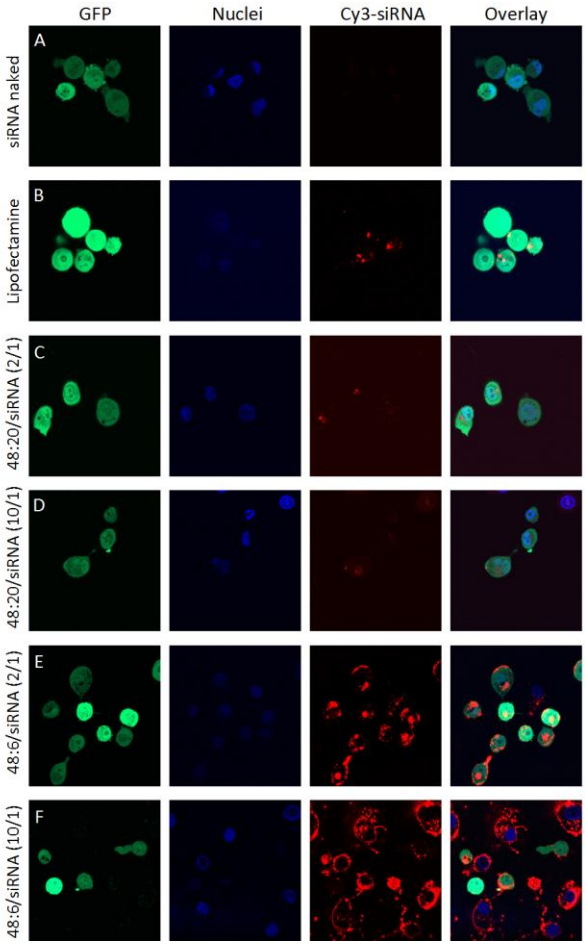

Figure 9.3 siRNA internalization mediated by different polymer-based systems at 37 °C. HT1080 cells (green) were incubated with the different complexes containing 50 nM of non-target Cy3-labelled siRNA (red). Cell nuclei were labeled with Hoechst 33342 dye (blue). Representative confocal microscopy images of each experimental condition (630x), taken after 4 h of cell incubation with the complexes are presented (A-F). Representative results of siRNA internalization in cells treated with Lipofectamine siRNAmax™/Cy3-siRNA (B), 48:20 polymer/Cy3-siRNA (C-D) and 48:6 polymer/Cy3-siRNA (E-F) complexes, at the indicated charge ratios, are presented. Results for cells treated with Cy3-siRNA only (siRNA naked) are shown as a control (A).

9.4.4 siRNA PROTECTION CONFERRED BY THE POLYMERS

The ability of the generated copolymers to confer protection to the siRNA was assessed by Picogreen fluorescence at 25 and 37 °C (**Figure 9.4**). This assay takes advantage of the probe fluorescence emission only occurring upon probe intercalation in the nucleic acid structure. Therefore, the fluorescence measured in this assay reflects the accessibility of the nucleic acid in solution.

As observed, all the polymers studied herein were able to efficiently shield the siRNA molecules at 25 °C, with protection levels between 70 and 87%, over the range of the tested charge ratios. However, results obtained from parallel experiments performed at 37 °C showed that the copolymers essentially lost the capacity to protect the carried siRNAs. As observed, the

maximum protection (30%) was attained for complexes produced from the n:m 48:6 block copolymer and siRNA at the (+/-) charge ratio of 2/1. Surprisingly, at this temperature (37 °C), the polymers showed a tendency for decreased ability to protect the siRNA molecules with increasing (+/-) charge ratio. In fact, it should be expected that increasing the relative amount of the cationic molecule would increase the "wrapping" of the siRNAs, leading to a more efficient shielding of the carried nucleic acid molecules. That behavior was particularly noticed for polyplexes prepared from the copolymer n:m 48:20, while for the polyplexes based on n:m 48:6, 48:10 and 65:20 copolymers, the degree of protection did not vary significantly with the (+/-) charge ratio.

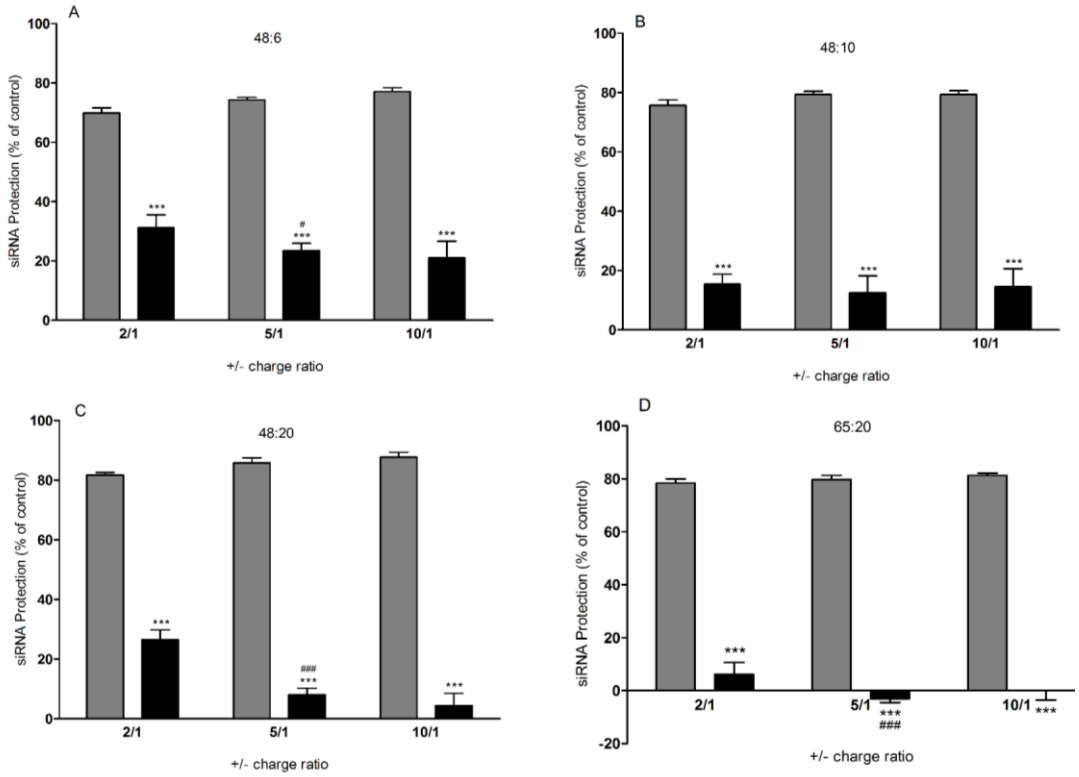

Figure 9.4 Effect of composition and (+/−) charge ratio of PNIPAAM-*b*-PAMPTMA-based polyplexes on siRNA protection, as assessed by measurement of the PicoGreen fluorescence at 25 °C (■) and at 37 °C (■). Polyplexes, prepared by incubating the copolymers n:m 48:6 (A), 48:10 (B), 48:20 (C) and 65:20 (D) with 14 pmol of siRNA, were added to a PicoGreen solution, as described in the Material and Methods section. The results represent the mean ± SD obtained from triplicates of three independent experiments. The degree of protection conferred by each polyplex formulation to siRNA at 37 °C was compared to that conferred by the same formulation at 25 °C (***$p<0.001$) and to that conferred by the same formulation at the immediately precedent polymer/siRNA (+/-) charge ratio ($^{\#}p < 0.05$, $^{\#\#\#}p < 0.001$).

9.5 DISCUSSION

The temperature dependence of the structural properties exhibited by PNIPAAM-based block copolymers has been extensively exploited in recent years, with the purpose of producing delivery systems with controlled release ability for pDNA and other therapeutic molecules (Ward & Georgiou 2011).

In this study, four cationic diblock copolymers differing in terms of the length of the thermoresponsive and the charged blocks were used. In a previous work (Pamies et al. 2009; Calejo et al. 2013b), it was shown that the length and ratio between these blocks are determinant of the structural changes taking place as the temperature is increased, influencing the transfection efficiency. For a constant length of the PNIPAAM block, increasing length of the PAMPTMA(+) block led to an increase in the hydrodynamic radius of the polyplexes at 25 °C (48:6 < 48:10 < 48:20, **Table 9.2**). This trend may be explained by the molecular weight increase and also by an enhancement of the repulsive electrostatic interactions leading to the complex expansion. However, the smaller hydrodynamic diameter of complexes formed with the highest molecular weight copolymer (65:20) as compared to the complexes formed with 48:20 suggests that the temperature-responsive block also plays a role in that physical parameter. Furthermore, the fact that this temperature-responsive contraction is observed at 25 °C suggests that the complexation of the polymer with the nucleic acids can shift the transition temperature of PNIPAAM to lower temperatures, in agreement with the charge neutralization of the copolymer.

The increase of temperature from 25 to 37 °C apparently did not promote statistically significant differences in the hydrodynamic radii for the polyplexes prepared with 48:6, 48:10 and 65:20 copolymers. However, the cloud point values and the thermoresponsive behavior of the copolymers suggest that structural changes take place as the temperature is increased. Interplay between temperature-induced contraction of the polyplexes (contributing to hydrodynamic diameter decrease) and an increased aggregation number (higher number of associating chains, contributing to hydrodynamic diameter increase) may explain the apparently unchanged hydrodynamic diameter of the polyplexes as the temperature is raised. Furthermore, with the exception of polyplexes based on 48:20 copolymers, the hydrodynamic

diameter of the polyplexes increased with the increase of (+/-) charge ratio, reflecting an increase of the aggregation number, caused by a higher number of polymer molecules in solution. Interestingly, at 37 °C the hydrodynamic diameter of the polyplexes prepared with 48:20 copolymers was found to be reduced as the charge ratio increased. This suggests a significant degree of electrostatic repulsion between the complexes formed with the long PAMPTMA(+) block. In the 65:20-containing complexes the electrostatic repulsions are minimized by an extremely long PNIPAAM block.

In a therapeutic context, a siRNA delivery system must be able to carry the nucleic acid molecules to target cells, preventing their degradation by extracellular nucleases, and promote their cellular internalization and release into the cytosol. Because of the inhibitory effect exerted by serum on transfection mediated by non-viral systems, nucleic acid delivery is usually performed in the absence of serum. However, the presence of serum proteins is unavoidable under *in vivo* conditions. Therefore, in the present work, aiming at predicting the *in vivo* behavior of the generated PNIPAAM$_n$-*b*-PAMPTMA(+)$_m$-based polyplexes towards their successful clinical application, the knockdown efficiency was evaluated in the presence of serum.

The presence of serum during cell incubation with the complexes caused a mild decrease in their biological activity, as compared to that observed in the absence of serum. This may reflect an unspecific interaction between the cationic moiety of the PNIPAAM-*b*-PAMPTMA(+) copolymers and the negatively charged serum proteins, thus preventing some complexes to reach the cells, and thereby decreasing the knockdown levels. Moreover, the silencing efficiency achieved in the presence of serum was less specific than in its absence, indicating the occurrence of off-target effects. The unspecific silencing should be avoided as it can lead to gene mutations and cell transformation, with severe consequences, such as impairment of the cellular machinery responsible for the production of important cell survival proteins (Birmingham et al. 2006; Jackson et al. 2006).

The cloud point of the polymers (**Table 9.1**) showed to influence both cytotoxicity and silencing efficiency. In this regard, at the highest polymer/siRNA charge ratios tested, the cytotoxicity induced by the complexes was inversely correlated with the cloud point of the polymers. Both in the absence and presence of 10% serum, the polymer

with the lowest cloud point (n:m 65:20) originated complexes that were highly toxic to the cells. Similar observations have been made when this polymer was used as a carrier for plasmid DNA, and this was then associated with the formation of a compact structure decorated with a highly charged corona (Calejo et al. 2013b). On the other hand, the knockdown efficiency of the polyplexes at the 10/1 (+/-) charge ratio in the absence of serum was found to be also inversely correlated with the polymer transition temperature. Indeed, the silencing activity was most effective for complexes formed by the polymer with the lowest cloud point, with a progressive increase in silencing efficiency according to the following order: 48:20 < 48:10 < 48:6 < 65:20 (**Figure 9.3**). This can be explained by the effect of the siRNAs on the cloud point of the copolymers. Due to their negative charges, siRNA molecules may change the ionic strength of the environment or neutralize the charges of the cationic units of the copolymer (which are responsible for increasing the LCST), thus altering the thermal behavior of the complexes (Ward & Georgiou 2011), and eventually promoting their dissociation, by contraction of the polymer in a coil-to-globule transition (Volden et al. 2012).

Most cationic systems used to deliver nucleic acids to cells present a protection pattern to siRNA that is consistent with the amount of the cationic moiety employed to formulate the complexes, increasing from the lowest to the highest charge ratios (Crombez et al. 2009; Tsai et al. 2011). However, the thermoresponsive copolymers studied herein did not present such behavior. Apparently, the polymer/siRNA charge ratio did not affect the release of the siRNAs or showed an opposite effect to that described for non-thermoresponsive systems (**Figure 9.4**). In general, at 25 °C (temperature of complex preparation), a very efficient complexation was achieved and the siRNAs were highly shielded, similarly to what has been described for other cationic polymers used as delivery systems (Crombez et al. 2009). However, at 37 °C, the siRNA protection decreased, as the polymers collapsed and dissociated from the nucleic acids. This suggests that at this temperature the increase in polymer concentration mostly results in enhanced intra- and intermolecular hydrophobic associations between the PNIPAAM blocks, contributing to the formation of aggregated and compact structures. In other words, the thermoresponsive properties of the copolymers are dominant in the system, and an increase in charge ratio mostly

contributes to increase the associative behavior of PNIPAAM, rather than contributing to protect the siRNA. In this context, the polymer cloud point may also have guided the efficacy of siRNA release, as previously discussed. On the other hand, the polymer molecular weight and the number of charged PAMPTMA units determine the number of polymer molecules needed in each case to reach the desired complex charge ratio. Therefore, the organization of the polymeric moieties around the siRNAs was probably sufficiently diverse to lead to the observed differential behavior regarding the nucleic acid release.

In spite of the much lower extent of internalization detected by confocal microscopy, the n:m 48:20 polyplexes, at 10/1 (+/-) charge ratio, showed a relatively high level of GFP knockdown (66%) as compared to that induced by n:m 48:6 complexes (85%), which should be attributed to their efficiency in promoting siRNA release. Parallel silencing experiments using Lipofectamine RNAi max revealed that the n:m 48:20 copolymer is as efficient as this commercial reagent (65%) in promoting gene knockdown. Interestingly, the polyplexes formulated with the 48:20 copolymer, at the 10/1 (+/-) charge ratio, were those presenting, at this charge ratio, the largest hydrodynamic diameter at 25 °C (>580 nm) and were the smallest (140 nm) at 37 °C. If, on the one hand, the large hydrodynamic diameter at 25 °C might be associated with a high siRNA load, the decay in size at 37 °C, on the other hand, can reflect a collapse of the structure upon heating, promoting the release of the entrapped nucleic acids, as described for other drugs (Ward & Georgiou 2011). Due to their small size, the siRNA molecules are exposed after contraction of the copolymers at high temperatures and their subsequent release by the temperature-induced contraction of the copolymers favors the gene silencing efficiency.

The general picture that emerges from this work is that the silencing efficacy of the studied polyplexes depends on a delicate interplay between repulsive electrostatic forces and hydrophobic interactions, whose balance can be tuned by changing the length of the PNIPAAM or PAMPTMA blocks, which, in turn, defines polymer transition temperature and charge density. The cloud point of the polymer showed, as expected, high relevance for the biological activity achieved upon interaction of the complexes with the cells. It should be stressed that, in the present work, two promising siRNA delivery systems were generated with the n:m 48:6 and n:m 48:20 copolymers and

siRNA at the 10/1 (+/-) charge ratio, which revealed high efficiency in silencing a reporter gene in a fibrosarcoma cell line, even in the presence of serum. Under these conditions, the formulation containing n:m 48:20 combines the best relationship between a relatively low-toxic (65% of cell viability) and highly efficient gene silencing system, with 68% of GFP knockdown and only 33% of unspecific gene silencing. Although the size and nucleic acid protection levels of the complexes may limit their application for intravenous administration, the complexes under study can be useful for local delivery into target cells (Hruby et al. 2011).

Overall, this study opens new trends for the engineering of innovative therapeutic delivery systems from the combination of materials whose properties can synergistically contribute to enhance the efficacy of nucleic acid delivery. With a growing understanding of polymeric drug delivery mechanisms, this approach may be therefore of great relevance to generate new and promising systems for gene therapies.

Chapter 10

Concluding remarks and future perspectives

Concluding remarks and future perspectives

The present work contributes to shed light on the relevance of the structural characteristics and ability of a variety of nucleic acid delivery systems to interact with lipid membranes for their efficiency in transfecting cells.

In this context, some of the most significant conclusions drawn from the studies on the three main groups of nucleic acid delivery systems developed in the present work are mentioned below.

The efficiency of transfection mediated by gemini surfactants depends on an intricate combination of unique features of these compounds regarding their headgroups, spacer, and hydrophobic tails. Therefore, the establishment of clear-cut structure–activity relationships for these compounds is challenging. Structural characteristics, such as tail and spacer length and flexibility define the phases formed by gemini surfactants in aqueous medium and the supramolecular complexes they form with DNA. Conventional m-s-m gemini surfactants containing increasingly long tails formed vesicular complexes with DNA and helper lipids (12-2-12) and also irregularly-shaped aggregates of flocculated smaller vesicles (14-2-14 and 16-2-16). The variation of the headgroup-spacer linkage in serine-derived gemini surfactants, originating different spacer flexibility and different effective lengths between the two charged headgroups, resulted in complexes presenting different arrangements. The ester derivative, which presented the most flexible spacer, also formed the smallest complexes. The strength of gemini surfactant-DNA interactions and the extent of the interactions established by gemini surfactant-based complexes with cellular membranes determine, in turn, whether DNA is efficiently complexed and delivered into the cell or, in contrast, DNA is entrapped in the complex, being unable to reach its target organelle, or to be released from the endosomes, being degraded. Complexes of conventional gemini surfactants, internalized mostly by macropinocytosis and direct membrane translocation, benefited from a strong gemini surfactant-DNA interaction and a mild destabilization upon contact with lipid membranes, which lead to efficient transfection. Serine-derived gemini surfactants produced complexes that were shown to be internalized by a variety of endocytic mechanisms, as well as by direct

membrane translocation. The most efficient complexes in mediating transfection presented low propensity to be destabilized upon interactions with membranes, which most likely leads to a late disassembly of the complexes, allowing them to reach the proximities of the nucleus before nucleic acid release.

On the other hand, the use of conventional and serine-derived gemini surfactants as nucleic acid carriers opens a window for the application of gene delivery to treat mitochondrial diseases. Thus, the ability of gemini surfactants (14-2-14, (14Ser)2N5 and (16Ser)2N5)) to deliver a plasmid DNA that is selectively expressed by the mitochondrial machinery was demonstrated. Additionally, the most competent nucleic acid complexes in promoting gene delivery and expression in mitochondria were shown to be distinct from those able to induce expression of pDNA in the nucleus.

Regarding CPPs, the ability to promote lipid domain segregation and to induce nonlamellar phases, thus destabilizing the membrane and increasing its permeability, has been correlated with the efficient DNA delivery mediated by S4(13)-PV. The inability of S4(13)-PV to efficiently deliver siRNAs was attributed to endosomal entrapment. Structural alteration of the delivery system, either by addition of the helper lipid DOPE or by the chemical modification of the peptide itself through the addition of a histidine tail, with the purpose of inducing endosomal destabilization and nucleic acid release, were shown to improve the transfection efficiency of the complexes.

A temperature-induced phase transition of thermoresponsive polymers near the physiological temperature range was found to improve the silencing efficacy of the corresponding polyplexes. Structural alterations promoted by small changes in the relative proportions of the cationic (AMPTMA) and thermoresponsive (NIPAAM) blocks, which define polymer transition temperature and charge density, by modulating the delicate interplay between repulsive electrostatic forces and hydrophobic interactions, showed to be highly relevant for the biological activity achieved upon interaction of the complexes with the cells.

Overall, these data provided deep insights into the mechanisms through which the composition, the physicochemical properties and the final architecture of a variety of nonviral delivery systems, whose structure was susceptible of systematic modulation,

influence their efficiency in mediating transfection. **Table 10.1** summarizes the structural properties modulated in the delivery systems used in the present work and their influence on the success of transfection.

Table 10.1 Structural characteristics of gene delivery systems suitable for modulation and their influence on the success of transfection.

Delivery system	Structural characteristic modulated	Findings (correlations)	Conclusions
Gemini surfactant-based	• Tail length • Headgroup • Spacer length • Spacer-headgroup linkage	• Surfactants with long tails and small headgroups (m-s-m) or with short tails and large headgroups (serine derivatives) produce the most efficient delivery systems. • Surfactants with long spacers produce cytotoxic complexes • Surfactants with ester linkage produce the most efficient delivery systems.	• Ability for gene delivery and cytotoxicity of gemini surfactants can be modulated by modifying structural properties that guide the strength of the interactions with DNA and the supramolecular structures adopted by DNA complexes.
CPP-based	• Sequence of aminoacids • NLS reversion • Histidine tail addition	• S4(13)-PV promotes phase separation in model membranes and induces H_{II} structures in cell membranes, whereas its scrambled analogue does not. • S4(13)-PVrev is highly cytotoxic. • H_5-S4(13)-PV mediates gene silencing more efficiently than S4(13)-PV.	•Transfection efficiency and cytotoxicity of complexes containing peptides from S4(13)-PV family showed to depend on: *i*) peptide aminoacid sequence, which drives peptide-membrane interactions, membrane destabilization and formation of nonlamellar phases; *ii*) peptide His content, which impacts on nucleic acid endosomal escape
Thermo-responsive copolymer-based	• Relative proportions of cationic and thermoresponsive blocks	• Complexes formed with the copolymer with LCST at 37 °C are the most efficient in mediating gene silencing.	• Transfection efficiency of polyplexes can be enhanced by modulating structural properties of the thermoresponsive polymer in order to obtain efficient nucleic acid complexation at room temperature and high dissociation at physiological temperatures.

These studies also allowed defining critical aspects that should be taken into consideration in the formulation of gene delivery systems, such as their capacity to interact with membranes, thus providing data to reinforce the importance of membrane interactions in determining the mechanisms by which delivery systems are taken up by cells and reach their target organelle.

In fact, a variety of pathways may be used by cells to internalize nucleic acid complexes, leading to more or less efficient transfection depending on an intricate set of circumstances, which ensure or avoid the intracellular trafficking of complexes or their cargo to the target organelle. Our results clearly showed that several mechanisms are available in the same type of cells to internalize different nucleic acid delivery systems and complexes with similar composition but different transfection efficiency are taken up through different pathways in the same cell type. These results pointed to the possibility of manipulating formulations in order to optimize intracellular delivery under a specific set of *in vitro* conditions, which, however, may not work equally well for different cells or cells integrated in the living organism, thus significantly hindering clinical applications. Therefore, a long way can be anticipated for developing new gene delivery systems endowed with properties that ensure their efficiency in transfection, such as those allowing to a precise and universal control of the endocytosis pathway, which may involve functionalizing the delivery systems with receptor-specific ligand moieties. Our results suggested that the physicochemical characteristics of the complexes, namely size and surface charge, are important parameters that dictate their cellular processing. On the other hand, it is expectable that the presence of chemical groups recognized by membrane receptors and intracellular transporters have an increased impact on the fate of nucleic acid complexes inside the cell (Georgieva et al., 2011). An alternative means of addressing gene delivery systems to the target cells or the target intracellular organelle consists of developing complexes with certain surface characteristics that make them able to interact selectively with lipid membranes of specific composition. Cardiolipin, the mitochondria lipid trademark, has been used as target for drugs and nanoparticles intended to enter mitochondria. Consistently, we have observed that gemini-based gene carriers that strongly interact with cardiolipin-containing membrane models succeeded in delivering mtpDNA into mitochondria. The differential lipid composition of diseased vs. healthy cells could also contribute to the design of gene delivery systems towards specific targets. In particular, cancer cells and tissues present several characteristics that suit specific targeting. Besides the particular lipid and protein composition of the cytoplasmic membranes, the lack of lymphatic drainage and the enhanced permeation and retention (EPR) effect, which characterizes the highly permeable tumor vasculature (pore sizes 400–800 vs. 5–10

nm), allow colloidal systems to extravasate across tumor vasculature while being unable to enter healthy tissue (Abulateefeh et al. 2011). Together, these characteristics make cancer cells particularly susceptible to gene delivery strategies, allowing to reducing the doses of complexes to be administered and, consequently, cytotoxicity.

After cellular internalization, nucleic acids or the corresponding complexes are actively transported through the cytoplasm, a process mediated by the microtubule network (Won et al. 2009). However, the small functional size of the nuclear pore complex (≈ 10 nm) of a non-dividing ("postmitotic") cell poses an important barrier to the nuclear import of complexes (or DNA) (Won et al. 2009). Complexes favor DNA nuclear import presumably due to the reduced size of DNA upon complexation with polycations. In this regard, it would be interesting to study in detail the stages of intracellular trafficking and the process of complex dissociation, since premature decompression of DNA can result in a less efficient nuclear uptake. In addition, tracking the fate of the components resulting from complex dissociation and their metabolites, which can be kept inside the cells or secreted to the extracellular medium, would enable the determination of the nature of the cytotoxicity mechanisms.

Overall, an important driving force behind all types of nonviral gene delivery systems (gemini surfactant-based, cell-penetrating peptide-based and thermoresponsive polymer-based systems, included) seems to reside in their ability to undergo a structural or conformational change in physiological conditions. This alteration can occur upon selective interaction with cell membranes, or in response to a stimulus, such as pH, oxidative/reductive environment or temperature. The conformational change should be triggered in order to allow nucleic acid release near the appropriate target.

Considering that humans have over 220 distinct cell types and the success of nucleic acid delivery varies from one cell type to another, ingenious approaches should be needed to devise synthetic, highly efficient materials with tunable selectivity for the different types of cells. In conclusion, there is still much work to be done towards a future precise molecular therapy for life-threatening diseases, but we believe that great strides are being made in this direction based on the development of nonviral delivery systems.

References

References

Abes, S. et al., 2006a. Vectorization of morpholino oligomers by the (R-Ahx-R)4 peptide allows efficient splicing correction in the absence of endosomolytic agents. *Journal of Controlled Release*, 116(3), 304–13.

Abes, S., Williams, D., et al., 2006b. Endosome trapping limits the efficiency of splicing correction by PNA-oligolysine conjugates. *Journal of Controlled Release*, 110(3), 595–604.

Abulateefeh, S. R., Spain, S. G., Aylott, J. W., Chan, W. C., Garnett, M. C., & Alexander, C., 2011. Thermoresponsive polymer colloids for drug delivery and cancer therapy. *Macromolecular Bioscience*, *11*(12), 1722–34.

Akbar, J., Tavakoli N., Marangoni D.G., Wettig, S.D., 2012. Mixed aggregate formation in gemini surfactant/1,2-dialkyl-sn-glycero-3-phosphoethanolamine systems. *Journal of Colloid and Interface Science*, 377, 237-43.

Alami, E., Levy, H. & Zana, R., 1993. Alkanediyl-a,o-bis(dimethylalky1ammonium bromide) Surfactants. 2. Structure of the Lyotropic Mesophases in the Presence of Water. *Langmuir*, 9, 940–4.

Aleandri, S. et al., 2013. Fusion of gemini based cationic liposomes with cell membrane models: Implications for their biological activity. *Biochimica et Biophysica Acta*, 1828(2), 382–90.

Alexander, C., 2006. Temperature- and pH-responsive smart polymers for gene delivery. *Expert Opinion on Drug Delivery*, 3(5), 573–81.

Almeida, J.A.S. et al., 2010. The effect of cationic gemini surfactants upon lipid membranes. An experimental and molecular dynamics simulation study. *Physical Chemistry Chemical Physics.*, 12(43), 14462–76.

Almeida, J.A.S. et al., 2011. Dicationic alkylammonium bromide gemini surfactants. Membrane perturbation and skin irritation. *PloS One*, 6(11), p.e26965.

Altieri, D.C., 2008. New wirings in the Survivin Networks. *Oncogene*, 27(48), 6276–84.

Alves, I.D. et al., 2008. Membrane interaction and perturbation mechanisms induced by two cationic cell penetrating peptides with distinct charge distribution. *Biochimica et Biophysica Acta*, 1780, 948–59.

Alves, I.D. et al., 2009. The interaction of cell-penetrating peptides with lipid model systems and subsequent lipid reorganization: thermodynamic and structural characterization. *Journal of Peptide Science*, 15, 200–9.

Åmand, H.L., Nordén, B. & Fant, K., 2012. Functionalization with C-terminal cysteine enhances transfection efficiency of cell-penetrating peptides through dimer formation. *Biochemical and Biophysical Research Communications*, 418(3), 469–74.

Anderson, S. et al., 1981. Sequence and Organization of the Human Mitochondrial Genome. *Nature*, 290, 457–65.

Andrich, M. P., & Vanderkooi, J. M., 1976. Temperature dependence of 1,6-diphenyl-1,3,5-hexatriene fluorescence in phospholipid artificial membranes. *Biochemistry*, *15*(6), 1257–61.

Arduíno, D. et al., 2012. Mitochondrial Metabolism in Parkinson's Disease Impairs Quality Control Autophagy by Hampering Microtubule-Dependent Traffic. *Human Molecular Genetics*, 21(21), 4680–702.

Arsov, Z. et al., 2008. Cholesterol prevents interaction of the cell-penetrating peptide transportan with model lipid membranes. *Journal of Peptide Science*, 14, 1303–8.

Badea, I. et al., 2005. In vivo cutaneous interferon-gamma gene delivery using novel dicationic (gemini) surfactant-plasmid complexes. *Journal of Gene Medicine*, 7, 1200–14.

Badea, I. et al., 2007. Topical non-invasive gene delivery using gemini nanoparticles in interferon-gamma-deficient mice. *Eur. J. Pharm. Biopharm.*, 65(3), 414–22.

Badr, E.E., Kandeel, E.M. & El-Sadek, B.M., 2010. Novel gemini cationic surfactants based on N, N-dimethyl fatty hydrazide and 1,3-dibromopropane: synthesis, evaluation of surface and antimicrobial properties. *Journal of Oleo Science*, 59(12), 647–52.

Bajaj, A., Kondaiah, P. & Bhattacharya, S., 2007. Synthesis and gene transfer activities of novel serum compatible cholesterol-based gemini lipids possessing oxyethylene-type spacers. *Bioconjugate Chemistry*, 18(5), 1537–46.

Bajaj, A., Kondaiah, P. & Bhattacharya, S., 2008a. Effect of the nature of the spacer on gene transfer efficacies of novel thiocholesterol derived gemini lipids in different cell lines: a structure-activity investigation. *Journal of Medicinal Chemistry*, 51(8), 2533–40.

Bajaj, A., Paul, B., et al., 2008b. Structure-activity investigation on the gene transfection properties of cardiolipin mimicking gemini lipid analogues. *Bioconjugate Chemistry*, 19(6), 1283–300.

Baker, a et al., 1997. Polyethylenimine (PEI) is a simple, inexpensive and effective reagent for condensing and linking plasmid DNA to adenovirus for gene delivery. *Gene Therapy*, 4(8), 773–82.

Balazs, D. A. & Godbey, W.T., 2011. Liposomes for use in gene delivery. *Journal of Drug Delivery*, Article ID 326497, 12 pages.

Barenholz, Y., 2001. Liposome application: problems and prospects. *Current Opinion in Colloid & Interface Science*, 6(1), 66–77.

Bartlett, G.R., 1958. Phosphorus Assay in Column Chromatrography. *The Journal of Biological Chemistry*, 234(3), 466–8.

Bell, P.C. et al., 2003. Transfection mediated by gemini surfactants: engineered escape from the endosomal compartment. *Journal of the American Chemical Society*, 125(6), 1551–8.

Beltrami, E. et al., 2004. Acute ablation of survivin uncovers p53-dependent mitotic checkpoint functions and control of mitochondrial apoptosis. *The Journal of Biological Chemistry*, 279(3), 2077–84.

Bhattacharya, S. & De, S., 1999. Synthesis and Vesicle Formation from Dimeric Pseudoglyceryl Lipids with (CH2)m Spacers: Pronounced m-Value Dependence of Thermal Properties, Vesicle Fusion, and Cholesterol Complexation. *Chemistry: A European Journal*, 5(8), 2335–47.

Birmingham, A. et al., 2006. 3' UTR seed matches, but not overall identity, are associated with RNAi off-targets. *Nature Methods*, 3(3), 199–204.

Blunk, D. et al., 2006. New speciality surfactants with natural structural motifs. *New Journal of Chemistry*, 30(12), 1705-17.

Boddapati, S. V. et al., 2005. Mitochondriotropic Liposomes. *Journal of Liposome Research*, 15(1), 49–58.

Bombelli, C., Faggioli, F., et al., 2005a. Efficient transfection of DNA by liposomes formulated with cationic gemini amphiphiles. *Journal Medicinal Chemistry*, 48(16), 5378–82.

Bombelli, C., Borocci, S., et al., 2005b. Role of the spacer of cationic gemini amphiphiles in the condensation of DNA. *Langmuir*, 21(23), 10271–4.

Bottcher, C. J. F., van Gent, C. M., & Pries, C., 1961. A rapid and sensitive sub-micro phosphorus determination. *Analytica Chimica Acta*, 24, 203–4.

Boussif, O. et al., 1995. A versatile vector for gene and oligonucleotide transfer into cells in culture and in vivo: polyethylenimine. *Proceedings of the National Academy of Sciences of the United States of America*, 92(16), 7297–301.

Brito, R.O. et al., 2006. Self-assembly in a catanionic mixture with an aminoacid-derived surfactant: from mixed micelles to spontaneous vesicles. *The Journal of Physical Chemistry. B*, 110(37), 18158–65.

Brito, R. O., Oliveira, I. S., Araújo, M. J., & Marques, E. F., 2013. Morphology, thermal behavior, and stability of self-assembled supramolecular tubules from lysine-based surfactants. *The Journal of Physical Chemistry B*, *117*(32), 9400–11.

Brower, V., 2010. RNA Interference Advances to Early-Stage Clinical Trials. *Journal of the National Cancer Institute*, 102(19), 1459–61.

Buijnsters, P.J.J.A. et al., 2002. Cationic Gemini Surfactants Based on Tartaric Acid: Synthesis, Aggregation, Monolayer Behaviour, and Interaction with DNA. *European Journal of Organic Chemistry*, (8), 1397–406.

Bunton, C. et al., 1971. Catalysis of Nucleophilic Substitutions by Micelles of Dicationic Detergents. *Journal of Organic Chemistry*, 36(16), 2346–50.

Burrows, H.D. et al., 2007. Interplay of electrostatic and hydrophobic effects with binding of cationic gemini surfactants and a conjugated polyanion: experimental and molecular modeling studies. *Journal of Physical Chemistry B*, 111(17), 4401–10.

Calejo, M.T., Sande, S.A. & Nyström, B., 2013a. Thermoresponsive polymers as gene and drug delivery vectors: architecture and mechanism of action. *Expert Opinion on Drug Delivery*, 10(12), 1669–86.

Calejo, M.T. et al., 2013b. Temperature-responsive cationic block copolymers as nanocarriers for gene delivery. *International Journal of Pharmaceutics*, 448(1), 105–14.

Camilleri, P. et al., 2000. A novel class of cationic gemini surfactants showing efficient in vitro gene transfection properties. *Chemical Communications*, 29712(14), 1253–4.

Caplen, N.J., 2004. Gene therapy progress and prospects. Downregulating gene expression: the impact of RNA interference. *Gene therapy*, 11(16), 1241–8.

Cardoso, A. L. C., et al., 2007. siRNA delivery by a transferrin-associated lipid-based vector : a non-viral strategy to mediate gene silencing. *The Journal of Gene Medicine*, *9*, 170–83.

Cardoso, A.L.C. et al., 2008. Tf-lipoplexes for neuronal siRNA delivery: a promising system to mediate gene silencing in the CNS. *Journal of Controlled Release*, 132(2), 113–23.

Cardoso, A. et al., 2009. Targeted Lipoplexes for siRNA Delivery. *Methods in Enzymology*, 465(09), 267–87.

Cardoso, A., Trabulo, S., Moreira, J. N., Duzgunes, N., & Pedroso de Lima, M. C. (2009). Targeted Lipoplexes for siRNA Delivery. *Methods in Enzymology*, *465*(09), 267–87.

Cardoso, A.L. et al., 2012. miR-155 modulates microglia-mediated immune response by down-regulating SOCS-1 and promoting cytokine and nitric oxide production. *Immunology*, 135(1), 73–88.

Cardoso, A.M.S. et al., 2011. Gemini surfactant dimethylene-1,2-bis(tetradecyldimethyl-ammonium bromide)-based gene vectors: a biophysical approach to transfection efficiency. *Biochimica et Biophysica Acta*, 1808(1), 341–51.

Cardoso, A.M. et al., 2013. Comparison of the Efficiency of Complexes Based on S4(13)-PV Cell-Penetrating Peptides in Plasmid DNA and siRNA Delivery. *Molecular Pharmaceutics*, 10, 2653–66.

Cardoso, A. M. et al., 2014. Bis-quaternary gemini surfactants as components of nonviral gene delivery systems: A comprehensive study from physicochemical properties to membrane interactions. *International Journal of Pharmaceutics*, *474*(1-2), 57–69.

Carl R, M., Mark R, G. & John C, P., 1971. Bacterial virus gene expression in human cells. *Nature*, 233(5319), 398–400.

Carpino, L.A. et al., 2003. Rapid, Continuous Solution-Phase Peptide Synthesis: Application to Peptides of Pharmaceutical Interest. *Organic Process Research & Development*, 7(1), 28–37.

Carver, E R, Blout, J.P., 1967. Polypeptide models for collagen. In G. N. Ramachandran, ed. *Treatise on Collagen* (p.441–523) London: Academic Press.

Castellani, R. et al., 2002. Role of mitochondrial dysfunction in Alzheimer's disease. *Journal of Neuroscience Research*, 70(3), 357–60.

Check, E., 2005. Gene therapy put on hold as third child develops cancer. *Nature*, 433, p.561.

Chen, L. A., Dale, R. E., Roth, S., & Brand, L., 1977. Nanosecond Time-dependent Fluorescence Diphenylhexatriene in Dimyristoyllecithin Determination of "Microviscosity ." *The Journal of Biological Chemistry*, *252*(7), 2163–9.

Chen, X. et al., 2009. The structure of detergent-resistant membrane vesicles from rat brain cells. *Biochimica et biophysica acta*, 1788(2), 477–83.

Chinnery, P.F. et al., 1999. Peptide nucleic acid delivery to human mitochondria. *Gene therapy*, 6(12), 1919–28.

Chrzanowska-Lightowlers, Z.M. et al., 1999. Conversion of a reporter gene for mitochondrial gene expression using iterative mega-prime PCR. *Gene*, 230(2), 241–7.
Collins, J.M. & Leadbeater, N.E., 2007. Microwave energy: a versatile tool for the biosciences. *Organic & Biomolecular Chemistry*, 5, 1141–50.
Colomer, A. et al., 2011. Cationic surfactants derived from lysine: effects of their structure and charge type on antimicrobial and hemolytic activities. *Journal of Medicinal Chemistry*, 54(4), 989–1002.
Conner, S.D. & Schmid, S.L., 2003. Regulated portals of entry into the cell. *Nature*, 422(6927), 37–44.
Crombez, L. et al., 2008. Peptide-Based Nanoparticle for Ex Vivo and In Vivo Dug Delivery. *Current Pharmaceutical Design*, 14(34), 3656–65.
Crombez, L. et al., 2009. A new potent secondary amphipathic cell-penetrating peptide for siRNA delivery into mammalian cells. *Molecular Therapy*, 17(1), 95–103.
da Cruz, M.T. et al., 2001. Kinetic analysis of the initial steps involved in lipoplex--cell interactions: effect of various factors that influence transfection activity. *Biochimica et biophysica acta*, 1510(1-2), 136–51.
Cullen, B.R., 2004. Transcription and processing of human microRNA precursors. *Molecular Cell*, 16(6), 861–5.
Damen, M. et al., 2010. Delivery of DNA and siRNA by novel gemini-like amphiphilic peptides. *Journal of Controlled Release*, 145(1), 33–9.
Danner, S. et al., 2008. Structure and thermotropic behavior of the Staphylococcus aureus lipid lysyl-dipalmitoylphosphatidylglycerol. *Biophysical Journal*, 94(6), 2150–9.
Dauty, E. et al., 2001. Dimerizable Cationic Detergents with a Low cmc Condense Plasmid DNA into Nanometric Particles and Transfect Cells in Culture. *Journal of the American Chemical Society*, 123(38), 9227–34.
Dedinaite, A. et al., 2010. Friction in aqueous media tuned by temperature-responsive polymer layers. *Soft Matter*, 6, 2489–98.
Dennison, S.R. et al., 2007. Interactions of cell penetrating peptide Tat with model membranes: a biophysical study. *Biochemical and Biophysical Research Communications*, 363(1), 178–82.
Derossi, D. et al., 1994. The third helix of the Antennapedia homeodomain translocates through biological membranes. *The Journal of biological chemistry*, 269(14), 10444–50.
Derossi, D., Chassaing, G. & Prochiantz, A., 1998. Trojan peptides: the penetratin system for intracellular delivery. *Trends in Cell Biology*, 8(2), 84–7.
Deshayes, S. et al., 2004. Primary Amphipathic Cell-Penetrating Peptides: Structural Requirements and Interactions with Model Membranes†. *Biochemistry*, 43(24), 7698–706.
DiMauro, S. & Schon, E.A, 2001. Mitochondrial DNA mutations in human disease. *American Journal of Medical Genetics*, 106(1), 18–26.
Ding, M. et al., 2011. Cellular uptake of polyurethane nanocarriers mediated by gemini quaternary ammonium. *Biomaterials*, 32(35), 9515–24.
Dohi, T. et al., 2004. Mitochondrial survivin inhibits apoptosis and promotes tumorigenesis. *The Journal of Clinical Investigation*, 114(8), 1117–27.
Donkuru, M. et al., 2010. Advancing nonviral gene delivery: lipid- and surfactant-based nanoparticle design strategies. *Nanomedicine*, 5(7), 1103–27.
van Doren, H. a. et al., 2000. Mesogenic sugars. From aldoses to liquid crystals and surfactants. *Chemical Society Reviews*, 29(3), 183–99.
Doyle, S.R. & Chan, C.K., 2008. Mitochondrial gene therapy: an evaluation of strategies for the treatment of mitochondrial DNA disorders. *Human Gene Therapy*, 19(12), 1335–48.
D'Souza, G.G.M. et al., 2003. DQAsome-mediated delivery of plasmid DNA toward mitochondria in living cells. *Journal of Controlled Release*, 92(1-2), 189–97.
Dunlap, D.D. et al., 1997. Nanoscopic structure of DNA condensed for gene delivery. *Nucleic Acids Research*, 25(15), 3095–101.

Duzgunes, N., Simões, S., Lopez-Mesas, M., & Pedroso de Lima, M. C., 2007. Intracellular Delivery of Therapeutic Oligonucleotides in pH-Sensitive and Cationic Liposomes. In G. Gregoriadis (Ed.), *Liposome Technology: Interaction of Liposomes with the Biological Milieu* (3rd ed., pp. 253–275). New York: Informa Healthcare.

Eguchi, A. & Dowdy, S.F., 2009. siRNA delivery using peptide transduction domains. *Trends in Pharmacological Sciences*, 30(7), 341–5.

Elbashir, S.M. et al., 2001. Duplexes of 21-nucleotide RNAs mediate RNA interference in cultured mammalian cells. *Nature*, 411, 494–8.

El-Sayed, A. & Harashima, H., 2013. Endocytosis of gene delivery vectors: from clathrin-dependent to lipid raft-mediated endocytosis. *Molecular Therapy*, 21(6), 1118–30.

Evans, E. & Needham, D., 1987. Physical properties of surfactant bilayer membranes: thermal transitions, elasticity, rigidity, cohesion and colloidal interactions. *The Journal of Physical Chemistry*, 91(16), 4219–28.

Fan, H. et al., 2008. Active control of surface properties and aggregation behavior in amino acid-based Gemini surfactant systems. *Journal of Colloid and Interface Science*, 321(1), 227–34.

Faneca, H., Simões, S. & de Lima, M.C.P., 2002. Evaluation of lipid-based reagents to mediate intracellular gene delivery. *Biochimica et Biophysica Acta*, 1567(1-2), 23–33.

Faneca, H., Simões, S. & Pedroso de Lima, M.C., 2004. Association of albumin or protamine to lipoplexes: enhancement of transfection and resistance to serum. *The Journal of Gene Medicine*, 6(6), 681–92.

Feigenson, G.W., 2006. Phase behavior of lipid mixtures. *Nat. Chem. Biol.*, 2(11), 560–3.

Felgner, P.L. et al., 1987. Lipofection: a highly efficient, lipid-mediated DNA-transfection procedure. *Proceedings of the National Academy of Sciences of the United States of America*, 84(21), 7413–7.

Fields, G.B. & Noble, R.L., 1990. Solid phase peptide synthesis utilizing 9-fluorenylmethoxycarbonyl amino acids. *International Journal of Peptide and Protein Research*, 35, 161–214.

Fire, A. et al., 1998. Potentandspecific genetic interference by double-stranded RNA in Caenorhabditis elegans. *Nature Letters*, 391, 806–11.

Fischer, A., Hacein-Bey, S. & Cavazzana-Calvo, M., 2002. Gene therapy for severe combined immunodeficiencies. *Nature Reviews: Immunology*, 2, 615–21.

Foldvari, M. et al., 2006. Structural characterization of novel gemini non-viral DNA delivery systems for cutaneous gene therapy. *Journal of Experimental Nanoscience*, 1(2), 165–76.

Fonseca, S.B., Pereira, M.P. & Kelley, S.O., 2009. Recent advances in the use of cell-penetrating peptides for medical and biological applications. *Advanced Drug Delivery Reviews*, 61, 953–64.

de Fougerolles, A. et al., 2007. Interfering with disease: a progress report on siRNA-based therapeutics. *Nature Reviews Drug Discovery*, 6, 443–54.

de Fougerolles, A.R., 2008. Delivery vehicles for small interfering RNA in vivo. *Human Gene Therapy*, 19, 125–32.

Frankel, A.D. & Pabo, C.O., 1988. Cellular uptake of the tat protein from human immunodeficiency virus. *Cell*, 55, 1189–93.

Frindi, M. & Michels, B., 1994. Alkanediyl-alpha,omega-bis(dimethylalkylammonium bromide) Surfactants. 4. Ultrasonic Absorption Studies of Amphiphile Exchange between Micelles and Bulk Phase in Aqueous Micellar Solutions. *Langmuir*, 10, 1140–5.

Fuller, S. et al., 1996. Thermotropic and Lyotropic Mesophase Behavior of Amphitropic Diammonium Surfactants. *Langmuir*, 12(3), 1117–23.

Gabrielson, N.P. & Pack, D.W., 2009. Efficient polyethylenimine-mediated gene delivery proceeds via a caveolar pathway in HeLa cells. *Journal of Controlled Release*, 136(1), 54–61.

Garnon, J. et al., 2005. Fragile X-related protein FXR1P regulates proinflammatory cytokine tumor necrosis factor expression at the post-transcriptional level. *The Journal of Biological Chemistry*, 280(7), 5750–63.
Gavrilov, K. & Saltzman, W.M., 2012. Therapeutic siRNA: Principles, challenges, and Strategies. *Yale Journal of Biology and Medicine*, 85, 187–200.
Gennis, R.B., 1989. *Biomembranes: Molecular Structure and Function* 1st ed. C. R. Cantor, ed., New York: Springer-Verlag.
Georgieva, J. V. et al., 2011. Surface characteristics of nanoparticles determine their intracellular fate in and processing by human blood-brain barrier endothelial cells in vitro. *Molecular Therapy*, *19*(2), 318–25.
Gerbal-Chaloin, S. et al., 2007. First step of the cell-penetrating peptide mechanism involves Rac1 GTPase-dependent actin-network remodelling. *Biology of the Cell,* 99(4), 223–38.
Glover, D.J., Lipps, H.J. & Jans, D. A, 2005. Towards safe, non-viral therapeutic gene expression in humans. *Nature Reviews. Genetics*, 6(4), 299–310.
Grayson, A.C.R., Doody, A.M. & Putnam, D., 2006. Biophysical and structural characterization of polyethylenimine-mediated siRNA delivery in vitro. *Pharmaceutical Research*, 23(8), 1868–76.
Griffiths, P.C. et al., 2008. Physicochemical Characterization of Thermoresponsive Poly(N-isopropylacrylamide)-poly(ethylene imine) Graft Copolymers. *Biomacromolecules*, 9, 1170–8.
Grigoriev, I. V et al., 2012. Cationic gemini surfactants as new agents for plasmid DNA delivery into cells. *Doklady Biochemistry and Biophysics*, 445(3), 197–9.
Grosmaire, L. et al., 2002. Alkanediyl-α,ω-bis(dimethylalkylammonium bromide) surfactants 9. Effect of the spacer carbon number and temperature on the enthalpy of micellization. *Journal of Colloid and Interface Science*, 246(1), 175–81.
Groth, C. et al., 2004. Kinetics of the self-assembly of gemini surfactants. *Journal of Surfactants and Detergents*, 7(3), 247–55.
Guo, J. et al., 2010. Therapeutic targeting in the silent era: advances in non-viral siRNA delivery. *Molecular BioSystems*, 6, 1143–61.
Guterstam, P. et al., 2009. Elucidating cell-penetrating peptide mechanisms of action for membrane interaction, cellular uptake, and translocation utilizing the hydrophobic counter-anion pyrenebutyrate. *Biochimica et Biophysica Acta*, 1788(12), 2509–17.
Hacein-bey-Abina, S. & Schmidt, M., 2003. A Serious Adverse Event after Successful Gene Therapy for X-Linked Severe Combined Immunodeficiency. *The New England Journal of Medicine*, 384, 255–66.
Hallock, K. et al., 2002. Membrane Composition Determines Pardaxin's Mechanism of Lipid Bilayer Disruption. *Biophysical Journal*, 83(2), 1004–13.
Hannon, G.J., 2002. RNA interference. *Nature*, 418, 24–6.
Hannon, G.J. & Rossi, J.J., 2004. Unlocking the potential of the human genome with RNA interference. *Nature*, 431(7006), 371–8.
Hariton-Gazal, E. et al., 2002. Targeting of nonkaryophilic cell-permeable peptides into the nuclei of intact cells by covalently attached nuclear localization signals. *Biochemistry*, 41(29), 9208–14.
He, L. & Hannon, G.J., 2004. MicroRNAs: small RNAs with a big role in gene regulation. *Nature reviews. Genetics*, 5(7), 522–31.
Heitz, F., Morris, M.C. & Divita, G., 2009. Twenty years of cell-penetrating peptides: from molecular mechanisms to therapeutics. *British Journal of Pharmacology*, 157, 195–206.
Hillaireau, H. & Couvreur, P., 2009. Nanocarriers' entry into the cell: relevance to drug delivery. *Cellular and Molecular Life Sciences*, 66(17), 2873–96.
Hinrichs, W.L. et al., 1999. Thermosensitive polymers as carriers for DNA delivery. *Journal of Controlled Release*, 60(2-3), 249–59.
Hoekstra, D. et al., 2007. Gene delivery by cationic lipids: in and out of an endosome. *Biochemical Society Transactions*, 35(Pt 1), 68–71.

Hoffman, W.H. et al., 2002. Transcriptional repression of the anti-apoptotic survivin gene by wild type p53. *The Journal of Biological Chemistry*, 277(5), 3247–57.
Hoque, J. et al., 2012. Cleavable cationic antibacterial amphiphiles: synthesis, mechanism of action, and cytotoxicities. *Langmuir*, 28(33), 12225–34.
Horobin, R.W., Trapp, S. & Weissig, V., 2007. Mitochondriotropics: a review of their mode of action, and their applications for drug and DNA delivery to mammalian mitochondria. *Journal of Controlled Release*, 121(3), 125–36.
Howell, N., 1999. Human Mitochondrial Diseases: Answering Questions and Questioning Answers. *International Review of Cytology*, 186(409), 49–116.
Hruby, M. et al., 2011. Thermoresponsive polymeric radionuclide delivery system-an injectable brachytherapy. *European Journal of Pharmaceutical Sciences*, 42(5), 484–8.
Hui, S.W. et al., 1996. The Role of Helper Lipids in Cationic Liposome-Mediated Gene Transfer. *Biophysical Journal*, 71, 590–9.
Ibrahim, N. et al., 2011. DNA delivery to mitochondria: sequence specificity and energy enhancement. *Pharmaceutical Research*, 28(11), 2871–82.
Ilekti, P. et al., 1999. Effects of Polyelectrolytes on the Structures and Interactions of Surfactant Aggregates. *The Journal of Physical Chemistry B*, 103(45), 9831–40.
Ilies, M. A., et al., 2006. Lipophilic pyrylium salts in the synthesis of efficient pyridinium-based cationic lipids, gemini surfactants, and lipophilic oligomers for gene delivery. *Journal Medicinal Chemistry*, *49*(13), 3872–87.
In, M. & Zana, R., 2007. Phase Behavior of Gemini Surfactans. *Journal of Dispersion Science and Technology*, 28, 143–54.
Jackson, A.L. et al., 2006. Widespread siRNA "'off-target'" transcript silencing mediated by seed region sequence complementarity. *RNA*, 12, 1179–87.
Jain, S. & Bates, F.S., 2003. On the Origins of Morphological Complexity in Block Copolymer Surfactants. *Science*, 300(5618), 460–4.
Jeong, G.-J. et al., 2007. Biodistribution and tissue expression kinetics of plasmid DNA complexed with polyethylenimines of different molecular weight and structure. *Journal of Controlled Release,* 118(1), 118–25.
Jiang, N. et al., 2004. Micellization of Cationic Gemini Surfactants with Various Counterions and Their Interaction with DNA in Aqueous Solution. The *Journal of Physical Chemistry B*, 108, 15385–91.
Jinek, M. & Doudna, J.A, 2009. A three-dimensional view of the molecular machinery of RNA interference. *Nature*, 457(7228), 405–12.
Joanne, P. et al., 2009. Lipid reorganization induced by membrane-active peptides probed using differential scanning calorimetry. *Biochimica et Biophysica Acta*, 1788, 1772–81.
Johnsson, M. et al., 2003. Sugar-Based Gemini Surfactants with pH-Dependent Aggregation Behavior: Vesicle-to-Micelle Transition, Critical Micelle Concentration, and Vesicle Surface Charge Reversal. *Langmuir*, 19(11), 4609–18.
Joliot, A. et al., 1991. Antennapedia homeobox peptide regulates neural morphogenesis. *Proceedings of the National Academy of Sciences of the United States of America*, 88, 1864–8.
Jurado, A.S., Pinheiro, T.J. & Madeira, V.M., 1991. Physical studies on membrane lipids of Bacillus stearothermophilus temperature and calcium effects. *Archives of Biochemistry and Biophysics*, 289(1), 167–79.
Kabir-ud-Din, Koya, P.A. & Khan, Z.A., 2010. Conductometric studies of micellization of gemini surfactant pentamethylene-1,5-bis(tetradecyldimethylammonium bromide) in water and water-organic solvent mixed media. *Journal of Colloid and Interface Science*, 342(2), 340–7.
Kappler, M. et al., 2005. Radiosensitization, after a combined treatment of survivin siRNA and irradiation, is correlated with the activation of caspases 3 and 7 in a wt-p53 sarcoma cell line, but not in a mt-p53 sarcoma cell line. *Oncology Reports*, 13, 167–72.
Karaborni, S. et al., 1994. Simulating the Self-Assembly of Gemini (Dimeric) Surfactants. *Science*, 266, 254–6.

Karlsson, L., van Eijk, M.C.P. & Söderman, O., 2002. Compaction of DNA by gemini surfactants: effects of surfactant architecture. *Journal of Colloid Interface Science*, 252(2), 290–6.

Khan, I.A., Mohammad, R. & Alam, M.S., 2010. Surface Properties and Mixed Micellization of Cationic Gemini Surfactants with Ethyleneamines. *Journal of Chemical & Engineering Data*, 55(1), 370–80.

Kim, B.-K. et al., 2011. Synthesis and Optimization of Cholesterol-Based Diquaternary Ammonium Gemini Surfactant (Chol-GS) as a New Gene Delivery Vector. *Journal of Microbiology and Biotechnology*, 21(1), 93–9.

Kim, C. et al., 2010. Thermally triggered cellular uptake of quantum dots immobilized with poly(N-isopropylacrylamide) and cell penetrating peptide. *Langmuir*, 26(18), 14965–9.

Kirby, A.J. et al., 2003. Gemini surfactants: new synthetic vectors for gene transfection. *Angew. Chem.*, 42(13), 1448–57.

Kjøniksen, A.-L. et al., 2009. Novel transition behavior in aqueous solutions of a charged thermoresponsive triblock copolymer. *Colloids and Surfaces A: Physicochemical and Engineering Aspects*, 333(1-3), 32–45.

Klijn, J.E. et al., 2006. pH-dependent phase behavior of carbohydrate-based gemini surfactants. Effect of the length of the hydrophobic spacer. *Journal of Physical Chemistry B*, 110(43), 21694–700.

Klijn, J.E. et al., 2007. pH-dependent phase behavior of carbohydrate-based gemini surfactants. The effects of carbohydrate stereochemistry, head group hydrophilicity, and nature of the spacer. *Journal of Physical Chemistry B*, 111(19), 5204–11.

Konopka, K. et al., 1996. Human immunodeficiency virus type-1 (HIV-1) infection encreases the sensitivity of macrophages and THP-1 cells to cytotoxicity by cationic liposomes. *Biochimica et Biophysica Acta*, 1312, 186–96.

Koppelhus, U. et al., 2002. Cell-dependent differential cellular uptake of PNA, peptides, and PNA-peptide conjugates. *Antisense Nucleic Acid Drug Development*, 12(2), 51-63.

Koulintchenko, M. et al., 2006. Natural competence of mammalian mitochondria allows the molecular investigation of mitochondrial gene expression. *Human Molecular Genetics*, 15(1), 143–54.

Koynova, R., Wang, L. & MacDonald, R.C., 2006. An intracellular lamellar-nonlamellar phase transition rationalizes the superior performance of some cationic lipid transfection agents. *Proceedings of the National Academy of Sciences of the United States of America*, 103(39), 14373–8.

Lamazière, A. et al., 2007. Non-metabolic membrane tubulation and permeability induced by bioactive peptides. *PloS one*, 2(2), e201.

Lamazière, A. et al., 2010. Lipid domain separation, bilayer thickening and pearling induced by the cell penetrating peptide penetratin. *Biochimica et Biophysica Acta*, 1798(12), 2223–30.

Langel, Ü. et al., 1996. A galanin-mastoparan chimeric peptide activates the Na+,K+-ATPase and reverses its inhibition by ouabain. *Regulatory Peptides*, 62(1), 47–52.

Lavigne, M.D. et al., 2007. Enhanced gene expression through temperature profile-induced variations in molecular architecture of thermoresponsive polymer vectors. *The Journal of Gene Medicine*, 9, 44–54.

Layn, K.M., Debenedetti, P.G. & Prud'homme, R.K., 1998. A theoretical study of Gemini surfactant phase behavior. *Journal of Chemical Physics*, 109(13), 5651-8.

Lee, M. et al., 2007. DNA delivery to the mitochondria sites using mitochondrial leader peptide conjugated polyethylenimine. *Journal of Drug Targeting*, 15(2), 115–22.

Lee, M., Choi, J.S. & Ko, K.S., 2008. Mitochondria targeting delivery of nucleic acids. *Expert Opinion on Drug Delivery*, 5(8), 879–87.

Lee, M.S. et al., 2013. Enhanced transfection by antioxidative polymeric gene carrier that reduces polyplex-mediated cellular oxidative stress. *Pharmaceutical Research*, 30(6), 1642–51.

Lehrman, S., 1999. Virus treatment questioned after gene therapy death. *Nature*, 401(6753), 517–8.
Lentz, B.R., 1989. Membrane "fluidity" as detected by diphenylhexatriene probes. *Chemistry and Physics of Lipids*, 50, 171–90.
Lewis, R. N., & Mannock, David & McElhaney, R. N., 1997. *Membrane Lipid Molecular Structure and Polymorphism*. In R. Epand (Ed.), Lipid Polymorphism and Membrane Properties (pp. 25–103). San Diego, California: Academic Press.
Li, F. et al., 1998. Control of apoptosis and mitotic spindle checkpoint by survivin. *Nature*, 396, 580–4.
Li, F. et al., 1999. Pleiotropic cell-division defects and apoptosis induced by interference with survivin function. *Nature Cell Biology*, 1, 461–6.
Li, F., 2003. Survivin study: what is the next wave? *Journal of Cellular Physiology*, 197(1), 8–29.
Li, S. & Huang, L., 2000. Nonviral gene therapy: promises and challenges. *Gene Therapy*, 7(1), 31–4.
Li, X. et al., 2005. Synthesis and solution properties of gemini surfactants containing oleyl chains. *Physical Chemistry Chemical Physics*, 7(17), 3172–8.
Liu, S. et al., 2013. A novel type of highly effective nonionic gemini alkyl O-glucoside surfactants: a versatile strategy of design. *Langmuir*, 29(27), 8511–6.
Liu, T. et al., 2006. Activation of Dual Apoptotic Pathways in Human Melanocytes and Protection by Survivin. *Journal of Investigative Dermatology*, 126(10), 2247–56.
Liu, Y. et al., 1997. Factors influencing the efficiency of cationic liposome-mediated intravenous gene delivery. *Nature Biotechnology*, 15(2), 167–73.
Lo, S.L. & Wang, S., 2008. An endosomolytic Tat peptide produced by incorporation of histidine and cysteine residues as a nonviral vector for DNA transfection. *Biomaterials*, 29, 2408–14.
Luciani, P. et al., 2007. Influence of the spacer of cationic gemini amphiphiles on the hydration of lipoplexes. *Biomacromolecules*, 8(6), 1999–2003.
Lúcio, M. et al., 2008. Binding of Nonsteroidal Anti-inflammatory Drugs to DPPC: Structure and Thermodynamic Aspects. *Langmuir*, 24(8), 4132–9.
Luckzynski, J. et al., 2012. Chemodegradble Gemini Alanine-based Cationic Surfactants: Synthesis and Anti-fungal Activity. *Chemistry Letters*, 41(10), 1176–7.
Lundberg, P. et al., 2007. Delivery of short interfering RNA using endosomolytic cell-penetrating peptides. *FASEB Journal*, 21(11), 2664–71.
Luzzati, V. et al., 1997. *Lipid polymorphism and membrane properties.* Academic P. R. Epand, ed., San Diego, California.
Lyrawati, D., Trounson, A. & Cram, D., 2011. Expression of GFP in the mitochondrial compartment using DQAsome-mediated delivery of an artificial mini-mitochondrial genome. *Pharmaceutical Research*, 28(11), 2848–62.
Manet, S. et al., 2010. Counteranion effect on micellization of cationic gemini surfactants 14-2-14: Hofmeister and other counterions. *Langmuir,* 26(13), 10645–56.
Mano, M. et al., 2005. On the mechanisms of the internalization of S4(13)-PV cell-penetrating peptide. *Biochemical Journal*, 390, 603–612.
Mano, M. et al., 2006. Cellular uptake of S4(13)-PV peptide occurs upon conformational changes induced by peptide–membrane interactions. *Biochimica et Biophysica Acta*, 1758, 336–46.
Mano, M. et al., 2007. Interaction of S4(13)-PV cell penetrating peptide with model membranes: relevance to peptide translocation across biological membranes. *Journal of Peptide Science*, 13, 301–13.
Masci, G., Ladogana, R.D. & Cametti, C., 2012. Assemblies of thermoresponsive diblock copolymers: micelle and vesicle formation investigated by means of dielectric relaxation spectroscopy. *The Journal of Physical Chemistry B*, 116(7), 2121–30.
Mason, P. A., 2003. Mismatch repair activity in mammalian mitochondria. *Nucleic Acids Research*, 31(3), 1052–8.

McGregor, C. et al., 2001. Rational approaches to the design of cationic gemini surfactants for gene delivery. *Journal of the American Chemical Society*, 123(26), 6215–20.
Meade, B.R. & Dowdy, S.F., 2008. Enhancing the cellular uptake of siRNA duplexes following noncovalent packaging with protein transduction domain peptides. *Advanced Drug Delivery Reviews*, 60(4-5), 530–6.
Mellott, A.J., Forrest, M.L. & Detamore, M.S., 2013. Physical non-viral gene delivery methods for tissue engineering. *Annals of Biomedical Engineering*, 41(3), 446–68.
Menger, F. & Littau, C., 1991. Gemini Surfactants: Synthesis and Properties. *Journal of the American Chemical Society*, 113(4), 1451–2.
Menger, F.M. & Littau, C.A., 1993. Gemini surfactants: a new class of self-assembling molecules. *Journal of the American Chemical Society*, 115(22), 10083–90.
Menger, F.M. & Keiper, J.S., 2000. Gemini Surfactants. *Angewandte Chemie*, 39, 1906–20.
Menger, F.M. & Mbadugha, B.N., 2001. Gemini surfactants with a disaccharide spacer. *Journal of the American Chemical Society*, 123(5), 875–85.
Mesri, M. et al., 2001. Cancer gene therapy using a survivin mutant adenovirus. *Journal of Clinical Investigation*, 108(7), 981–90.
Midoux, P. & Monsigny, M., 1999. Efficient gene transfer by histidylated polylysine/pDNA complexes. *Bioconjugate Chemistry*, 10(3), 406–11.
Milletti, F., 2012. Cell-penetrating peptides: classes, origin, and current landscape. *Drug Discovery Today*, 17(15–16), 850–60.
Misra, S.K. et al., 2013. Gene transfection in high serum levels: case studies with new cholesterol based cationic gemini lipids. *PloS One*, 8(7), p.e68305.
Mitchell, D.J. et al., 2000. Polyarginine enters cells more efficiently than other polycationic homopolymers. *The Journal of Peptide Research*, 56(5), 318–25.
Mohammed-Saeid, W. et al., 2012. Development of lyophilized gemini surfactant-based gene delivery systems: influence of lyophilization on the structure, activity and stability of the lipoplexes. *Journal of Pharmacy & Pharmaceutical Sciences*, 15(4), 548–67.
Molinaro, R. et al., 2013. Polyethylenimine and chitosan carriers for the delivery of RNA interference effectors. *Expert Opinion on Drug Delivery*, 10(12), 1653–68.
Morán, M. C., et al., 2004. "Green" amino acid-based surfactants. *Green Chemistry*, *6*(3), 233–40.
Morein, S. et al., 2000. The effect of peptide/lipid hydrophobic mismatch on the phase behavior of model membranes mimicking the lipid composition in Escherichia coli membranes. *Biophysical Journal*, 78(5), 2475–85.
Morris, M.C. et al., 1997. A new peptide vector for efficient delivery of oligonucleotides into mammalian cells. *Nucleic Acids Research*, 25(14), 2730–6.
Morris, M.C. et al., 2001. A peptide carrier for the delivery of biologically active proteins into mammalian cells. *Nature Biotechnology*, 19(12), 1173–6.
Morris, M.C., Deshayes, S., Heitz, F., 2008. Cell-penetrating peptides: from molecular mechanisms to therapeutics. *Biology of the Cell*, 100, 201–17.
Mountain, A., 2000. Gene therapy: the first decade. *Trends in Biotechnology*, 18(3), 119–28.
Mukhopadhyay, A. & Weiner, H., 2007. Delivery of drugs and macromolecules to mitochondria. *Advanced Drug Delivery Reviews*, 59(8), 729–38.
Muñoz-Morris, M.A. et al., 2007. The peptide carrier Pep-1 forms biologically efficient nanoparticle complexes. *Biochemical and Biophysical Research Communications*, 355(4), 877–82.
Muñoz-Úbeda, M. et al., 2012. How does the spacer length of cationic gemini lipids influence the lipoplex formation with plasmid DNA? Physicochemical and biochemical characterizations and their relevance in gene therapy. *Biomacromolecules*, 13(12), 3926–37.
Murata, M. et al., 2003. Novel DNA/Polymer conjugate for intelligent antisense reagent with improved nuclease resistance. *Bioorganic & Medicinal Chemistry Letters*, 13(22), 3967–70.

Muratovska, A. et al., 2001. Targeting peptide nucleic acid (PNA) oligomers to mitochondria within cells by conjugation to lipophilic cations: implications for mitochondrial DNA replication, expression and disease. *Nucleic Acids Research*, 29(9), 1852–63.

Murguía, M.C. et al., 2008. Synthesis, Surface-Active Properties, and Antimicrobial Activities of New Double-Chain Gemini Surfactants. *Journal of Oleo Science*, 57(5), 301–8.

Murphy, J. & Riley, J., 1962. A modified single solution method for the determination of phosphate in natural waters. *Analytica Chimica Acta*, 27, 31–6.

Nambi, P., Rowe, E.S. & McIntosh, T.J., 1988. Studies of the ethanol-induced interdigitated gel phase in phosphatidylcholines using the fluorophore 1,6-diphenyl-1,3,5-hexatriene. *Biochemistry*, 27(26), 9175–82.

Napoli, C., Lemieux, C. & Jorgensen, R., 1990. Introduction of a Chimeric Chalcone Synthase Gene into Petunia Results in Reversible Co-Suppression of Homologous Genes in trans. *The Plant Cell*, 2(4), 279–89.

Neves, S.S. et al., 2006. Transfection of oral cancer cells mediated by transferrin-associated lipoplexes: mechanisms of cell death induced by herpes simplex virus thymidine kinase/ganciclovir therapy. *Biochimica et biophysica acta*, 1758(11), 1703–12.

Nguyen, Q.N. et al., 2006. Light controllable siRNAs regulate gene suppression and phenotypes in cells. *Biochimica et Biophysica Acta*, 1758(3), 394–403.

Niidome, T. & Huang, L., 2002. Gene therapy progress and prospects: nonviral vectors. *Gene Therapy*, 9(24), 1647–52.

Obłąk, E. et al., 2013. Antifungal activity of gemini quaternary ammonium salts. *Microbiological Research*, 168(10), 630–8.

Obłąk, E. et al., 2014. Antibacterial activity of gemini quaternary ammonium salts. *FEMS Microbiology Letters*, 350(2), 190–8.

Oda, R., Candau, S.J. & Huc, I., 1997. Gemini surfactants, the effect of hydrophobic chain length and dissymmetry. *Chemical Communicaions*, (21), 2105–6.

Oda, R. et al., 1999. Elongated Aggregates Formed by Cationic Gemini Surfactants. *Langmuir*, 15(7), 2384–90.

Oh, Y.-K. & Park, T.G., 2009. siRNA delivery systems for cancer treatment. *Advanced Drug Delivery Reviews*, 61, 850–62.

Olie, R.A. et al., 2000. A Novel Antisense Oligonucleotide Targeting Survivin Expression Induces Apoptosis and Sensitizes Lung Cancer Cells to Chemotherapy. *Cancer Research*, 60, 2805–9.

Opalinska, J.B. & Gewirtz, A.M., 2002. Nucleic-acid therapeutics: basic principles and recent applications. *Nature Reviews. Drug discovery*, 1(7), 503–14.

Pabst, G. et al., 2007. On the propensity of phosphatidylglycerols to form interdigitated phases. *Biophysical Journal*, 93(2), 513–25.

Padari, K. et al., 2010. S4(13)-PV Cell-Penetrating Peptide Forms Nanoparticle-Like Structures to Gain Entry Into Cells. *Bioconjugate Chemistry*, 21(4), 774–83.

Pai, S.I. et al., 2006. Prospects of RNA interference therapy for cancer. *Gene Therapy*, 13, 464–77.

Palm-Apergi, C. et al., 2009. The membrane repair response masks membrane disturbances caused by cell-penetrating peptide uptake. *FASEB Journal*, 23(1), 214–23.

Pamies, R. et al., 2009. Thermal response of low molecular weight poly-(N-isopropylacrylamide) polymers in aqueous solution. *Polymer Bulletin*, 62(4), 487–502.

Panov, A. V et al., 2002. Early mitochondrial calcium defects in Huntington's disease are a direct effect of polyglutamines. *Nature Neuroscience*, 5(8), 731–6.

Patrizi, M.L. et al., 2009. Synthesis and association properties of thermoresponsive and permanently cationic charged block copolymers. *Polymer*, 50(2), 467–74.

Pedersen, T.B. et al., 2005. Phase behavior and nanoscale structure of phospholipid membranes incorporated with acylated C14-peptides. *Biophysical Journal*, 89(4), 2494–503.

Pedroso de Lima, M. C., Faneca, H., Mano, M., Penacho, N., Düzgüneş, N., & Simões, S., 2003. Biophysical characterization of cationic liposome-DNA complexes and their interaction with cells. *Methods in Enzymology*, *373*, 298–312.

Peetla, C., Stine, A. & Labhasetwar, V., 2009. Biophysical Interactions with Model Lipid Membranes: Applications in Drug Discovery and Drug Delivery. *Molecular Pharmaceutics*, 6(5), 1264–76.

Penacho, N. et al., 2008. Transferrin-associated lipoplexes as gene delivery systems: relevance of mode of preparation and biophysical properties. *Jounal of Membrane Biology*, 221(3), 141–52.

Peoples, R. W., Li, C., & Weight, F. F., 1996. Lipid vs protein theories of alcohol action in the nervous system. *Annual Review of Pharmacology and Toxicology*, *36*, 185–201.

Pérez, L. et al., 1996. Synthesis, Aggregation, and Biological Properties of a New Class of Gemini Cationic Amphiphilic Compounds from Arginine, bis (Args). *Langmuir*, 12(22), 5296–301.

Pérez, L. et al., 2002. Biological Properties of Arginine-based Gemini Cationic Surfactants. *Environmental Toxicology and Chemistry*, 21(6), 1279–85.

Pérez, L. et al., 2007. Investigation of the Micellization Process of Single and Gemini Surfactants from Arginine by SAXS , NMR Self-Diffusion , and Light Scattering. *Journal of Physical Chemistry*, 111, 11379–87.

Pérez, L. et al., 2014. Gemini surfactants from natural amino acids. *Advances in Colloid and Interface Science*, 205, 134–55.

Pfeifer, A. & Verma, I.M., 2001. Gene therapy: promises and problems. *Annual Review of Genomics and Human Genetics*, 2, 177–211.

Pfeiffer, T. et al., 2006. Lipoplex gene transfer of inducible nitric oxide synthase inhibits the reactive intimal hyperplasia after expanded polytetrafluoroethylene bypass grafting. *Journal of vascular surgery*, 43(5), 1021–7.

Pooga, M. et al., 1998. Cell penetration by transportan. *FASEB Journal*, 12(1), 67–77.

Prendergast, F. G., Haugland, R. P., & Callahan, P. J., 1981. 1-[4-(Trimethylamino)pheny1]-6-phenylhexa-1,3,5-triene: Synthesis, Fluorescence Properties, and use as a Fluorescence Probe of Lipid Bilayers. *Biochemistry*, *20*, 7333–8.

Prossnigg, F. et al., 2010. Packing behaviour of two predominant anionic phospholipids of bacterial cytoplasmic membranes. *Biophysical Chemistry*, 150(1-3), 129–35.

Rashid, F. & Horobin, R.W., 1990. Histochemistry Interaction of molecular probes with living cells and tissues. Part 2 A structure-activity analysis of mitochondrial staining by cationic probes, ans a discussion of the synergistic nature of image-based and biochemical approaches. *Histochemistry*, 94, 303–8.

Rejman, J. et al., 2004. Size-dependent internalization of particles via the pathways of clathrin- and caveolae-mediated endocytosis. *The Biochemical journal*, 377(Pt 1), 159–69.

Richard, J.P. et al., 2003. Cell-penetrating peptides. A reevaluation of the mechanism of cellular uptake. *The Journal of Biological Chemistry*, 278(1), 585–90.

Robbins, P.D. & Ghivizzani, S.C., 1998. Viral vectors for gene therapy. *Pharmacology & Therapeutics*, 80(1), 35–47.

Ronsin, G. et al., 2001. Novel spermine-based cationic gemini surfactants for gene delivery. *Chemical Communications*, (21), 2234-5.

Rosenzweig, H.S., Rakhmanova, V.A. & MacDonald, R.C., 2001. Diquaternary ammonium compounds as transfection agents. *Bioconjugate Chemistry*, 12(2), 258–63.

Ruthaven NAH, L. and R. N. M., 2005. *The Mesomorphic Phase Behaviour of Lipid Bilayers.* In P. L. Yeagle (Ed.), The Structure of Biological Membranes (2nd ed., pp. 53–107). CRC Press.

Ryan, B.M., O'Donovan, N. & Duffy, M.J., 2009. Survivin: a new target for anti-cancer therapy. *Cancer Treatment Reviews*, 35, 553–62.

Ryther, R.C.C. et al., 2005. siRNA therapeutics: big potential from small RNAs. *Gene Therapy*, 12, 5–11.

Scarpelli, M. et al., 2010. Current Options in the Treatment of Mitochondrial Disease. *Recent Patents on CNS Drug Discovery*, 5, 203–9.
Schild, H.G., 1992. Poly(N-isopropylacrylamide): experiment, theory and application. *Progress in Polymer Science*, 17(2), 163–249.
Schmaljohann, D., 2006. Thermo- and pH-responsive polymers in drug delivery. *Advanced Drug Delivery Reviews*, 58(15), 1655–70.
Schwarze, S. et al., 1999. In vivo protein transduction: delivery of a biologically active protein into the mouse. *Science*, 285(5433), 1569–72.
Seibel, P. et al., 1995. Transfection of mitochondria: strategy towards a gene therapy of mitochondrial DNA diseases. *Nucleic Acids Research*, 23(1), 10–7.
Shinitzky, M., & Barenholz, Y. (1974). Dynamics of the Hydrocarbon Layer in Liposomes of Lecithin and Sphingomyelin Containing Dicetylphosphate. *The Journal of Biological Chemistry*, *249*, 2652–7.
Shinitzky, M. & Barenholz, Y., 1978. Fluidity parameters of lipid regions determined by fluorescence polarization. *Biochimica et Biophysica Acta*, 515(4), 367–94.
Shokolenko, I.N. et al., 2010. The Approaches for Manipulating Mitochondrial Proteome. *Environmental and Molecular Mutagenesis*, 51, 451–61.
Shotton, D. M., 1988. Review: Video-enhanced light microscopy and its applications in cell biology. *Journal of Cell Science*, *89*, 129–50.
Siegel, D.P., 1993. Energetics of intermediates in membrane fusion: comparison of stalk and inverted micellar intermediate mechanisms. *Biophysical Journal*, 65(5), 2124–40.
Siegel, D.P. & Epand, R.M., 1997. The mechanism of lamellar-to-inverted hexagonal phase transitions in phosphatidylethanolamine: implications for membrane fusion mechanisms. *Biophysical Journal*, 73(6), 3089–111.
Silva, S.G. et al., 2009. Towards novel efficient monomeric surfactants based on serine, tyrosine and 4-hydroxyproline: synthesis and micellization properties. *Tetrahedron*, 65(21), 4156–64.
Silva, S.G. et al., 2012. Serine-Based Bis-quat Gemini Surfactants: Synthesis and Micellization Properties. *European Journal of Organic Chemistry*, (2), 345–52.
Silva, S.G. et al., 2013. Synthesis of Gemini Surfactants and Evaluation of Their Interfacial and Cytotoxic Properties: Exploring the Multifunctionality of Serine as Headgroup. *European Journal of Organic Chemistry*, 2013(9), 1758–69.
Simeoni, F., 2003. Insight into the mechanism of the peptide-based gene delivery system MPG: implications for delivery of siRNA into mammalian cells. *Nucleic Acids Research*, 31(11), 2717–24.
Simões, S. et al., 1998. Gene delivery by negatively charged ternary complexes of DNA, cationic liposomes and transferrin or fusigenic peptides. *Gene therapy*, 5(7), 955–64.
Simões, S. et al., 1999. Mechanisms of gene transfer mediated by lipoplexes associated with targeting ligands or pH-sensitive peptides. *Gene Therapy*, 6, 1798–807.
Simões, S. et al., 2005. Cationic liposomes for gene delivery. *Expert Opinion on Drug Delivery*, 2(2), 237–54.
Simons, K. & Gerl, M.J., 2010. Revitalizing membrane rafts: new tools and insights. *Nature Reviews. Molecular Cell Biology*, 11(10), 688–99.
Singh, J. et al., 2012. Evaluation of cellular uptake and intracellular trafficking as determining factors of gene expression for amino acid-substituted gemini surfactant-based DNA nanoparticles. *Journal of Nanobiotechnology*, 10(1), 7.
Somia, N. & Verma, I.M., 2000. Gene therapy: trials and tribulations. *Nature Reviews. Genetics*, 1(2), 91–9.
Spelbrink, J.N., 2010. Functional organization of mammalian mitochondrial DNA in nucleoids: history, recent developments, and future challenges. *IUBMB Life*, 62(1), 19–32.
Sternberg, B., Sorgib, F.L. and Huang, L. 1994. New structures in complex formation between DNA and cationic liposomes visualized by freeze-fracture electron microscopy. *FEBS Letters, 356*, 361-6.

Struck, D. K., Hoekstra, D., & Pagano, R. E., 1981. Use of resonance energy transfer to monitor membrane fusion. *Biochemistry*, *20*(14), 4093–9.
Talelli, M. & Hennink, W.E., 2011. Thermosensitive polymeric micelles for targeted drug delivery. *Nanomedicine*, 6(7), 1245–55.
Tamm, I. et al., 1998. IAP-Family Protein Survivin Inhibits Caspase Activity and Apoptosis Induced by Fas (CD95), Bax, Caspases, and Anticancer Drugs. *Cancer Research*, 58, 5315–20.
Takeda, N. et al., 2004. Temperature-responsive polymeric carriers incorporating hydrophobic monomers for effective transfection in small doses. *Journal of Controlled Release*, 95(2), 343–55.
Tardani, F., Masci, G. & La Mesa, C., 2011. Block co-polymers undergoing supra-molecular association. *Colloids and Surfaces A,* 384(1-3), 374–80.
Templeton, N.S. et al., 1997. Improved DNA:liposomes complexes for increased systemic delivery and gene expression. *Nature Biotechnology*, 15, 647–52.
Theato, P. et al., 2013. Stimuli responsive materials. *Chemical Society Reviews*, 42(17), 7055-6.
Trabulo, S. et al., 2008. S4(13)-PV cell penetrating peptide and cationic liposomes act synergistically to mediate intracellular delivery of plasmid DNA. *The Journal of Gene Medicine*, 10, 1210–22.
Trabulo, S. et al., 2010a. A non-covalent strategy combining cationic lipids and CPPs to enhance the delivery of splice correcting oligonucleotides. *Journal of Controlled Release*, 145, 149–58.
Trabulo, S., Cardoso, A.L., Mano, M., Pedroso de Lima, M.C., 2010b. Cell-penetrating peptides—mechanisms of cellular uptake and generation of delivery systems. *Pharmaceuticals*, 3, 961–93.
Trabulo, S. et al., 2012. Cell-penetrating peptide-based systems for nucleic acid delivery: a biological and biophysical approach. *Methods in Enzymology*, 509, 277–300.
Trabulo, S. et al., 2013. Cell-penetrating Peptides as Nucleic Acid Delivery Systems: From Biophysics to Biological Applications. *Current Pharmaceutical Design*, 19(16), 2895–923.
Tripathi, S. K., Gupta, K. C., & Kumar, P., 2013. Polyethyleneglycol crosslinked N-(2-hydroxyethyl)-polyethylenimine nanoparticles as efficient non-viral vectors for DNA and siRNA delivery in vitro and in vivo. *Molecular bioSystems*, *9*(9), 2322–30.
Troiber, C. & Wagner, E., 2011. Nucleic acid carriers based on precise polymer conjugates. *Bioconjugate Chemistry*, 22(9), 1737–52.
Trotter, P.J. & Storch, J., 1988. 3-[p-(6-Phenyl)-1,3,5-hexatrienyl]phenylpropionic acid (PA-DPH): characterization as a fluorescent membrane probe and binding to fatty acid binding proteins. *Biochimica et Biophysica Acta*, 982, 131–9.
Tsai, L.-R. et al., 2011. A single-monomer derived linear-like PEI-co-PEG for siRNA delivery and silencing. *Biomaterials*, 32(14), 3647–53.
Tunnemann, R.M. Martin, S. Haupt, C. Patsch, F. Edenhofer, M.C.C., 2006. Cargo-dependent mode of uptake and bioavailability of TAT-containing proteins and peptides in living cells. *FASEB Journal*, 20, 1775–84.
Twaites, B.R. et al., 2004. Thermo and pH responsive polymers as gene delivery vectors: effect of polymer architecture on DNA complexation in vitro. *Journal of Controlled Release*, 97(3), 551–66.
Twaites, B.R. et al., 2005. Thermoresponsive polymers as gene delivery vectors: cell viability, DNA transport and transfection studies. *Journal of Controlled Release*, 108(2-3), 472–83.
Uchida, H. et al., 2004. Adenovirus-mediated transfer of siRNA against survivin induced apoptosis and attenuated tumor cell growth in vitro and in vivo. *Molecular Therapy*, 10(1), 162–71.

Uhríková, D. et al., 2005. Interaction of gemini surfactants butane-1,4-diyl-bis(alkyldimethylammonium bromide) with DNA. *Colloids and Surfaces, B*, 42(1), 59–68.
Veis, A. & Nawrot, C., 1970. Basicity Differences among Peptide Bonds. *Journal of the American Chemical Society*, 92(13), 3910–4.
Vereb, G. et al., 2003. Dynamic, yet structured: The cell membrane three decades after the Singer-Nicolson model. *Proceedings of the National Academy of Sciences of the United States of America*, 100(14), 8053–8.
Verma, I.M. & Somia, N., 1997. Gene therapy - promises, problems and prospects. *Nature*, 389(6648), 239–42.
Verma, I.M. & Weitzman, M.D., 2005. Gene therapy: twenty-first century medicine. *Annual Review of Biochemistry*, 74(1), 711–38.
Vile, R.G., Russell, S.J. & Lemoine, N.R., 2000. Cancer gene therapy: hard lessons and new courses. *Gene Therapy*, 7(1), 2–8.
Vivès, E. et al., 2003. TAT peptide internalization: seeking the mechanism of entry. *Current Protein and Peptide Science*, 4(2), 125–32.
Volden, S. et al., 2012. Interactions between bovine serum albumin and Langmuir films composed of charged and uncharged poly(N-isopropylacrylamide) block copolymers. *Colloids and surfaces. B: Biointerfaces*, 98, 50–7.
Wallace, D.C., 1999. Mitochondrial diseases in man and mouse. *Science*, 283(5407), 1482–8.
Wallace, D.C., 2007. Why do we still have a maternally inherited mitochondrial DNA? Insights from evolutionary medicine. *Annual Review of Biochemistry*, 76, 781–821.
Wang, C. et al., 2007. Investigation of complexes formed by interaction of cationic gemini surfactants with deoxyribonucleic acid. *Physical Chemistry Chemical Physics*, 9(13), 1616–28.
Wang, H. & Wettig, S.D., 2011. Synthesis and aggregation properties of dissymmetric phytanyl-gemini surfactants for use as improved DNA transfection vectors. *Phys. Chem. Chem. Phys.*, 13(2), 637–42.
Wang, H. et al., 2013. Transfection and structural properties of phytanyl substituted gemini surfactant-based vectors for gene delivery. *Physical Chemistry Chemical Physics*, 15(47), 20510–6.
Ward, M.A. & Georgiou, T.K., 2011. Thermoresponsive Polymers for Biomedical Applications. *Polymers*, 3(3), 1215–42.
Wasungu, L., Stuart, M.C.A., et al., 2006a. Lipoplexes formed from sugar-based gemini surfactants undergo a lamellar-to-micellar phase transition at acidic pH. Evidence for a non-inverted membrane-destabilizing hexagonal phase of lipoplexes. *Biochimica et Biophysica Acta*, 1758(10), 1677–84.
Wasungu, L., Scarzello, M., et al., 2006b. Transfection mediated by pH-sensitive sugar-based gemini surfactants; potential for in vivo gene therapy applications. *Journal of Molecular Medicine*, 84(9), 774–84.
Weber-Lotfi, F. et al., 2009. Developing a genetic approach to investigate the mechanism of mitochondrial competence for DNA import. *Biochimica et Biophysica Acta*, 1787(5), 320–7.
Weihs, D. et al., 2005. Self-aggregation in dimeric arginine-based cationic surfactants solutions. *Colloids and Surfaces A*, 255(1-3), 73–8.
Weissig, V. et al., 1998. DQAsomes: A Novel Potential Drug and Dene Delivery System Made from Dequalinium. *Pharmaceutical Research*, 15(2), 334–7.
Weissig, V., D'Souza, G.G. & Torchilin, V.P., 2001a. DQAsome/DNA complexes release DNA upon contact with isolated mouse liver mitochondria. *Journal of Controlled Release*, 75(3), 401–8.
Weissig, V. & Torchilin, V.P., 2001b. Towards mitochondrial gene therapy: DQAsomes as a strategy. *Journal of Drug Targeting*, 9(1), 1–13.

Weissig, V. & Torchilin, V.P., 2001c. Cationic bolasomes with delocalized charge centers as mitochondria-specific DNA delivery systems. *Advanced Drug Delivery Reviews*, 49(1-2), 127–49.
Weissig, V. & Torchilin, V.P., 2001d. Mitochondriotropic cationic vesicles: a strategy towards mitochondrial gene therapy. *Current Pharmaceutical Biotechnology*, 2(2), 208–29.
Weissig, V., 2005. Targeted drug delivery to mammalian mitochondria in living cells. *Expert Opinion on Drug Delivery*, 2(1), 89–102.
Wender, P. a et al., 2000. The design, synthesis, and evaluation of molecules that enable or enhance cellular uptake: peptoid molecular transporters. *Proceedings of the National Academy of Sciences of the United States of America*, 97(24), 13003–8.
Wettig, S.D. & Verrall, R.E., 2001. Thermodynamic Studies of Aqueous m-s-m Gemini Surfactant Systems. *Journal of Colloid and Interface Science*, 235(2), 310–316.
Wettig, S.D. et al., 2007. Structural and transfection properties of amine-substituted gemini surfactant-based nanoparticles. *J. Gene Med.*, 9, 649–58.
Wettig, S.D., Verrall, R.E. & Foldvari, M., 2008. Gemini surfactants: a new family of building blocks for non-viral gene delivery systems. *Current Gene Therapy*, 8(1), 9–23.
Wheeler, V.C. et al., 1996. Synthesis of a modified gene encoding human ornithine transcarbamylase for expression in mammalian mitochondrial and universal translation systems: a novel approach towards correction of a genetic defect. *Gene*, 169(2), 251–5.
Whitehead, K. A., Langer, R. & Anderson, D.G., 2009. Knocking down barriers: advances in siRNA delivery. *Nature reviews. Drug Discovery*, 8(2), 129–38.
Wilkinson, D.A. & McIntosh, T.J., 1986. A subtransition in a phospholipid with a net charge, dipalmitoylphosphatidylglycerol. *Biochemistry*, 25(2), 295–8.
Winter, R., & Köhling, R., 2004. Static and time-resolved synchrotron small-angle x-ray scattering studies of lyotropic lipid mesophases, model biomembranes and proteins in solution. *Journal of Physics: Condensed Matter*, *16*(5), S327–52.
Won, Y.-Y., Sharma, R. & Konieczny, S.F., 2009. Missing Pieces in Understanding the Intracellular Trafficking of Polycation/DNA Complexes. *Journal of Controlled Release*, 139(2), 88–93.
Wong, S.Y., Pelet, J.M. & Putnam, D., 2007. Polymer systems for gene delivery—Past, present, and future. *Progress in Polymer Science*, 32(8-9), 799–837.
Wu, S.Y. & McMillan, N.A.J., 2009. Lipidic systems for in vivo siRNA delivery. *The American Association of Pharmaceutical Scientists Journal*, 11(4), 639–52.
Yang, P. et al., 2010. Enhanced gene expression in epithelial cells transfected with amino acid-substituted gemini nanoparticles. *European Journal of Pharmaceutics and Biopharmaceutics*, 75(3), 311–20.
Yasuzaki, Y., Yamada, Y. & Harashima, H., 2010. Mitochondrial matrix delivery using MITO-Porter, a liposome-based carrier that specifies fusion with mitochondrial membranes. *Biochemical and Biophysical Research Communications*, 397(2), 181–6.
Yonesaka, K. et al., 2006. Small interfering RNA targeting survivin sensitizes lung cancer cell with mutant p53 to adriamycin. *International Journal of Cancer*, 118, 812–20.
Yoon, Y.G., Koob, M.D. & Yoo, Y.H., 2010. Re-engineering the mitochondrial genomes in mammalian cells. *Anatomy & Cell Biology*, 43(2), 97–109.
Zana, R., Benrraou, M. & Rueff, R., 1991. Alkanediyl- α,ω-bis(dimethylalkylammonium bromide) surfactants. 1. Effect of the spacer chain length on the critical micelle concentration and micelle ionization degree. *Langmuir*, 7(6), 1072–5.
Zana, R. & Lévy, H., 1997. Alkanediyl-α,ω-bis(dimethylalkylammonium bromide) surfactants (dimeric surfactants) Part 6. CMC of the ethanediyl-1,2-bis(dimethylalkylammonium bromide) series. *Colloids and Surfaces, A*, 127(1-3), 229–32.
Zana, R., 2002a. Dimeric (gemini) surfactants: effect of the spacer group on the association behavior in aqueous solution. *Journal of Colloid and Interface Science*, 248(2), 203–20.
Zana, R., 2002b. Dimeric and oligomeric surfactants. Behavior at interfaces and in aqueous solution: a review. *Advances in Colloid and Interface Science*, 97(1-3), 205–53.

Zana, R. & In, M., 2005. *Phase Behavior of Gemini Surfactants in Gemini Surfactants - Synthesis, Interfacial and Solution-Phase Behavior, and Applications* R. Zana & J. Xia, eds., New York: Marcel Dekker, Inc.

Zeta Sizer Nano Series (Malvern Instruments), User Manual, Mano317, Issue 1.1, 2014, United Kingdom, Chapters 1 and 13.

Zhang, C. et al., 2006. siRNA-containing liposomes modified with polyarginine effectively silence the targeted gene. *Journal of Controlled Release*, 112(2), 229–39.

Zhao, J., Christian, S.D. & Fung, B.M., 1998. Mixtures of Monomeric and Dimeric Cationic Surfactants. *The Journal of Physical Chemistry B*, 102, 7613–8.

Zhao, X. et al., 2008. Biophysical characterization of complexation of DNA with oppositely charged Gemini surfactant 12-3-12. *Biophysical Chemistry*, 138(3), 144–9.

Zhou, T. et al., 2013. High Transfection Efficiency of Homogeneous DNA Nanoparticles Induced by Imidazolium Gemini Surfactant as Nonviral Vector. *The Journal of Physical Chemistry C*, 117(50), 26573–81.

Zuhorn, I.S. et al., 2002. Phase behavior of cationic amphiphiles and their mixtures with helper lipid influences lipoplex shape, DNA translocation, and transfection efficiency. *Biophysical Journal*, 83(4), 2096–108.

Zuhorn, I.S., Engberts, J.B.F.N. & Hoekstra, D., 2007. Gene delivery by cationic lipid vectors: overcoming cellular barriers. *European Biophysics Journal*, 36, 349–62.

Zuidam, N.J., Barenholz, Y. & Minsky, A., 1999. Chiral DNA packaging in DNA-cationic liposome assemblies. *FEBS Letters*, 457(3), 419–22.

Apendix

Copyright Licence Agreements

SPRINGER LICENSE
TERMS AND CONDITIONS

Aug 21, 2014

This is a License Agreement between Ana Cardoso ("You") and Springer ("Springer") provided by Copyright Clearance Center ("CCC"). The license consists of your order details, the terms and conditions provided by Springer, and the payment terms and conditions.

All payments must be made in full to CCC. For payment instructions, please see information listed at the bottom of this form.

License Number	3453070321290
License date	Aug 20, 2014
Licensed content publisher	Springer
Licensed content publication	Cellular and Molecular Life Sciences
Licensed content title	Nanocarriers' entry into the cell: relevance to drug delivery
Licensed content author	Hervé Hillaireau
Licensed content date	Jan 1, 2009
Volume number	66
Issue number	17
Type of Use	Thesis/Dissertation
Portion	Figures
Author of this Springer article	No
Order reference number	None
Original figure numbers	Fig 5
Title of your thesis / dissertation	NUCLEIC ACID DELIVERY SYSTEMS: FROM BIOPHYSICS TO BIOLOGICAL ACTIVITY
Expected completion date	Sep 2014
Estimated size(pages)	300
Total	0.00 EUR
Terms and Conditions	

Introduction

The publisher for this copyrighted material is Springer Science + Business Media. By clicking "accept" in connection with completing this licensing transaction, you agree that the following terms and conditions apply to this transaction (along with the Billing and Payment terms and conditions established by Copyright Clearance Center, Inc. ("CCC"), at the time that you opened your Rightslink account and that are available at any time at http://myaccount.copyright.com).

Limited License

With reference to your request to reprint in your thesis material on which Springer Science and Business Media control the copyright, permission is granted, free of charge, for the use indicated in your enquiry.

Licenses are for one-time use only with a maximum distribution equal to the number that you identified in the licensing process.

This License includes use in an electronic form, provided its password protected or on the university's intranet or repository, including UMI (according to the definition at the Sherpa website: http://www.sherpa.ac.uk/romeo/). For any other electronic use, please contact Springer at (permissions.dordrecht@springer.com or permissions.heidelberg@springer.com).

The material can only be used for the purpose of defending your thesis limited to university-use only. If the thesis is going to be published, permission needs to be re-obtained (selecting "book/textbook" as the type of use).

Although Springer holds copyright to the material and is entitled to negotiate on rights, this license is only valid, subject to a courtesy information to the author (address is given with the article/chapter) and provided it concerns original material which does not carry references to other sources (if material in question appears with credit to another source, authorization from that source is required as well).

Permission free of charge on this occasion does not prejudice any rights we might have to charge for reproduction of our copyrighted material in the future.

Altering/Modifying Material: Not Permitted
You may not alter or modify the material in any manner. Abbreviations, additions, deletions and/or any other alterations shall be made only with prior written authorization of the author(s) and/or Springer Science + Business Media. (Please contact Springer at (permissions.dordrecht@springer.com or permissions.heidelberg@springer.com)

Reservation of Rights
Springer Science + Business Media reserves all rights not specifically granted in the combination of (i) the license details provided by you and accepted in the course of this licensing transaction, (ii) these terms and conditions and (iii) CCC's Billing and Payment terms and conditions.

Copyright Notice:Disclaimer
You must include the following copyright and permission notice in connection with any reproduction of the licensed material: "Springer and the original publisher /journal title, volume, year of publication, page, chapter/article title, name(s) of author(s), figure number(s), original copyright notice) is given to the publication in which the material was originally published, by adding; with kind permission from Springer Science and Business Media"

Warranties: None

Example 1: Springer Science + Business Media makes no representations or warranties with respect to the licensed material.

Example 2: Springer Science + Business Media makes no representations or warranties with respect to the licensed material and adopts on its own behalf the limitations and disclaimers established by CCC on its behalf in its Billing and Payment terms and conditions for this licensing transaction.

Indemnity
You hereby indemnify and agree to hold harmless Springer Science + Business Media and CCC,

and their respective officers, directors, employees and agents, from and against any and all claims arising out of your use of the licensed material other than as specifically authorized pursuant to this license.

No Transfer of License
This license is personal to you and may not be sublicensed, assigned, or transferred by you to any other person without Springer Science + Business Media's written permission.

No Amendment Except in Writing
This license may not be amended except in a writing signed by both parties (or, in the case of Springer Science + Business Media, by CCC on Springer Science + Business Media's behalf).

Objection to Contrary Terms
Springer Science + Business Media hereby objects to any terms contained in any purchase order, acknowledgment, check endorsement or other writing prepared by you, which terms are inconsistent with these terms and conditions or CCC's Billing and Payment terms and conditions. These terms and conditions, together with CCC's Billing and Payment terms and conditions (which are incorporated herein), comprise the entire agreement between you and Springer Science + Business Media (and CCC) concerning this licensing transaction. In the event of any conflict between your obligations established by these terms and conditions and those established by CCC's Billing and Payment terms and conditions, these terms and conditions shall control.

Jurisdiction
All disputes that may arise in connection with this present License, or the breach thereof, shall be settled exclusively by arbitration, to be held in The Netherlands, in accordance with Dutch law, and to be conducted under the Rules of the 'Netherlands Arbitrage Instituut' (Netherlands Institute of Arbitration).***OR:***

All disputes that may arise in connection with this present License, or the breach thereof, shall be settled exclusively by arbitration, to be held in the Federal Republic of Germany, in accordance with German law.

Other terms and conditions:

v1.3

You will be invoiced within 48 hours of this transaction date. You may pay your invoice by credit card upon receipt of the invoice for this transaction. Please follow instructions provided at that time.
To pay for this transaction now; please remit a copy of this document along with your payment. Payment should be in the form of a check or money order referencing your account number and this invoice number RLNK501381974.
Make payments to "COPYRIGHT CLEARANCE CENTER" and send to:

Copyright Clearance Center
Dept 001
P.O. Box 843006
Boston, MA 02284-3006
Please disregard electronic and mailed copies if you remit payment in advance.
Questions? customercare@copyright.com or +1-855-239-3415 (toll free in the US) or +1-978-646-2777.

Gratis licenses (referencing $0 in the Total field) are free. Please retain this printable license for your reference. No payment is required.

ELSEVIER LICENSE
TERMS AND CONDITIONS

Aug 21, 2014

This is a License Agreement between Ana Cardoso ("You") and Elsevier ("Elsevier") provided by Copyright Clearance Center ("CCC"). The license consists of your order details, the terms and conditions provided by Elsevier, and the payment terms and conditions.

All payments must be made in full to CCC. For payment instructions, please see information listed at the bottom of this form.

Supplier	Elsevier Limited The Boulevard,Langford Lane Kidlington,Oxford,OX5 1GB,UK
Registered Company Number	1982084
Customer name	Ana Cardoso
Customer address	Largo Marquês de Pombal Coimbra, 3004-517
License number	3453090116467
License date	Aug 20, 2014
Licensed content publisher	Elsevier
Licensed content publication	International Journal of Pharmaceutics
Licensed content title	Temperature-responsive cationic block copolymers as nanocarriers for gene delivery
Licensed content author	Maria Teresa Calejo,Ana Maria S. Cardoso,Anna-Lena Kjøniksen,Kaizheng Zhu,Catarina M. Morais,Sverre Arne Sande,Ana Luísa Cardoso,Maria C. Pedroso de Lima,Amália Jurado,Bo Nyström
Licensed content date	1 May 2013
Licensed content volume number	448
Licensed content issue number	1
Number of pages	10
Start Page	105
End Page	114
Type of Use	reuse in a thesis/dissertation
Intended publisher of new work	other
Portion	figures/tables/illustrations
Number of figures/tables/illustrations	2
Format	electronic
Are you the author of this	Yes

Elsevier article?	
Will you be translating?	No
Title of your thesis/dissertation	NUCLEIC ACID DELIVERY SYSTEMS: FROM BIOPHYSICS TO BIOLOGICAL ACTIVITY
Expected completion date	Sep 2014
Estimated size (number of pages)	300
Elsevier VAT number	GB 494 6272 12
Permissions price	0.00 USD
VAT/Local Sales Tax	0.00 USD / 0.00 GBP
Total	0.00 USD
Terms and Conditions	

INTRODUCTION

1. The publisher for this copyrighted material is Elsevier. By clicking "accept" in connection with completing this licensing transaction, you agree that the following terms and conditions apply to this transaction (along with the Billing and Payment terms and conditions established by Copyright Clearance Center, Inc. ("CCC"), at the time that you opened your Rightslink account and that are available at any time at http://myaccount.copyright.com).

GENERAL TERMS

2. Elsevier hereby grants you permission to reproduce the aforementioned material subject to the terms and conditions indicated.

3. Acknowledgement: If any part of the material to be used (for example, figures) has appeared in our publication with credit or acknowledgement to another source, permission must also be sought from that source. If such permission is not obtained then that material may not be included in your publication/copies. Suitable acknowledgement to the source must be made, either as a footnote or in a reference list at the end of your publication, as follows:

"Reprinted from Publication title, Vol /edition number, Author(s), Title of article / title of chapter, Pages No., Copyright (Year), with permission from Elsevier [OR APPLICABLE SOCIETY COPYRIGHT OWNER]." Also Lancet special credit - "Reprinted from The Lancet, Vol. number, Author(s), Title of article, Pages No., Copyright (Year), with permission from Elsevier."

4. Reproduction of this material is confined to the purpose and/or media for which permission is hereby given.

5. Altering/Modifying Material: Not Permitted. However figures and illustrations may be altered/adapted minimally to serve your work. Any other abbreviations, additions, deletions and/or any other alterations shall be made only with prior written authorization of Elsevier Ltd. (Please contact Elsevier at permissions@elsevier.com)

6. If the permission fee for the requested use of our material is waived in this instance, please be advised that your future requests for Elsevier materials may attract a fee.

7. Reservation of Rights: Publisher reserves all rights not specifically granted in the combination of (i) the license details provided by you and accepted in the course of this licensing transaction, (ii)

these terms and conditions and (iii) CCC's Billing and Payment terms and conditions.

8. License Contingent Upon Payment: While you may exercise the rights licensed immediately upon issuance of the license at the end of the licensing process for the transaction, provided that you have disclosed complete and accurate details of your proposed use, no license is finally effective unless and until full payment is received from you (either by publisher or by CCC) as provided in CCC's Billing and Payment terms and conditions. If full payment is not received on a timely basis, then any license preliminarily granted shall be deemed automatically revoked and shall be void as if never granted. Further, in the event that you breach any of these terms and conditions or any of CCC's Billing and Payment terms and conditions, the license is automatically revoked and shall be void as if never granted. Use of materials as described in a revoked license, as well as any use of the materials beyond the scope of an unrevoked license, may constitute copyright infringement and publisher reserves the right to take any and all action to protect its copyright in the materials.

9. Warranties: Publisher makes no representations or warranties with respect to the licensed material.

10. Indemnity: You hereby indemnify and agree to hold harmless publisher and CCC, and their respective officers, directors, employees and agents, from and against any and all claims arising out of your use of the licensed material other than as specifically authorized pursuant to this license.

11. No Transfer of License: This license is personal to you and may not be sublicensed, assigned, or transferred by you to any other person without publisher's written permission.

12. No Amendment Except in Writing: This license may not be amended except in a writing signed by both parties (or, in the case of publisher, by CCC on publisher's behalf).

13. Objection to Contrary Terms: Publisher hereby objects to any terms contained in any purchase order, acknowledgment, check endorsement or other writing prepared by you, which terms are inconsistent with these terms and conditions or CCC's Billing and Payment terms and conditions. These terms and conditions, together with CCC's Billing and Payment terms and conditions (which are incorporated herein), comprise the entire agreement between you and publisher (and CCC) concerning this licensing transaction. In the event of any conflict between your obligations established by these terms and conditions and those established by CCC's Billing and Payment terms and conditions, these terms and conditions shall control.

14. Revocation: Elsevier or Copyright Clearance Center may deny the permissions described in this License at their sole discretion, for any reason or no reason, with a full refund payable to you. Notice of such denial will be made using the contact information provided by you. Failure to receive such notice will not alter or invalidate the denial. In no event will Elsevier or Copyright Clearance Center be responsible or liable for any costs, expenses or damage incurred by you as a result of a denial of your permission request, other than a refund of the amount(s) paid by you to Elsevier and/or Copyright Clearance Center for denied permissions.

LIMITED LICENSE

The following terms and conditions apply only to specific license types:

15. **Translation**: This permission is granted for non-exclusive world **English** rights only unless your license was granted for translation rights. If you licensed translation rights you may only translate this content into the languages you requested. A professional translator must perform all

translations and reproduce the content word for word preserving the integrity of the article. If this license is to re-use 1 or 2 figures then permission is granted for non-exclusive world rights in all languages.

16. **Posting licensed content on any Website**: The following terms and conditions apply as follows: Licensing material from an Elsevier journal: All content posted to the web site must maintain the copyright information line on the bottom of each image; A hyper-text must be included to the Homepage of the journal from which you are licensing at http://www.sciencedirect.com/science/journal/xxxxx or the Elsevier homepage for books at http://www.elsevier.com; Central Storage: This license does not include permission for a scanned version of the material to be stored in a central repository such as that provided by Heron/XanEdu.

Licensing material from an Elsevier book: A hyper-text link must be included to the Elsevier homepage at http://www.elsevier.com . All content posted to the web site must maintain the copyright information line on the bottom of each image.

Posting licensed content on Electronic reserve: In addition to the above the following clauses are applicable: The web site must be password-protected and made available only to bona fide students registered on a relevant course. This permission is granted for 1 year only. You may obtain a new license for future website posting.

For journal authors: the following clauses are applicable in addition to the above: Permission granted is limited to the author accepted manuscript version* of your paper.

***Accepted Author Manuscript (AAM) Definition:** An accepted author manuscript (AAM) is the author's version of the manuscript of an article that has been accepted for publication and which may include any author-incorporated changes suggested through the processes of submission processing, peer review, and editor-author communications. AAMs do not include other publisher value-added contributions such as copy-editing, formatting, technical enhancements and (if relevant) pagination.

You are not allowed to download and post the published journal article (whether PDF or HTML, proof or final version), nor may you scan the printed edition to create an electronic version. A hyper-text must be included to the Homepage of the journal from which you are licensing at http://www.sciencedirect.com/science/journal/xxxxx. As part of our normal production process, you will receive an e-mail notice when your article appears on Elsevier's online service ScienceDirect (www.sciencedirect.com). That e-mail will include the article's Digital Object Identifier (DOI). This number provides the electronic link to the published article and should be included in the posting of your personal version. We ask that you wait until you receive this e-mail and have the DOI to do any posting.

Posting to a repository: Authors may post their AAM immediately to their employer's institutional repository for internal use only and may make their manuscript publically available after the journal-specific embargo period has ended.

Please also refer to Elsevier's Article Posting Policy for further information.

18. **For book authors** the following clauses are applicable in addition to the above: Authors are permitted to place a brief summary of their work online only.. You are not allowed to download and post the published electronic version of your chapter, nor may you scan the printed edition to create an electronic version. **Posting to a repository:** Authors are permitted to post a summary of

their chapter only in their institution's repository.

20. **Thesis/Dissertation**: If your license is for use in a thesis/dissertation your thesis may be submitted to your institution in either print or electronic form. Should your thesis be published commercially, please reapply for permission. These requirements include permission for the Library and Archives of Canada to supply single copies, on demand, of the complete thesis and include permission for UMI to supply single copies, on demand, of the complete thesis. Should your thesis be published commercially, please reapply for permission.

Elsevier Open Access Terms and Conditions

Elsevier publishes Open Access articles in both its Open Access journals and via its Open Access articles option in subscription journals.

Authors publishing in an Open Access journal or who choose to make their article Open Access in an Elsevier subscription journal select one of the following Creative Commons user licenses, which define how a reader may reuse their work: Creative Commons Attribution License (CC BY), Creative Commons Attribution – Non Commercial - ShareAlike (CC BY NC SA) and Creative Commons Attribution – Non Commercial – No Derivatives (CC BY NC ND)

Terms & Conditions applicable to all Elsevier Open Access articles:

Any reuse of the article must not represent the author as endorsing the adaptation of the article nor should the article be modified in such a way as to damage the author's honour or reputation.

The author(s) must be appropriately credited.

If any part of the material to be used (for example, figures) has appeared in our publication with credit or acknowledgement to another source it is the responsibility of the user to ensure their reuse complies with the terms and conditions determined by the rights holder.

Additional Terms & Conditions applicable to each Creative Commons user license:

CC BY: You may distribute and copy the article, create extracts, abstracts, and other revised versions, adaptations or derivative works of or from an article (such as a translation), to include in a collective work (such as an anthology), to text or data mine the article, including for commercial purposes without permission from Elsevier

CC BY NC SA: For non-commercial purposes you may distribute and copy the article, create extracts, abstracts and other revised versions, adaptations or derivative works of or from an article (such as a translation), to include in a collective work (such as an anthology), to text and data mine the article and license new adaptations or creations under identical terms without permission from Elsevier

CC BY NC ND: For non-commercial purposes you may distribute and copy the article and include it in a collective work (such as an anthology), provided you do not alter or modify the article, without permission from Elsevier

Any commercial reuse of Open Access articles published with a CC BY NC SA or CC BY NC

ND license requires permission from Elsevier and will be subject to a fee.

Commercial reuse includes:

- Promotional purposes (advertising or marketing)
- Commercial exploitation (e.g. a product for sale or loan)
- Systematic distribution (for a fee or free of charge)

Please refer to Elsevier's Open Access Policy for further information.

21. **Other Conditions**:

v1.6

You will be invoiced within 48 hours of this transaction date. You may pay your invoice by credit card upon receipt of the invoice for this transaction. Please follow instructions provided at that time.
To pay for this transaction now; please remit a copy of this document along with your payment. Payment should be in the form of a check or money order referencing your account number and this invoice number RLNK501382019.
Make payments to "COPYRIGHT CLEARANCE CENTER" and send to:

Copyright Clearance Center
Dept 001
P.O. Box 843006
Boston, MA 02284-3006
Please disregard electronic and mailed copies if you remit payment in advance.
Questions? customercare@copyright.com or +1-855-239-3415 (toll free in the US) or +1-978-646-2777.

Gratis licenses (referencing $0 in the Total field) are free. Please retain this printable license for your reference. No payment is required.